

The University of Nottingham

UNITED KINGDOM • CHINA • MALAYSIA

Development of existing and novel tyrosinase inhibitors for skin pigmentation: intradermal delivery, biological evaluation and mechanistic studies

Zhiwei Li

Submitted to the University of Nottingham for the degree of Doctor of Philosophy

Feb 2023

General Abstract

Hyperpigmentation is a common skin disorder caused by the abnormal production and accumulation of melanin, including sunspots, post-inflammatory hyperpigmentation, and melasma. Melanin is produced by melanocytes in melanosomes through a complex process called melanogenesis, in which tyrosinase plays a critical role. Therefore, exploration of the permeation capacity, biological activity, and metabolic mechanisms of existing and novel tyrosinase inhibitors is necessary and will help to improve the problem of hyperpigmentation. One of the main problems regarding the existing tyrosinase inhibitor, Alpha-Arbutin, is its poor permeation ability. In this thesis, it is proposed that the ability of the drug to permeate within the skin can be enhanced by solid microneedles and dissolving polymeric microneedles. It was found that both solid microneedle post-treatment and dissolving polymeric microneedles were able to facilitate the intradermal penetration of Alpha-Arbutin. Interestingly, the soluble polymeric microneedle was able to reach deeper into the skin, targeting delivery to the basal layer, making it a more desirable option. Also, given the compliance and safety issues associated with solid microneedles, dissolving polymeric microneedles overall have better prospects.

Although we found that the use of dissolving polymeric microneedles is an effective way to improve the permeation of Alpha-Arbutin, there still exists a need to develop a novel compound with strong tyrosinase inhibition and optimal partition coefficient. Thus, in this thesis, we have identified the new compound 11c as a promising tyrosinase inhibitor with excellent anti-

tyrosinase activity shown in melanoma cells A375. Compound 11c is hydrophobic and demonstrated good *in vitro and in vivo* penetration ability. Most importantly, compound 11c was able to successfully improve UV-induced skin pigmentation in guinea pigs in the *in vivo* experiments. All suggest that compound 11c may serve as a promising and effective novel tyrosinase inhibitor that could be used to develop potential therapies for the treatment of skin hyperpigmentation.

After having evaluated the biological activity as well as the physicochemical properties of 11c, we turned our attention to its mechanism of action. In this thesis, the metabolic pathway of tyrosinase modulators in melanoma cells was investigated. A combination of LC-MS targeted metabolomics and OrbiSIMS analysis was used to investigate the differences in metabolites in melanoma cells from different experimental groups. It was found that disorders of Malate-Aspartate Shuttle and fatty acids were associated with the role of tyrosinase modulators in melanoma cells. This suggests that fatty acids and respiration have important functions in melanoma cells. This also provides a strong contribution to subsequent scholars searching for new therapeutic targets for pigmentation and melanoma.

Declaration

I declare that except where acknowledged in the text, this thesis is my work and is based on research undertaken at the School of Pharmacy, Faculty of Science, University of Nottingham.

Supervisors:

Dr. Zheying Zhu, Associate Professor in International Pharmacy & Traditional Medicines, Course Director of BSc International Pharmacy, School of Pharmacy, The University of Nottingham, UK

Dr. Maria Marlow, Associate Professor in Formulation Science and Pharmaceutical Materials, School of Pharmacy, The University of Nottingham, UK

Dr. David Scurr, Principal Research Fellow in Surface Analysis, School of Pharmacy, The University of Nottingham, UK

Acknowledgements

This thesis represents the end of a long and memorable journey, accompanied by many challenges and difficulties. It has been four years not only of PhD studies but also of being affected by the pandemic. Despite this adversity, I believe I have already overcome it successfully.

First and foremost, I would like to express my gratitude to my supervisor, Dr Zheying Zhu. I would like to thank her for her continued enthusiasm and wealth of knowledge in supporting and guiding me. Her motivation and guidance have helped me and enabled me to successfully complete my project. Without her support and companionship, this would have been an impossible task. In addition, I would like to extend my thanks to my second supervisor, Dr David Scurr, for his help and guidance throughout my PhD project, especially the OrbiSIMS part. He is a very patient person and was willing to answer all my academic concerns. I would also like to express my deepest gratitude to my third supervisor, Dr Maria Marlow. She gave me ample guidance and advice throughout the project, especially on the intradermal drug delivery and microneedle fabrication part.

I would also want to thank Mohammed Khan for all his guidance and dedication to my experimental manipulation.

I would also like to thank Prof Jinyi Xu from China Pharmaceutical University and her research team for supplying the novel tyrosinase inhibitors 11c and 11m. I am also very grateful to the technical staff at the School of Pharmacy and the School of Life Sciences at the University of Nottingham for their help and training. I am also grateful to my thesis

examiners, Professor Lodewijk Dekker and Professor Gary Moss. I would like to thank them for their helpful feedback and suggestions, which helped me to develop a strong argument in my thesis.

I would like to thank all my lab mates for their company and help. I would also like to thank all the friends I have made in Nottingham who have made my four years of education life so much more enjoyable and memorable.

I am extremely appreciative of my cousin, Irene Xue, for her insightful comments on my thesis over the past month. She has taught me how to present the content in a more authentic and clear manner. Finally, I must give credit to my parents for all their hard work and efforts in my upbringing, and for their support and financial assistance. They are my main source of providing me with a sense of security.

Attended Conferences

The beauty lab 2022, Royal Institution, London, 5 May 2022

2022 UKICRS Workshop & Symposium, Manchester, 9-10 June, 2022

13th PharmSci International Conference, Belfast, 7-9 September 2022

Publications:

Songtao Xue,[‡,#] Zhiwei Li,[†,#] Xiaotong Ze,[‡] Xiuyuan Wu,[‡] Chen He,[‡] Wen Shuai,[‡] Maria Marlow,[†] Jian Chen,[Δ] David Scurr,[†,*] Zheying Zhu,[†,*] Jinyi Xu,[‡,*] Shengtao Xu[‡,Δ,*], Design, Synthesis and Biological Evaluation of Novel Hybrids Containing Dihydrochalcone as Tyrosinase Inhibitors to Treat Skin Hyperpigmentation, 2023, *Journal of Medicinal Chemistry*, https://doi.org/10.1021/acs.jmedchem.3c00012

Zhiwei Li[#], Maria Marlow, David Scurr, Felicia Goh Xia Yee, Zheying Zhu*, Evaluation of enhanced Intradermal delivery of Alpha-Arbutin by applications of microneedles and 3D OrbiSIMS, 2023, *Molecular Pharmaceutics* (to be submitted)

Zhiwei Li[#], Li Lu, David Scurr, Maria Marlow, Zheying Zhu*, Implications of tyrosinase modulators for malate-aspartate shuttle and fatty acid metabolism in melanoma cells A375 revealed by metabolomics and lipidomics, 2023, *Molecular Omics* (to be submitted)

CONTENTS

Chapter 1. General Introduction 20

1.1 Skin pigmentation disorders 21

1.1.1 Hyperpigmentation 22

1.1.2 Hypopigmentation 24

1.2 Melanocytes 24

1.2.1 Melanin and melanosomes 25

1.2.2 Factors regulating melanogenesis within melanocytes 27

1.2.3 Mechanism of tyrosinase involving production of melanin 30

1.3 Tyrosinase modulators 32

1.3.1 Tyrosinase stimulator - L-DOPA 32

1.3.2 Advances of research in tyrosinase inhibitors 34

1.4 Skin penetration 42

1.4.1 Skin structure and function 42

1.4.2 The route of skin administration 47

1.4.3 Microneedles 51

1.5 Skin cancer - melanoma 58

1.6 Metabolomics 61

1.6.1 Application of metabolomics in tumour crippling research 63

1.7 Lipidomics 65

1.7.1 Lipid metabolites 66

1.7.2 The relationship between melanoma and lipids 71

1.8 Experimental methods to assess drug penetration 74

1.8.1 Franz diffusion cell 74

1.8.2 Analytical techniques 76

1.9 Aims of this thesis 81

Chapter 2. Evaluation of enhanced Intradermal delivery of Alpha-Arbutin by applications of microneedles and 3D OrbiSIMS 84

2.1 Abstract 85

2.2 Introduction 86

2.3 Materials and methods 92

2.3.1. Materials 92

2.3.2 Methods 94

2.4 Results and discussion 101

2.4.1 Formulation and fabrication of dissolving MNs 101

2.4.2 HPLC analysis of Alpha-Arbutin in skin permeation study 102

2.4.3 Visualisation of Alpha-Arbutin within the skin by 3D OrbiSIMS 111

2.5. Conclusion 116

Chapter 3. Design, Synthesis and Biological Evaluation of Novel Hybrids Containing Dihydrochalcone as Tyrosinase Inhibitors to Treat Skin Hyperpigmentation 118

3.1 Abstract 120

3.2 Introduction 120

3.3 Methods 126

3.3.1 Chemical synthesis 126

3.3.2 Mushroom TYR inhibitory activity of tested compounds 127

3.3.3 Cytotoxicity of 11c and 11m 128

3.3.4 TYR inhibitory activity of 11c and 11m 128

3.3.5 Inhibition of 11c and 11m on melanin content 129

3.3.6 Western blotting 130

3.3.7 HPLC analysis of 11c and kojic acid in skin permeation study 131

3.3.8 Linearity, limit of detection and limit of quantitation 131

3.3.9 In vitro skin permeation efficiency of 11c and kojic acid by Franz cell components 132

3.3.10 Franz cell set-up 132

3.3.11 Post Franz cell skin tissue preparation 133

3.3.13 3D OrbiSIMS imaging analysis 134

3.4 Result and discussion 135

3.4.1 Chemical synthesis 135

3.4.2 Mushroom TYR inhibitory activity of tested compounds 136

3.4.3 TYR inhibitory activity of 11c and 11m in murine cell line B16F10 140

3.4.4 TYR inhibitory activity of 11c and 11m in human cells A375 142

3.4.5 In vitro skin permeation efficiency of compound 11c by Franz cell component 145

3.4.6 Visualization of compound 11c within the skin by OrbiSIMS 147

3.4 Conclusion 151

Chapter 4. Implications of tyrosinase modulators for malate-aspartate shuttle and fatty acid metabolism in melanoma cells A375 revealed by metabolomics and lipidomics 153

4.1 Abstract 154

4.2 Introduction 155
4.3 Methods 159
4.3.1 Bioevaluation of 11c and 11m on human cell line A375 159
4.3.2 Cell sample preparation for LC-MS 161
4.3.3 LC-MS analysis 162
4.3.4 Cell sample preparation for OrbiSIMS 163
4.3.5 OrbiSIMS experimental methods 163
4.3.6 Identification and annotation of metabolites 164
4.3.7 Pathway and enrichment analysis 165
4.4 Results and Discussion 165
4.4.1 Compounds 11c and 11m have negligible cytotoxicity in cell A375 165
4.4.2 Compounds 11c and 11m inhibit tyrosinase activity and reduce melanin content in cell A375. 166
4.4.3 LC-MS Metabolic profiles of melanoma cell A375 treated with L-DOPA only, or along with Alpha-Arbutin, 11c, and 11m. 168
4.4.4 Tyrosinase modulators significantly perturb phenylalanine, tyrosine and tryptophan biosynthesis and Malate-Aspartate Shuttle 174
4.4.5 OrbiSIMS lipid metabolic profiles of melanoma cell A375 in the presence of L-DOPA only, or with Alpha-Arbutin, 11c and 11m. 180
4.4.6 Tyrosinase modulators significantly perturb the fatty acid metabolism 185
4.5 Conclusion 187

Chapter 5. General conclusions, future work and perspectives 189

5.1 General conclusion 189

5.2 Future work and perspectives 194

Chapter 6. References 197

Chapter 7. Appendices 271

List of Figures

Figure 1-1 Factors that regulate melanogenesis within melanocytes. 28

Figure 1-2 Tyrosine metabolism and the enzymatic action of tyrosinase. 32

Figure 1-3 Chemical structures of existing tyrosinase inhibitors. 36

Figure 1-4 Chemical structure of Chalcone related derivatives. 40

Figure 1-5 The structure of skin. 43

Figure 1-6 The epidermis of thick skin with the designations of different layers. 44

Figure 1-7 Schematic diagram of the 'bricks and mortar' structure and functional composition of the stratum corneum. 46

Figure 1-8 Illustration of nanoparticle skin penetration pathways. 49

Figure 1-9 Schematic diagram of the microneedle patch and other common injection routes into human skin. 53

Figure 1-10 4 types of MNP and their route of administration. 55

Figure 1-11 Schematic illustration of the static Franz diffusion cell. 75

Figure 2-1 Photograph, Optical microscopy and scanning electron microscope images of Alpha-Arbutin-loaded PVPVA microneedle. 102

Figure 2-2 Calibration curves for Arbutin and Alpha-Arbutin. 103

Figure 2-3 HPLC analysis of mean percentage of permeation.____ 107

Figure 2-4 HPLC analysis of mean percentage of Alpha-Arbutin remaining within skin after a 24-hours permeation test._____ 111

Figure 2-5 HE-stained cross-section of DMNs dosed porcine dermatomed skin (4 mm thick)._____ 112

Figure 2-6 Negative polarity ion images of 3D OrbiSIMS from various fragment ions of the skin cross-section dosed by DMNs and CMNs._____ 114

Figure 2-7 Images of 3D OrbiSIMS from various fragment ions overlay._____ 116

Figure 3-1 . Catalytic cycle of TYR._____ 123

Figure 3-2 . Structures of commercially available TYR inhibitors.__ 124

Figure 3-3 . Design strategy of novel dihydrochalcone hybrids as TYR inhibitors._____ 125

Figure 3-4 The synthesis and structure of compounds 11c and 11m.__ _____ 136

Figure 3-5 Summary of the structure-activity relationship of dihydrochalcone TYR inhibitors._____139

Figure 3-6 . Evaluation in murine cell line B16F10._____142

Figure 3-7 . Evaluation in human A375 cells._____144

Figure 3-8 . HPLC analysis of the mean percentage of permeation of

11c in different Franz cell components._____147

Figure 3-9 . HE-stained cross-section and 3D OrbiSIMS imaging of dermatomed porcine skin (4 mm thick) dosed with 11c at 2 mg/mL._____ 149

Figure 3-10 . Overlay images of 3D OrbiSIMS from various fragment ions of the skin cross section dosed by 2 mg/mL of 11c in dermatomed porcine skin (4 mm thickness)._____ 151

Figure 4-1 Cytotoxicity, melanin content and tyrosinase activity of 11c, 11m, and Alpha-Arbutin in cell A375._____ 168

Figure 4-2 LC-MS Metabolic profiles of melanoma cell A375 treated with L-DOPA only, or along with Alpha-Arbutin, 11c and 11m(1). _____ 170

Figure 4-3 LC-MS Metabolic profiles of melanoma cell A375 treated with L-DOPA only, or along with Alpha-Arbutin, 11c and 11m(2).__ _____ 172

Figure 4-4 The relative normalized intensity of significantly identified lipid metabolites detected from LC-MS. _____ 173

Figure 4-5 The pathway enrichment analysis of the control and 5 μM L-DOPA group in A375 cells. _____ 175

Figure 4-6 The pathway network mapping._____ 179

Figure 4-7 OrbiSIMS Metabolic profiles of melanoma cell A375 treated with L-DOPA only, or along with Alpha-Arbutin, 11c and

11m.. 183

Figure 4-8 The relative normalized intensity of significantly identified lipid metabolites detected from OrbiSIMS. 184

List of Tables

Table 1-1 Lipid categories of the comprehensive classification system and the number of structures in the LIPID MAPS database. 67

Table 1-2 Abbreviations and examples of glycerophospholipid main classes. 69

Table 3-1 Inhibitory activity of tested compounds on TYR. 138

Table 3-2 The Log P and pK_a value of tested compounds on TYR 139

Table 4-1 Cytotoxicity of 11c, 11m, and Alpha-Arbutin in cell A375 in 48h 168

Table 4-2 Inhibition of Tyrosinase and Melanin of by 11c, 11m, and Alpha-Arbutin in cell A375 in 48h 168

Table 4-3 The classification of annotated lipid metabolites detected by OrbiSIMS. 184

List of Abbreviations

3D OrbiSIMS	Three dimensional Orbitrap Secondary Ion Mass Spectrometry
AA	Ordinary® Ascorbic Acid 8% + Alpha-Arbutin 2%
ATP	Adenosine triphosphate
BCC	Basal cell carcinoma
CMM	Cutaneous malignant melanoma
CMNs	Commercial Microneedle
CP	Carbopol Polymer
CT	Chamber temperature
DMNs	Dissolving microneedle
DO	Dopa oxidation
DPPH	2,2-diphenyl-1-picrylhydrazyl
DTS	Dermal therapy system
EB	Epidermis basal layer
ER	Endoplasmic reticulum
FA	Fatty acids
FASN	Fatty acid synthase
FATP2	Fatty Acid Transport Protein 2
GCIB	Gas cluster ion beam
HA	Ordinary® Alpha- Arbutin 2% + Hyaluronic Acid
HPLC	High Performance Liquid Chromatography
INK	The INKEY® List 2% Alpha-Arbutin Serum
LC-MS	Liquid chromatography - mass spectrometry

L-DOPA	Dihydroxyphenylalanine
MALDI	Matrix-assisted laser desorption ionisation
MAS	Malate-aspartate shuttle
MC1R	Melanocortin-1 receptor
MITF	Melanocyte inducing transcription factor
MNs	Microneedles
MTT	3-(4,5-dimethylthiazol-2-yl)-2,5-diphenyltetrazolium bromide
OT	Object temperature
PCA	Principal component analysis
PD	Parkinson's disease
PDMS	Polydimethylsiloxane
PE	Glycerophosphoethanolamines,
PG	Propylene glycol
PLS-DA	Partial least squares-discriminant analysis
ROS	Reactive oxygen species
SC	Stratum corneum
SCC	Squamous cell carcinoma
SM	Sphingomyelins
TCA	Tricarboxylic acid
TG	Triglycerides
TH	Tyrosine hydroxylase
TYR	Tyrosinase
TYRP-1	Tyrosine-related protein 1

TYRP-2	Tyrosine-related protein 2
UVR	Ultraviolet radiation
α-KG	Alpha-ketoglutarate
α-MSH	α-Melanocyte stimulating hormone

Chapter 1. General Introduction

In this introductory chapter, I will discuss skin disorders associated with abnormal melanin deposition and their common treatment modalities. Among these treatment modalities, tyrosinase inhibitors have been widely reported as effective anti-melanogenic agents[1,2]. This article will briefly review the characteristics of existing tyrosinase inhibitors and the limitations of current treatment options for hyperpigmentation. It will also provide theoretical support for research into the development of more effective tyrosinase inhibitors and further study of their mechanisms as well as metabolic pathways. Furthermore, this study will not only explore the intracellular action and mechanism of tyrosinase at the biological level, but it will also focus on the intradermal drug delivery capability of tyrosinase inhibitors. This chapter will then describe the anatomical structure and function of the skin, as well as the routes of drug delivery. In addition, this chapter will review different ways of enhancing intradermal drug delivery, where microneedles are used as a viable drug delivery strategy to aid in treating disease. Different microneedle types and applications will also be covered here. Lastly, different applications of various experimental methods are presented in this article, including LC-MS and OrbiSIMS.

There is now considerable evidence showing how skin disorders can lead to psychological problems and a poor quality of life. Skin lightening and skin cancer have been in the spotlight for decades[3,4]. In Asia, a large

market exists for skin lightening. Most women seek to make their skin whiter and brighter in various ways, mostly for aesthetic purposes[5]. In addition, the incidence of skin cancer has been high in both Europe and the United States[6]. Excessive UV exposure and melanin accumulation can cause severe damage to the skin and significantly increase the risk of skin cancer[7]. Studies on melanin suppression would be effective in improving both of these skin problems. Therefore, there is a need for more in-depth research into existing as well as newly synthesised tyrosinase inhibitors.

1.1 Skin pigmentation disorders

In humans, changes in skin colour occur at the functional level of epidermal melanin[8,9]. Essentially, this system is related to the density of melanocytes; the number, size, and distribution of melanin vesicles transferred to epidermal keratin-forming cells; the properties and degradation rate of the melanin, and its degradation rate[10]. In turn, the regulation of pigmentation involves many factors required for the development, heterogeneity, regeneration, and ageing of melanocytes and their precursor cells[11]. This can determine the structure of melanosomes, melanin synthesis, transport and distribution of melanosomes, and the melanocyte-specific transcription factors that control the expression and function of all these genes[12]. Also, the mutations of several of these genes are now known to be associated with human pigmentary disorders[13], which include hyperpigmentation and hypopigmentation.

1.1.1 Hyperpigmentation

Skin hyperpigmentation arises from three distinct processes: (i) biogenesis and transport of melanin within melanocytes; (ii) transfer of melanin from melanocytes to keratinocytes; and (iii) internalisation and processing of melanin by keratinocytes. Within keratinocytes, melanin accumulates in the supranuclear region and protects nuclear genetic material from UV-induced damage[9,14]. The relationship between skin pigmentation and photoprotection still remains uncertain, but we do know that excessive melanin accumulation can also lead to many skin problems[15–18].

Hyperpigmentation disorders can be classified as congenital hyperpigmentation disorders or as acquired hyperpigmentation disorders[19,20]. Acquired hyperpigmentation disorders include age-related freckles/freckles, melasma, penile/vaginal melanosis, facial follicular red melanosis, UV-induced hyperpigmentation (tanning), post-burn hyperpigmentation (frictional melanosis and grey skin disease), and chemical/pharmaceutical-induced hyperpigmentation[21–23].

Of these, the most common are sunspots, post-inflammatory hyperpigmentation, and melasma[24,25]. Sunspots, also known as liver spots, are associated with prolonged exposure to the sun. Generally, they appear in areas exposed to the sun, such as the hands and face. Post-inflammatory hyperpigmentation is the result of skin damage or inflammation. Common causes may be due to acne or reactions to certain

drugs[26].

Melasma, also known as chloasma, is a discrete, localised, and non-inflammatory hyperpigmentation disorder that often occurs on the eyes, mouth, cheeks, and forehead[27]. The leading patient group is middle-aged women. As an acquired facial pigmentation disorder, melasma is thought to be caused by hormonal changes - specifically, the elevation of serum progesterone levels[26, 28]. Pathological studies have found melasma to be associated with increased melanin deposition within the epidermis, particularly in the supranuclear region of the basal cells[29]. In contrast, melasma does not cause an increase in melanocytes within the epidermis. Thus, the pigmentation in melasma is functional and reversible. Because of the slow onset of hyperpigmentation, long-term treatment can prevent hyperpigmentation in melasma[30,31].

Bioinformatics analysis studies of melasma have showed that melanin and melanogenesis-related proteins were significantly more highly expressed in the lesioned epidermis, as were mRNA levels of tyrosinase-related protein I, suggesting a regulatory role at the mRNA level[32]. In contrast, the expression of melasma-related genes, including Wnt and other genes related to lipid metabolism, was significantly downregulated in the presence of impaired barrier function due to melasma[32]. Interestingly, however, a subset of Wnt signalling regulators, including Wnt blocker I, secretory frizzled-associated protein II, and Wnt5a, were found to be more highly expressed in melasma lesions[33–35].

This abnormal amount of melanin can become an aesthetic problem[36]. In Western countries, a large patient population uses skin lighteners to prevent and treat this type of irregular pigmentation. In summary, there is a large potential market and good prospects for further exploration of the mechanisms of hyperpigmentation and the development of new agents for its treatment.

1.1.2 Hypopigmentation

Hypopigmentation is the loss of skin colour due to a decrease in the amount of melanin, such as vitiligo and albinism[37,38]. Disruptions in the function of many factors associated with hyperpigmentation, such as GABRB3, are thought to be the cause of hypopigmented disorders. Delahanty et al[39] suggest that deletion of GABRB3 results in almost total loss of retinal pigment. Although mostly benign, acquired hypopigmentation can have significant cosmetic, psychological, economic, and social impacts. For example, vitiligo can lead to smooth skin with white patches, which can cause aforementioned impacts for the individual. In some people, these patches can appear all over the body. It is an autoimmune disease where the cells that produce pigment are damaged. At the current time of writing, there is no cure for vitiligo[40].

1.2 Melanocytes

Pigmentation disorders of the human skin are usually caused by abnormal lesions of melanocytes or melanosomes, resulting in aberrant changes in melanin[41]. This is why the structure of melanosomes and the mechanism

of melanin formation are the focus of research into these disorders.

1.2.1 Melanin and melanosomes

Melanin is a complex polymer produced by melanocytes in human skin, eyes, and hair[42]. In humans, melanin exists in three forms: eumelanin, pheomelanin, and neuromelanin[43]. The most common of these is eumelanin, which is manufactured and deposited in melanosomes. Production of melanin first occurs in the epidermis before being transferred to keratin-forming cells via their dendritic structure[44]. The amount of melanin present determines our skin colour and thus our ethnicity and phenotypic appearance. There is no significant difference in the number of melanocytes between races. The main factors affecting differences in skin colour are the proportion of melanin and the number and distribution of melanosomes in keratin-forming cells[45]. It also plays an important role in protecting our skin from UV radiation and photocarcinogenesis and in removing toxic drugs and chemicals[46]. Melanin also reduces the risk of folate intake and skin degeneration[47]. Many epidemiological studies have shown that people with darker skin are less likely to develop skin cancer compared to those with fairer skin[48]. However, excessive accumulation of melanin can lead to skin diseases such as freckles, melasma, and even melanoma and skin cancer[49]. Although the presence of melanin may prevent the development of skin cancers, including cutaneous melanoma, the presence of melanin may be necessary for the malignant transformation of melanocytes. The poor photostability of brown melanin creates a mutagenic environment upon

exposure to short-wave UV light and displays cytotoxic, genotoxic properties. This demonstrates the complex role of melanogenesis in the development of melanoma and explains the association of exposure to UV radiation with an increased risk of malignant melanoma, a cancer of melanocyte[50].

Melanosomes belong to the LRO (lysosome-associated organelle) family[51]. Their formation involves the interaction of rough endoplasmic reticulum (RER) structures with vesicles and trans-Golgi network (TGN) channels[52]. Melanosomes can be divided into four stages depending on their level of maturation[53,54]. Early melanosomes, particularly stage I melanosomes, are similar to lysosomes and are formed by the smooth membrane outgrowth of RER. In the second stage of the melanosome production pathway, a fibrillar matrix is formed. Late melanosomes contain a structurally intact matrix and a high density of melanin deposits. Further maturation is driven by the delivery and activation of structural and enzymatic proteins and the delivery of substrates. Melanosomes can therefore be defined as organelle containing tyrosinase and located in melanocytes that have a unique capacity to synthesise melanin[55].

It is generally believed that melanogenesis begins when tyrosinase and other related enzymes are cleaved and tyrosinase hydroxylates L-tyrosine to L-DOPA. Initiation of this activity requires an acidic pH[56]. Another theory suggests that tyrosine hydroxylase is involved in producing L-DOPA much earlier[57], and the initial hydroxylation reaction requires an acidic environment provided by the pre-melanosome, whose pH is

regulated by the proton pump system[58–60]. However, due to the acidification will inhibit the synthesis of melanin[60,61], once L-DOPA is present, the formation of melanin pigments requires a neutral or alkaline environment[61,62]. Therefore, the environmental conditions required for melanin synthesis needs to be further investigated.

1.2.2 Factors regulating melanogenesis within melanocytes

In addition to the influence of melanosomes and the melanogenic environment, the key elements regulating melanogenesis within melanocytes are pigment-specific factors usually located in, on, or near melanosomes. They can be divided into three types: proteins involved in the structure of melanosomes, enzymes that regulate melanin synthesis, and proteins involved in melanosome composition and melanosome transport[42], as shown in **Figure 1-1**. Transcription factors such as MITF are clearly expressed by melanocytes and melanoma cells and are able to regulate the expression and function of many pigment-specific factors[11,63–65].

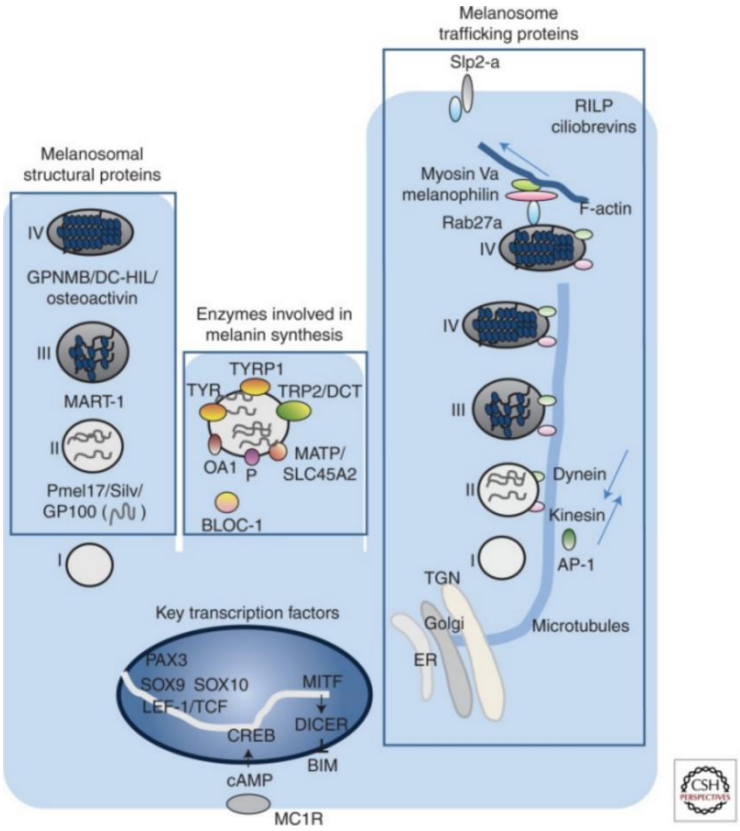


Figure 1-1 Factors that regulate melanogenesis within melanocytes. Key factors include proteins that affect melanosome structure (Pmel17, MART-1 and GPNMB) and proteins that directly or indirectly regulate melanin synthesis (TYR, TYRP1, DCT, BLOC-1)[42].

One of the most well-known receptors on melanocytes that regulate their function is the melanocortin-1 receptor (MC1R)[66,67]. Activation of MC1R increases the production of cAMP and leads to phosphorylation of the transcription factor of the cAMP-response element binding protein (CREB) and its motif[68,69]. This process is illustrated at the bottom of **Figure 1-1**.

Currently, known MC1R agonists include alpha-melanocyte stimulating hormone (α-MSH) and adrenocorticotropic hormone (ACTH), the

antagonist of MC1R is Agouti signaling protein (ASP), which regulates true melanogenesis[70]. And, polymorphisms in the MC1R gene have been extensively studied, one of the most critical transcription factors regulating cellular function is the Microphtalmia Transcription Factor (MITF). Regarding MITF, the promoter is regulated by a variety of other transcription factors including PAX3, SOX9[71], and SOX10[72]. Various physiological factors from keratin-forming cells, fibroblasts, and other sources can also regulate the level and function of MITF expression[73,74].

In addition to the MC1R receptor, multiple proteins also influence melanin production in melanocytes. Three important structural proteins make up melanosomes: PMEL17/Silv/GP100, MART-1 and GPNMB[75]. These structural melanosome proteins provide the scaffolding material for the enzymes required for melanin deposition[76]. Several other proteins are also involved in melanin synthesis. In melanosomes, there are three key enzymes: TYR (tyrosinase), TYRP1 (tyrosinase-related protein-1), and TRP2/DCT (dopachrome interconversion isomerase)[77]. A number of other factors, including block-1, OA1, P, and SLC45A2 (formerly known as MATP) affect the transport of these enzymes and thus their function[78,79]. According to current research, over 150 genes are involved in the production and regulation of melanin. Melanin biosynthesis is controlled by multiple extracellular signaling pathways[80].

Overall, melanin formation is a combination of enzymatic catalysis and chemical reactions. The biosynthetic pathway for melanin formation in various life forms was first elucidated by Raper[81] and Mason[82], but has

recently been modified[83,84]. Factors that stimulate melanogenesis include direct UV irradiation and the action of melanocyte-stimulating hormone (α-MSH) secreted by keratin-forming cells, which promotes the tyrosinase reaction to produce melanin. Tyrosinase can therefore be considered as the key enzyme responsible for the regulation of melanin and melanogenesis in the body. The regulation of tyrosinase activity is now widely used to reduce dark spots and promote skin lightening[85]. The exploration of novel tyrosinase inhibitors is a popular route to alleviate skin pigmentation problems[86].

1.2.3 Mechanism of tyrosinase involving production of melanin

The discovery of tyrosinase dates back to 1895, when Bourquelot et al.[87] found that instead of turning blue as previously observed, the mushrooms *Russula Foetens* and *Rhizopus Nigricans* turned red and then dark brown during oxidation. Tyrosine was later isolated from *Aspergillus niger* and was shown to be a precursor of melanin[88]. After that, tyrosinase, a new enzyme that oxidises tyrosine to the corresponding quinone, was named by Bertrand et al.[89]

Tyrosinase (TYR, EC 1.14.18.1) is a copper-containing oxidoreductase and a critical rate-limiting enzyme[90]. Tyrosinase has multiple mechanistic pathways of action. For example, enzymatic inhibition of natural products by tyrosinase is often caused by the synergistic action of macromolecules and small molecules[91]. The active site of tyrosinase contains two copper ions. When exposed to UV light, these copper ions cause tyrosinase to

become more active. This means a compound could potentially block melanin production by trapping the copper ions and preventing them from activating tyrosinase[92].

Tyrosinase is involved in two main reactions: catalysing the hydroxylation of L-tyrosine to produce L-DOPA, and the oxidation of L-DOPA to produce dopaquinone[93] (**Figure 1-2**). The first stage is stimulated by copper ions which catalyse the conversion of monophenols (e.g. tyrosine) to o-diphenols (monophenolase activity), followed by the oxidation of o-diphenols to the corresponding o-quinone derivatives (biphenolase activity) to form L-DOPA[94,95]. This is followed by further oxidation of L-dopamine to produce dopamine quinone (hydroquinonase)[96]. which is then further oxidised to eumelanin and brown melanin through other related enzymatic reactions[97]. Tyrosinase thus has a unique dual catalytic function[98,99]. As tyrosinase plays a crucial role in melanin production, reducing melanin production through tyrosinase inhibition has attracted the interest of many medicinal chemists and cosmetic researchers. Currently, most cosmetic products or emollients are tyrosinase inhibitors. Since tyrosinase is produced only by melanocytes, tyrosinase inhibitors specifically inhibit intracellular melanin production without any side effects, making it an attractive strategy.

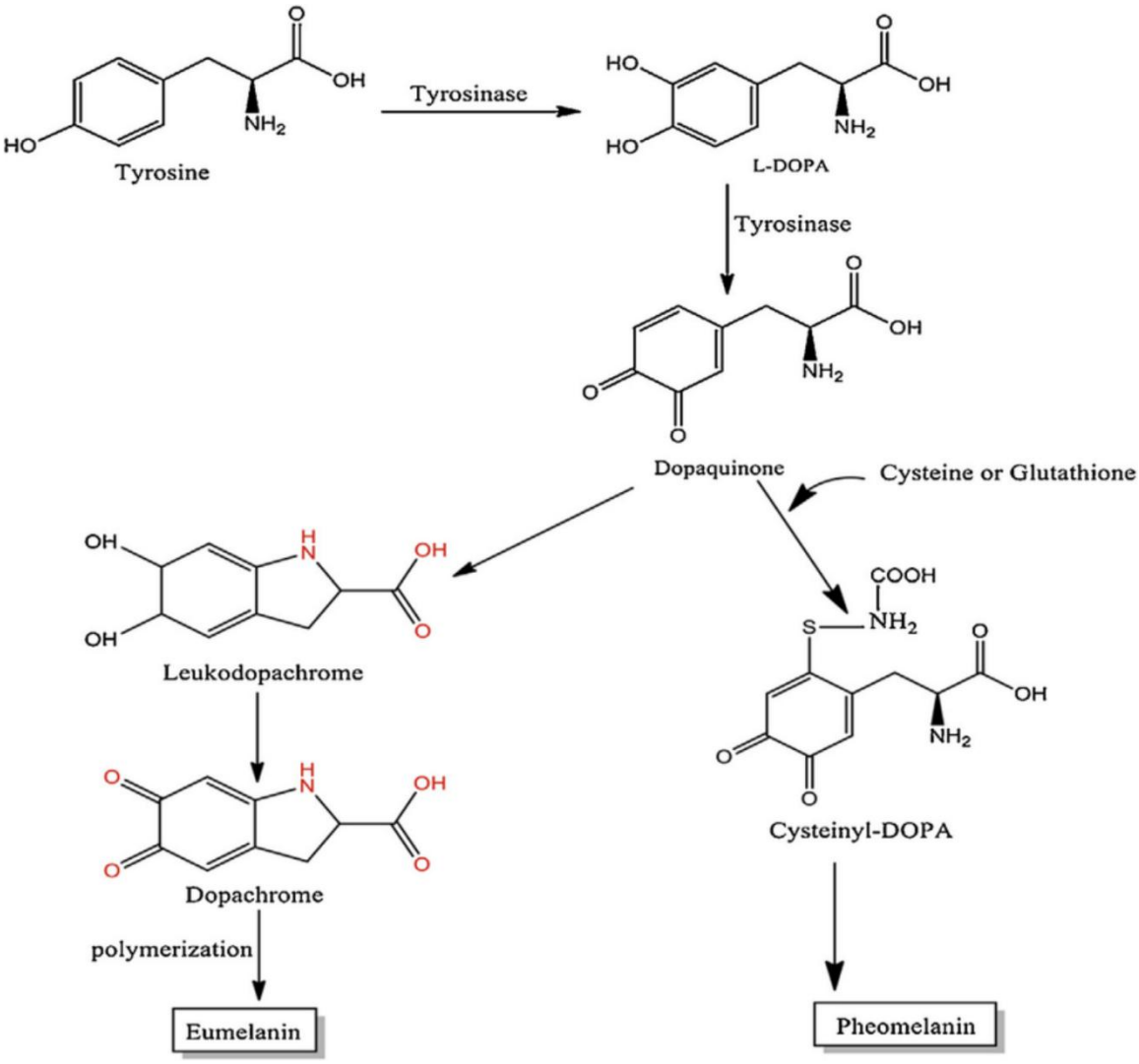


Figure 1-2 Tyrosine metabolism and the enzymatic action of tyrosinase.

1.3 Tyrosinase modulators

1.3.1 Tyrosinase stimulator - L-DOPA

L-DOPA is a precursor of melanin and is an important cofactor in tyrosinase catalysis[100]. In hamster melanoma cells, L-DOPA induces a rapid and dose-dependent increase in tyrosinase activity, with peak activity at 25 or 50 μM. It also induces moderate pigmentation and the

formation of predominantly immature melanosomes[101]. It had long been known that L-DOPA is a potent activator and substrate for human tyrosinase, but lacked sufficient theoretical support. Today, it has been shown that both the substrate L-tyrosine and the activator L-DOPA have independent binding sites on the tyrosinase enzyme[83,102,103]. Furthermore, both L-tyrosine and L-DOPA are required for the correct folding of the tyrosinase in the endoplasmic reticulum (ER), preventing it from entering the degradation pathway[104,105]. This strongly suggests that L-DOPA leads to a dramatic increase in tyrosinase activity and melanin content, accompanied by the appearance of many melanosomes.

It has been found that in melanoma cell lines, L-tyrosine and L-DOPA also each have a regulatory role in melanogenesis, in addition to their known functions as substrates and cofactors[101,106]. L-tyrosine and L-DOPA initiate the tyrosine hydroxylase (TH) and dopa oxidation (DO) cycles respectively[107,108]. Both phenolics may bind axially to the catalytic centre, but L-tyrosine binds preferentially to the CuA site, while L-DOPA binds to CuB[108,109].

L-DOPA is a direct product of L-tyrosine hydroxylation and a cofactor of TH. The Tyr affinity of L-DOPA as a TH cofactor is approximately 100-fold higher than that of L-DOPA as a DO substrate, suggesting that L-DOPA may bind to both sites of the enzyme[110]. However, it is also the dual role of L-DOPA as a substrate for DO activity and a cofactor for TH activity that complicates the understanding of the mechanism of the Tyr response[111]. Furthermore, in human melanoma, increased MSH binding is

observed within hours after exposure to L-tyrosine or L-DOPA[112]. α-MSH binds to the melanocortin-1 receptor (MC1R) on the cell surface and activates adenylate cyclase, leading to the upregulation of the cAMP/PKA signaling pathway and the induction of MITF expression[68,113–115]. This suggests that L-DOPA acts as a positive regulator of melanogenesis by stimulating MSH receptor activity.

It has also been suggested that L-DOPA at micromolar or lower concentrations stimulates cell proliferation[116,117]. Current literature[104,118,119] suggests that L-DOPA could also regulate cellular function and cellular metabolism through non-receptor-mediated processes that act directly or through melanogenic intermediates produced by its non-enzymatic or enzymatic oxidation. Therefore, further studies are required on the metabolic pathways and mechanisms of action of levodopa in melanoma cells.

1.3.2 Advances of research in tyrosinase inhibitors

There are four categories of tyrosinase inhibitors: competitive, non-competitive, mixed (competitive/non-competitive), and uncompetitive inhibitors[120,121]. Competitive inhibitors may be inhibitors that prevent substrate binding by binding to free tyrosinase, such as copper ion chelators, substrate analogues of tyrosinase, or derivatives of L-tyrosine or L-DOPA. In contrast, non-competitive inhibitors bind only to tyrosine complexes.

Over the past few decades, medical and cosmetic industries have been

investigating the treatment of skin diseases. Numerous studies have shown that compounds derived and isolated from a variety of natural sources and compounds have strong antioxidant and skin lightening properties[122]. Tyrosinase inhibitors have now become important ingredients in medical cosmetic products for depigmentation.

Although synthetic tyrosinase inhibitors have been widely reported at this stage, only a few have been used for commercial purposes, such as resorcinol, arbutin[123] and kojic acid[92,124]. Among this, resorcinol is banned mainly because of its high cytotoxicity, arbutin and kojic acid is limited by the insufficient permeability, low activity, or poor stability[125]. Vitamin C and its derivatives can also be used as whitening agents. However, the level of tyrosinase inhibitory activity in these compounds is still not high enough for widespread use. The tyrosinase inhibitors commonly used in the market today, such as tretinoin and cysteine, have good inhibitory capacity. However, studies have found that they may produce undesirable side effects such as dermatitis, skin irritation, and even skin cancer[126]. Traditional skin lightening products such as hydroquinone[127], corticosteroids, and mercury-containing products have been banned. These compounds have been found to be potentially mitogenic, making them genotoxic to melanocytes[128]. Therefore, there is a need to develop natural whitening products that do not contain harmful side effects. The chemical structures of existing tyrosinase inhibitors are shown in **Figure 1-3**.

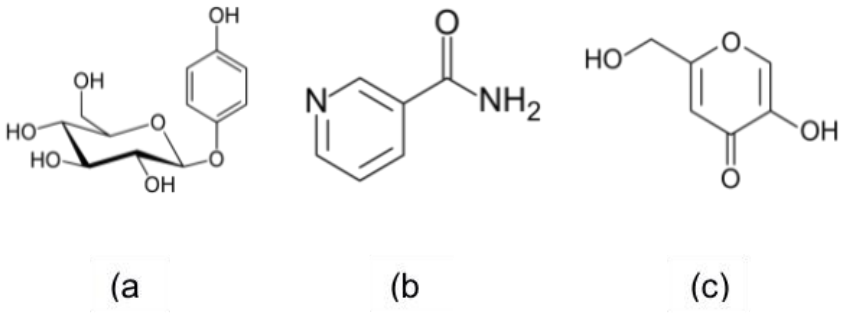


Figure 1-3 Chemical structures of existing tyrosinase inhibitors. (a) Arbutin (b) Nicotinamide (c) Kojic acid.

As tyrosinase plays a key role in mammalian melanin production, tyrosinase inhibitors have been a hot topic of research in this field. However, regarding the study of commercial tyrosinase inhibitors at this stage, the choice of research target is an issue. All these compounds have certain defects in their physicochemical properties, among which arbutin is the most lipophilic and has difficulty in crossing the stratum corneum to the inner skin. For this reason, arbutin is considered to be of high research interest. Moreover, due to the limitations of the experimental method, only arbutin could be detected among these three compounds as shown by the Orbi-SIMS. Therefore, the choice of arbutin as a research target is feasible and has sufficient scientific implications.

1.3.2.1 Naturally derived tyrosinase inhibitors

Naturally derived tyrosinase inhibitors are mainly of animal, plant, and microbial origin[129]. Chai et al[130] extracted and isolated proanthocyanidins from avocados, and found that proanthocyanidins are reversible competitive tyrosinase inhibitors as well as that the neighbouring hydroxyl

group on the B-ring can integrate with the copper ion at the active centre of the enzyme. Xiong et al.[131] found that apigenin is a mixed tyrosinase inhibitor that can be inserted into the hydrophobic lumen of the enzyme and interact with a number of amino acid residues. Passi et al[132] isolated C9 and C11 dicarboxylic acids from cereal spore cultures and found them to be competitive tyrosinase inhibitors with tyrosinase inhibitory capacity[133].

1.3.2.1.1 Arbutin

Arbutin, also known as 4-hydroxyphenyl-β-d-glucopyranoside, is a naturally occurring phenolic component found in various plants such as rockweed, bearberry, lingonberry, and pear[134]. Arbutin is a safe and mild competitive inhibitor of melanogenesis with negligible toxicity to melanocytes and other skin cells[135]. Instead, it inhibits the tyrosinase activity of melanosomes rather than inhibiting the synthesis and expression of melanocyte tyrosinase[136]. In addition, arbutin inhibits melanogenesis in melanocytes co-cultured with keratin-forming cells more effectively than in melanocyte cultures alone[137]. As a result, arbutin is widely used in both the cosmetic and medical fields[123].

1.3.2.1.2 Isomers of arbutin and Alpha-Arbutin

One of the isomers of natural arbutin is Alpha-Arbutin (4-hydroxyphenyl-α-d-glucopyranoside, α-arbutin), which is produced by the glycosidic bond as an Alpha - isomer[138]. In 2003, researchers found that Alpha-Arbutin inhibited melanogenesis by directly inhibiting tyrosinase activity [139]. So far,

the results of skin lightening agents screened using human tyrosinase suggest that Alpha-Arbutin is a more effective lightening agent than arbutin[140]. One researcher studied the effects of Alpha- and Beta-Arbutin on tyrosinase activity in mushrooms and mouse melanomas and found that Beta-Arbutin was able to inhibit their tyrosinase activity. In contrast, Alpha-Arbutin only inhibited tyrosinase in mouse melanoma with an IC_{50} of 0.48 mM, with a mixed mechanism of inhibition. However, its effect was 10 times greater than that of Beta -arbutin[141]. As a result, Alpha-Arbutin has become one of the most widely used skin lightening agents.

1.3.2.1.3 Physicochemical properties of arbutin

The chemical formula of arbutin is $C_{12}H_{16}O_7$ with a specific spin value of -64.00 ± 1.00. It appears as a white powder that is soluble in hot water, slightly soluble in cold water, and soluble in organic solvents such as methanol[142]. Arbutin should be kept in a tightly closed environment, avoiding contact with oxides. It is easily hydrolysed under acidic conditions. This is due to the presence of several hydroxyl groups in the Alpha-Arbutin molecule that can form hydrogen bonds with water molecules, making it highly hydrophilic with a log P value of -1.49[143]. It makes Alpha-Arbutin difficult to cross the epidermis of the skin to reach the melanocyte site for action, as the stratum corneum is more resistant to hydrophilic substances[144]. However, due to the advantages of Alpha-Arbutin over other harmful skin lightening agents, there is a need to investigate the development of multiple dosage forms or transdermal delivery systems to improve the bioavailability of arbutin, such as through

microneedles, nanosystems, microsystems, and lipid systems[143,145].

1.3.2.2 Synthetic tyrosinase inhibitors

Many scholars have studied the inhibition mechanism of tyrosinase inhibitors and have synthesised a series of effective inhibitors. Xing et al.[146] synthesised and characterised $Na_7PMo_{11}CuO_{40}$. Their experimental results showed that this compound was a reversible competitive inhibitor that could effectively inhibit tyrosinase activity with an IC_{50} of 4.8×10^{-4} mol/L. Yi et al.[147] also synthesised some salicylic acid analogues based on salicylic acid and investigated their inhibition of tyrosinase activity, finding that a 4, 6 -O- phenethyl on the glycosyl group could be a potential tyrosinase inhibitor with an IC_{50} of 5.2×10^{-5} mol/L.

These studies have led to the synthesis of novel tyrosinase inhibitors using natural products as lead compounds. Common lead compounds with specific backbone structures include flavonoids or polyphenols.

1.3.2.2.1 Chalcones and flavonoid inhibitors

Chalcone is an important substrate for the biosynthesis of flavonoids and can be converted to flavonoids in plants by the action of chalcone isomerase[148]. Chalcones are widely distributed in the flowers, leaves, bark, and roots of plants and play an important role in a variety of phytopharmaceuticals commonly used in Asia, Europe, Africa, and South America[149,150]. Chalcones have a flexible backbone structure that allows them to bind to a wide range of receptors. In addition, they have a wide

range of biological activities: anti-cancer[151,152], antioxidant[153], antibacterial[154], antimalarial[155], and anti-inflammatory[156]. The use of chalcones in clinical practice has become a major research topic. Nowadays, various drugs used clinically, such as Metochalcone for gallbladder diseases and Sofalcone for gastric ulcers, are available[157]. Their structures are shown in **Figure 1-4**. Chalcone compounds show considerable promise and have received widespread attention. In recent years, research into their biological activity has been very active.

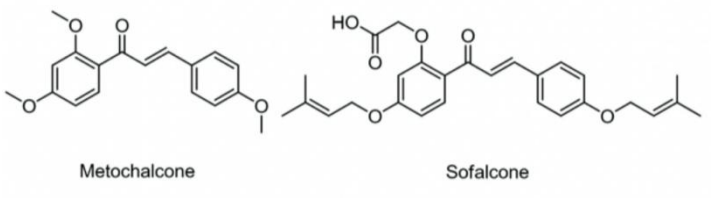


Figure 1-4 Chemical structure of Chalcone related derivatives.

However, little research has been reported on the ability of chalcones to activate tyrosinase activity. Nishida et al.[158] synthesised a series of hydroxychalcone analogues and selected four compounds that showed strong inhibition of tyrosinase activity, with the best inhibition at an IC_{50} concentration of only 1 μmol/L. Nixha et al.[159] synthesised chalcone analogues from carbazole and modified them to obtain several new compounds with tyrosinase activating activity. Sonmez et al.[160] obtained a series of tyrosinase activating chalcone derivatives by introducing different substituted phenylureas and phenylthioureas into the a-ring of chalcone.

Such preliminary studies demonstrate the feasibility of novel tyrosinase inhibitors using chalcone as a backbone. In order to develop safer and more effective tyrosinase inhibitors, other preliminary studies have been carried out on dihydrochalone and its homologues in the flavonoid family. Dihydrochalone is a non-planar water-soluble molecule containing a 1,3-diphenylacetone structure and is considered to be a "minority flavonoid" naturally occurring in plants[161–163]. It is an important, safe, and biodiverse natural compound with hypoglycaemic, hepatoprotective, antioxidant, antitumour, whitening, memory improvement, blood pressure regulation, analgesic, anti-inflammatory, and antibacterial properties[164,165]. It is also commonly used in food additives. Therefore, synthesising dihydrochalcone as a backbone and introducing other active groups to produce tyrosinase inhibitors with better activity and safety is worthy of being tried and studied.

1.3.2.3 Limitations of tyrosinase inhibitors

Despite the large number of in vitro tyrosinase inhibitors available, only a few have been able to produce results in clinical trials[166,167]. This is due to the rate-limiting step of tyrosinase catalysis during pigmentation. The gap between in vitro and in vivo studies suggests that other innovative strategies are needed to validate their efficacy and safety. Besides the drug’s tyrosinase inhibition ability, other parameters related to the cytotoxicity, solubility, skin absorption, permeability, and stability of the drug should also be considered. Screening test systems are also crucial as keratin-forming cells play a positive regulatory role in melanogenesis

within melanocytes[168]. Therefore, the use of animal skin, keratin-forming cells co-cultured with melanocytes, or 3D skin should be considered for mammalian skin models. If only melanocytes or soluble tyrosinase are used, the reliability of the data is not strong enough.

1.4 Skin penetration

Skin penetration for intradermal or transdermal drug delivery is a limiting factor for success. One of the main issues in achieving effective depigmentation is the choice of the intradermal delivery system and drug formulation, as we need to ensure that useful drug concentrations will reach the melanocyte[166]. Poor bioavailability and penetration into melanosomes are the main reasons why many potential inhibitors of melanin synthesis have failed in *in vitro* and *in vivo* trials[169].

1.4.1 Skin structure and function

The human skin is a highly complex multilayered structure and is the largest organ of the body, accounting for approximately 16% of body mass and an average area of 2 m^2 in a typical adult[170]. The main function of the skin is to act as a barrier between the body and the external environment[171]. This barrier prevents the entry of chemicals, microorganisms, and UV radiation, and the loss of water and body fluids[172]. In addition, the skin regulates body temperature and acts as a sensory organ. The human skin can be divided into three layers: the

epidermis, the dermis, and the subcutaneous fat layer[173], as shown in **Figure 1-5**. The basal layer in the epidermis and is the target region for drug administration.

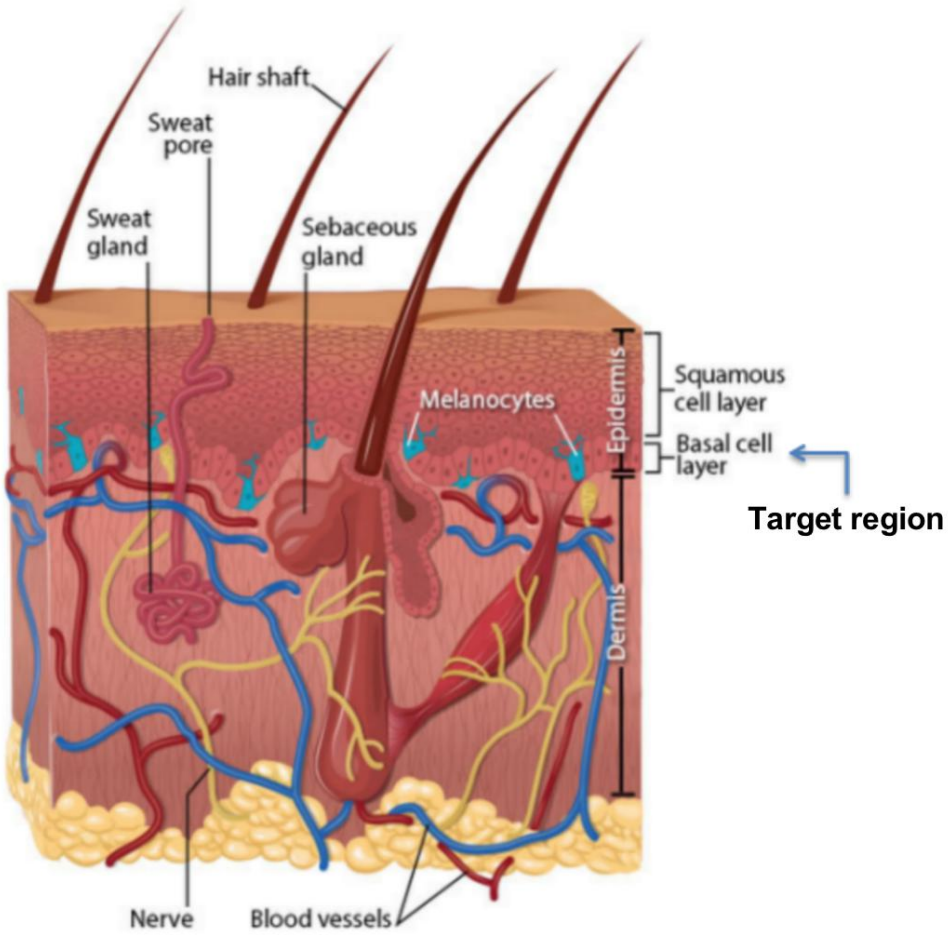


Figure 1-5 The structure of skin[174].

1.4.1.1 The epidermis

The epidermis is the outermost layer of the skin and protects the rest of the body from the environment. The thickness of the epidermis varies depending on the area of the body; the eyelids are only 0.05 mm thick,

while the palms of the hands and soles of the feet are 1.5 mm thick. The epidermis contains melanocytes (melanoma-forming cells), Langerhans cells (involved in the skin's immune system), Merkel cells, and sensory nerves[175,176]. It consists of a stratum corneum, a hyaline layer (stratum lucidum), a granular layer, a spinous layer, and a basal layer, which has no blood vessels but contains free nerve endings[177]. The melanocytes are located in the basal lamina. This is illustrated in **Figure 1-6**.

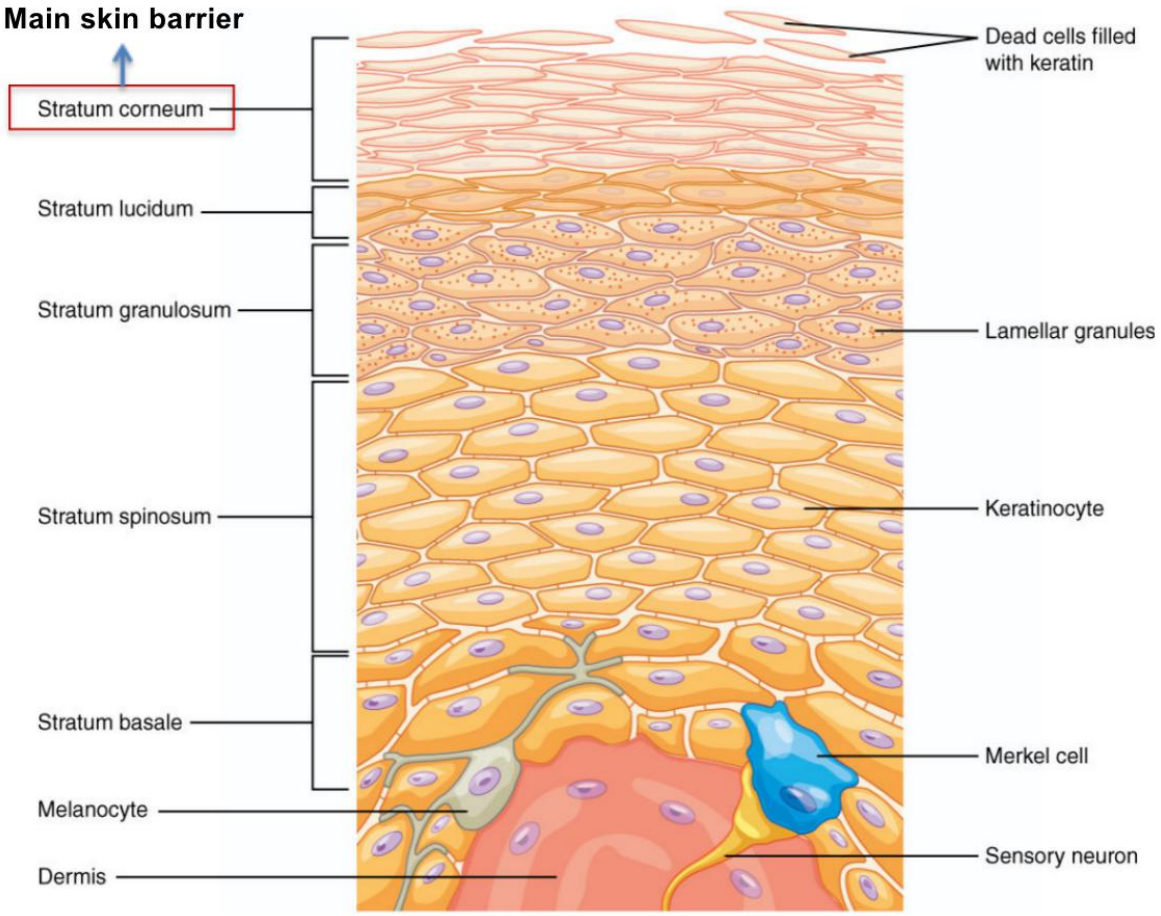


Figure 1-6 The epidermis of thick skin with the designations of different layers[178].

The human epidermis is a complex squamous epithelium that is constantly renewing itself. Its innermost basal cells are a population of stem cells which have the ability to proliferate and divide. Once their dividing progeny leave the basal layer and migrate upwards, they begin the terminal differentiation process, forming the characteristic morphological layers of the spindle, granule, and stratum corneum[179].

1.4.1.2. The stratum corneum

The epidermis is mainly composed of keratinocyte (95%), which form the initial basis of the 'bricks and mortar' structure[180] (with the exception of trace components such as pigment cells, Ranges cells, and Merkel cells) (**Figure 1-7**). Keratinocyte expand and give rise to daughter cells which eventually differentiate to form the stratum corneum (SC), consisting of 10 - 25 layers of dead cells (corneocytes). The corneocytes act as "bricks" embedded in a "mortar" consisting of various lipid bilayers such as ceramide, fatty acids, cholesterol, and cholesteryl esters, also known as the intercellular platelet lipid membrane. This creates the structural basis of the epidermal permeability barrier[181], where the intercellular platelet lipid membrane forms the functional part of the skin barrier[182]. The epidermal barrier function usually prevents excess water from entering or leaving the body[183].

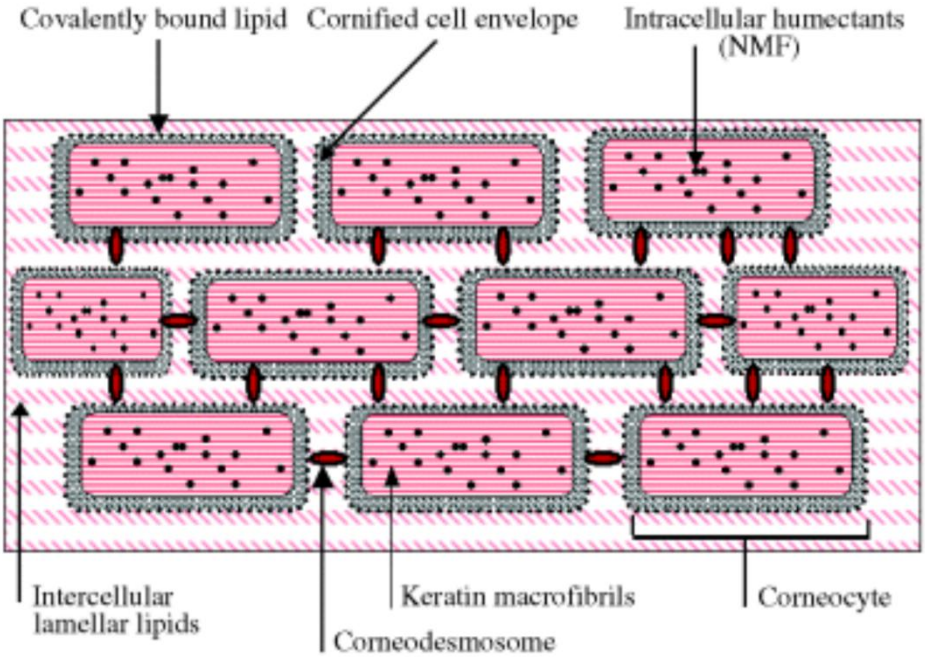


Figure 1-7 Schematic diagram of the 'bricks and mortar' structure and functional composition of the stratum corneum[184].

The stratum corneum can be removed by the classic tape peeling method. The cuticle is selectively and completely transferred to the tape by pressing the tape onto the skin and then abruptly removing it. This process is repeated 10-20 times. This way, active skin can be obtained for experiments or used to determine drug concentrations in the stratum corneum and the rest of the skin respectively[185].

1.4.1.3. The basal cell layer

The basal layer is the innermost layer of the epidermis and contains small round cells called basal laminae. The cells of the basal layer are constantly dividing, with new cells pushing older cells to the surface of the skin and eventually shedding them. The basal cell layer is also known as

the germ layer because it is constantly producing new cells[186].

The basal cell layer contains melanocytes. Melanocytes produce a skin pigment called melanin, which gives the skin its tan colour and helps protect the deeper layers of the skin from the harmful effects of the sun[187]. Sunlight exposure causes melanocytes to increase melanin production to protect the skin from UV rays which can cause sunburn. Melanin spots on the skin can lead to birthmarks, freckles, and age spots.

1.4.2 The route of skin administration

Skin administration can be divided into topical, intradermal, and transdermal drug delivery[188]. When the intended site of action is superficial to the skin, the drug delivery system is considered to be topical[189]. When the intended target site of action is deep in the skin, such as within the dermis, the drug delivery system is considered intradermal[190–192]. Lastly, when the drug passes through the skin and enters the systemic circulation, the drug delivery system is considered transdermal[193,194]. In the last 20 years, transdermal and intradermal drug delivery systems have increased in their usage. These systems have various advantages over oral administration and are a novel painless route of drug delivery, thanks in large part to their non-invasive nature[193,195]. The risk of oral or injectable drug overdose is reduced while early metabolism of the drug in the liver can be avoided. These systems are also able to produce controlled drug delivery and sustained release, resulting in satisfactory efficacy[196,197].

Unfortunately, the protective function of human skin imposes physicochemical limitations on the type of penetrant that can cross the barrier[198]. For passive drug delivery through the skin, adequate lipophilicity with a logarithmic partition coefficient preferably between 1-3.5, low molecular weight <500 Da, and reasonable water solubility >100 µg/mL is required in order to penetrate the barrier[199,200]. These requirements limit the number of commercially available products that are based on transdermal or dermal delivery[201].

The SC is a key factor in regulating the passage of drugs through the tissue[200,202]. This uppermost layer of the skin consists of keratinocytes embedded in a lipid-rich matrix and is approximately 10-15 µm thick. However, most active pharmaceutical ingredients (APIs) are quite hydrophilic, electrically charged, or of large molecular size, making them far from ideal for skin penetration[203]. Recent developments in intra-/transdermal drug delivery have therefore raised the need for strategies to overcome the function of the SC barrier to facilitate rapid and effective penetration of a wider range of molecules, including large molecule therapeutics and genetic material[204,205].

1.4.2.1 Pathways across the stratum corneum

At this stage, three routes of crossing the SC are currently being employed[206–208](**Figure 1-8**). The first consists of crossing the SC and epidermis using different hair follicles to reach the dermis directly, also known as the appendageal route[209]. The other two routes involve crossing

the SC then passing through the keratinocytes (intracellular route) or passing between keratinocytes through lipid cements (intercellular route). Of these, the intracellular route is more polar due to the keratin-containing cells of the stratum corneum. And due to the lipid cements, intercellular route is thus considered to be the main route for transdermal drug delivery[210,211]. Water-soluble drugs readily enter the intracellular route and lipid-soluble drugs mainly pass through the intercellular route[212–214]. It is noteworthy that the penetration of external molecules into the skin occurs simultaneously through these three parallel permeation pathways. However, their relative contribution may depend to a large extent on the physicochemical properties of the drug. Knowing that it is usually not possible to select their properties according to the intended application, it is necessary to develop strategies that facilitate skin transport.

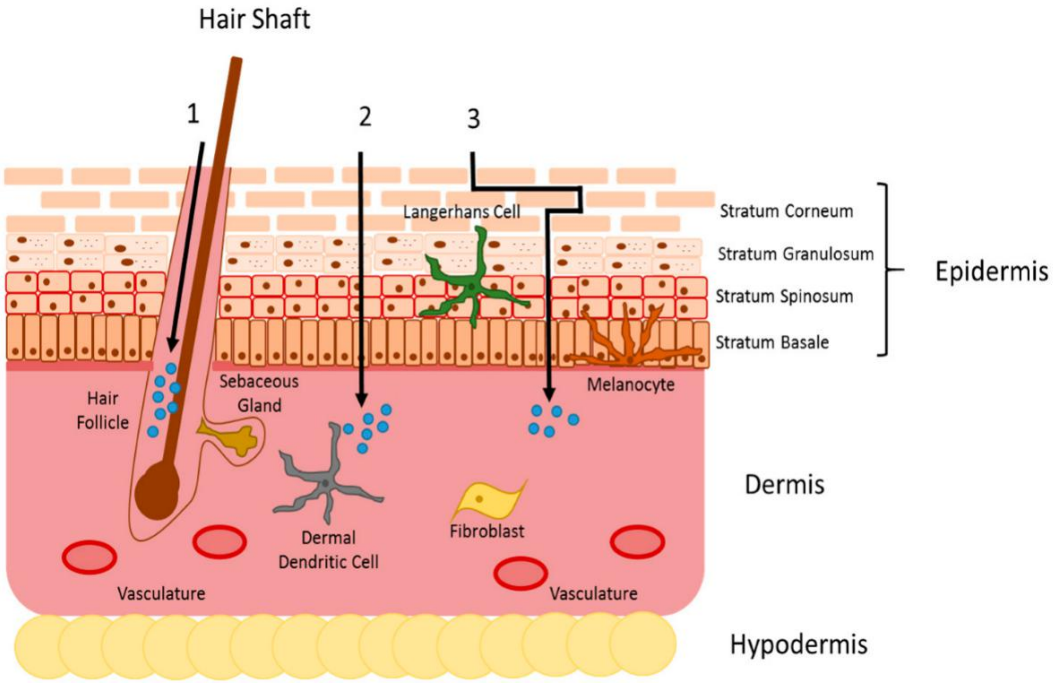


Figure 1-8 Illustration of nanoparticle skin penetration pathways. Topically

applied nanoparticles can penetrate the skin in one of three different ways: (1) through the appendageal route, (2) through the intracellular route, or (3) through the intercellular route[215] .

1.4.2.2 Intradermal drug delivery for the treatment of hyperpigmentation

As melanin is secreted by melanocytes in the basal layer[216,217], in order to effectively inhibit melanin production, the drug needs to cross the stratum corneum and reach the deepest basal layers of the epidermis. However, it is not necessary for the drug to cross the skin into the circulatory system, so a route with little systemic absorption and accumulation is ideal. Intradermal drug delivery, also known as dermal therapy system (DTS), is thus an appropriate delivery method and is often used to treat skin diseases. Through topical treatment, the drug is distributed or passes through the outer layer of the skin to the lesion[218].

Some of the available tyrosinase inhibitors are essentially hydrophilic[219,220]. It is difficult for hydrophilic compounds to penetrate the skin because they do not readily enter the hydrophobic stratum corneum[221,222]. Therefore, it is worth investigating how the active ingredient penetrates the skin and delivers the drug to the basal layer. DTS is appropriate in this aspect as it can ensure that more of the drug stays in the skin rather than penetrating the whole body.

Drugs delivered via DTS target the skin, including the stratum corneum, active epidermis, and dermis. DTS treatment requires both partial

retention in the stratum corneum and the passage of drugs across the skin surface into the active epidermis or dermis[223,224]. Unlike other organs of the body, drugs can easily be delivered directly to the skin. The challenge is that the outermost layer of the skin, the stratum corneum, acts as a barrier to drugs and varies greatly in its ability to bind to different drugs. Successful DTS designs are able to deliver drugs to the interior of the skin without excessive entry into the body's circulation[225], producing high concentrations within the skin while minimising absorption into the bloodstream to avoid side effects[226].

1.4.3 Microneedles

With the rapid development of biomaterials, microelectronics, micro and nano manufacturing, and nanotechnology, various methods of promoting penetration to facilitate penetration agents such as drug carriers, iontophoresis, microneedle injections, ultrasound, electrothermal pores, and needleless injections have begun to break through the barrier of the stratum corneum, allowing transdermal absorption of large molecules previously thought to be difficult to administer transdermally (**Figure 1-9**).

In recent years, with the rapid rise in the incidence of skin diseases such as acne, psoriasis, and skin tumours, there has been a growing demand for topical treatments for skin diseases. Many of the drugs used in the treatment of dermatological conditions have a high degree of systemic toxicity or skin irritation, such as retinoids, corticosteroids, potomytoxin, and anti-melanoma drugs. The use of carrier technology to improve the

dermal targeting of these drugs can improve local absorption and reduce systemic toxicity in the skin and is becoming a popular area of research in transdermal drug delivery systems.

One simple and feasible way to do this is through the microneedle. The development of an effective microneedle system is necessary in order to avoid harming other normal body cells. Microneedles are a hybrid of a hypodermic needle and a transdermal patch and are slowly revolutionising the field of transdermal and intradermal drug delivery[227]. This new finding also speaks volumes about the importance of intradermal drug delivery.

When applied to the skin, microneedles achieve increased transdermal drug absorption by selectively puncturing or removing the stratum corneum, creating micron-sized pores through which the drug travels[228]. Typically, microneedles have an axis length between 250-1000 microns and possess a sharper tip than hypodermic needles[229,230]. Studies have shown that microneedles can penetrate the stratum corneum[231] without touching nerves or blood vessels, leaving patients pain-free[232,233].Microneedles have also been shown to greatly improve the bioavailability of various therapeutic agents and large molecular weight compounds. This is a significant advantage over conventional transdermal drug delivery[234].

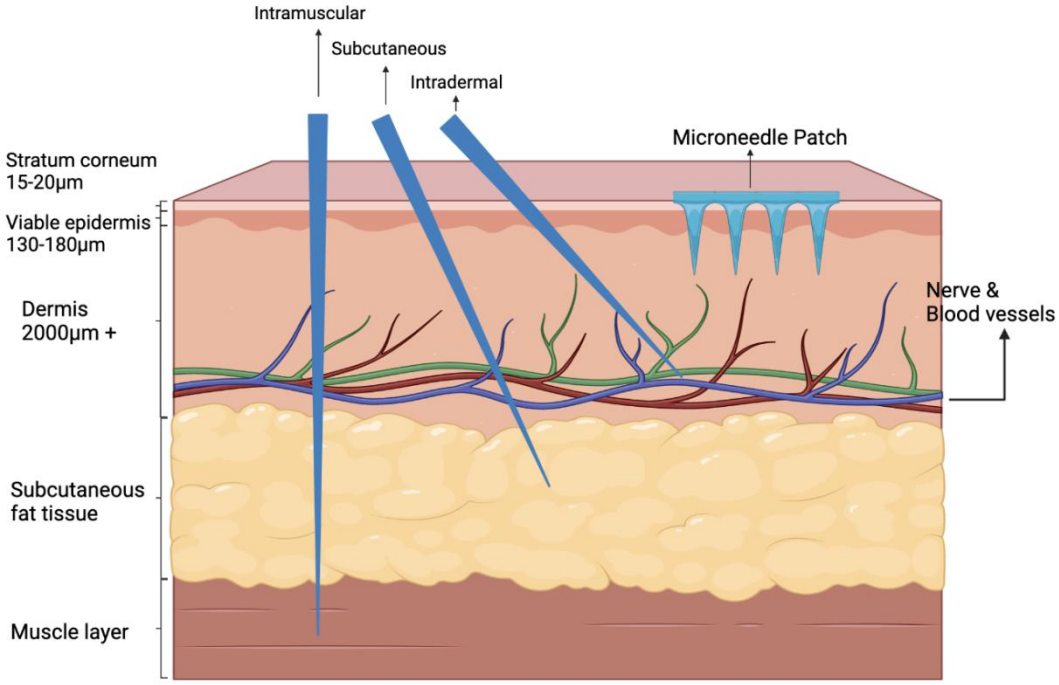


Figure 1-9 Schematic diagram of the microneedle patch and other common (intramuscular, subcutaneous and intradermal) injection routes into human skin.

In 1952, the Journal of Science published a paper on the construction and application of microneedles, initiating research into their use in biomedicine[235]. In 1976, the first microneedle patent was applied for by Gerstel and Place of Alza. It was thought that this micron-sized needle could be used for transdermal drug delivery in a painless manner[236]. However, it was not until 1995 that the first paper on microneedle arrays was published, where they developed a hollow microneedle array injected with bacterial plasmids for genetic transformation of nematodes[237]. In 1998, Prausnitz et al. first applied microneedles to the field of intradermal drug delivery[238]. Since then, more and more scientists have been

exploring the field of microneedles and have discovered that not only small molecules but also large molecules such as peptides, proteins, oligonucleotides, and even supramolecular complexes can be administered transdermally using microneedles[239].

Most microneedles on the market today are used for aesthetic purposes, such as for hyperpigmentation. This suggests that patients with hyperpigmentation are more receptive to using microneedles as a form of drug delivery and thus further exploration into this field is warranted.

1.4.3.1 Types of microneedles

Most of the early microneedle arrays were made of silicon, but new materials such as silicon nitride, glass, metals, and polymers have now come into use[240,241]. Processing techniques for microneedles originate mainly from the semiconductor industry from lithography, chemical etching, or optical techniques[242–244]. Currently, microneedles can generally be classified into four main categories depending on the preparation process and material used. These include solid microneedles, coated microneedles, hollow microneedles, and dissolving microneedles[245,246], as shown in **Figure 1-10**.

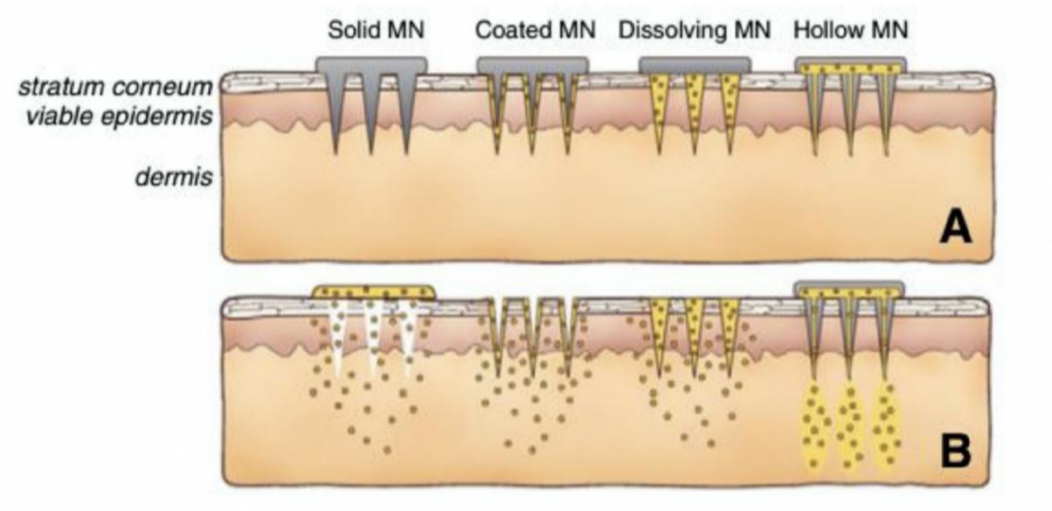


Figure 1-10 4 types of MNP and their route of administration[247].

Solid microneedles can be loaded by applying a drug to the surface or by pre-treating the skin to induce microchannel infiltration[248]. Coated microneedles are a modified version of solid microneedles and contain an additional drug-polymer coating[249,250]. After insertion into the skin, the microneedle is left in place for a certain period of time in order to allow the coating to dissolve, resulting in the release of the drug. The hollow microneedle can be loaded with liquid drugs and injected into the skin for microneedle delivery, similar to traditional subcutaneous injections[247,251]. This method allows for more control of the drug delivery rate through pressure-driven flow. Recently, drugs have been delivered through this method[252].

Each of these different microneedling methods has its own advantages. Among them, solid microneedles can be used directly overlaid with commercial products, enabling a visual comparison of their enhancing capacity. Soluble microneedling is widely used for its good compliance,

especially for patients with excessive melanin deposition, where long-term use of microneedle patches is the best treatment option.

1.4.3.1 Solid microneedles

Solid microneedles are micron-length arrays of microneedles made from polymers containing biocompatible properties. These types of microneedles are commonly used as skin pre-treatments to create microneedle channels. These micropores are deeper and easily penetrate the outermost layer of the skin. Topical preparations are then applied. Solid microneedles are now used by dermatologists for skin treatments[253]. Among others, Akmal et al[227] found that skin post-treatment of solid microneedles, like a "stick-and-poke" strategy where the drug is administered first and then the solid microneedle is applied, can greatly enhance drug delivery. However, some studies have found that microneedle channels are difficult to keep open for longer periods of time due to the regenerative and elastic nature of the skin. It has been reported that microneedle channels can only maintain activity for just 15 minutes using the 'poke-stick' method[254]. This is the biggest limiting factor found to date and may reduce the amount of drug ultimately delivered[255,256]. Therefore, strategies need to be developed to prolong the pore viability for drug delivery.

1.4.3.2 Dissolving microneedles

Dissolving microneedles are made by encapsulating drug molecules with a biodegradable polymer[257,258]. When the dissolving microneedle is

inserted into the skin, the tip dissolves and the drug is then released into the skin. This is a single step process as the polymer degrades completely and does not need to be removed after insertion. There is no need to consider whether it will break off in the skin and have biocompatibility issues[231]. In addition, dissolving microneedles have been shown to be very effective in controlling drug release. Due to the bioacceptability of the polymer and its solubility in the skin, it is one of the best options for long-term treatment to improve patient compliance[259,260].

It is worth noting that the matrix polymer and manufacturing method of DMNs can affect the properties and enhance the ability of microneedles[192]. To investigate the binding of Alpha-Arbutin to microneedles, Aung et al developed dissolved microneedles loaded with Alpha-Arbutin and hydrogel-forming microneedles using polyvinyl alcohol (PVA) and poly (acrylic acid-maleic acid) copolymer (PAMA)[261,262]. The results showed that the dissolving microneedles and hydrogel-forming microneedles were able to provide intradermal delivery of Alpha-Arbutin. This illustrates the importance of continuing to investigate better microneedles containing Alpha-Arbutin and their feasibility.

Currently, a large number of microneedles are used mainly for immune system diseases, diabetes, and cancer[196,263,264]. This has been a major breakthrough in improving vaccinations. However, for dermatological diseases, especially skin lightening, the question of whether the absorption rate of intradermal administration can be effectively improved and the accuracy of targeted delivery improved is a question that requires

further research.

1.5 Skin cancer - melanoma

Skin cancer is one of the most common malignancies worldwide[265]. It can generally be classified as either malignant melanoma or non-melanoma skin cancer[266,267]. Malignant melanoma is a serious form of skin cancer that begins in the pigmented system of the skin. Its incidence is relatively low, accounting for only 4% of skin cancers, but it causes 79% of skin cancer-related deaths[268]. Non-melanoma skin cancers, mainly basal cell carcinoma (BCC) and squamous cell carcinoma (SCC), occur mainly on exposed areas of the face and can be extremely disfiguring[269–271]. Cutaneous malignant melanoma (CMM) is a malignant tumour of melanocytic origin, usually caused by skin pigmentation and by unregulated and abnormal proliferation of melanocytes within the epidermis[272]. In people of colour, malignant melanoma occurs in areas that are rarely exposed to UV light, such as the feet[273]. In contrast, in Caucasians, 90% of the original lesions are cutaneous, with the most common lesions occurring on the back, male chest, and female legs[274]. It is more dangerous than other types of skin cancer such as BCC and SCC as it spreads more rapidly to other organs[275]. The incidence of melanoma has continued to rise in recent decades, often affecting young people. Therefore, the importance of research and development of new treatment strategies has increased greatly[265].

Based on their histopathology, primary cutaneous melanomas can be

classified into four groups: superficial spreading melanoma, nodular melanoma, melanotic melanoma, and acantholytic melanoma[276–278]. Primary cutaneous melanomas are characterised by their ability to invade and metastasise and are one of the most common forms of skin cancer. Cancer cells usually arise from the transformation and proliferation of melanocytes that normally reside in the basal cell layer of the epidermis, but can also develop when melanocytes no longer respond to the normal control mechanisms of cell growth[216,279]. They may then invade nearby structures or spread to other organs of the body (metastases) where they again invade and impair the function of that organ. Although melanoma is almost always curable in its early stages, it may be considered advanced if it spreads to other parts of the body[280]. Therefore, early diagnosis of melanoma is very important and careful examination is necessary for further melanoma treatment.

In addition to early diagnosis, successful treatment requires the right type of therapy e.g. chemotherapy. Many active compounds that have an effect on the cytotoxicity of malignant melanoma cells exist and can be used as effective agents for further treatment[281,282]. Melanoma can be inhibited through a variety of mechanisms. Studies have shown that inhibition can be achieved through apoptosis, a common mechanism of action of cancer-targeting drugs[283–285]. Different proteins induce apoptosis in different ways, but all ultimately lead to nuclear DNA damage. For example, sangenol has been reported as an anti-cancer drug. Its expression in ovarian cancer cells can activate and inhibit the NF-KB

signaling pathway through caspases[286]. However, the mechanism by which *sangenol L.* induces melanoma cell death is unclear. Interestingly, important data exists suggesting that the purinergic signalling pathway plays an immunosuppressive role in the pathophysiology of melanoma and in the ATP signaling pathway[287,288]. Therefore, as shown in other tumours, the purinergic signaling pathway should be considered as a potential target for melanoma management and treatment and may offer new therapeutic perspectives.

Although chemotherapeutic drugs can kill cancer cells, they may damage some normal cells and cause side effects, including effects on other cellular and molecular mechanisms in the melanoma system[289–291]. The type of side effects induced depend on the type of drug used, the amount taken, and the length of treatment. The impact of resistance to chemotherapy on the treatment of melanoma has also been mentioned in recent studies[292–294]. Moreover, the immunosuppressive effect of excess melanin can lead to melanoma progression and resistance to immunotherapy[50]. Therefore, inhibition of tyrosinase can inhibit the production of excess melanin, thereby alleviating the progression of melanoma and improving the efficiency of immunotherapy such as chemotherapy.

In summary, the study of tyrosinase inhibitors and their mechanism of action is of great value. Better targeting and overcoming resistance to chemotherapy are essential to improve the overall efficacy of melanoma treatment. In addition, research into the mechanisms of inhibition of

melanoma skin cancer and the development of new effective compounds are also important research directions.

Among these, the malignant melanoma cell A375 was chosen to be used in my studies as it is a human melanoma cell. A375 was derived from a 54-year-old woman and is one of a series of cell lines established by Geiard et al[295]. It formed rapidly growing subcutaneous tumours resembling malignant melanoma in NIH Swiss mice treated with anti-thymocyte globulin and serum, and was cloned on normal fibroblasts and agar. The karyotype is a triploid with chromosomes[296]. There are 9 marker chromosomes per cell and normal precent of N2, N6, and N22[297].

1.6 Metabolomics

Metabolism is the general term for all the chemical reactions and chemicals in a biological system (cells, tissues, organisms) that are used to maintain life activities[298]. Whether or not an object has metabolism determines whether or not it can be considered a living being[299]. In a biological system, the variety of metabolites and the number of metabolic reactions is enormous. The systematic study of these metabolite changes and the regulation of metabolic reactions is of great importance to the life sciences, not only for revealing the regulatory mechanisms and molecular mechanisms of certain metabolic genes, but also for the diagnosis, prognosis, and treatment of certain metabolism-related diseases[300,301]. Metabolomics is a reliable tool that can be used to study the complex changes in metabolites of biological systems[302,303].

Since the emergence of the concept of genomics at the end of the 20th century[304], a wide range of -omics have emerged and studies have been published. These include transcriptomics, proteomics, and metabolomics. Among these, metabolomics has become a hot topic of research for medical researchers[305,306]. Metabolomics is different from other ‘omics’, as it is the study of the changes of metabolites in the dynamic process of metabolism as well as the changes of metabolites over time after the biological system is stimulated or perturbed. Metabolomics enables us to elucidate the metabolic pathways of the biological system and reveals the metabolic nature of the organism's life activities[307,308]. With the development of life sciences, the depth of research on metabolites has increased and gradually metabolomics has become established. A metabolome can be defined as the collection of all metabolites in a cell, tissue, organ, or individual, generally referring to small endogenous molecules with a molecular weight of less than 1000 Da which often exert biological effects at lower blood concentrations[309,310]. As metabolites are at the end of the regulation of biochemical activity in biological systems, they contain biomarker information that directly reflects the physiological phenotype[311–313]. Metabolomics is therefore able to describe the metabolic reactions that are taking place in a given biological system and can allow us to visualise the metabolic profile. As a result, metabolomics is increasingly becoming a very powerful analytical tool for the holistic study of functional changes in living systems[314]. With the rapid development of systems biology, it is equally important to establish information on the correlations and interactions between these groups.

The concept of Metabolomics was first introduced by Oliver[315] in 1997 and Metabonomics by Jeremy K. Nicholson[316] in 1999. Metabolomics and Metabonomics form the current mainstream field of metabolomics[317]. The former is generally considered to be a cell-based study and focuses on the comprehensive, quantitative analysis of all metabolites in the system. The latter, on the other hand, places more emphasis on the study of biological fluids and tissues, and is the quantitative determination of the dynamic, multi-indicator metabolic response of living systems to pathophysiological stimuli or genetic modifications. Later, 'Metabolomics' gradually came to stand in for both and became the mainstream term used.

Within metabolomics, there are also two different directions of future development. One way is to study metabolite changes in biological systems as a way to find the regulatory pathways involved in metabolism and to find metabolic biomarkers associated with certain changes[318]. The other way is to improve the equipment and find new ways to find more metabolites, which can reveal more metabolite changes and thus new mechanisms of metabolite changes[319].

1.6.1 Application of metabolomics in tumour crippling research

Tumour cells are metabolically active and undergo a series of metabolic reorganisations compared to normal cells[320–322]. Denkert et al.[323] used a GC-MS metabolomics research platform to analyse the metabolic network of cancerous tissues from colon cancer patients and found that cancerous

tissues had lower tricarboxylic acid cycle intermediates and higher levels of nucleic acid molecules (such as purines and pyrimidines and amino acids) than normal tissues. In a metabolomic study of cancerous tissues from gastric and colon cancer, Hirayama et al.[324] found that cancerous tissues had lower glucose concentrations and higher concentrations of glycolytic intermediates and lactate, with an overall upregulation of amino acid concentrations except for glutamine. This suggests that glycolysis is the main mode of energy supply in cancerous tissues and that there is active glutamine catabolism and protein degradation in cancerous tissues. Catchpole et al.[325] applied a metabolomic approach to characterise the metabolic phenotype of kidney cancer cells. Levels of glucose 1-phosphate, fructose 1-phosphate, inositol, mangiferin, and a-tocopherol were found to be significantly different from those of normal kidney cells, and fatty acids such as arachidonic acid, as well as proline and uracil, were important in the metastatic process of kidney cancer.

The use of metabolomics has great significance in studying cancer. Cancer cells dividing in large numbers require large amounts of nutrients and energy to support them. This can lead to abnormalities in cell metabolism, and these abnormalities can help explain the cause of cancer as well as help us find suitable biomarkers.[326,327] The application of metabolomics in cancer in general comprises two areas. One area is concerned with the application of metabolomics to the clinical aspects of cancer, mainly the search for metabolic markers, including diagnosis and prognostsis[328]. The second area is concerned with the application of

metabolomics to the study of metabolic mechanisms, including the detection of metabolites in cancer cells to reveal alterations in metabolic pathways[329], as well as the study of the relationship between certain genes or proteins on metabolism through the combined application of metabolomics and other histologies[330].

1.7 Lipidomics

The structural diversity and complexity of metabolites in living organisms have made it difficult for researchers, As a result, a series of new branches of metabolomics, such as Glycomics and Lipidomics, have emerged based on the in-depth classification of metabolites in the body according to their characteristics[331]. Of these, lipidomics is an important branch in the development of metabolomics[332,333]. Lipidomics was first proposed by Han et al. in 2003[334], and is a discipline that provides a systematic analysis of lipid-like metabolites and their interacting molecules. This facilitates the understanding of the structure and function of lipids, which in turn reveals the relationship between lipid metabolism and the physiological and pathological processes of cells, organs, and even the organism.[335]. Lipidomics is important for revealing lipids' metabolic regulation, biological functions, and mechanisms of action[336,337]. Once the concept of lipidomics was introduced, it quickly became an international research hotspot. Nowadays, lipidomics has been widely used for marker screening, pathological mechanism research, drug action target screening, evaluation of drug action effect, and mechanism of action research.

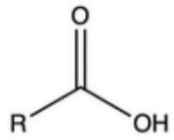
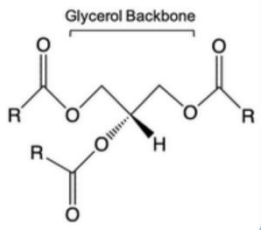
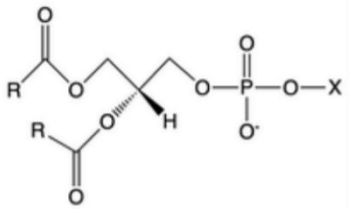
1.7.1 Lipid metabolites

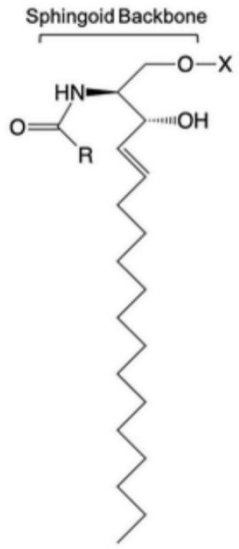
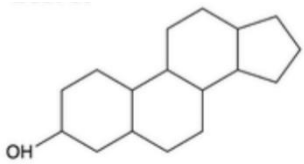
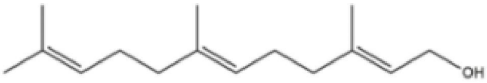
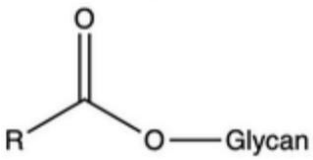
Lipid metabolites are chemically non-homogeneous compounds that occur in nature and are highly soluble in organic solvents. They were later redefined as 'hydrophobic or amphiphilic small molecules'[335]. Lipid metabolites are mainly classified as Fatty acids (FA), Glycerolipid (GL), Glycerophospholipid (GP) (details in Table 2), Sphingolipid (SP), Sterol lipid (ST), Prenol lipid (PR), saccharolipid (SL), and polyketide (PK)[338,339]. Among them, the first five lipid components are relatively high in mammalian cells (Table 1). Lipid metabolites are a major component of biological membranes and act as energy storage sources while also participating in many important life activities, such as signal recognition, signalling transduction, cell differentiation, and apoptosis[340–342]. Therefore, changes in the metabolism and function of lipids can affect cellular function and cause pathological disorders in the organism. Studies have found that metabolic diseases[343], cardiovascular diseases[344], tumours[345], and neurological diseases[346] are closely related to abnormal lipid metabolism. Therefore, the study of the metabolic processes of lipid compounds can provide a new basis for disease pathogenesis, diagnosis, treatment, and even pharmaceutical research and development. All of these findings are biologically significant.

The diversity of lipid functions is reflected in the great variation in the structure of lipid molecules. Unlike genes and proteins, which consist mainly of linear combinations of four nucleic acids and 20 amino acids respectively, lipid structures are often much more complex because of the

many different biochemical transformations that take place during their biosynthesis[339,347,348]. This degree of diversity means it is important to develop a comprehensive system of classification, nomenclature, and chemical representation to accommodate the myriad of lipid species that exist in nature(**Table 1-1** & **Table 1-2**).

Table 1-1 Lipid categories of the comprehensive classification system and the number of structures in the LIPID MAPS database.

Category	Abbreviation	Structures in Database
Fatty acyls	FA	
Glycerolipids	GL	
Glycerophospholipids	GP	

Category	Abbreviation	Structures in Database
Sphingolipids	SP	
Sterol Lipids	ST	
Prenol Lipids	PR	
Saccharolipids	SL	

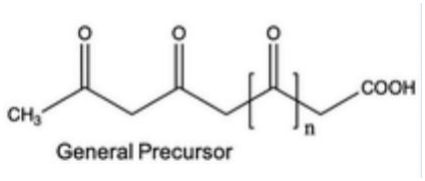
Category	Abbreviation	Structures in Database
Polyketides	PK	 General Precursor

Table Lipid categories of the comprehensive classification system and the number of structures in the LIPID MAPS database.

Table 1-2 Abbreviations and examples of glycerophospholipid main classes.

Class	Abbreviation	Examples
Glycerophosphocholines	PC (LPC for lyso species)	PC(P-16:0/18:2(9Z,12Z))
Glycerophosphoethanolamines	PE (LPE for lyso species)	PE(O-16:0/20:4(5Z,8Z,11Z,14Z))
Glycerophosphoserines	PS (LPS for lyso species)	PS(16:0/18:1(9Z))
Glycerophosphoglycerols	PG (LPG for lyso species)	–

Glycerophosphates	PA (LPA for lyso species)	PA(16:0/0:0) or LPA(16:0)
Glycerophosphoinositols	PI (LPI for lyso species)	PI(18:0/18:0)
Glycerophosphoinositol monophosphates	PIP	–
Glycerophosphoinositol bis-phosphates	PIP2	–
Glycerophosphoinositol tris-phosphates	PIP3	–
Glycerophosphoglycerophosphoglycerols (Cardiolipins)	CL	CL(1′-[16:0/18:1(11Z)],3′-[16:0/18:1(11Z)])
Glycerophosphoglycerophosphates	PGP	–
Glyceropyrophosphates	PPA	–
CDP-glycerols	CDP-DG	–
Glycosylglycerophospholipids	[glycan]-GP	–

Glycerophosphoinositolglycans	[glycan]-PI	–
Glycerophosphonocholines	PnC	–
Glycerophosphonoethanolamines	PnE	–

1.7.2 The relationship between melanoma and lipids

Melanoma is a devastating form of skin cancer characterised by an impressive capacity for metabolic reprogramming[349,350]. Melanoma cells are able to adapt to the tumour's microenvironment by using a variety of fuels that contribute to tumour growth and progression[351]. One of the obvious manifestations is an increased rate of lipid synthesis. Lipids are a source of energy and form the structural basis of all membranes, but also appear as mediators that not only influence classical oncogenic signaling pathways but also contribute to melanoma progression[349,352]. Various alterations in fatty acid metabolism have been reported and can promote the aggressiveness of melanoma cells[353]. Elevated expression of key lipogenic fatty acid synthases is associated with aggressive and poor prognosis of tumour cells. Fatty acid uptake from the surrounding microenvironment, β-oxidation of fatty acids, and storage also appear to play an important role in tumour cell migration[354–356]. It has been documented that some specific lipid classes such as glycerophospholipids,

sphingolipids, sterols, and eicosanoids are significantly altered in lipid metabolism in melanoma.

Studies have now explored the metabolism of lipids in melanoma cells by comparing melanoma cells with normal melanocytes, with the most striking difference being an increased rate of lipogenesis[357,358]. In this case, carbohydrates from nutrients are converted into fatty acids (FA), sterols, and complex lipids[359]. The synthesis of FA begins with the carboxylation of acetyl-CoA to malonyl-CoA, dependent on the availability of acetyl-CoA from the tricarboxylic acid (TCA) cycle[360]. Specific inhibition of FASN activity with the anti-obesity drug orlistat has been reported to reduce the occurrence and number of lung metastases in a mouse model of melanoma[361,362].

Furthermore, a recent study reported that oleic acid, a FA abundant in the lymph, protects melanoma cells from iron toxicity in an ACSL3-dependent manner and increases their ability to form metastases[349,363]. In addition to their role in providing fuel for various lipid metabolisms, FAs are involved in protein acylation, thereby controlling protein translocation, membrane localisation, and signalling activities. For example, S-palmitoylation of the melanocortin-1 receptor (MC1R), which corresponds to the covalent attachment of palmitic acid to cysteine residues of proteins, has been linked to the activation of MC1R, thereby reducing melanin formation in mice[364].

Furthermore, FAs, a valuable source of acetyl CoA, contribute to citrate

formation upon entry into the TCA cycle and provide ATP elevation to tumour cells under nutrient-deprived conditions, emphasising the importance of FA uptake for melanoma progression[365,366]. Increased FA biosynthesis and FA uptake may lead to increased levels of multiple lipids with signaling functions, thereby affecting numerous cellular processes, including melanoma cell differentiation and motility[367]. Among these, reduced expression of MITF increases the metastatic nature of melanoma cells. In contrast, a variety of enzymes associated with FA metabolism can reduce MITF expression[368,369]. Thus, it is demonstrated that FA metabolism can regulate the differentiation and progression of melanoma cells.

In FA, studies have been reported regarding the changes in the ratio of saturated and unsaturated fatty acids. In mice[370] and human melanomas[371], the type of PI with saturated and monounsaturated FA chains increased with the tumour stage. A previous lipidomics study showed an increased ratio of saturated to unsaturated FA in highly metastatic B16F10 cells compared to poorly metastatic B16F1 cells, suggesting that membrane fluidity may in turn decrease during melanoma progression[372].

The uptake of fatty acids by melanoma cells occurs via fatty acid transporters, specifically the family consisting of fatty acid transporters 1-6 (FATP1-6)[373]. Of these, FATP2 is essential for the esterification of long-chain fatty acids to triglycerides (TG) and acts as both a fatty acid synthase and a fatty acid transporter[374,375]. According to data from the

Metabolic Cancer Study (Me-Can), patients with increased serum TG are at increased risk of melanoma and accumulation of TG in melanoma cells also increases resistance to targeted therapy[376,377]. The literature suggests that targeting FATP2 attenuates the uptake of lipids.

Overall, fatty acid uptake and subsequent fatty acid oxidation (FAO) play an important role in the survival and metastasis of tumour cells[378,379]. However, melanoma cells can also take up lipids from other sources, such as adipocytes. Regardless of the source, melanoma cells take up lipids and use them to promote aggressive behaviour, such as metastasis or resistance to treatment, which allows them to survive[380].

1.8 Experimental methods to assess drug penetration

1.8.1 Franz diffusion cell

Due to the difficulties of in vivo experiments, most topical and transdermal drug penetration studies have used in vitro experiments as an alternative. In addition to being used in risk assessment experiments for many drugs, in vitro permeation tests can also provide a platform for the initial assessment of the permeability of topical and transdermal formulations. In vitro permeation assays are usually performed using static diffusion cells (Franz cells) followed by HPLC[381]. The stratum corneum is the main resistance to drug penetration through the skin and therefore the majority of in vitro drug release studies are based on this.

A common device used for in vitro transdermal studies is the Franz

diffusion cell which reflects the in vivo absorption process[382,383], consisting of a supply chamber, a receiving chamber, an angular sampling port, a thermostatic water circulation, and a drug delivery skin, as shown in **Figure 1-11**.

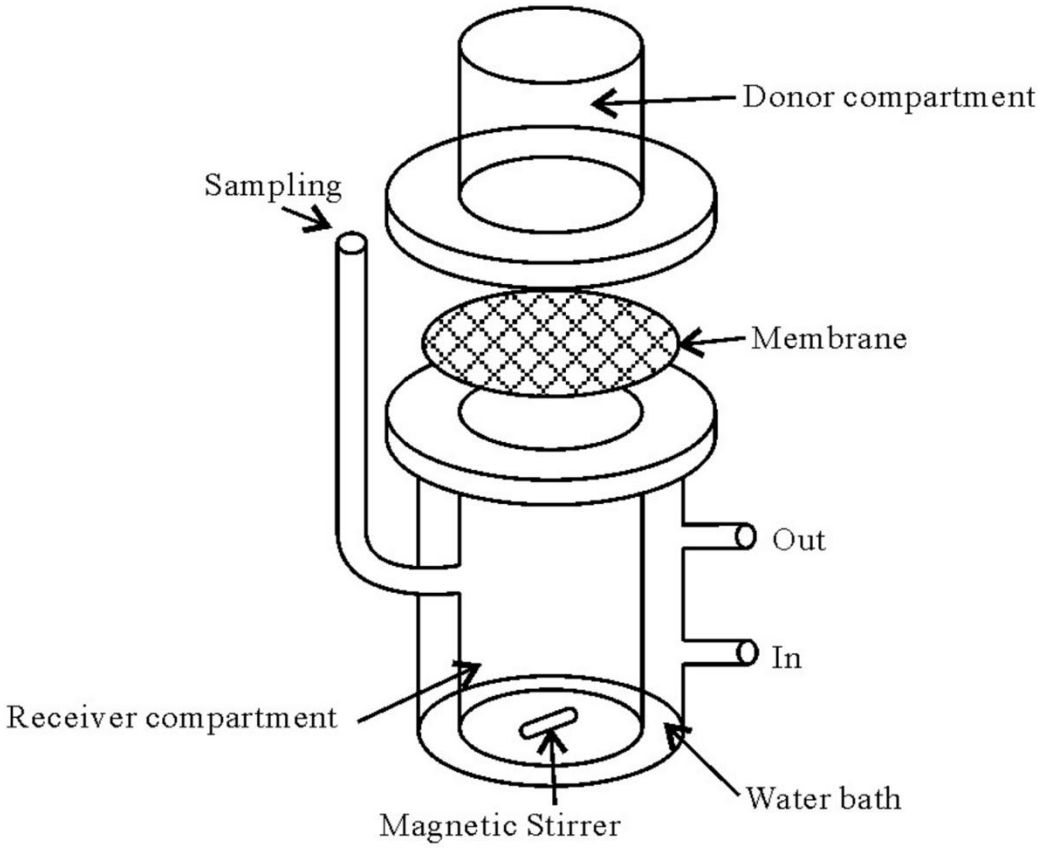


Figure 1-11 Schematic illustration of the static Franz diffusion cell.

The Franz diffusion cell is commonly used to determine the transdermal and cumulative transdermal rates of topical formulations for in vitro transdermal administration[384,385]. The basic operation is to place a treated animal skin or skin model between the recipient and donor compartments, with the stratum corneum against the donor compartment for dermal drug delivery models. The drug is placed on the cuticle of the skin and the

receptor chamber is filled with receptor fluid. The concentration of the drug in the receptor fluid is determined by high-performance liquid chromatography and the kinetics of drug passage through the skin is then analysed.

In terms of the choice of laboratory materials, human skin is considered to be the most reliable model for *in vitro* experiments[386]. However, animal skin can be used as a substitute for human skin due to legal restrictions, unavailability of human skin, and sample variation due to differences in age, sex, race, and anatomical location[387]. It has been observed that diffusion experiments conducted through the skin of some animals, particularly small animals such as mice and rats, show higher penetration rates than experiments using human skin due to their increased thinness[388]. The best natural membrane for diffusion studies is pig skin, particularly pig ear skin, which has similar thickness, histology, and permeability to human skin[389].

In addition, according to Baert and colleagues[384], they evaluated various solvents used in the preparation of interstitial fluids for tissue sample culture. It was found that PBS was the best fluid for this study and could be used as the tissue fluid for their simulations[261,262]. In addition, PBS can also be used to simulate biological fluids. The ionic composition of PBS includes Na^+, K^+, Ca^{2+}, Mg^{2+}, Cl^-, and HCO_3^-, and its phosphate and pH values are similar to those of interstitial fluids[390].

1.8.2 Analytical techniques

1.8.2.1 High-performance liquid chromatography

The most widely used technique for determining the concentration of drugs that penetrate or cross the skin is the traditional chromatographic method, usually HPLC[391]. HPLC and penetrant concentrations can be analysed from different Franz cell elements (e.g. donor chamber wash, skin wash, tape strips, remaining within skin, and recipient fluid). As HPLC is a relatively rapid, quantitative, and versatile analytical method, it can be used for most permeable substances through the appropriate selection of columns, flow equations etc.

However, some difficulties exist when using HPLC. Detection and quantification may be problematic if the sensitivity is low[392]. In addition, in liquid chromatography, the sample should be in solution and therefore an effective solvent extraction step is required before injection into the HPLC system. This increases the complexity of the method and the time required for analysis. Also, as HPLC does not have any imaging capability, it cannot determine the exact depth of penetration or provide information on the spatial distribution of topical formulation penetrants within the skin.

1.8.2.2 Orbi-SIMS

1.8.2.2.1 Imaging capabilities

Secondary ion mass spectrometry (SIMS) is an effective technique for displaying molecular structures[393]. SIMS has two main platforms, ToF-SIMS and nanoscale SIMS, which are capable of imaging different types

of biomolecules at single-cell and organelle level resolution respectively[394]. Three-dimensional OrbiSIMS is a new TOF-based label-free chemical imaging instrument[395]. It combines the state-of-the-art Orbitrap analyser with TOF-SIMS to allow chemical imaging and in-depth analysis of cells with minimal sample preparation. The Orbitrap analyser offers high-quality accuracy (sub p.p.m.), high-quality resolution (from 15,000 at m/z 200 to 480,000 at m/z 200, acquisition rate > 20 spectra for 1 spectrum), high sensitivity, and high spectral dynamic range (total ion number to noise ratio of 105). On the other hand, TOF-SIMS uses a multi-atom primary beam, offering the advantage of high molecular yields and low subsurface damage[396].

Due to these properties, the most important advantage of 3D - OrbiSIMS is thus that metabolic imaging at sub-cellular resolution can be achieved. It combines the high field orbitals of biomass spectroscopy to address the poor mass resolution of TOF-SIMS and improve the confident identification of endogenous metabolites[395]. Previously, a commonly used imaging analysis method was matrix-assisted laser desorption ionisation (MALDI)[397]. However, it cannot achieve subcellular spatial resolution[398] and even the most advanced microscopy applications rely on labelling, which can compromise the physicochemical properties of drug molecules. SIMS fills this gap as it improves spatial resolution, drug molecules no longer need to be labelled in in vitro or in vivo systems, and minimal sample preparation is required. When used in conjunction with Orbitrap, SIMS can also provide three-dimensional information and even potential

metabolomic information.

1.8.2.2.2 OrbiSIMS for metabolomics

OrbiSIMS can be used not only for imaging, which provides information on the location of compounds, but also for metabolomic analysis[399]. At this stage, it has been shown to be able to release and unambiguously identify large diagnostic chemical species, such as lipids and peptides. Passarelli[395] et al. used this new technique for metabolite analysis of macrophages treated with different concentrations of an exogenous compound (the drug amiodarone). In a tissue section of a mouse brain, they identified lipid and amino acid fragments and were able to image individual cells in the tissue section. Hodgkinson et al.[400] recently used three-dimensional OrbiSIMS images to observe the metabolites of multiple mesenchymal stem cells (MSCs) using ToF and Orbitrap. Suvannapruk et al.[399] also used 3D OrbiSIMS to study the metabolic profiles of human monocyte-derived M0, M1, and M2 macrophages at the single cell level, identifying characteristic ions associated with known biological processes in each subpopulation.

This OrbiSIMS-based metabolomics analysis platform provides an important aid for in situ metabolic analysis of tissues and cells due to the low sample preparation, small sample size, and fast analysis time required, enabling rapid screening of significant changes in metabolites in different experimental groups[395,401]. This fully demonstrates the feasibility of applying OrbiSIMS to metabolomics analysis, especially lipidomics.

1.8.2.3 LC-MS based metabolomics assays

Liquid chromatography-mass spectrometry (LC-MS) is a powerful tool for quantifying a range of small biomolecules and identifying known and unknown metabolites present in biological samples[402]. This technique has been widely used for the identification of biomarkers of inflammatory diseases, drug discovery, and studies of cellular metabolic profiles[403]. Unlike OrbiSIMS, which is a completely new analytical method, LC-MS or UPLC-MS technology has already developed into one of the mainstream technical tools for metabolomics research. It allows the separation and detection of a wide range of polar or non-polar metabolites with high resolution and sensitivity[404,405]. While typical diode array detectors (DADs) are sensitive to the nmol range, mass spectrometry has higher sensitity to the pmol range, and for metabolites that have been derivatised, the detection limit of mass spectrometry can reach the fmol range[406,407]. Furthermore, this tool has also been used for the identification of metabolites such as amino acids.

In addition, hydrophilic interaction liquid chromatography (HILIC), a chromatographic technique used to improve the retention behaviour of strongly polar substances that are poorly retained in reversed-phase chromatography, has replaced conventional reversed-phase chromatography[408]. HILIC works by using a strongly polar stationary phase in combination with a mobile phase consisting of a high proportion of organic phase/low proportion of aqueous phase. Furthermore, the HILIC column was found to be more stable than reversed-phase

chromatography, demonstrating the potential of HILIC for metabolomics research[409].

Despite recent advances in determining the metabolic phenotypes of various conditions using traditional LC-MS-based techniques, there are still many drawbacks[410,411]. For example, large numbers of cells (>1 million cells) are required to obtain sufficient signal for single cell analysis[412,413]. In addition, sample preparation procedures are complex and include the use of organic solvents for metabolic quenching and extraction of intracellular metabolites, these procedures will result in incomplete sampling. And biases exist in the quantification of small molecules in biological samples due to the rapid turnover and loss of metabolites. Furthermore, cell samples are homogenised (metabolite extraction) during preparation, thereby losing the structural integrity and physiologically relevant structure of tissues and cells and eliminating the possibility of correlating the spatial distribution of metabolites with morphology[414]. Therefore, exploring better methods for metabolomic analysis is an important future research direction.

1.9 Aims of this thesis

Taking into consideration the current state of research on tyrosinase inhibitors, this thesis aims to explore and develop suitable tyrosinase inhibitors and ways of enhancing permeation as well as explore the relationship between tyrosinase modulators and melanoma in order to further our understanding in this field.

The first aim of this thesis is to assess the skin permeation ability of commercial products containing Alpha Alpha-Arbutin and to find ways to enhance their intradermal delivery. To achieve this goal, we first produced dissolving microneedles containing Alpha-Arbutin and then compared the magnitude of enhancement of pre-treatment, post-treatment, and dissolving microneedles against Alpha-Arbutin permeation by HPLC analysis of Franz cell. The analysis was then visualised using 3D OrbiSIMS to see how well dissolving microneedles could deliver drug to a targeting site compared to solid microneedles. The combined analysis was then used to help identify a more effective method of enhancing intradermal drug delivery. This composes the second chapter of this thesis and will explore and discuss the objectives of improving the bioavailability of Alpha-Arbutin.

The second aim of this thesis is to assess the biological activity of the newly synthesised tyrosinase inhibitor and its permeation capacity via intradermal administration. To achieve this goal, I chose two new dihydrochalcone backbone heterodimers, 11c and 11m, synthesised and provided by our collaborators, and investigated their ability to inhibit tyrosinase activity as well as determined their melanin content. The goal was to find promising new tyrosinase inhibitors. In addition, their permeation capacity was analysed by HPLC analysis and 3D OrbiSIMS imaging visualisation with the aim of discovering new compounds that can target intradermally for drug delivery. The whole evaluation process will be presented in Chapter 3.

The third aim of this thesis is to explore the potential mechanisms of tyrosinase modulators in melanoma cells to find new therapeutic targets for melanoma. L-DOPA and Alpha-Arbutin, as well as 11c and 11m, are tyrosinase modulators that were chosen for differential analysis in this study. They are capable of stimulating either up- or down-regulation of tyrosinase and are closely related to tyrosinase activity as well as tyrosine metabolism. As presented and described in Chapter 4 of the thesis, this study used a combination of LC-MS and OrbiSIMS to analyse the metabolite changes of tyrosinase modulators in melanoma cells, thus identifying metabolites with significant changes and exploring their pathways.

Chapter 2. Evaluation of enhanced Intradermal delivery of Alpha-Arbutin by applications of microneedles and 3D OrbiSIMS

Zhiwei Li[#], Maria Marlow, David Scurr, Felicia Goh Xia Yee, Zheying Zhu*

School of Pharmacy, The University of Nottingham, Nottingham, NG7 2RD, United Kingdom

This chapter is written in the format of a published article that will be submitted to the journal *Molecular Pharmaceutics*.

Keywords: Intradermal Delivery, Hyperpigmentation, Alpha-Arbutin, Microneedle, OrbiSIMS

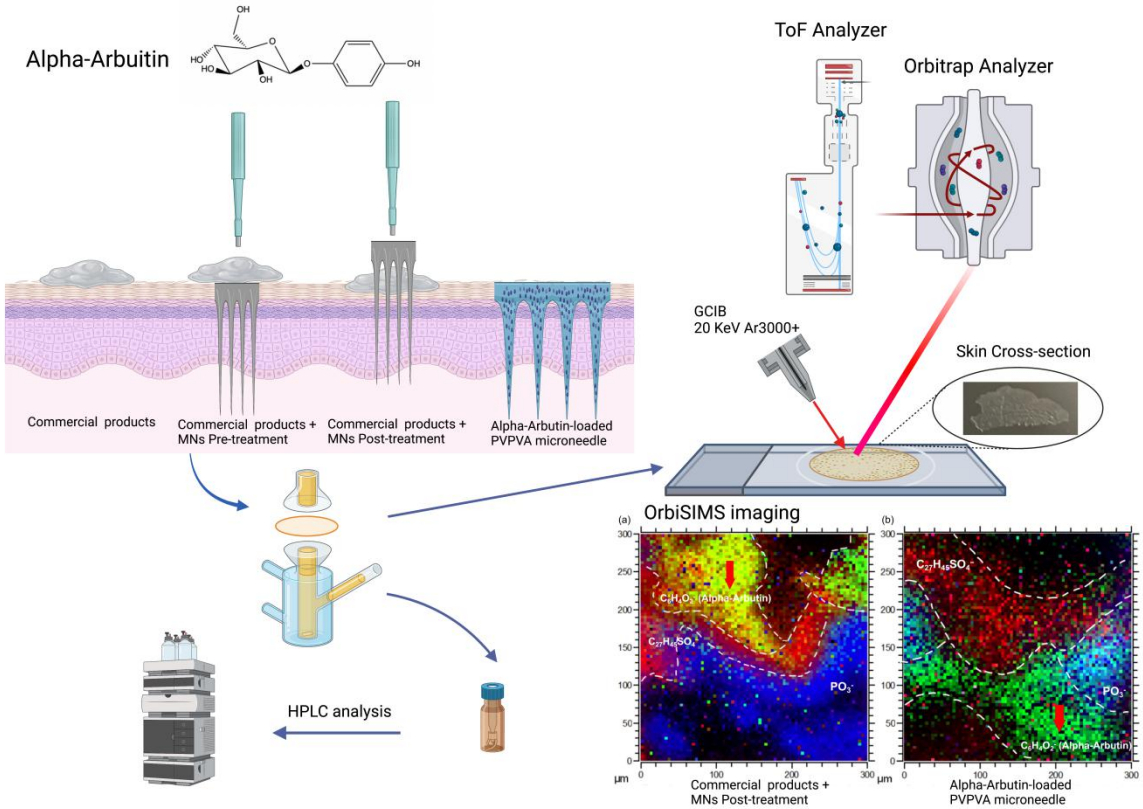
2.1 Abstract

Hyperpigmentation is a common dermatological disorder caused by abnormal production and accumulation of melanin. This can lead to various other skin disorders, including ephelides, hemochromatosis, and lentigines. Alpha-Arbutin has been widely used to treat hyperpigmentation disorders through tyrosinase. However, its hydrophilicity makes it challenging for it to permeate through the stratum corneum and to reach the basal layer where its target site melanosomes are located. Therefore, it is necessary to explore the applications of commercial solid steel microneedle (CMNs) and dissolving microneedle (DMNs) techniques and assess their effectiveness in improving skin permeation of Alpha-Arbutin.

This skin permeation study was carried out by application of three commercial products with different formulations on porcine skin of full thickness mounted on Franz cell for 24 hours. In addition, we assessed the effectiveness of commercial solid steel microneedles in delivering commercial Alpha-Arbutin products into the basal layer using the oscillating microneedle device, Dermapen®, as a pre-treatment and post-treatment. Furthermore, an Alpha-Arbutin-loaded Polyvinylpyrrolidone-Co-Vinyl Acetate (PVPVA) dissolving microneedle was fabricated using 2% w/w Alpha-Arbutin and the effectiveness of the Alpha-Arbutin-loaded PVPVA dissolving microneedle in promoting Alpha-Arbutin permeation was then evaluated. Subsequent HPLC analysis was carried out to analyze the amounts of Alpha-Arbutin remaining in each of the Franz cell components. Further 3D Orbitrap Secondary Ion Mass Spectrometry

(OrbiSIMS) imaging was conducted for visual analysis.

Our results showed that although skin permeation of Alpha-Arbutin was limited (less than 1%), a large enhancement (4-5%) was achieved after application of CMNs or DMNs. We found that DMNs demonstrate a more sustainable and robust capacity through visual analysis by OrbiSIMS. In addition, enhance skin permeation of Alpha-Arbutin by delivering the compound to the basal layer within the skin. Overall, this study demonstrates that DMNs could be a promising delivery system for promoting intradermal delivery of Alpha-Arbutin to achieve the highest effectiveness in the treatment of hyperpigmentation disorders.



2.2 Introduction

Melanin is the primary pigment responsible for the pigmentation of skin,

eyes, and hair and has a multitude of properties. It has a crucial role in photoprotection, and is a broadband ultraviolet absorbent, an antioxidant, and a radical scavenger. Melanin protects the skin against damage from the harmful ultraviolet radiation from sunlight[16]. It also protects the skin against stress from different sources, including environmental pollutants, toxic drugs, and chemicals. Although melanin plays an important role in protecting the skin, abnormally increased production and accumulation of melanin leads to various hyperpigmentation disorders, including melasma, postinflammatory hyperpigmentation, solar lentigines, ephelides, and café au lait macules[414]. These conditions are generally not harmful but can have a considerable psychological effect on the affected patients due to the effect on their physical appearance[415].

In general, these skin disorders are caused by several intrinsic and extrinsic factors, including ultraviolet radiation, radicals, inflammatory mediators, and hormones[416]. These all lead to the upregulation of melanogenesis. Several approaches to achieve depigmentation include regulation of the transcription and activity of tyrosinase, tyrosinase-related protein-1, tyrosinase-related protein-2, and peroxidase, as well as regulation of the uptake and distribution of melanosomes in recipient keratinocytes, regulation of the degradation of melanin and melanosomes, and the turnover of pigmented keratinocytes[417]. Current treatment options for hyperpigmentation include topical agents, chemical peels, cryotherapy, and light or laser therapy[418]. Approximately 15% of the world's population is estimated to be using depigmenting products[79]. Among them, Alpha-

Arbutin is a common commercial ingredient used to improve skin pigmentation and a naturally occurring reversible tyrosinase inhibitor. Its IUPAC name is (2R,3S,4S,5R,6S)-2 hydroxymethyl-6-(4-hydroxyphenoxy) oxane-3,4,5-triol.

The alpha-isomer Alpha-Arbutin (4-hydroxyphenyl-Alpha-D-glucopyranoside) has superior tyrosinase inhibition[139]. Alpha-Arbutin is able to inhibit the synthesis of melanin in patients with hyperactive melanocytes and hyperpigmentation disorders. The main mechanism of action of Alpha-Arbutin is through inhibition of melanosomal tyrosinase activity directly, or by acting as a substrate to compete with tyrosinase for the active site of the enzyme[123]. Several studies show that Alpha-Arbutin has similar effectiveness to hydroquinone due to its molecular structure, but it demonstrates less irritation and melanocytotoxicity[419]. Hence, it may be a great alternative for treating skin hyperpigmentation disorders.

However, since the treatment of hyperpigmentation is generally administered topically, it is necessary for the drug to pass through the stratum corneum of the skin to ensure successful delivery. Corneocytes are thought to be the main barrier[420,421] to skin penetration, and consist of an extremely insoluble keratin matrix that does not permit diffusion of hydrophilic molecules[422].

Melanocytes are located in the basal layer, which is the target site of Alpha-Arbutin. In order to reach the target site, Alpha-Arbutin thus needs to permeate through the stratum corneum. The log P of a drug is an indication of its lipophilicity. Substances with a log P greater than 2 readily

permeate across the skin[423]. However, Alpha-Arbutin is hydrophilic and has a log P value of – 1.49[424], thus it exhibits poor permeation across the skin[142].

Although there are other depigmenting agents with better active effects, Alpha-Arbutin has a much lower toxic effect profile and does not cause serious adverse effects with long-term exposure[142]. Therefore, it is crucial to improve the permeation of Alpha-Arbutin across the skin. This can be done by developing novel delivery systems such as microneedles[425], nanosystems[426], microsystems[427,428], lipidic systems[429], and more[142]. Among these, microneedle technology has been widely explored for improving the skin permeation ability of intradermal and transdermal delivery systems of hydrophilic molecules[180]. Donnelly et al.[430] used solid microneedles to enhance the skin penetration of the hydrophilic compound ALA and to reduce the amount of ALA used. Oh et al.[431] found that biocompatible PC microneedles enhance the skin penetration of calcein, a hydrophilic molecule, and thus they believe it is a suitable tool for transdermal drug delivery systems for hydrophilic molecules.

Microneedles are arrays of micro-size projections with lengths ranging from 250 μm to 1000 μm that pierce the skin to create microchannels through the stratum corneum in order to deliver drug molecules to the target site in the skin [432]. Microneedles can be categorised into five main groups: solid, coated, dissolving, hollow, and hydrogel-forming microneedles[197].

The solid microneedle is normally used for skin pre-treatment based on

the "poke-and-patch" technique[433]. The needle tips penetrate into the skin, forming microchannels through which the drug directly enters the skin layers on the application of a drug patch, thus increasing skin permeation[258]. However, the closure of microchannels created after microneedle insertion is a critical aspect when evaluating microneedles as it influences the drug diffusion rate to the skin microvasculature and interstitial fluid. In a previous study by S Bal et al., the microchannels generated after solid microneedle application were shown to close very rapidly - after 15 minutes in most of the cases[434]. Currently, no study has been carried out to investigate the effectiveness of commercial solid steel microneedles in improving the skin permeation of Alpha-Arbutin. Therefore, commercial solid stainless steel microneedles were used in this study not only as the pre-treatment but also as the skin post-treatment based on the “coat-and-poke” technique with slight modifications[226]. The drug was first applied to the skin surface, followed by microneedle insertion. This was done to overcome the transient period of microchannels opening for more effective transportation of Alpha-Arbutin across the skin[435].

One advantage of dissolving microneedles is their ability to improve patient compliance. Dissolving microneedles are typically fabricated using hydrophilic polymers (eg. PVA or PVP) and by incorporating drug molecules either in solution or nano/microparticle suspension at the casting stage. Upon insertion of the dissolving microneedle in the skin, dissolution takes place, and the drug is released into the skin. This is a

single-step process without the need for the microneedle to be removed after insertion. Therefore, it is one of the best choices for long-term therapy as it can improve patient compliance[436].

Recently, Aung et al. developed Alpha-Arbutin-loaded dissolving microneedles and hydrogel-forming microneedles using polyvinyl alcohol (PVA) and poly (acrylic acid-co-maleic-acid) copolymer (PAMA)[260]. The results were promising as the dissolving microneedles and hydrogel-forming microneedles showed 4.5 times and 2.8 times increase in the permeation of Alpha-Arbutin respectively, compared to the commercial gel and cream[261]. This data suggests that the dissolving microneedle and hydrogel-forming microneedle offer superior intradermal delivery of Alpha-Arbutin. However, further attempts to improve targeted delivery of dissolving microneedles through different polymer (PVPVA) formulations are necessary. Previous studies have only focused on the total amount of drug delivered into the skin by microneedles, neglecting the specific location. As melanocytes are located between the epidermis and the dermis, if the drug stays only in the upper epidermis, it will not reach the target location. Therefore, a good microneedle system should provide a more precise target position.

In order to find a better microneedle system, the latest OrbiSIMS imaging technique was chosen to be combined with HPLC analysis in this study. Although HPLC analysis provides useful quantitative results, this analytical technique does not confer any detail regarding the distribution of Alpha-Arbutin within individual layers of skin. Hence, additional visual

analytical techniques must be explored to provide spatial detail regarding Alpha-Arbutin permeation. Previously, time-of-flight secondary ion mass spectrometry (ToF-SIMS) has been widely used as a tool for imaging drug spatial distribution in skin layers [226,437,438]. Recently, it has been noted that with the incorporation of OrbiTrap to ToF-SIMS, also known as 3D OrbiSIMS, has been shown to provide higher mass-resolution capabilities[439], allowing the visual analysis to act as a powerful complementary technique[393]. 3D OrbiSIMS combines the high speed and spatial resolution of secondary ion mass spectrometry (SIMS; under 200 nm for inorganics and under 2 μm for biomolecules) with the high mass resolving power of an Orbitrap (>240,000 atm/z200)[394]. OrbiSIMS also yields significantly more and stronger peaks than ToF-SIMS which greatly facilitates further analysis[440]. However, there is still a knowledge gap regarding OrbiSIMS as a visual analysis tool for skin, as its application to skin so far has only been by depth profile and tapes strips imaging. Thus, this study will be the first to apply 3D OrbiSIMS to the visualization of the skin distribution of Alpha-Arbutin, with many advantages including subcellular resolution and no need for radiolabelling or fluorescent labels.

Overall, this study aims to evaluate the skin permeation of Alpha-Arbutin commercial products and investigate the effects of commercial solid stainless steel microneedles and polymeric dissolving microneedles in improving skin permeation of Alpha-Arbutin.

2.3 Materials and methods

2.3.1. Materials

Alpha-Arbutin analytical standard was purchased from Merck Life Sciences UK Limited by Scientific Laboratory Supplies Ltd. Ordinary® Alpha-Arbutin 2% + Hyaluronic Acid (HA) and Ordinary® Ascorbic Acid 8% + Alpha-Arbutin 2%(AA) were purchased from Deciem Beauty Group Inc. The INKEY® List 2% Alpha-Arbutin Serum (INK) was purchased from The INKEY List. Sodium acetate was purchased from Sigma-Aldrich, UK. Phosphate buffered saline (pH 7.4), Acetic acid, and Methanol (HPLC grade) were purchased from Fisher Scientific, UK. Teepol® solution (multipurpose detergent) was purchased from Scientific Laboratory Supplies, UK. D-Squame standard sampling discs (adhesive discs) were ordered from CUDERM corporation, USA. Deionized water was obtained from an ELGA reservoir, PURELAB® Ultra, ELGA, UK. All reagents were of analytical grade, unless otherwise stated. Hypersil BDS C18 column (150 mm length x 4.6 mm inner diameter, 3.0 µm particle size) and UltiMate™ 3000 HPLC were obtained from Fisher Scientific, UK. Centrifuge 5417R was purchased from Eppendorf UK Limited.

Dermapen®, a microneedling pen, was purchased from ZJchao, China. The microneedles on Dermapen® have a tapered conical structure. The microneedle has a base diameter of 370 µm with a tip radius of 53.4 µm. The distance between the microneedles (pitch) is 620 µm. For the purpose of the permeation study, we selected a microneedle length of 1000 µm and an oscillation speed of 8000 RPM. Dermastamp™, a microneedle stamp, was purchased from Teoxy Beauty, Wuhan, China. PVPVA Kollidon® (vinyl acetate 64 molecular weight 15-20 kDa) was

kindly provided by BASF, Ludwigshafen, Germany. Kollisolv® PEG E 400 and Glycerol were purchased from Merck Life Sciences UK Limited by Scientific Laboratory Supplies Ltd. Carboxymethylcellulose sodium salt high viscosity was purchased from Scientific Laboratory Supplies, UK. OCT media was obtained from VWR International Ltd., Belgium.

Pig skin was used to study the ability of microneedles to promote permeability, rather than ex-vivo human skin. Because unlike human skin, it does not have limited availability and does not need to pass ethical scrutiny. In addition, various studies have highlighted that pig skin is a suitable substitute for human skin. The pig skin samples were taken from a local abattoir of animals raised specifically for food.

The skin samples were collected without any steam cleaning. The skin is then prepared by distilled water washing and drying it with tissues. Full thickness skin is generally used to avoid altering the biomechanical properties of the skin. Afterwards, skin samples are stored at -20 ˚ C and used for six months.

2.3.2 Methods

2.3.2.1 Fabrication of Alpha-Arbutin-loaded polyvinylpyrrolidone-co-vinyl acetate (PVPVA) microneedles

Alpha-Arbutin-loaded PVPVA microneedles were fabricated using polydimethylsiloxane (PDMS) moulds based on the method developed by Sabri et al.[226]. Briefly, the moulds consist of a 10 x 10 array of 300 µm x 300 µm x 1000 µm (W x L x H) obelisk microneedles with tip-to-tip spacing of 800 µm. The microneedle matrixes were prepared by

dissolving 16.2% w/v PVPVA and 2% v/v PEG 400 in HPLC water at room temperature and pressured for one hour. Then, 2% w/w Alpha-Arbutin was added to the polymer solution, which was further degassed for 30 minutes. Afterwards, 150 µl of the polymer solution was pipetted into each PDMS mould using positive displacement pipettes and centrifuged at 4000 revolutions per minute (RPM) for 15 minutes at room temperature to fill the needle cavities. Finally, excessive polymer solution was removed before leaving the needle layers to be dried overnight in a desiccator.

The backing layer of microneedle patches was prepared by dissolving 5.2% w/w sodium carboxymethyl cellulose (CMC) in HPLC water while stirring at 75 °C for two hours. Then, glycerol (0.66% v/w) was added to the backing layer solution to act a plasticizer. 200 µl of backing layer solution was pipetted on top of the needle layers using positive displacement pipettes and centrifuged at 3500 RPM for 10 minutes. The moulds were dried at room temperature for 48 hours in a desiccator. The polymeric microneedles were then demoulded and stored in a desiccator until further use.

2.3.2.2 Visualization of PVPVA microneedles by SEM

Polymeric microneedle images were captured using an optical microscope (Zeiss Axioplan, Germany) and an environmental scanning electron microscopy (ESEM) (FEI Quanta 650) in low vacuum mode to visualize the shape and dimensions of the microneedles. For ESEM imaging, the microneedles were mounted on a metal stub using double-

sided carbon tape prior to imaging.

2.3.2.3. HPLC analysis of Alpha-Arbutin in skin permeation study

2.3.2.3.1 Chromatographic conditions

Hypersil BDS C18 Columns, 150mm L x 4.6mm ID, 3.0µm was used as chromatographic column. The system was operated at a flow rate of 0.5 mL/min and injection volume of 10.00µL. Column temperature was maintained at 30°C and UV detection at λ max = 280nm with an emission wavelength setting. The run time for each sample was 20 minutes. 0.1M acetate buffer (pH 4.0) and methanol in a ratio of 95:5 (v/v) were used as the mobile phase.

2.3.2.3.2. Linearity, LOD and LOQ

The linearity of the method was assessed over a range of concentrations. Twelve different concentrations between 0.1 and 1024 µg/mL were chosen. The calibration curves were obtained by plotting the peak areas against the corresponding Alpha-Arbutin concentrations. The slope, y-intercept, and correlation ccoefficient (R^2) of the curve were determined by linear regression analysis[441].

According to FDA regulations[442], the theoretical limits of detection (LOD) and quantification (LOQ) values for the developed method were calculated using the standard deviation of the response (σ) and slope (S) of the calibration curve according to the following equations :

LOD = 3.3σ/S, LOQ = 10σ/S

2.3.2.4. Skin preparation

Skin samples were prepared from 6-month-old pigs obtained from local abattoirs. The skin was kept at 4 °C for a maximum of 24 hours, the tissue was washed with ultrapure water only, and the hair was trimmed with scissors. Excess subcutaneous fat was removed, and the skin was wrapped in aluminium foil and stored at -20 °C for a maximum of 3 months. The entire full thickness of the skin was used for the Franz cell permeation experiments to prevent alteration of the biomechanical properties of the skin.

2.3.2.5. Franz cell set-up

Prior to permeation studies, skin samples were thawed at room temperature for at least one hour. Afterward, circular skin samples were cut and mounted between the donor and recipient compartments of the Franz-type static diffusion cell device[443] with the dermal side facing downwards and an exposed surface area of 0.64 cm^2 and a recipient compartment volume of 3mL. The trimmed skin samples were placed over the recipient compartment for 15 minutes to allow equilibration prior to skin treatment. The integrity of each skin sample was assessed by resistance using the method and guidelines described by Davies et al.[444], and only skin that yielded resistance readings greater than 10 kΩ was used. PBS solution (pH 7.4) was used as the recipient medium. The water bath conditions needed to be maintained throughout the experiment, such as temperature at 36.5°C. The maximum duration of the study was 24 hours.

2.3.2.6. Permeation of commercial Alpha-Arbutin products using

solid microneedles Dermapen®

Franz cell experiments were performed with three commercial products (HA, AA, and INK) with and without the application of the Dermapen®. Firstly, 200mg of each product was applied to the skin, and 200 ml of distilled water was used as a control. For the microneedles pre-treatment, the Dermapen® (1000 µm, oscillation speed of 8000 RPM) was applied to the skin, followed by the application of the three commercial products. For the post-treatment, three commercial products were applied to the skin first, followed by the application of the Dermapen®. For both pre- and post-treatments, the application time of the Dermapen® was kept to 1 minute with a mild pressure application. The skin was then mounted on Franz cells. Each experiment was run in triplicate to ensure accurate results.

2.3.2.7. Permeation of Alpha-Arbutin-loaded polyvinylpyrrolidone-co-vinyl acetate (PVPVA) microneedles

In order to investigate the utility of dissolving microneedles in enhancing skin permeation of Alpha-Arbutin, Franz cell experiments were performed using Alpha-Arbutin-loaded PVPVA microneedles (DMNs). Prior to assembling the Franz cells, Alpha-Arbutin-loaded PVPVA microneedles were punctured into the skin in quadruplicate for 1 minute using thumb force and 200 ml of distilled water was used as a control. The skin samples were then mounted on Franz cells.

Upon assembling the Franz cells, all the permeation experiments were conducted over a period of 24 hours in a thermostatically controlled water

bath set at 36.5 °C.

2.3.2.8. Post Franz cell skin tissue preparation

After the permeation experiments, the excess liquid was removed and collected from the skin surface by careful application of sponges soaked with 3% v/v Teepol solution. The sponges were pooled for HPLC analysis as a total skin wash. Any formulation which might have spread to the donor chamber was collected by the sponges and stored for HPLC analysis as a donor chamber wash. Upon removing the excess formulation from the skin surface, 15 sequential tape strips were collected from the skin. The amount from the different Franz cell components (skin wash, donor chamber wash, pooled tape strips, and remaining skin after tape stripping) was extracted by the addition of 5, 5, 10, and 5 mL of methanol extraction mixture (methanol 30%: water) respectively. Samples were then vortexed for 1 minute and sonicated for 30 minutes. Then, 1 mL of mixture was collected from each sample. For the receptor fluid, 1 mL of the solution from each Franz cell was collected. All the samples were centrifuged at 4 ºC at 14000 rpm for 10 minutes and then filtered through a 0.22 µm membrane.

2.3.2.9. Visualization of Alpha-Arbutin within the skin by 3D OrbiSIMS

2.3.2.9.1 Sample preparation

The skin samples from the Franz cell experiment in section 2.2.7 were chosen for the visualization analysis. The surface of the skin was

scrubbed with a sponge moistened with distilled water to remove excess formulation. The skin was then scrubbed with a dry sponge. The skin samples were then immediately frozen using liquid nitrogen to avoid morphological distortion and tissue damage caused by autolysis or decay. The skin samples were then placed on a Cryostat (Leica Biosystems, Wetzlar, Germany) for frozen sectioning (CT -24°C, OT -30°C), and 20 µm thick transverse skin sections were cut, with three sections per sample being placed on the slide. For each sample, adjacent 20 µm thick sections were used for standard hematoxylin-eosin staining.

2.3.2.9.2 3D OrbiSIMS imaging analysis

For permeation analysis, skin cross-sections were used. A 3D OrbiSIMS (Hybrid SIMS, IONTOF GmbH, Germany) analysis was performed and for the Orbitrap image acquisition, a 20 KeV Ar3000+ analysis beam with a diameter of 20 µm was used as the primary ion source. Samples were analyzed at room temperature across a 300 × 300 µm area in negative polarity. Ar3000+ primary ions were used with a filament current of 2.30 A with charge compensation performed using a low-energy (-20 eV) electron flood gun. Duty cycle was set to 4.4% and cycle time to 200 µs. Argon gas flooding was in operation to aid with charge compensation, which led to a pressure of $9.0 \times 10\text{-}7$ mbar in the main chamber. The optimal target surface potential was at 136.6 V. Mass spectra were recorded at a resolution of 240,000 at m/z 200 in the mass range of 75 to 1,125 m/z. The automatic gain control (AGC) target was off, with the maximum injection time set at 500 ms. Both data acquisition and the

subsequent data processing were performed using SurfaceLab 7 software (IONTOF GmbH). Orbitrap data was acquired using a Thermo Fisher Orbitrap HF mass spectrometer.

2.3.2.10 Statistical Analysis

All results were reported as mean ± standard deviation ($n \geq 3$). Statistical calculations were performed using Prism8. Statistically, a significant difference is denoted using an unpaired student's t-test (*, $p < 0.05$; **, $p < 0.01$).

2.4 Results and discussion

2.4.1 Formulation and fabrication of dissolving MNs

The Alpha-Arbutin-loaded PVPVA microneedle was successfully fabricated using a two step casting process as previously reported. The rigidity of the needle tips was increased by the introduction of PEG 400. According to previous reports[445], the dissolving microneedles formed from PVPVA and PEG 400 materials have good mechanical strength and puncture capacity, so their properties will not be expanded on in detail here. The backing layer of the microneedles is flexible due to the combination of glycerol and CMC, and as such, demoulding is easily manipulated.

The images of a top view and side view of the Alpha-Arbutin-loaded PVPVA microneedle are illustrated in **Figure 2-1**(a-b). **Figure 2-1**(c) shows an optical microscope side view image of the Alpha-Arbutin-loaded

PVPVA microneedle with needle tip lengths of 1000 nm. As shown in **Figure 2-1**(d-g), the needles have an obelisk design with a base width of 284.2 μm and 276.1 μm. It can also be seen that, this is 10×10 array of microneedles with the tip-to-tip spacing of 800 μm.

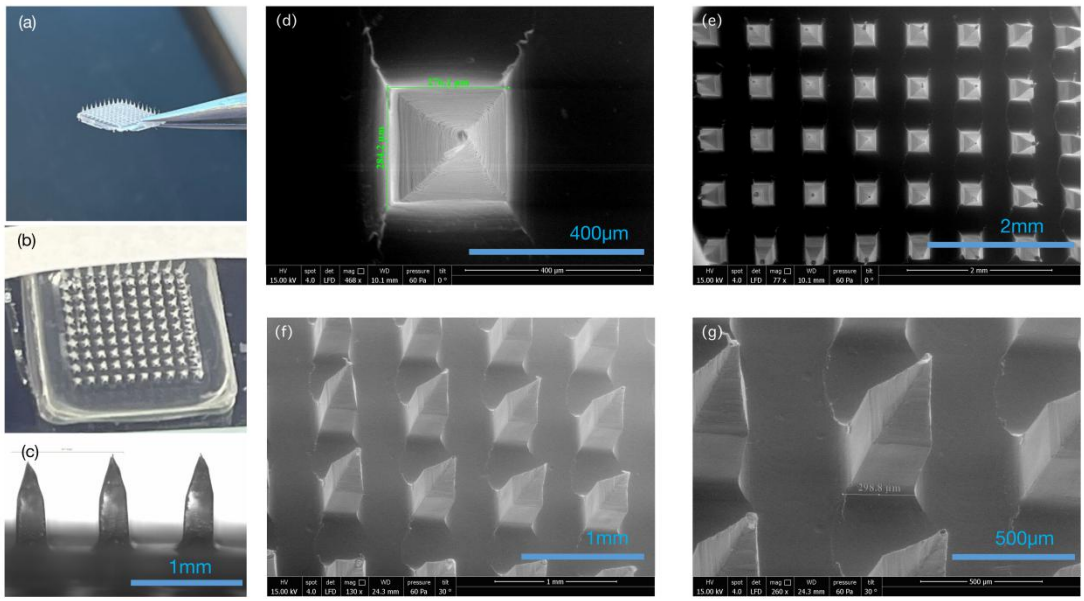


Figure 2-1 Photograph, optical microscopy and scanning electron microscope images of Alpha-Arbutin-loaded PVPVA microneedle (a) Photograph of side view (b) Photograph of top view (c) Optical microscopy image of side view. (d-g) Scanning electron microscope images of Alpha-Arbutin-loaded PVPVA microneedle. (d&e) Top view (f&g) Side view.

2.4.2 HPLC analysis of Alpha-Arbutin in skin permeation study

2.4.2.1 Linearity, LOD, and LOQ

The calibration curves, limits of detection and limits of quantification

for Alpha-Arbutin were determined according to the chromatographic conditions described in section 2.3.2.3.

As shown in Figure 2-2, a calibration curve for Alpha-Arbutin was obtained by selecting 12 points between the concentrations of 0.1 and 1024 μg/mL concentrations. The equation for the relationship between concentration and area was obtained as y = 0.0862x + 0.2359, where the coefficient of determination was 0.9999. The detection limit of Alpha-Arbutin was 0.0646 μg/mL, and the limit of Alpha-Arbutin quantification was 0.1937 μg/mL. This shows that the curves are accurate and the regression effect is significant and credible.

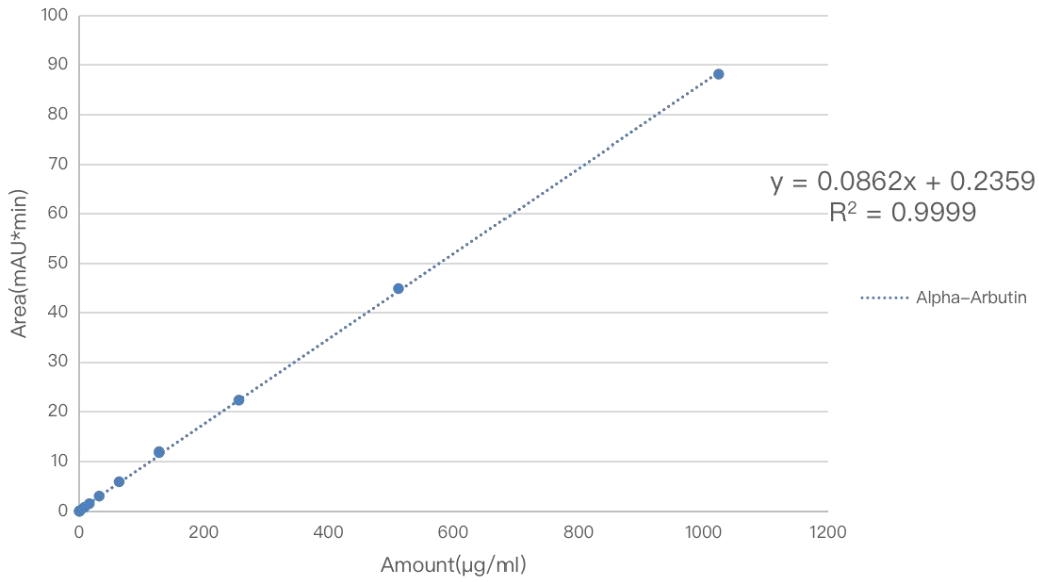


Figure 2-2 Calibration curves for Arbutin and Alpha-Arbutin (a) Calibration curves for arbutin; (b) Calibration curves for Alpha-arbutin Calibration curves for arbutin standards were obtained by selecting 12 points between 0.1 and 1024 μg/ml concentration. And x is concentration of the compounds solution in μg/ml and y is peak area (mAU*min) of the

compound.

2.4.2.2 Alpha-Arbutin skin permeation from commercial products

The mean percentage of permeation of commercial Alpha-Arbutin products in different Franz cell components following a 24-hour permeation test is illustrated in **Figure 2-3**(A). The mean percentage of permeation of Alpha-Arbutin was the highest outside the skin (in donor wash and skin wash) compared to the other Franz cell components.

This indicates that the vast majority of the Alpha-Arbutin failed to penetrate the skin. Indeed, limited drug penetration into the skin was observed, with only about 0.7-1.1% of the active ingredient being found within the remaining skin in the target layer where melanocytes reside. Also, less than 0.02% of Alpha-Arbutin for all three products was able to penetrate through the dermis to reach the receptor compartment (**Figure 2-3**(A, d)). Overall, we found that the Alpha-Arbutin has limited permeation into the skin (tape strips and remaining skin) and across the skin (receptor fluid). This can be attributed to the high hydrophilicity of Alpha-Arbutin that makes it difficult for it to permeate through the hydrophobic stratum corneum, as also reported by Won et al[415]. In Won's study, 2% Alpha-Arbutin eventually resulted in only 0.97 ± 1.76 μg/mL deposited in the epidermis and dermis.

2.4.2.3 Alpha-Arbutin skin permeation from commercial products with Dermapen® pre-treatment

As shown in **Figure 2-3**(B, b), following Dermapen® application pre-treatment, the mean percentage of permeation of Alpha-Arbutin of HA, AA, and INK remaining within the skin was increased by approximately 1.5 times, 2.2 times, and 1.4 times, respectively. The mean percentage permeation of Alpha-Arbutin in the receptor fluid (across the skin) for HA, AA, and INK in **Figure 2-3**(B,c), although increased, remains no more than 0.6% of the total dose administered.

2.4.2.4 Alpha-Arbutin permeation from commercial products with Dermapen® post-treatment

The mean percentage of permeation of commercial Alpha-Arbutin products with Dermapen® application post-treatment in different Franz cell components following 24-hour permeation test is shown in **Figure 2-3**(C).

Following Dermapen® application post-treatment, the mean percentage of permeation of Alpha-Arbutin from the commercial HA formulation in tape strips, remaining skin, and receptor fluid was increased by approximately 9 times, 3 times and 30 times respectively; the mean percentage of permeation of Alpha-Arbutin of AA in tape strips, remaining skin and receptor fluid was increased by approximately 10 times, 14 times and 74 times respectively; and the mean percentage of permeation of Alpha-Arbutin of INK in tape strips, remaining skin, and receptor fluid was increased by approximately 6 times, 17 times and 261 times respectively. This indicates the permeation into the skin (tape strips and remaining skin)

was improved. This provides a better opportunity for Alpha-Arbutin to act as a skin-lightening agent and treat hyperpigmentation disorders. However, attention needs to be paid to the fact that the proportion permeating across skin into the receptor fluid was also increasing in parallel.

2.4.2.5. Alpha-Arbutin release of Alpha-Arbutin-loaded Polyvinylpyrrolidone-Co-Vinyl Acetate (PVPVA) microneedle

The mean percentage of permeation of Alpha-Arbutin with Alpha-Arbutin-loaded PVPVA microneedle application in different Franz cell components following 24-hour permeation test is illustrated in **Figure 2-3**(D).

Following Alpha-Arbutin-loaded PVPVA microneedle application, since the concentration of the drug in the soluble microneedle and in the commercial product was controlled to be the same at 2% w/w, comparisons could be made between them. The mean percentage of permeation of Alpha-Arbutin remaining within skin was a 6-fold increase compared to the group without microneedles application. This indicates that the permeation into the skin (tape strips and remaining skin) was improved. In addition, the drug content of the receptor fluid (transdermal delivery) was also significantly higher, up to 1%.

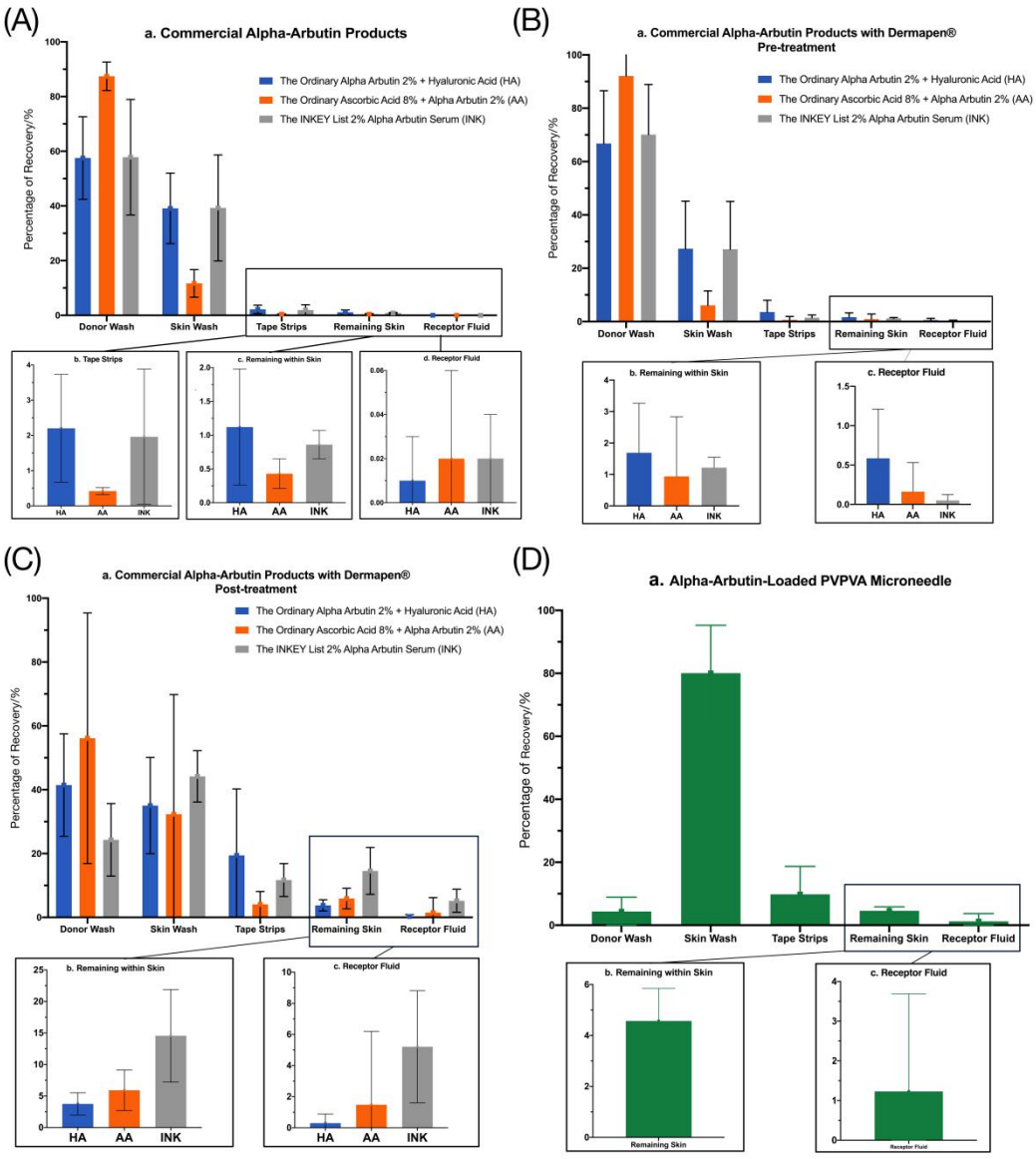


Figure 2-3 HPLC analysis of mean percentage of permeation of (A)commercial Alpha-Arbutin products, n=3; (B)commercial Alpha-Arbutin products with Dermapen® pre-treatment, n=6; (C)commercial Alpha-Arbutin products with Dermapen® post-treatment, n=6; and (D) Alpha-Arbutin-loaded PVPVA microneedle application (n=4), in different Franz cell components (donor wash, skin wash, tape strips, remaining skin and receptor fluid) following 24-hour permeation test. The insets provide details on the mean percentage of permeation of commercial Alpha-

Arbutin products in (A) Tape strips (b), Remaining within skin (c) and Receptor fluid (d). (B-D) Remaining within skin (b), and Receptor fluid (c). The data are expressed as means ± SD (n≥3). HA stands for The Ordinary Alpha Arbutin 2% + Hyaluronic Acid; AA stands for The Ordinary Ascorbic Acid 8% + Alpha Arbutin 2%; INK stands for The INKEY List 2% Alpha Arbutin Serum.

2.4.2.6 Comparison between different types of microneedles.

The statistical comparison between the percentage of permeation of Alpha-Arbutin in the remaining skin shows that the percentage of permeation of Alpha-Arbutin with Dermapen® application pre-treatment has no significant difference compared to the group without microneedle. For the solid microneedles post-treatment, a significantly higher percentage of permeation of Alpha-Arbutin in the formulation of HA and INK was found compared to the percentage of permeation of Alpha-Arbutin without microneedle, as illustrated in **Figure 2-4**.

In addition, the statistical comparison between the percentage of permeation of Alpha-Arbutin in the remaining skin shows that the percentage of permeation of Alpha-Arbutin with Alpha-Arbutin-loaded PVPVA microneedle application was also significantly higher than the percentage of permeation of Alpha-Arbutin without microneedle as illustrated in **Figure 2-4**.

Theoretically, the percentage of permeation of Alpha-Arbutin should have a greater improvement following dissolving microneedle (DMNs)

application as all the drugs can be loaded and released into the skin[416,417] whereas solid microneedle application cannot deliver the full dose. However, when comparing the percentage of permeation of Alpha-Arbutin with Dermapen® and Alpha-Arbutin-loaded PVPVA microneedle application, there is no significant difference between both treatment modalities, as illustrated in **Figure 2-4**.

Although the percentage of permeation of Alpha-Arbutin with Dermapen® application is only slightly different compared with the percentage of permeation of Alpha-Arbutin with Alpha-Arbutin-loaded PVPVA microneedle application, the standard error of the mean is higher. This indicates that the results are not consistent and may vary between each application[418], which may be due to the drug loss caused by the Dermapen® during application.

Normally, solid microneedle is used as skin pre-treatment prior to drug application, and the channels generated in the dermal layer of the skin immediately recoil and reseal after microneedle application[419]. Therefore, commercial solid steel microneedle was used after drug application in this study. However, a large amount of the formulation is left in the microneedle cartridge when solid microneedles are used for post-treatment, as shown in Appendix **Figure A-1**. This leads to a large amount of composition being wasted and reduces the permeation rate of the drug. Furthermore, as different formulations have different viscosities for the needle, the amount left in the cartridge is varied, as shown in Appendix **Table A-1**. Therefore, if solid microneedles are to be utilized for

reprocessing in the future, the formulation needs to be improved to decrease the likeliness of it remaining inside the cartridge. This also gives a reason to explore new delivery methods, such as dissolvable microneedles.

Since both CMNs and DMNs are able to pierce the outermost layer of skin and create microchannels reaching the depth of the dermal papillae, an increase in the percentage of Alpha-Arbutin penetration in the receptor fluid was expected and obserived. Higher amounts of Alpha-Arbutin bypassed the skin barriers through the microchannels created and were presented in the receptor fluid[448]. However, these results were not as we hoped, as the excessive amount of Alpha-Arbutin that crosses the skin may enter the blood circulation. Overall though, CMNs post-treatment has a higher transdermal delivery rate compared to DMNs.

Overall, from the comparison of the percentage of permeation of Alpha-Arbutin in remaining skin following the three treatment modalities, as illustrated in **Figure 2-4**, microneedles in general improve the permeation of Alpha-Arbutin into the skin. This provides a good opportunity to improve Alpha-Arbutin's effect as skin-lightening agent. However, in terms of compliance and safety, DMNs offer better prospects.

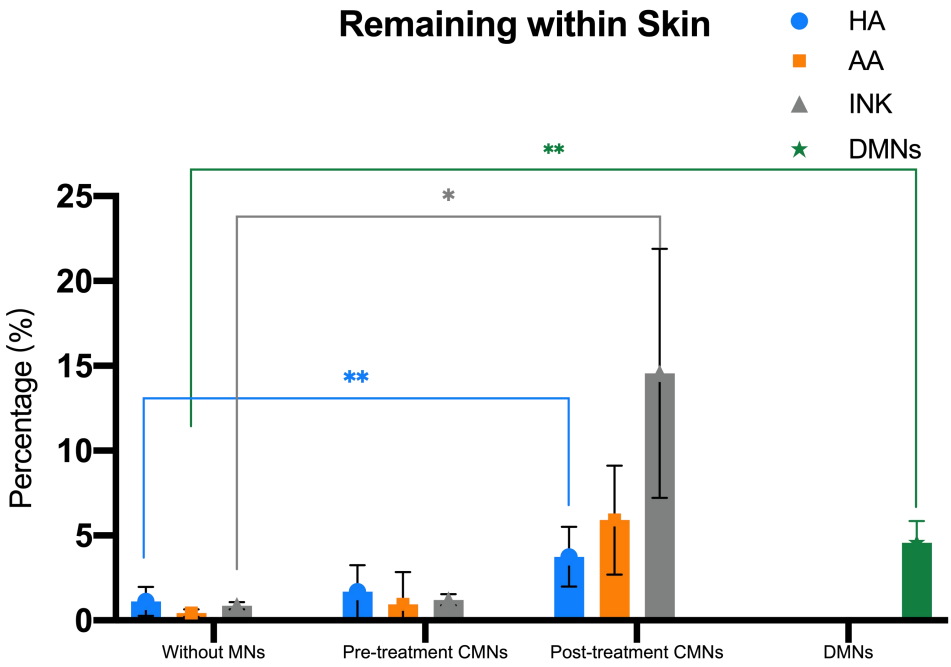


Figure 2-4 HPLC analysis of mean percentage of Alpha-Arbutin without microneedles (Without MNs), with Dermapen® pre/post treatment(CMNs) and with Alpha-Arbutin-loaded PVPVA microneedles(DMNs) remaining within skin after a 24-hour permeation test. The data are expressed as means ± SD (n=3 without microneedle; n=6 with Dermapen®; n=4 with Alpha-Arbutin-loaded PVPVA microneedle). Unpaired student's t-test was used to determine statistical significance(* indicates $p < 0.05$; ** indicates $p < 0.01$; no significant difference (ns) indicates $p > 0.05$).

2.4.3 Visualisation of Alpha-Arbutin within the skin by 3D OrbiSIMS

Although the use of HPLC analysis provides useful insights into the permeation of compounds within the skin, it is unable to provide more precise information on specific skin layers. Therefore, using skin sections in combination with 3D OrbiSIMS imaging is required to investigate the

depth distribution of Alpha Arbutin within the skin. Due to the variation in pig skin thickness, it is important to identify the thickness of the epidermis based on sections from the adjacent site. For example, **Figure 2-5** shows that the thickness of the stratum corneum at this site is 10-15 μm, and the thickness of the epidermis is 20-150 μm. The melanocytes containing tyrosinase are located between the epidermis and the dermis in a structure with only one layer of cells, located around 150-160 μm from the surface of the skin.



Figure 2-5 HE-stained cross-section of DMNs dosed porcine dermatomed skin (4 mm thick). The epidermal thickness of the skin sample is labelled on the image. Image from 20μm Cryocut tissue sections at a 10-fold magnification.

According to Nichola[451], palmitic acid ($C_{16}H_{31}O_2^-$) and cholesterol sulfate ($C_{27}H_{45}SO_4^-$) can be used to localize the uppermost layers of the stratum

corneum and epidermis. Alternatively, PO_3^-, which is usually found in the epidermis and dermis[440], can also be used to help with localization, as shown in **Figure 2-6** (I). In our study, high-intensity Arbutin fragment ions were detectable by OrbiSIMS analysis, with the fragment molecular ion of Arbutin ($C_{12}H_{16}O_7$) being $C_{12}H_{15}O_7^-$ (**Figure 2-6** II,d-f). It is clear that most of the Arbutin in the DMNs group is cleaved into fragments by the electron flood gun. The ion $C_6H_4O_2^-$ (**Figure 2-6** II, a-c) was found to have a significant signal intensity in the two samples, while it was barely visible on the blank skin group, indicating that $C_6H_4O_2^-$ is an exogenous substance and is not part of the ionic signal fragment present in the skin itself. Arbutin is a compound of hydroquinone and D-glucose. Some studies[124] suggest that arbutin will lose a glucose and break down naturally into hydroquinone ($C_6H_6O_2$) on the skin. It explains why the signal of ion $C_{12}H_{15}O_7^-$ is missing and leads to a logical inference that $C_6H_4O_2^-$ could be used as a representative ionic fragment of Alpha-Arbutin and could be used as a marker for the localized compound.

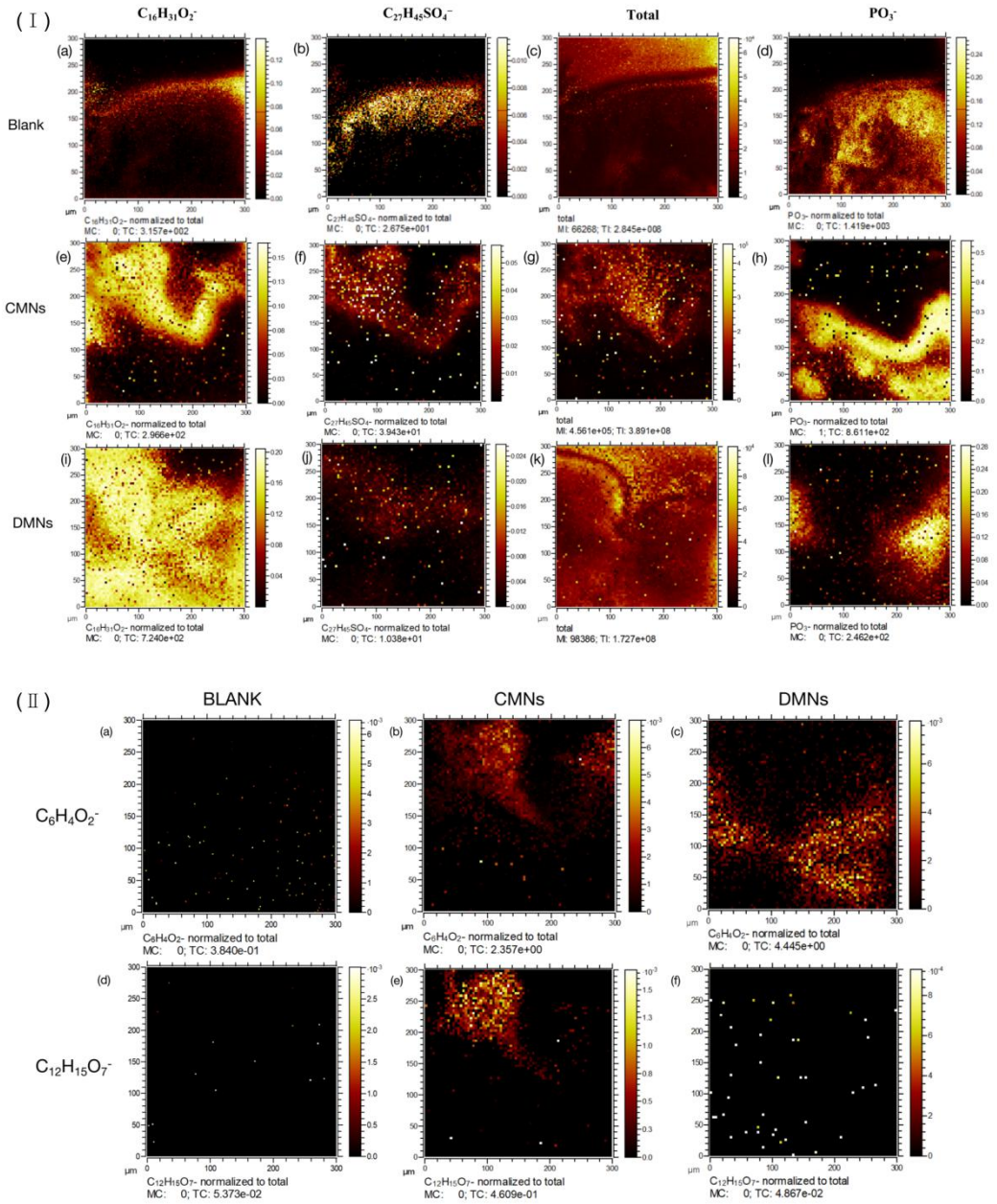


Figure 2-6 Negative polarity ion images of 3D OrbiSIMS from various fragment ions of the skin cross-section dosed by Alpha-Arbutin-Loaded PVPVA microneedles (DMNs) and Commercial Alpha-Arbutin Products with Dermapen® Application post-treatment(CMNs) in full thickness porcine skin (4 mm thickness), while water was used as blank group. The Field of View is 300.0 μm, and Pixelsize is 4.0 μm, MC stands for

maximum ion count per pixel and TC total ion count for the specific ion of interest. (I)The ion images illustrate the 2D spatial distribution for the following molecular ions: (a, e, i) Palmitic acid ($C_{16}H_{31}O_2^-$); (b,f,j) Cholesterol sulfate ($C_{27}H_{45}SO_4^-$); (c,g,k) Total ion; (d,h,l) Phospholipid marker (PO_3^-). And (a-d) is in the blank group, (e-h) in the CMNs group, and (i-l) in the DMNs group. All ion images have been normalized to the total ion image. (II) The ion images illustrate the 2D spatial distribution for the molecular ions of Alpha-Arbutin: (a&d) Alpha-Arbutin ($C_{12}H_{15}O_7^-$ and $C_6H_4O_2^-$) in the blank group (b&e); Alpha-Arbutin ($C_{12}H_{15}O_7^-$ and $C_6H_4O_2^-$) in CMNs group; (c) Alpha-Arbutin ($C_{12}H_{15}O_7^-$ and $C_6H_4O_2^-$) in DMNs group. All ion images have been normalized to the total ion image.

The ability to enhance the intradermal accessibility of Alpha-Arbutin using solid microneedle augmentation requires further definitive localization. As can be seen in **Figure 2-7** (a), the Alpha-Arbutin fragment signal overlaps substantially with molecular ion Cholesterol sulfate ($C_{27}H_{45}SO_4^-$), indicating that it is located primarily in the stratum corneum and upper epidermis and does not enter deeper parts of the skin. In contrast, the ionic signal of Alpha-Arbutin (green) in **Figure 2-7** (b) clearly appears below the stratum corneum. It overlaps with the position of the PO_3^- ion, indicating that it is distributed in the epidermis and located in the lower and middle epidermal layers and thus shows that DMNs have a significant enhancing effect on the permeation of this compound.

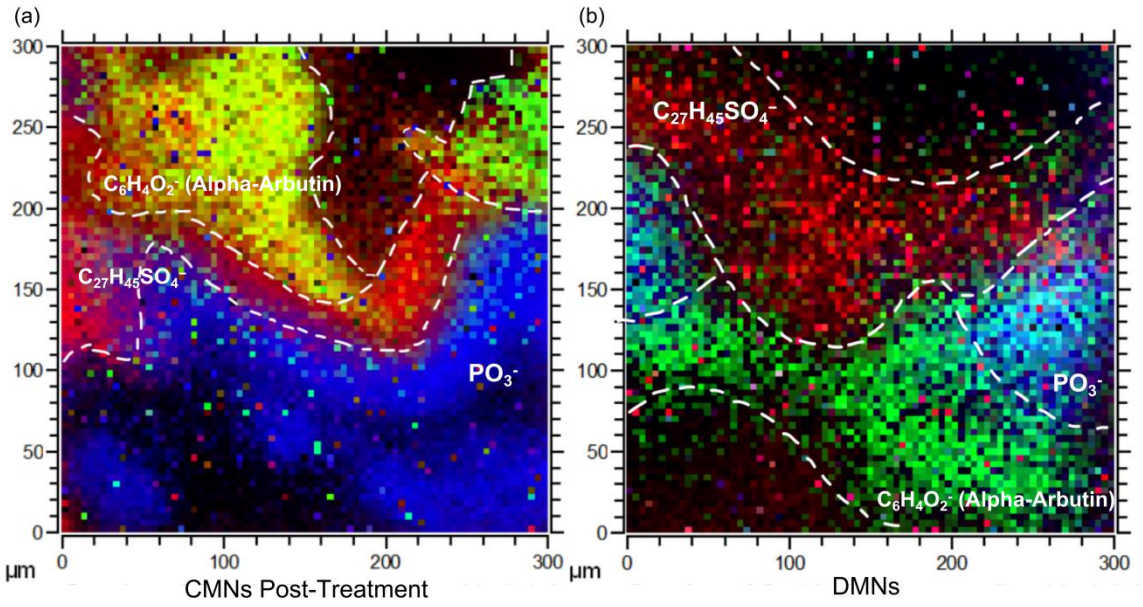


Figure 2-7 Images of 3D OrbiSIMS from various fragment ions overlay of the skin cross-section dosed by Commercial Alpha-Arbutin Products with Dermapen® Application post-treatment (a) and Alpha-Arbutin-Loaded PVPVA microneedles (b) in dermatomed porcine skin (4 mm thickness). The Field of View: 300.0 µm and Pixelsize: 4.0 µm. The ion images illustrate the 2D spatial distribution for the overlay of different molecular ions. Three color overlay between ion images; Stratum corneum and top of epidermal (cholesterol sulfate fragment, $C_{27}H_{45}SO_4^-$, red), epidermal (phospholipid marker, PO_3^-, blue) and Alpha-Arbutin fragment ($C_6H_4O_2^-$, green).

2.5. Conclusion

The permeation of Alpha-Arbutin through skin from three different commercial products was evaluated by HPLC, and for the first time,

OrbiSIMS was used to visualize the permeation of Alpha-Arbutin within the skin. In the absence of microneedles, a low percentage of permeation of Alpha-Arbutin was observed due to its high hydrophilicity.

Both solid microneedle post-treatment and dissolving polymer microneedles loaded with Alpha-Arbutin improved Alpha-Arbutin skin permeation as analysed by HPLC. Furthermore, the combination of 3D OrbiSIMS and skin cross-section analysis was used for the first time to evaluate the distribution of Alpha-Arbutin within the skin by 2D high-resolution imaging techniques, demonstrating the effectiveness of dissolving polymeric microneedles in improving the permeation of Alpha-Arbutin to the epidermal junction where melanocytes reside. Overall, the combination of HPLC results and OrbiSIMS image show that dissolving polymeric microneedles are more effective than solid microneedles at reaching the target, based on the same effective dose (2%). Moreover, in terms of compliance and safety, dissolving polymeric microneedles offer much better prospects. Thus, this study suggests that dissolving polymeric microneedles are a promising delivery system compared to solid microneedles to facilitate targeted intradermal delivery of Alpha-Arbutin for the treatment of skin hyperpigmentation disorders.

Chapter 3. Design, Synthesis and Biological Evaluation of Novel Hybrids Containing Dihydrochalcone as Tyrosinase Inhibitors to Treat Skin Hyperpigmentation

Songtao Xue,[‡,#] Zhiwei Li,[†,#] Xiaotong Ze,[‡] Xiuyuan Wu,[‡] Chen He,[‡] Wen Shuai,[‡] Maria Marlow,[†] Jian Chen,[Δ] David Scurr,[†,*] Zheying Zhu,[†,*] Jinyi Xu,[‡,*] Shengtao Xu[‡,Δ,*]

[‡]School of Pharmacy, China Pharmaceutical University, 639 Longmian Avenue, Nanjing, 211198, P. R. China

[†]School of Pharmacy, The University of Nottingham, University Park Campus, NG7 2RD, UK.

[Δ]Department of Hepatobiliary Surgery, The First People's Hospital of Kunshan, Suzhou, 215132, P. R. China

Author Contributions

The manuscript was written through contributions of all authors.

Zhiwei Li and [#]Songtao Xue contributed equally to this study.

The work done by Songtao Xue is in Section 3.3.1 Chemistry synthesis; 3.3.2 Mushroom TYR inhibitory activity of tested compounds; 3.3.6 Western blotting and Appendix B.

This chapter has been published in the *Journal of Medicinal Chemistry*

Although in the previous chapter, optimisation solutions were provided regarding the permeability of the existent tyrosinase inhibitor Alpha-Arbutin. Through a holistic approach, it was concluded that dissolving polymeric microneedles are a promising delivery system capable of facilitating intradermal delivery.

However, as the physico-chemical properties of Alpha-Arbutin are inherently flawed, and as all other existing melanin-reducing agents have some drawbacks to a greater or lesser extent, the development of a new effective melanin-reducing agent is necessary and urgent. As a key rate-limiting enzyme in the melanogenesis process, TYR has become the most important target for melanogenesis inhibition. Therefore, in this chapter 3, we will detail about the synthesis and the structure of new tyrosinase inhibitors and evaluate the medicinal potential of the new compounds by their biological activity and penetration capacity.

3.1 Abstract

Excessive melanin deposition may lead to a series of skin disorders. The production of melanin is carried out by melanocytes in melanosomes through a complex process called melanogenesis, in which the enzyme tyrosinase performs a key role. In this work, we identified a series of novel tyrosinase inhibitor hybrids with a dihydrochalcone skeleton and resorcinol structure, which can inhibit tyrosinase activity to reduce the melanin content in the skin. Of which, compound **11c** possessed the most potent activity against tyrosinase with the IC_{50} values at nanomolar concentration ranges, gratified antioxidant activity and showed low cytotoxicity. Furthermore, *in vitro* permeation tests, supported by HPLC analysis and 3D OrbiSIMS imaging visualisation, revealed the excellent permeation ability of **11c**, which is able to well permeate through the skin and is accommulated in the basal layer perfectly, targeting melanocytes in the skin. More importantly, compound **11c** could reduce the melanin content on UV-induced skin pigmentation in a guinea pig model *in vivo*. Herein, the present results suggested that compound **11c** may serve as a promising potent tyrosinase inhibitor for the development of a potential therapy to treat skin hyperpigmentation.

3.2 Introduction

Hyperpigmentation is a common skin disorder nowadays, which refers to the localized darkening of the skin due to an increase in melanin.[1] Melanin is an irregular light-absorbing substance produced by

melanocytes located in the basal layer of the epidermis.[2] While melanin can protect human skin from excessive ultraviolet radiation (UVR) and environmental pollutants, excessive melanin accumulation can lead to various of acute skin disorders, such as freckles, sun rash and chloasma,[3–6] as well as skin cancer[7] and post-inflammatory melanosis.[8] As hyperpigmentation such as melasma is functionally reversible, long-term treatment can prevent from more severe pigmentation.[9,10]

The pathogenesis of hyperpigmentation is generally thought to be related to genetic background, UV exposure and altered inbody hormone levels.[11] The current treatment for this type of disorder is generally topical. There are two main objectives, one is to inhibit melanin production, and the other is to inhibit melanin transport. The inhibition of melanin production is the main focus of research.

The molecular mechanism for small-molecular compounds to inhibit melanosynthesis usually involves the inhibition of melanocyte inducing transcription factor (MiTF).[12] Since melanogenesis is activated through the regulation of several intracellular signalling pathways, including Wnt/β-catenin pathway,[13] NO pathway,[14] MAPK pathway,[15] PI3K/Akt pathway, cAMP/MiTF-M signaling pathway[16] and MC1R/α pathway.[17] MiTF is an integral regulator of these five major signalling pathways and plays a critical role in the control of gene expression of the enzymes tyrosinase (TYR), tyrosine-related protein 1 (TYRP-1) and tyrosine-related protein 2 (TYRP-2).[12]

Melanin production involves complex synthetic pathways, including the

combination of enzymes and chemical catalytic reactions, in which TYR is a key rate-limiting enzyme. Moreover, TYR is expressed only by melanocytes, where melanin is synthesized.[18] As a result, inhibiting TYR can reduce melanin production in cells without toxic side effects.[19]

As shown in **Figure 3-1**, in the process of melanin synthesis, the active sites of TYR are in three states: reduced state, oxidation state and deoxidation state. The main difference between them lies in the oxidation state of copper ions.[20] In the presence of monophenol oxidase, deoxy TYR (E_{deoxy}) binds with oxygen to form oxidized TYR (E_{oxy}), and then E_{oxy} binds with L-Tyrosine (**1**) to further catalyze the formation of L-DOPA (**2**). In the presence of diphenol oxidase, E_{oxy} loses an oxygen atom to form reduced TYR (E_{met}), and L-Dopa is oxidized into dopaquinone (**3**). Two adjacent copper ions are bridged at the active site by water (hydroxyl) ligands. TYR exists mainly in the form of E_{met}, which cannot oxidize monophenolic compounds (such as L-Tyrosine) and needs to be reduced to E_{deoxy} by L-DOPA before tyrosine oxidation.[19]

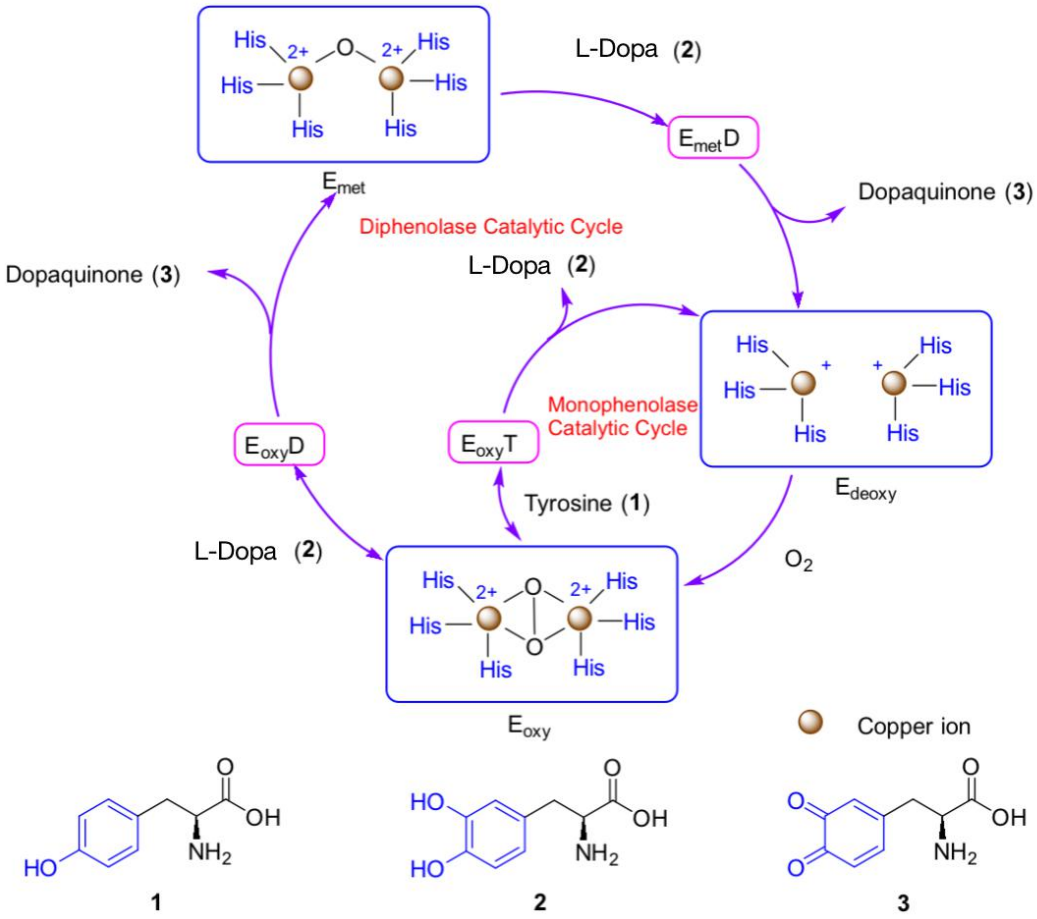


Figure 3-1. Catalytic cycle of TYR: catalytic cycle of monophenol oxidase and bisphenol oxidase. Three types of TYR are E_{oxy}, E_{met}, and E_{deoxy}, respectively. $E_{oxy}T$, $E_{oxy}D$, and $E_{met}D$ are E_{oxy}-tyrosine, E_{oxy}-dopamine, and E_{met}-dopamine complexes, respectively. Sphere shape represents copper ions with different oxidation states.

Nowadays, groups of compounds with TYR inhibitory activity have been developed, which can be divided into resveratrol analogues,[21–26] phenylthiourea analogues,[27–32] peptides[33–34] and flavonoids.[35–38] Although most of the inhibitors targeting TYR are proven to be effective *in vitro*, only a few have been in the clinical stage because of low bioavailability,

non-negligible skin irritation or poor stability. These in clinically used TYR inhibitors have been found to reduce skin pigmentation or cure skin disorders (**Figure 3-2**), such as hydroquinone (**4**),[39] arbutin (**5**),[40] azelaic acid (**6**),[41] L-ascorbic acid (**7**),[42] ellagic acid (**8**),[43] and kojic acid (**9**).[44] They have been mainly used in the cosmetics, with some side effects, such as low skin permeation, instability, high cytotoxicity and carcinogenicity.[45–48] Based on these factors, their applications are limited. Therefore, it is essential to develop more effective new agents with low toxicity and high skin permeability for the treatment of skin hyperpigmentation.

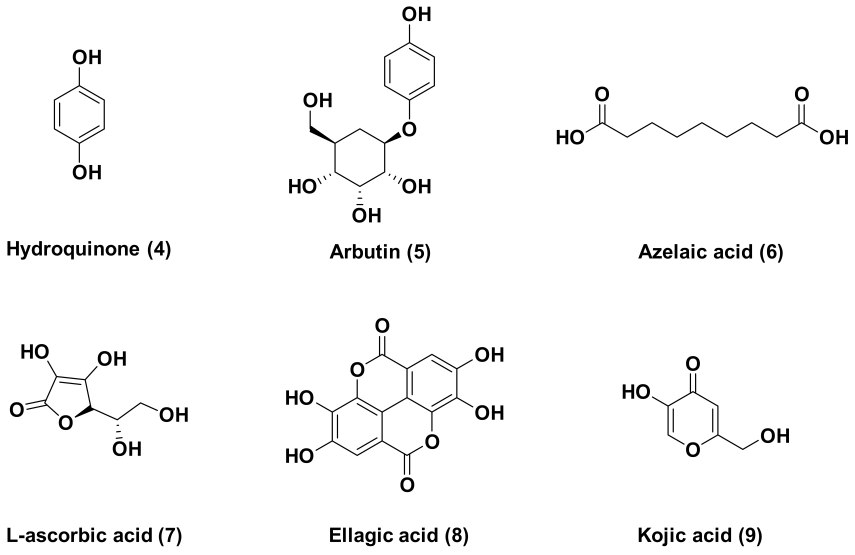


Figure 3-2. Structures of commercially available TYR inhibitors.

Dihydrochalcone (**10**) compounds belong to open-chain flavonoids with the structural skeleton of 1,3-diphenylacetone.[49] They have a variety of

biological activities, i.e., hypoglycemia, antioxidation, anti-tumor, hypopigmentation, and anti-inflammation. In this study, dihydrochalcone moiety is chosen as the synthetic backbone, aiming design and discovery of superior novel tyrosinase inhibitors. As reported previously,[45,46,50,51] the structure of resorcinol is the key pharmacophore of TYR inhibitors, and compounds containing this group have good TYR inhibitory activity. In order to obtain more effective tyrosinase inhibitors with better permeability, this study is sought to tackle this problem through design and synthesis of a series of novel dihydrochalcone hybrids by introducing resorcinol structure into the skeleton of dihydrochalcone (**Figure 3-3**) to explore the SAR of TYR inhibitors and identify a novel candidate agent for the potential treatment of skin hyperpigmentation.

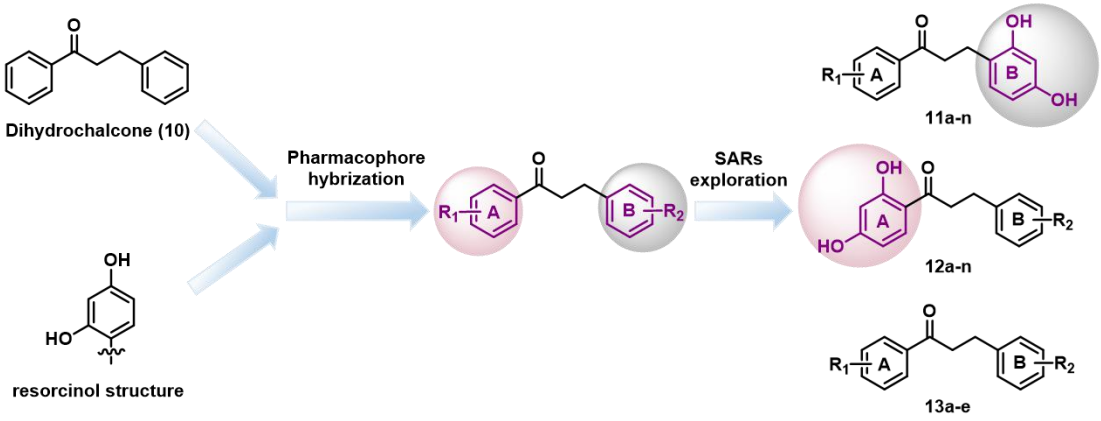


Figure 3-3. Design strategy of novel dihydrochalcone hybrids as TYR inhibitors.

Hererin, we would like to report the design, synthesis and biological

evaluation of these novel hybrids containing dihydrochalcone and resorcinol moieties. Their activity will be assessed in the *in vitro* enzyme and cell models. The most potent compound will be selected and assessed comprehensively using High Performance Liquid Chromatography (HPLC) analysis and 3D Orbitrap Secondary Ion Mass Spectrometry (OrbiSIMS) imaging to visualise and analyze the permeability of the compound. The effect of prophylaxis and repair will be assessed in the guinea pig skin models after topical administration.

3.3 Methods

3.3.1 Chemical synthesis

11a–n. A two-neck flask was charged with compounds **17a–n**, pentamethylbenzene (1.5 eq. per benzyl to be removed) and dry DCM. Under the protection of Ar at 0 ℃ (the intermediate without methoxyl) or -78 ℃ (the intermediate with methoxyl), inject 1 M BCl_3 (1.5 eq. per benzyl to be removed) into the flask, the solution turned orange and reacted for 20 min. After the reaction was completed, water was added to quench the reaction. Diluted with EtOAc and water, the biphasic solution was extracted three times with EtOAc. The combined organics were washed with brine, dried over anhydrous Na_2SO_4, and concentrated in vacuo. Purification of the residue by column chromatography with DCM/MeOH to give the target compounds **11a–n** with moderate yields.

*1,3-Bis(2,4-dihydroxyphenyl)propan-1-one (**11c**).* Yield 64.2%, yellow oil. ^{1}H NMR (300 MHz, DMSO-d_6) δ 12.71 (s, 1H), 9.25 (s, 1H), 9.02 (s, 1H), 7.78 (d, J = 8.7 Hz, 1H), 7.17 (d, J = 25.3 Hz, 2H), 6.85 (s, 1H), 6.28 (m, 2H), 6.12 (s, 1H), 3.10 (s, 2H), 2.73 (d, J = 8.1 Hz, 2H); ^{13}C NMR (75 MHz, DMSO-d_6) δ 205.0, 165.2, 164.8, 157.1, 156.3, 133.4, 130.6, 117.8, 112.9, 108.6, 106.4, 102.9, 92.5, 29.5, 25.4; HR-MS (ESI) *m/z*: calcd for $C_{15}H_{14}O_5$ $[M-H]^-$ 273.0768, found 273.0767; Purity: 99.671% (by HPLC).

*3-(2,4-Dihydroxyphenyl)-1-(4-hydroxy-3-methoxyphenyl)propan-1-one (**11m**).* Yield 63.2%, pink solid. ^{1}H NMR (300 MHz, MeOD) δ 7.57 (d, J = 7.7 Hz, 2H), 6.84 (dd, J = 11.8, 8.1 Hz, 2H), 6.29 (d, J = 2.4 Hz, 1H), 6.20 (dd, J = 8.2, 2.4 Hz, 1H), 3.89 (s, 3H), 3.15 (t, J = 7.7 Hz, 2H), 2.85 (t, J = 7.7 Hz, 2H); ^{13}C NMR (75 MHz, MeOD) δ 200.7, 156.4, 155.8, 152.3, 147.65, 130.2, 128.6, 123.3, 118.6, 114.5, 110.8, 106.0, 102.1, 54.9, 38.7, 19.5; HR-MS (ESI) *m/z*: calcd for $C_{16}H_{16}O_5$ $[M-H]^-$ 287.0925, found 287.0922; Purity: 95.521% (by HPLC).

For the rest of the chemical synthesis and the molecular docking method refer to Appendix B.

3.3.2 Mushroom TYR inhibitory activity of tested compounds

We analyzed the TYR inhibitory activity of target compounds based on methods reported in the literature[58] with minor modifications. Compounds were dissolved in DMSO, prepared as a 10 mM stock solution, and diluted to the desired concentration with 1×PBS at pH 6.8 (8 concentration gradients were set for each compound). TYR lyophilized powder and substrates (L-DOPA and L-Tyrosine) were dissolved in PBS, respectively,

to prepare 300 U/mL TYR solution and 2 mM L-DOPA solution or 1 mM L-Tyrosine solution. The total reaction volume was 200 μL, that was, 80 μL of PBS, 20 μL of sample and 60 μL of TYR solution were added to a 96-well plate, pre-incubated at 37 ℃ for 20 min, and then 40 μL of substrate solution was added to it, and pre-incubated at 37 ℃ for 5 min (L-DOPA) or 10 min (L-Tyrosine). Afterwards, absorbance at 490 nm was measured immediately with a microplate reader, PBS solvent used as blank control, and measured three times in parallel.

3.3.3 Cytotoxicity of 11c and 11m

B16F10 and A375 cells were used for determination of cytotoxicity of representative compounds **11c** and **11m**. The cells were cultured in DMEM high glucose medium containing 10% fetal bovine serum. The cells in logarithmic growth phase were digested, counted, suspended, and seeded into 96-well plates at a rate of 3×10^3 cells/well. After 24 h of culture, the compound solutions were added to the culture to make final concentrations of the compound at 5 μM, 10 μM and 50 μM for cell B16F10; 50 μM for cell A375. After incubatation at 37 ℃ in 5% CO_2 for 72 h, 20 μL of 5 mg/L MTT was then added to the culture. After incubation in the incubator for 4 days, the culture medium was sucked away, and methylzan was dissolved with 150 μL DMSO. The absorbance at 490 nm was measured with a microplate reader.

3.3.4 TYR inhibitory activity of 11c and 11m

The B16F10 and A375 cells in the logarithmic growth phase were

digested, resuspended, and counted, then seeded into 24-well plates at a rate of 3 × 10^4 cells/well, and incubated at 37 ℃ in a 5% CO_2 incubator for 24 h. 1 μM α-MSH was added to the blank control group, positive control group and experimental groups. For cells B16F10, the positive control group was treated with 25 μM kojic acid, the experimental groups was treated with 5, 10 and 25 μM **11c** or **11m**, respectively. For cells A375, the positive control group was treated with 20 μM kojic acid, the experimental groups were treated with 20 μM **11c** and **11m.** And the blank group was added with DMSO (< 0.3%). After 24 h of incubation, the cells were collected into centrifuge tubes, washed twice with 1 mL of PBS, and then added 100 μM of 1% TritonX-100 (with 50 mM PBS, pH 6.8) containing 0.1 mM PMSF to lyse cells. After incubating at -80 ℃ for 30 min, let it thaw at room temperature, then centrifuged at -4 ℃ at 12×10^3 rpm for 15 min, took 80 μL of the supernatant and added it to a 96-well plate, and then added 20 μL of bottom to the 96-well plate. The substance L-DOPA (2 mM) was transferred to 37 ℃ to react for 1 h, and its absorbance at 490 nm was measured with a microplate reader every 10 min. The experiment was repeated three times in parallel. % TYR activity = $OD_{experimental\ group}/OD_{control\ group}$ × 100%.

3.3.5 Inhibition of 11c and 11m on melanin content

The B16F10 cells and A375 cells in the logarithmic growth phase were digested, resuspended, and counted, then seeded into 24-well plates at a rate of 3×10^4 cells/well, and incubated at 37 ℃ in a 5% CO_2 incubator for 24 h. 1 μM α-MSH was added to the blank control group, positive control

group and experimental groups. For cells B16F10, the positive control group was treated with 25 μM kojic acid, the experimental groups was treated with 5, 10 and 25 μM **11c** and **11m**, respectively. For cells A375, the positive control group was treated with 20 μM kojic acid, the experimental groups was treated with 20 μM **11c** or **11m.** And the blank group was added with DMSO (< 0.3%). After incubating in the incubator for 24 h, the cells were collected into centrifuge tubes, washed twice with 1 mL PBS, and then added with 100 μL of 1 M NaOH, incubated at 60 ℃ for 1 h, and the supernatant was taken into a 96-well plate, the absorbance at 405 nm was measured with a microplate reader. The experiment was repeated three times in parallel. % Melanin content=$OD_{experimental\ group}/OD_{control\ group} \times 100\%$.

3.3.6 Western blotting

B16F10 cells (2×10^5 cells/well) were cultured in DMEM medium with 10% FBS and 1% penicillin/streptomycin (*v*/*v*) for 24 h and then incubated with various concentrations of compounds or DMSO for 72 h in six-well plates. Then, the cells were washed twice with ice-cold PBS and subsequently scraped in RIPA lysis buffer (Beyotime, China). The cell pellets were lysed on ice for 30 min, followed by centrifugation at 4 ℃ for another 30 min (13, 000 rpm/min) and the supernatant was quantified with BCA kit (Beyotime, China). The western blot operation process has been written in great detail in previous research. The specific primary antibodies used included those for TYR (1:1000, Abcam, Cambs, UK), MiTF (1:1000; Cell Signaling Technology, Beverly, MA), and GAPDH

(1:10000; Proteintech, Wuhan, China). The secondary antibody was HRP-conjugated goat anti-rabbit-IgG (1:10000; Biosharp Beijing, China). Immunoreactive bands were visualized by enhanced chemiluminescence using ECL plus (FUDE biology technology, Hangzhou, China) and Bio-Rad Versadoc (Tanon, Shanghai, China).

3.3.7 HPLC analysis of 11c and kojic acid in skin permeation study

Use Hypersil BDS C18 Columns, 150 mm L x 4.6 mm ID, 3.0 μm as chromatographic column. The system operated at a flow rate of 0.5 mL/min. Injection volume is 10.00 μL. Column temperature is kept at 30 °C, UV detection at λ max = 280 nm with an emission wavelength setting. And the run time for each sample is 20.00 min. Mobile phase is composed of 0.1 M acetate buffer (pH 4.0) and methanol in a ratio of 95:5 (*v*/*v*) for kojic acid and 40:60 (*v*/*v*) for **11c**.

3.3.8 Linearity, limit of detection and limit of quantitation

The linearity of the method was assessed over a range of concentrations. Thirteen different concentrations between 0.05 and 512 μg/mL are chosen for **11c** and kojic acid. The calibration curves were obtained by plotting the peak areas against the corresponding concentrations of **11c** or kojic acid. The slope, y-intercept and correlation co-efficient (R^2) of the curve were determined by linear regression analysis. According to FDA regulations[61], the theoretical LOD and LOQ for the developed method were calculated using standard deviation of the response (σ) and slope (S) of the calibration curve according to the following equations:

$$LOD = 3.3\sigma/S, LOQ = 10\sigma/S$$

The equation for the relationship between concentration and area was obtained as y=1.6456x−0.0178, where the coefficient of determination was 0.9998. Meanwhile, the calibration curve for kojic acid standard was obtained as, y=1.1165x+0.0091, and the regression coefficient was 0.9999. It indicates that the curves are accurate and the regression effect is more significant and credible. The detection limit of **11c** was 0.1323 μg/mL, and the limit of quantification was 0.4010 μg/mL. The detection limit of kojic acid was 0.1448 μg/mL and the limit of quantification was 0.4388 μg/mL.

3.3.9 In vitro skin permeation efficiency of 11c and kojic acid by Franz cell components

Skin samples were prepared from 6-month-old pigs obtained from local abattoirs and then steamed cleaned. The skin was kept at 4 ℃ for a maximum of no more than 24 hours, the tissue was washed with ultrapure water only and the hair was trimmed with scissors. Excess subcutaneous fat is removed and the skin is wrapped in aluminium foil and stored in the fridge at -20 ℃ for a maximum of 3 months. Ensure that the entire thickness of the skin is used for the Franz cell penetration experiments to prevent alteration of the biomechanical properties of the skin.

3.3.10 Franz cell set-up

Prior to infiltration studies, skin samples were thawed at room temperature for at least 1 h. Afterwards, circular skin samples were cut and mounted between the donor and recipient compartments of the Franz-type static diffusion cell device[62] with the dermal side facing

downwards and an exposed surface area of 0.64 cm^2 and a recipient compartment volume of 3 mL. The trimmed skin samples were placed over the recipient compartment for 15 min to allow equilibration prior to skin treatment. The integrity of each skin sample was assessed by resistance using the method and guidelines described by Davies et al., 2004[63], and only skin that yielded resistance readings greater than 10 kΩ was used. PBS solution (pH 7.4) was used as the recipient medium. 200 mL of 2 mg/mL of **11c** or kojic acid in PG were administered through the donor chamber. And 200 mL of distilled water was used as a control. The water bath temperature at 36.5℃ was maintained throughout the experiment. The skin was exposed to the compound preparation for various time points of 0.5, 1, 2, 4 and 24 h. Each preparation was run 3 times at each time point to ensure accuracy.

3.3.11 Post Franz cell skin tissue preparation

After the permeation experiments, the excess liquid was removed and collected from the skin surface by careful application of sponges soaked with 3% *v/v* Teepol solution. The sponges were pooled for HPLC analysis as a total skin wash. Any formulation which might have spread to the donor chamber was collected by the sponges and stored for HPLC analysis as a donor chamber wash. Upon removing the excess formulation from the skin surface, 15 sequential tape strips were collected from the skin as tape strips. The amount of **11c** from the different Franz cell components (skin wash, donor chamber wash, pooled tape strips, and remaining within skin after tape stripping) were extracted by the addition

of 5, 5, 10, and 5 mL of methanol extraction mixture (methanol 30%: water), respectively. Samples were then vortexed for 1 min and sonicated for 30 min. The extracts (1 mL) were collected. For the receptor fluid, 1 mL of the solution from each Franz cell was collected. And all the samples were centrifuged at 4 ℃ at 14000 rpm for 10 min and then filtered through the 0.22 μm membrane.

3.3.12 Visualization of 11c within the skin by OrbiSIMS

The 2 h skin samples were chosen from the Franz cell permeation test, the surface of the skin were scrubbed with a sponge moistened with distilled water to remove excess formulation. The skin was then scrubbed with a dry sponge. The skin samples were then immediately frozen using liquid nitrogen, to avoid morphological distortion and tissue damage caused by autolysis or decay. The skin samples were then placed on a Cryostat (Leica Biosystems, Wetzlar, Germany) for frozen sectioning (CT -24 ℃, OT -30 ℃), and 20 μm thick transverse skin sections were cut, with three sections per sample being placed on the slide. For each sample, adjacent 20 μm thick sections were used for standard hematoxylin-eosin staining controls.

3.3.13 3D OrbiSIMS imaging analysis

For permeation analysis, skin cross-sections were used. A 3D OrbiSIMS (Hybrid SIMS, IONTOF GmbH, Germany) analysis was performed on a hybrid instrument (IONTOF GmbH). For the Orbitrap image acquisition, a 20 KeV Ar3000+ analysis beam with a diameter of 20 μm was used as the primary ion source. Samples were analyzed at room temperature across a

300 × 300 μm area in negative polarity. Ar3000+ primary ions were used with a filament current of 2.30A with charge compensation performed using a low-energy (-20 eV) electron flood gun. Duty cycle was set to 4.4% and cycle time to 200 μs. Argon gas flooding was in operation to aid with charge compensation, which led to a pressure of 9.0×10^{-7} mbar in the main chamber. The optimal target surface potential was at 136.6 V. Mass spectra were recorded at a resolution of 240,000 at *m*/*z* 200 in the mass range of 75 to 1,125 *m*/*z*. The automatic gain control (AGC) target was off with the maximum injection time set at 500 ms. Both data acquisition and the subsequent data processing were performed using SurfaceLab 7 software (IONTOF GmbH). Orbitrap data were acquired using a Thermo Fisher Orbitrap HF mass spectrometer.

3.4 Result and discussion

3.4.1 Chemical synthesis

As shown in , compounds **11a–n** with ring B containing resorcinol structure were synthesized. Starting from commercially available 2,4-dihydroxybenzaldehyde (**14**), compound **15** with protected hydroxyl group was obtained by reaction with benzyl bromide. Compounds **16a–n** were prepared by aldol condensation between compound **15** and various acetophenone bearing different substituents, followed by the reduction of the double bond to give compounds **17a–n** in the presence of bis(pinacolato)diboron and catalyst Cs_2CO_3. Finally, in the present of BCl_3 as Lewis acid and pentamethylbenzene as acid-acceptor, benzyl group was removed to obtain the corresponding target compounds **11a–n**.

Among them, the chemical structure formulas of **11c** and **11m** are shown in the **Figure 3-4**.

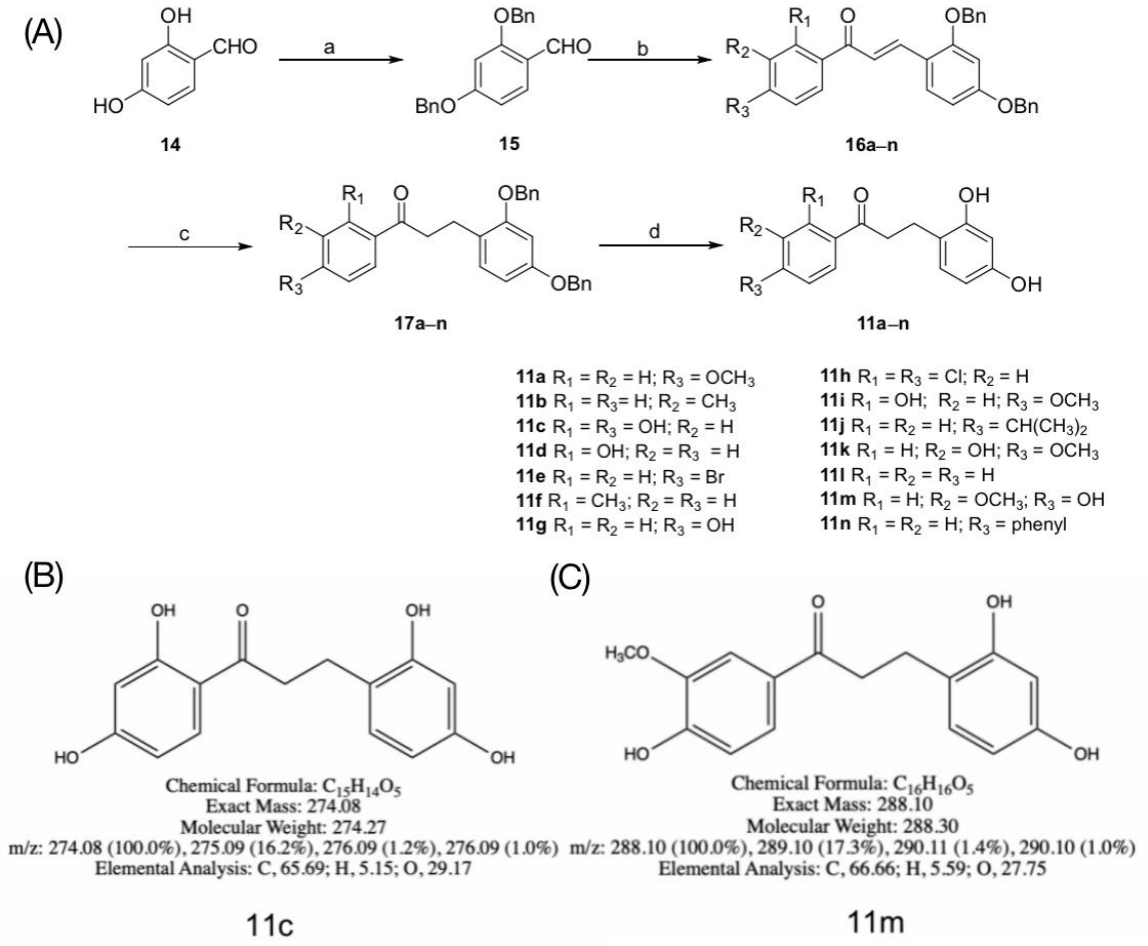


Figure 3-4 The synthesis and structure of compounds 11c and 11m.

For the rest of the chemical synthesis and the molecular docking results refer to Appendix B.

3.4.2 Mushroom TYR inhibitory activity of tested compounds

Due to the fact that TYR extracted from *Agaricus bisporus* (mTYR) is pure, stable and commercially available, it is often used as a model of human TYR to screen TYR inhibitors. L-Tyrosine and L-Dopa, substrates of monophenol oxidation and diphenol oxidation by TYR, were selected to

determine the TYR inhibitory activities of all target compounds by the method reported in the literature.[52] The results were shown in **Table 3-1**.

From the results of L-Tyrosine as substrate, it could be seen that when the B ring was 2',4'-dihydroxybenzyl ring, the TYR inhibitory activity of all target compounds was in nanomolar level; when the 2',4'-dihydroxy group on the B ring turned into 3',4'-dihydroxy group (such as **12m**), 2'-hydroxyl group (such as **12j**) or 4'-hydroxyl group (such as **12b**), its inhibitory activity decreased sharply. When the 2',4'-dihydroxy group on the B ring was methylated (such as **12n**), its inhibitory activity was also greatly reduced. These results suggested that a 2',4'-dihydroxybenzyl ring on the B-ring was necessary for TYR inhibitory activity. Among these compounds, whose A ring was 2,4-dihydroxyphenyl or 3-methoxy-4-hydroxyphenyl had the best TYR inhibitory activity, i.e., compound **11c** (L-Tyrosine IC_{50} = 0.050 μM; L-Dopa IC_{50} = 0.064 μM) and **11m** (L-Tyrosine IC_{50} = 0.054 μM; L-Dopa IC_{50} = 0.165 μM). When the substituent on the A ring was 3-hydroxy-4-methoxy (**11k**), its activity decreased slightly (L-Tyrosine IC_{50} = 0.069 μM; L-Dopa IC_{50} = 0.245 μM). When the A ring was substituted by alkyl or halogen groups, its activity decreased, and when the volume of alkyl substituents was large, such as 4-phenyl substituted **11n**, its activity decreased significantly. According to the results, the structure-activity relationship was summarized as follows: firstly, the B ring was resorcinol structure and essential for activity; secondly, for A ring, the activity of 2,4-dihydroxyphenyl and 3-methoxy-4-hydroxyphenyl was the best, followed by 2-hydroxy-4-methoxy. The activity would be reduced significantly when

it was substituted by highly hindered alkyl (Figure 3-5).

Table 3-1 Inhibitory activity of tested compounds on TYR.

Compd.	IC_{50} (μM) [a]		Compd.	IC_{50} (μM) [a]	
	L-Tyrosine	L-Dopa		L-Tyrosine	L-Dopa
11a	0.089 ± 0.008	0.171 ± 0.003	**12d**	> 10	> 10
11b	0.133 ± 0.036	0.189 ± 0.008	**12e**	> 10	> 10
11c	**0.050 ± 0.005**	**0.064 ± 0.005**	**12f**	> 10	> 10
11d	0.069 ± 0.006	0.286 ± 0.028	**12g**	> 10	> 10
11e	0.110 ± 0.010	0.184 ± 0.016	**12h**	> 10	> 10
11f	0.123 ± 0.013	0.239 ± 0.018	**12i**	> 10	> 10
11g	0.072 ± 0.017	0.212 ± 0.021	**12j**	> 10	> 10
11h	0.119 ± 0.012	0.189 ± 0.017	**12k**	> 10	> 10
11i	0.069 ± 0.007	0.183 ± 0.017	**12l**	> 10	> 10
11j	0.232 ± 0.024	0.644 ± 0.010	**12m**	> 10	> 10
11k	0.069 ± 0.007	0.245 ± 0.024	**12n**	> 10	> 10
11l	0.183 ± 0.016	0.625 ± 0.050	**13a**	> 10	> 10
11m	**0.054 ± 0.005**	**0.165 ± 0.018**	**13b**	> 10	> 10
11n	0.331 ± 0.033	1.431 ± 0.120	**13c**	> 10	> 10
12a	> 10	> 10	**13d**	> 10	> 10
12b	> 10	> 10	**13e**	> 10	> 10
12c	> 10	> 10	**Kojic acid**	29.7 ± 2.35	48.7 ± 3.85

[a] IC_{50} values are expressed as means ± SD (standard error) of at least three independent experiments.

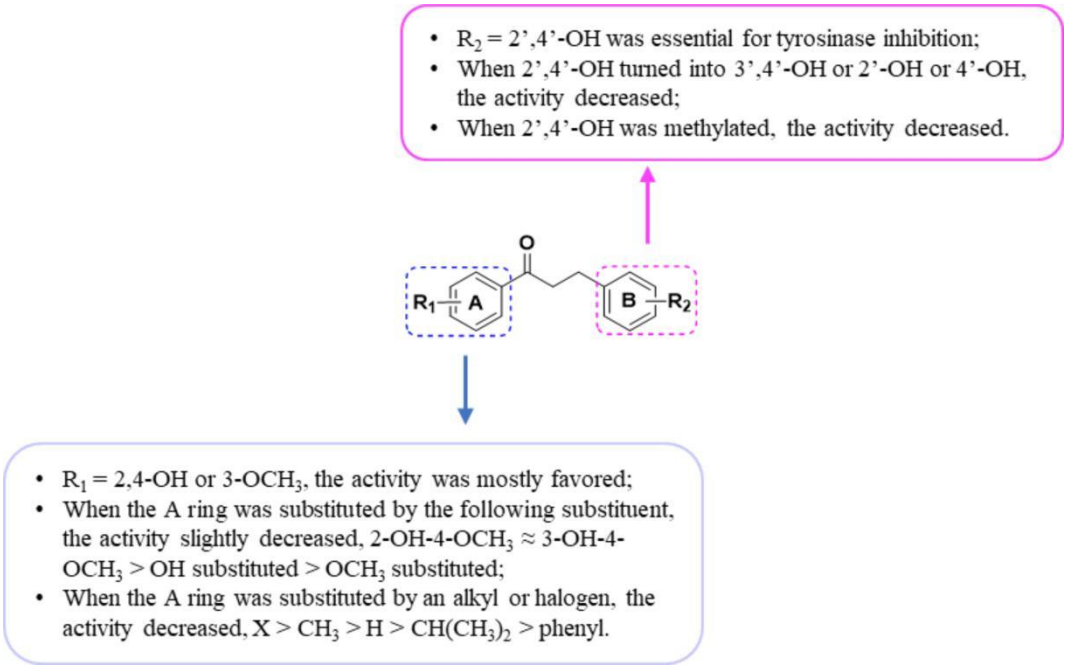


Figure 3-5. Summary of the structure-activity relationship of dihydrochalcone TYR inhibitors.

Based on the results obtained from the preliminary screening using mushroom tyrosinases, it was confirmed that the most active of these, 11c and 11m, were selected as the subjects for the study of their application as novel tyrosinase inhibitors in the anti-melanogenic field. The predicted physicochemical properties and PK parameters for 11c and 11m were obtained from data available through a dedicated prediction website, as shown in the table below(**Table 3-2**).

Table 3-2 The Log P and pK_a value of tested compounds on TYR

Compd.	IC_{50} (μM) [a]	
	L-Tyrosine	L-DOPA

11c	0.050 ± 0.005	0.064 ± 0.005
11m	0.054 ± 0.005	0.165 ± 0.018
Kojic acid	29.7 ± 2.35	48.7 ± 3.85

Based on the predicted results, both 11c and 11m have superior lipophilic properties. Therefore, it is expected that these compounds can have better permeability, compared to Kojic acid.

3.4.3 TYR inhibitory activity of 11c and 11m in murine cell line B16F10

MTT method was used to determine the cytotoxicity of compounds **11c** and **11m** in B16F10 cells at three concentrations (5 μM, 10 μM, and 50 μM) firstly. The results were shown in **Figure 3-6**A, even at a high concentration of 50 μM, the cytotoxicity of compounds **11c** and **11m** was minimal compared to the control group.

In order to evaluate the inhibitory effect of the optimal compounds on TYR activity and melanin content in B16F10 melanoma cells, α-Melanocyte stimulating hormone (α-MSH) was used to stimulate B16F10 cells to increase the level of TYR activity, and then compounds **11c** and **11m** (0, 5, 10 and 25 μM) or positive control (kojic acid, 25 μM) were used to treat B16F10 cells. L-DOPA was used as a substrate for TYR, and the results

of TYR activity assessment were shown in **Figure 3-6**B, compounds **11c** and **11m** had great inhibitory effects against TYR in cells in a dose-dependent manner and had better TYR inhibitory potential than the positive control kojic acid. Similar to the TYR activity assessment, melanin content in B16F10 cells decreased significantly when treated with **11c** and **11m** with the increase of concentration (**Figure 3-6**C).

As reported previously,[55] MiTF is an upstream transcription factor of TYR, which plays an important role in the transcription of TYR gene. Western blotting demonstrated that the protein levels of both TYR and MiTF in B16F10 cells treated with **11c** had decreased in a dose-dependent manner, whereas the inhibition of the protein levels of TYR and MiTF in B16F10 cells treated with kojic acid were relatively weaker compared with that of **11c** (**Figure 3-6**D). Altogether, the data indicated that **11c** probably suppressed melanin by both inhibiting the function of TYR and decreasing TYR contents.

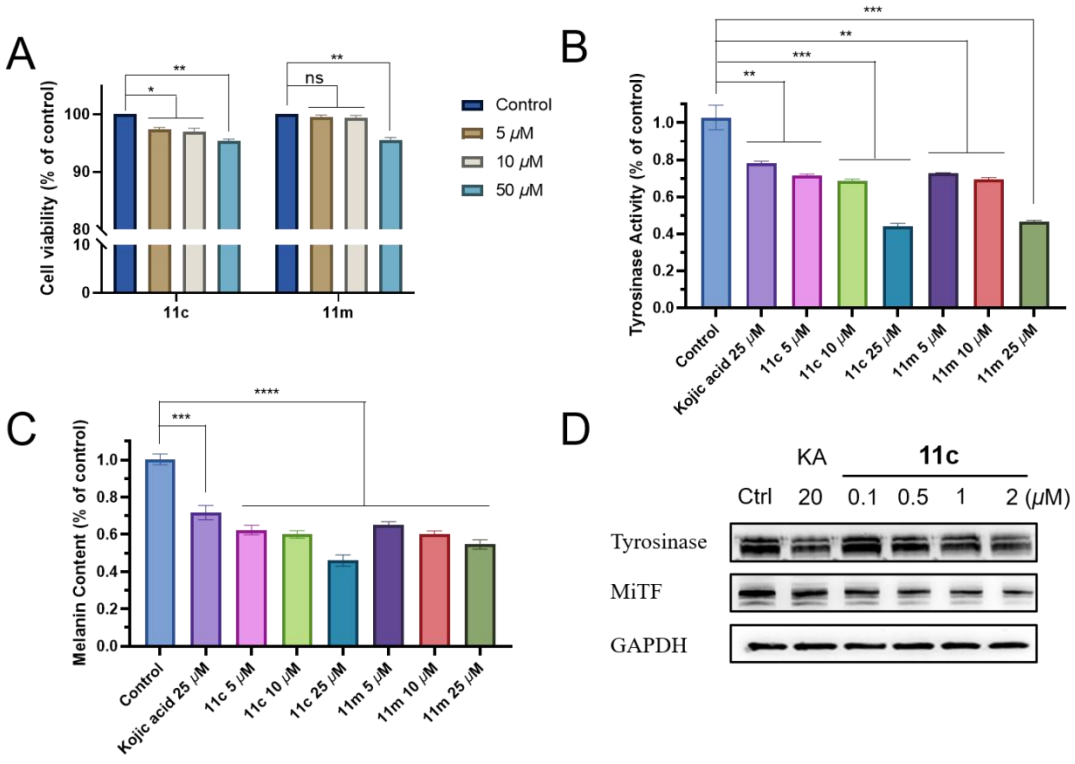


Figure 3-6. Evaluation in murine cell line B16F10. (A) Cytotoxicity of compounds **11c** and **11m** in B16F10 cells. Inhibitory activities of **11c** and **11m** on TYR (B) and melanin content (C) in B16F10 cells stimulated by α-MSH were tested. The cells were treated with 0, 5, 10, 25 μM of **11c** and **11m** or 25 μM of kojic acid, respectively. The data are expressed as means ± SD (n=3). Statistical significance of differences was assessed using multiple t-test. *, $p < 0.05$; **, $p < 0.01$; ***, $p < 0.001$; ****, $p < 0.0001$. (D) Western blotting. Effects of **11c** and kojic acid on TYR and MiTF levels in B16F10 cells.

3.4.4 TYR inhibitory activity of 11c and 11m in human cells A375

Since 11c and 11m have negligible toxicity at a low concentration (10 μM)

in murine-derived cells, and hypotoxicity at high concentration (50 μM), it is neccessory to verify whether it would be less toxicity in human-derived cells. Therefore, the human malignant melanoma cells A375 were chosen to determine the cytotoxicity of compounds **11c** and **11m** by MTT assay, using kojic acid as a positive control. The results are shown in **Figure 3-7**A. At a high concentration of 50 μM, the cytotoxicity of compound **11m** could be negligible compared to the control, while **11c** was slightly cytotoxic.

To ensure that the novel compounds had the same ability to inhibit melanin and TYR activity for human-derived cells, A375 cells were stimulated with α-MSH to increase the level of TYR activity. Then, A375 cells were treated with 20 μM of compounds **11c**, **11m** and the positive control (kojic acid). The results of the TYR activity and melanin content are shown in **Figure 3-7**B and 8C. Compounds **11c** and **11m** at 20 μM both had a significant inhibitory effect on TYR in A375 cells with a similar capacity to the positive control. Of these, **11c** had a slight superiority over **11m**. Similar to the assessment of TYR activity, melanin content in A375 cells was remarkably reduced with the treatment of **11c** and **11m** at 20 μM.

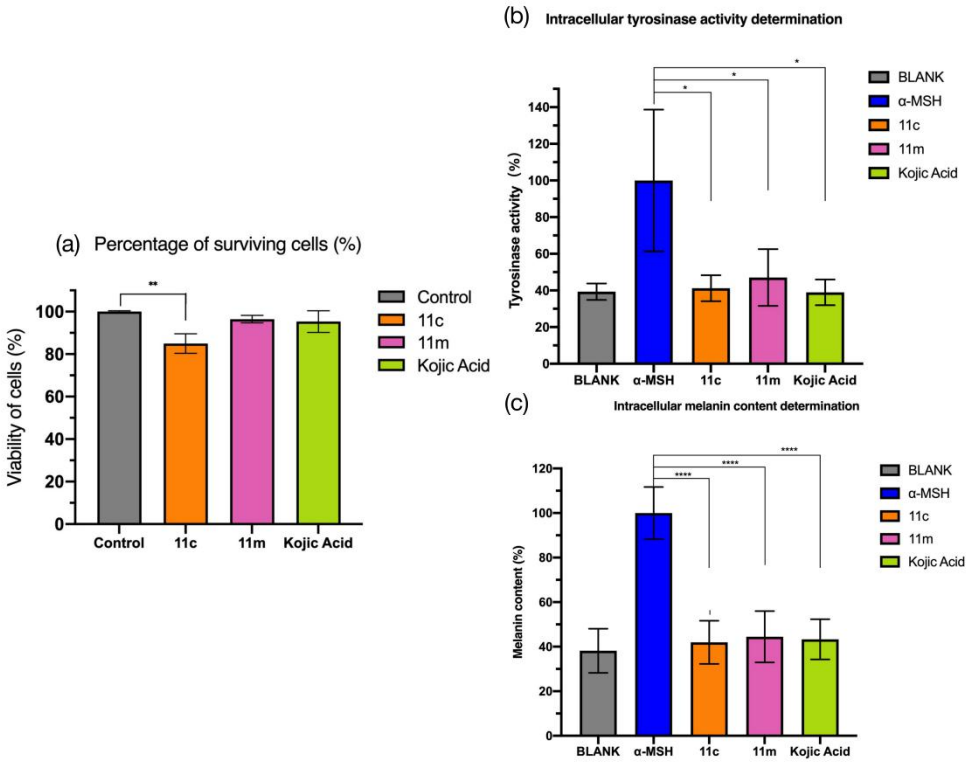


Figure 3-7. Evaluation in human A375 cells. (A) Cytotoxicity of compounds **11c**, **11m** and kojic acid in A375 cells. Inhibitory activities of **11c** and **11m** on TYR (B) and melanin content (C) in A375 cells stimulated by α-MSH were tested. The cells were exposed to 20 μM of **11c**, **11m** and kojic acid for 24 h. Statistical significance of differences was assessed using ANOVA one-way test. (A) Values were significantly different from those of the control group. (n=3, values are means ± SE). (B, C) Values were significantly different from those of the α-MSH group. (B, n=4, C, n=3, values are means ± SE)*, $p < 0.05$; **, $p < 0.01$; ****, $p < 0.0001$.

However, this raises the question that, unlike the excellent inhibitory

activity of 11c, 11m in mTYR, the activity was significantly reduced when targeting switched to hTYR. This may be due to a structural gap between the mushroom tyrosinase and the animal-derived tyrosinase. This has been identified in a number of studies[420], which have concluded that the catalytic activity and substrate specificity of mTYR has been shown to be significantly different from that of the mammalian enzyme, in particular the amino acid sequence of its active site region is significantly different from that of hTYR. Since small changes in enzyme-ligand interactions may also have a significant effect on binding affinity, the different inhibition results for hTYR and mTYR are not surprising.

3.4.5 In vitro skin permeation efficiency of compound 11c by Franz cell component

The skin permeation of **11c** was determined by HPLC analytical methods. Calibration curves, limits of detection and quantification for **11c** and kojic acid were firstly established according to the chromatographic conditions set up in the Experimental section.

The optimal compound **11c** was then assessed for its skin permeation studies by using the Franz diffusion cell. 2 mg/mL of **11c** in propylene glycol (PG) was used, and 2 mg/mL of kojic acid was chosen as a positive control. The highest skin permeation of **11c** was observed at 2 hours after application, with 26.77% remaining inside the skin (intradermal). In contrast, kojic acid reached its highest level at 4 hours after application,

with only 3.56% of the active ingredient remaining in the skin (**Figure 3-8**A). In addition, it can be seen from **Figure 3-8**B-F that from 0.5 h to 24 h, the amount of **11c** penetrated into receptor fluid (transdermal) is tiny, and the highest level (**Figure 3-8**F) doesn't exceed 1.2%. Overall, based on the skin permeation studies, the intradermal delivering capacity of **11c** was shown to be superior and far exceed that of kojic acid. In addition, only a tiny amount of **11c** would possibly be able to enter the circulatory system after transdermal permeation, most effectively avoiding toxic side effects.

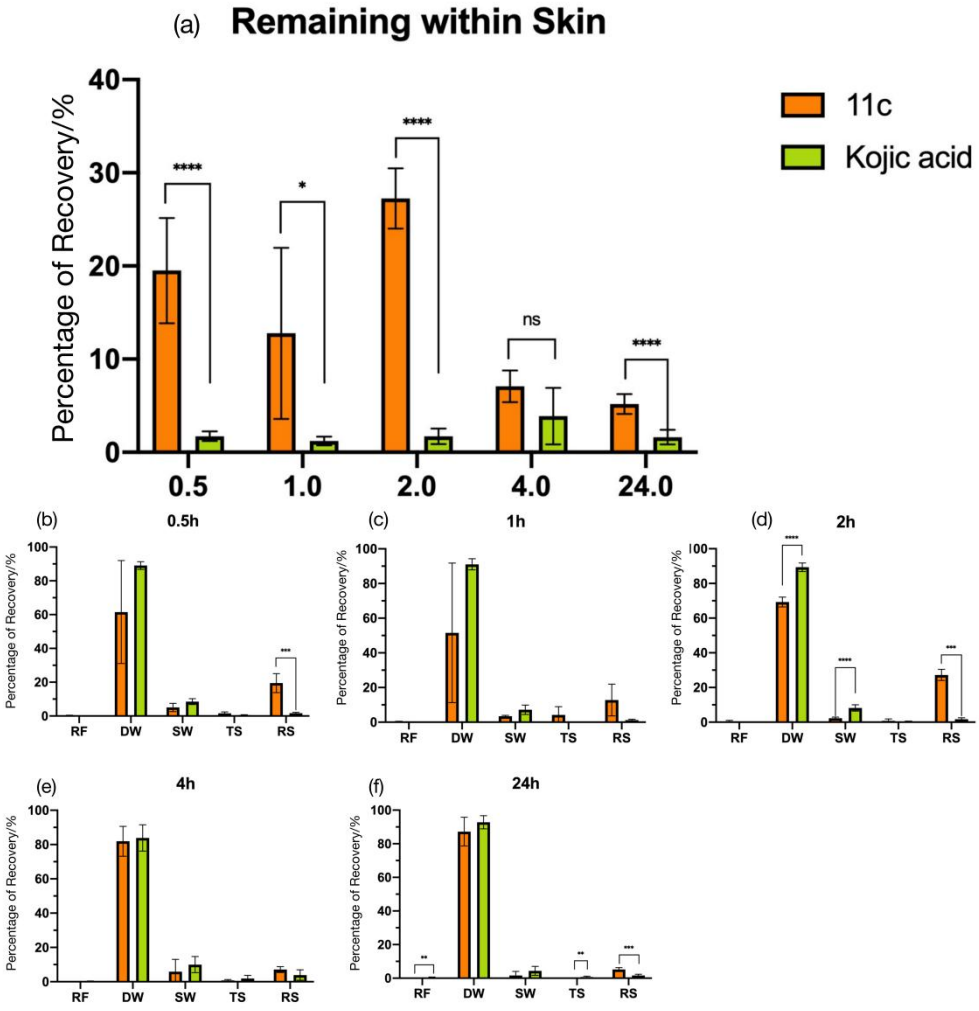


Figure 3-8. HPLC analysis of the mean percentage of recovery of **11c** in different Franz cell components (donor wash (DW), skin wash (SW), tape strips (TS), remaining within skin (RS) and receptor fluid (RF)) following permeation test at different hours ((B) 0.5h, (C) 1h, (D) 2h, (E) 4h, (F) 24h). (A) The percentage of **11c** remaining within skin (intradermal) at different hours. The data are expressed as means ± SD (n=6). Statistical significance of differences was assessed using multiple t-test (*, $p < 0.05$; **, $p < 0.01$; ***, $p < 0.001$; ****, $p < 0.0001$; no significant difference (ns) indicates $p > 0.05$).

3.4.6 Visualization of compound 11c within the skin by OrbiSIMS

Firstly, according to haematoxylin and eosin (H&E) staining (**Figure 3-9**A), the thickness of stratum corneum can be determined at 5-10 μm and the thickness of epidermis at 20-100 μm, where the melanocytes containing tyrosinase are located in the basal layer, between epidermis and dermis, and therefore should be located 100-110 μm from the skin surface.

According to the study of Nichola and co-workers,[56] palmitic acid ($C_{16}H_{31}O_2^-$) can be used to locate the stratum corneum. And cholesterol sulfate ($C_{27}H_{45}SO_4^-$) is used as an adjunct to locate the uppermost layer of epidermis. The white dashed line in Figure 11A indicates the boundary between stratum corneum and epidermis. The ion signal of **11c** clearly appeared below the stratum corneum and was distributed in the epidermis.

In addition, the signal ions of **11c** are mainly $C_{15}H_{13}O_5^-$ and $C_{15}H_{12}O_5Na^-$ in **Figure 3-9**B, c-d. $C_{15}H_{13}O_5^-$ resided more in the stratum corneum, and it lost a hydrogen ion and was bound a sodium ion when **11c** entered the epidermis. Alternatively, identification of the site of penetration of the compound was supported by the fact that the phospholipid marker (PO_3^-) would appear in the epidermis and upper dermis[57] (**Figure 3-9**C, f). Figure 3-10A shows remarkably that the ionic signal of 11c appears under palmitic acid ($C_{16}H_{31}O_2^-$), indicating that it has crossed the stratum corneum and entered the interior of the skin. As shown in **Figure 3-10**B, the distance of the green part of the **11c** ion from the skin surface is about 50-150 μm. This indicates that **11c** entered the skin and mainly stayed at the base of the epidermis and in the upper dermis. Further, according to **Figure 3-10**B, 11c is distributed in a line, showing that it has not permeated excessively into the dermis. Thus, it is suggested that compound **11c** targets the melanocytes in the basal layer adequately.

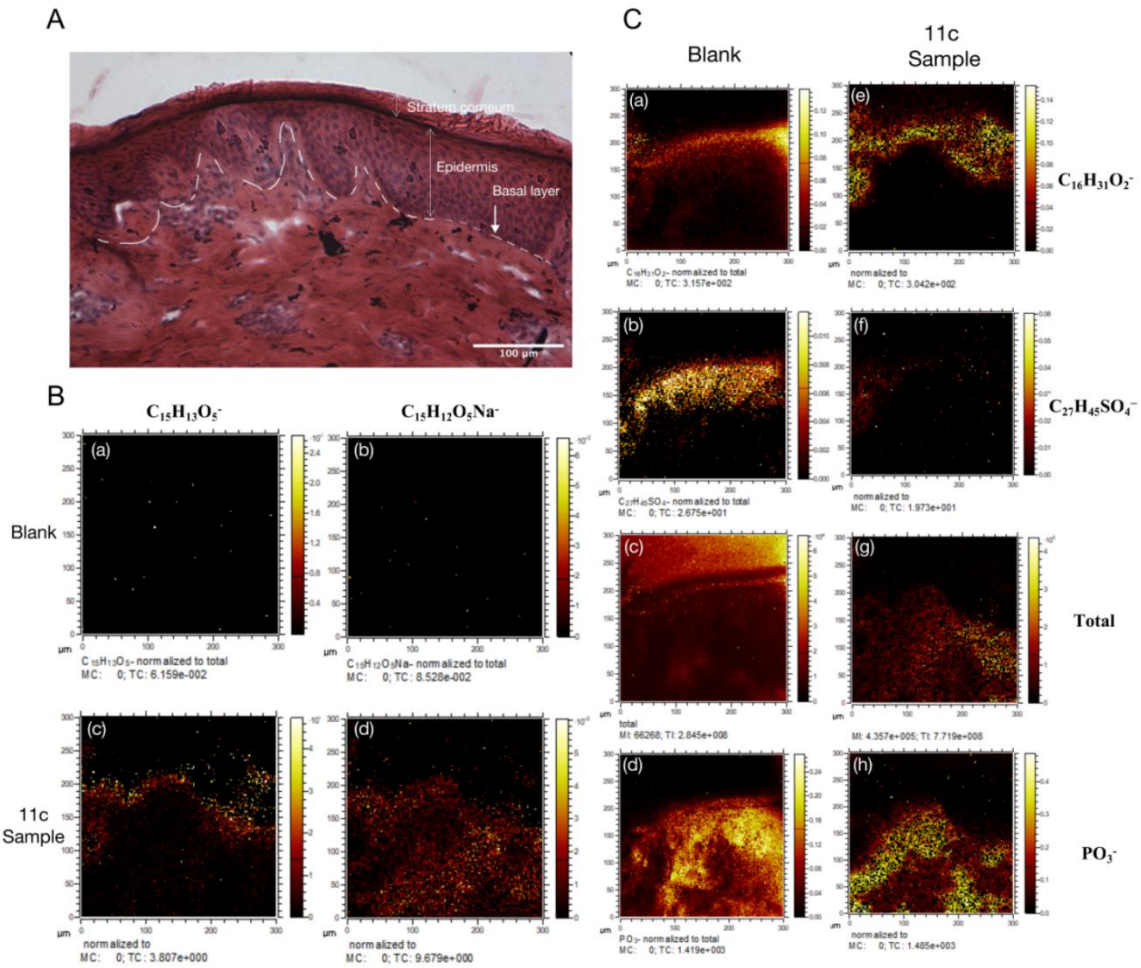


Figure 3-9. (A) HE-stained cross-section of dermatomed porcine skin (4 mm thick) dosed with **11c** at 2 mg/mL. The basal layer of epidermis is located above the white dashed line (the position indicated by the arrow). Image from 20 μm cryocut tissue section at a 10-fold magnification. (B & C) Negative polarity ion images of 3D OrbiSIMS from various fragment ions of the skin cross section dosed by compound **11c** at 2 mg/mL in dermatomed porcine skin (4 mm thickness), and use water as blank group. The field of view is 300.0 μm and pixelsize is 2.0 μm, MC maximum ion count per pixel and TC total ion count for the specific ion of interest. (B) The ion images illustrate the 2D spatial distribution for the molecular

ions of **11c**: (a) **11c** ($C_{15}H_{13}O_5^-$) in blank group; (b) **11c** ($C_{15}H_{12}O_5Na^-$) in blank group; (c) **11c** ($C_{15}H_{13}O_5^-$) in **11c** group; (d) **11c** ($C_{15}H_{12}O_5Na^-$) in **11c** group. All ion images have been normalized to the total ion image. (C) The ion images illustrate the 2D spatial distribution for the following molecular ions: (a)&(e) palmitic acid ($C_{16}H_{31}O_2^-$); (b)&(f) cholesterol sulfate ($C_{27}H_{45}SO_4^-$); (c)&(g) Total ion; (d)&(h) phospholipid marker (PO_3^-). And (a)-(d) in blank group and (e)-(h) in **11c** group. All ion images have been normalized to the total ion image.

Overall, the location of target compound penetration within the skin can be directly observed by the SIMS images. As in **Figure 3-10**, it is clear that 11c remains mainly between the epidermis and the dermis, facilitating rapid detection to obtain results. In addition, a comparison of **Figure 2-7** and **Figure 3-10** also shows that a greater amount of 11c can fully penetrate through the stratum corneum and into the skin compared to the low permeability of CMNs, fully illustrating the targeted permeability of 11c.

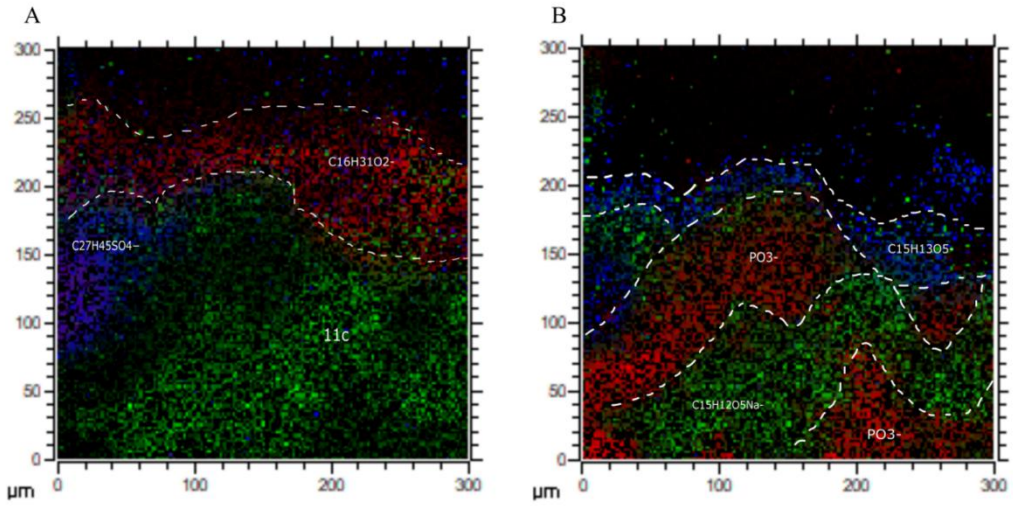


Figure 3-10. Images of 3D OrbiSIMS from various fragment ions of the skin cross section dosed by 2 mg/mL of **11c** in dermatomed porcine skin (4 mm thickness). The Field of View: 300.0 μm and Pixelsize: 2.0 μm. The ion images illustrate the 2D spatial distribution for the overlay of different molecular ions. (A) Three color overlay between ion images, Stratum corneum, SC (palmitic acid fragment, $C_{16}H_{31}O_2^-$, red), top of epidermis (cholesterol sulfate fragment, $C_{27}H_{45}SO_4^-$, blue) and **11c** ($C_{15}H_{13}O_5^-$, and $C_{15}H_{12}O_5Na^-$, green). (B) Three color overlay between ion images, **11c** ($C_{15}H_{13}O_5^-$, blue), **11c** ($C_{15}H_{12}O_5Na^-$, green), epidermis (phospholipid marker, PO_3^-, red).

3.4 Conclusion

As a key rate-limiting enzyme in the process of melanin formation, TYR has become the most important target to inhibit melanin production. In this study, by applying the pharmacophore fusion strategy, the resorcinol

structure is introduced into the skeleton of dihydrochalcone to discover potential TYR inhibitors. Thirty-three dihydrochalcone TYR inhibitors are designed and synthesized, and the TYR activities of all compounds are evaluated. The TYR inhibitory activity of fourteen compounds is stronger than that of positive control kojic acid, and the IC_{50} values reach the nanomolar levels. Compounds **11c** and **11m** show the most potent TYR inhibitory activity with IC_{50} of 0.050 μM and 0.054 μM, respectively (when the substrate was L-tyrosine). Mechanism validation experiments show that **11c** probably suppresses melanin production by inhibiting the function of TYR in a non-competitive manner and decreasing TYR contents.

Further experimental results show that compounds **11c** and **11m** have gratifying antioxidant activity and low cytotoxicity, and could inhibit TYR activity and melanin production in murine cell line B16F10 in a dose-dependent manner. In human-derived A375 cells, compounds **11c** and **11m** also show excellent TYR inhibition and melanin suppression. In addition, compound **11c** also shows outstanding performance in *in vitro* skin permeation assays, rapidly crossing the skin stratum corneum and remaining inside the skin, thus targeting the basal layer and focusing on the melanocytes. More importantly, we also found the compound **11c** exhibited powerful anti-melanogenesis ability in a guinea pig model *in vivo*.

Taken together, compound **11c** can be considered as a low-toxic and effective TYR inhibitor for further development of new therapeutic options for the treatment of skin hyperpigmentation.

Chapter 4. Implications of tyrosinase modulators for malate-aspartate shuttle and fatty acid metabolism in melanoma cells A375 revealed by metabolomics and lipidomics

Authors: Zhiwei Li, Li Lu, David Scurr, Maria Marlow, Zheying Zhu*

School of Pharmacy, The University of Nottingham, Nottingham, NG7 2RD, United Kingdom

Keywords: Metabolomics, lipidomics, tyrosinase modulators, malate-aspartate shuttle, fatty acid

This chapter is written in the form of a published paper and is scheduled for submission to *Molecular Omics*.

In the previous chapter we explored the possibility of novel tyrosinase inhibitors and, after evaluating the biological activity of compounds 11c and 11m, confirmed their potential as drugs for the treatment of hyperpigmentation. The next focus will thus be on studies on the mechanism of the new compounds' action. It is hoped that the analysis of the significant metabolite changes by tyrosinase modulators in melanoma cells A375 will provide a useful contribution to the search for new melanoma therapeutic targets.

4.1 Abstract

It is well known that hyperpigmentation is associated with melanocyte proliferation, which may lead to melanoma. As regulators of hyperpigmentation, the relationship between tyrosinase modulators and melanoma has been the focus of extensive attention. In this study, L-DOPA was chosen as the tyrosinase stimulator to be investigated, while Alpha-Arbutin and the new compounds 11c and 11m were chosen as the tyrosinase inhibitors. L-DOPA was chosen as there have been consistent cases suggesting a correlation between L-DOPA as a treatment for Parkinson's and the development of melanoma. Conversely, many tyrosinase inhibitors can alter or even inhibit the development of melanoma. Therefore, a combined metabolomics and lipidomics analysis was used to gain further insight into the molecular mechanisms of melanoma. The analysis yielded the metabolic pathways and effects of L-DOPA and tyrosinase inhibitors in melanoma cells. As a part of this, LC-MS targeted metabolomics was used to analyse metabolite changes in melanoma cells and a total of 108 metabolites was identified. LC-MS metabolite pathway analysis revealed that phenylalanine, tyrosine, and tryptophan biosynthesis and Malate- Aspartate Shuttle were the two most affected pathways. Subsequently, Orbitrap secondary ion mass spectrometry (OrbiSIMS) was applied as a novel technique for the analysis of metabolomics. As OrbiSIMS is sensitive to lipids, it was suitable to be used for a comparative analysis of the changes in lipids of tyrosinase regulators in melanoma cells. Combining the results of these

two analyses, we found that tyrosinase modulators can affect the normal physiological state of melanoma cells by modulating the levels of Malate-Aspartate Shuttle and fatty acids. Overall, this study provides a strong contribution to further exploration of the metabolic mechanisms of melanoma cells and the search for new therapeutic targets.

4.2 Introduction

Hyperpigmentation is a condition in which patches of skin are darker than the surrounding normal skin due to an upregulation of melanin synthesis, an increase in the number of melanocytes, and a decrease in melanosome breakdown. These new and localized hyperpigmented or irregularly pigmented lesions may be malignant melanoma if they cause pain or itching[166,421,422]. Abnormal hyperpigmentation is a hallmark sign of melanoma and can be used as a basis for diagnosis[423].

Melanoma is the deadliest form of skin cancer, and its incidence is growing faster than any other preventable cancer today[424]. In 2021, melanoma was the fifth most common cancer diagnosis in the United States, accounting for 5.6% of all cancer diagnoses[425]. While the incidence of many other tumour types has been declining, melanoma continues to increase worldwide and is very aggressive and lethal[426]. However, early-stage melanoma is treatable and has excellent long-term survival rates[427]. It is therefore important to explore the metabolic mechanisms of melanoma, find new targets for drug delivery, and thus to develop new drugs.

Studies have now found an association between Parkinson's disease (PD) treated with L-DOPA and an increased risk of developing malignant melanoma[428–431]. Patients with PD have an overall reduced risk of cancer diagnosis. However, breast cancer and melanoma have an unusually high co-morbidity rate with PD[432]. L-DOPA is the most common treatment for Parkinson's disease and is a substrate for melanin synthesis. However, there is concern that this therapy may lead to melanoma[433]. Following L-DOPA administration, tyrosinase activity has also been found to increase rapidly due to the higher substrate availability[434]. L-DOPA or its oxidation products stimulate intracellular tyrosinase concentrations and regulate tyrosinase mRNA levels in both a positive and negative manner, overall significantly increasing tyrosinase activity[435].

In contrast, it has also been suggested that whether or not PD patients are treated with L-DOPA has little or no effect on the development or progression of melanoma[436,437]. Therefore, whether L-DOPA is involved in this association remains controversial. However, there is no doubt that L-DOPA has a strong immunosuppressive effect, which must be somewhat problematic for the subsequent treatment of melanoma[438,439]. It is therefore important to explore the relationship between L-DOPA and melanoma, especially the effect of L-DOPA on melanoma cell metabolism.

In addition to L-DOPA, the massive accumulation of melanin can also lead to a failure of immunotherapy[440]. The overproduction of melanin is directly related to tyrosinase. Tyrosinase oxidises L-tyrosine to L-DOPA and then to L-DOPA quinone in melanocytes, which ultimately synthesise

melanin[441]. Unlike normal melanocytes, melanoma cells do not excrete melanin into neighbouring cells[442]. As a result, large amounts of melanin accumulate in melanoma cells, endogenously protecting them from radiation therapy and rendering immunotherapy ineffective[443]. In addition, melanin acts as a reactive oxygen species (ROS) scavenger and neutralises the effects of chemotherapy[444]. It is thus vital to find new melanoma treatment pathways. The overexpression of melanin during tumourigenesis is associated with tyrosinase. It is thought that tyrosinase inhibitors can be used to counteract the accumulation of high levels of melanin associated with many diseases, thus making it a potential molecular target in the treatment of melanoma[445]. It works by restoring the sensitivity of melanoma cells to external damage through inhibition of tyrosinase and reduction of melanin production. Therefore, it has been suggested that tyrosinase inhibitors could be used as sensitizers for melanoma treatment and adjuvant therapy. In addition, it has been suggested that tyrosinase overexpression can induce melanoma and that TYR can suspend apoptosis in melanoma cells under the regulation of the transcription factor MITF[74,446,447]. However, it has also been found that CRISPR/Cas9-mediated TYR knockdown (KO) increased Vasculogenic mimicry (VM) in melanoma cells, suggesting that TYR brings about anticancer function by negatively regulating VM[448]. These publications suggest the feasibility of using tyrosinase as a target for developing novel melanoma drugs.

Due to gaps in the metabolomics of tyrosinase modulators, the metabolic

pathways of L-DOPA and tyrosinase inhibitors in melanoma cells and their effects on melanoma cells need to be further investigated. A comprehensive analysis using metabolomics and lipidomics will be used in this study to further understand the molecular mechanisms of melanoma. L-DOPA, as well as Alpha-Arbutin, 11c, and 11m are tyrosinase modulators that stimulate the up- or down-regulation of tyrosinase and are closely related to tyrosinase activity and tyrosine metabolism[101,124,143]. Therefore, it is reasonable to choose tyrosine as the primary biomarker to be studied. In addition, much of the literature finds that the melanin suppression process is associated with multiple amino acids and nucleic acid metabolism, thus making metabolic pathway analysis targeting amino acid-related pathways necessary[449]. LC-MS is currently the most widely used metabolomics tool, as it can analyse a wide variety of small molecules, particularly amino acids[450]. Therefore, 247 standards, mainly amino acids, were used as references to target and analyse their metabolic pathways.

The literature shows that lipid metabolism signalling pathways are also strongly altered in melanoma cells[349,451]. Lipid metabolism, an important branch of metabolomics, is an analytical approach for the holistic study of the multiparametric response of living systems based on lipid metabolic signatures in complex biological samples. It has also attracted significant research interest. A new, sensitive instrument for lipids, 3D Orbitrap Secondary Ion Mass Spectrometry (OrbiSIMS), has now been applied to metabolomic analysis. Passarelli et al[395] imaged neurotransmitters in the

hippocampus of mice by 3D OrbiSIMS and was able to infer 127 lipids. 3D OrbiSIMS is characterised by the combination of the high resolution of Orbitrap (>240,000 at m/z 200) and the high spatial resolution of TOF mass spectrometry (<200 nm), with good results for lipid molecules. Therefore, OrbiSIMS was chosen as a complementary analytical tool to LC-MS, with its low sample preparation, small sample size, and fast analysis time making it suitable for the initial exploration of lipidomics.

Overall, this study is based on the analysis of L-DOPA and tyrosinase inhibitors, two substances with positive and negative effects on tyrosinase respectively, to analyse the metabolic mechanisms of melanoma cells and to try to find novel drug targets.

4.3 Methods

4.3.1 Bioevaluation of 11c and 11m on human cell line A375

4.3.1.1 Cytotoxicity of 11c and 11m in A375.

Each well in a 96-well plate was seeded with 1 x 10^4 cells/100 µl of A375 cell suspension and was left to develop overnight to attach to the bottom of each well. The next day, 100 µl of medium containing various concentrations (1, 2, 4, 8, 16, 32, 64, 100 µM) of 11c and 11m and Alpha-Arbutin was added. Control cells were grown in a medium with the same concentration of DMSO. After 48 hours, 25 ml of a 5 mg/ml MTT solution was added to each well without removing the medium. After 2 hours of incubation at 37 ° C, 100 ml of lysing buffer was added. A 96-well

multiscanner was then used and the optical densities at 490 nm were measured following an overnight incubation (20 hours) at 37 ° C. As a control, the medium/MTT/lysing buffer was incubated under identical conditions. Viability of cells (%) = $OD_{\text{test group}}$ /$OD_{\text{control group}}$ ×100%.

4.3.1.2 Intracellular tyrosinase activity determination of 11c and 11m in A375

$7x10^4$ A375 cells/Well vaccination were placed in 12-Well plates. 5 μM L-DOPA was added to the blank control group, positive control group and experimental groups. The positive control group was then treated with Alpha-Arbutin, the experimental groups with **11c** and **11m** (1, 2, 4, 8, 16, 32, 64, 100 μM), and blank group with DMSO (< 0.3%). After incubating for 48 hours, the cells were collected in centrifugal pipes with 200μL 1% Triton X-100, incubated in the freezer (- 40 °C) for 1 hour, and then left at room temperature until melted. After 12000 RPM centrifugation at 4 °C for 30 mins, 80 μL of each sample was placed in 96 - Well plates and 20μL L-DOPA(10 mM) was added. These were then incubated for 15 minutes in 37 °C water. The OD value at 490 nm was measured using a microplate, and tyrosinase activity (%) = $OD_{\text{test group}}$ /$OD_{\text{control group}}$ ×100%.

4.3.1.3 Intracellular melanin content determination of 11c and 11m in A375

A375 cells were seeded at a density of $7x10^4$ per well in 12-Well plates and cultured in a CO2 incubator at 37°C with a volume fraction of 5% for 24 hours. 5 μM L-DOPA was added to the blank control group, positive

control group and experimental groups. The positive control group was then treated with Alpha-Arbutin, the experimental groups with **11c** and **11m** (1, 2, 4, 8, 16, 32, 64, 100 μM), and blank group with DMSO (< 0.3%). Afterwards, the cells were removed from the 48 hours cell culture, washed twice with PBS, and digested with a pancreatic enzyme. The cells were then combined with 200 μL NaOH(1M) solution (10% DMSO) and left in an 80 °C water bath for one hour. The solution was then mixed uniformly and 100 μL of each solution was placed in 96-well plates, the absorbance at 405 nm was measured with a microplate reader. The experiment was repeated nine times in parallel. Melanin content (%) = OD test group /OD control group ×100%.

4.3.2 Cell sample preparation for LC-MS

A total of 5 groups of cells were cultured. 5 μM L-DOPA was added as an inducer of melanogenesis in 4 groups, excluding the control group. Three of these groups were then selected to be sample groups by adding 16 μM of 11c, 11m, and Alpha-Arbutin respectively. All five groups were cultured for 48 hours.

Afterwards, the culture medium was eliminated, and the cells were briefly rinsed with 37°C PBS. Methanol (500 μL) at -40°C was injected to stop the metabolism and remove the intracellular metabolites concurrently. The cells were scraped and aggressively vortexed for one hour on ice before being centrifuged at 14,000 rpm for 10 minutes at 4°C. The supernatants were transferring to fresh tubes and evaporated with a Jouan Centrifugal Evaporator. The leftover residue was then reconstituted in 70 μL of

methanol (4°C) and centrifuged for 10 minutes at 14,000 rpm and 4°C. The extract was put into an amber HPLC vial with a glass insert, labelled, and used for LC-MS analysis. 10 L of each sample was collected and used as a pooled QC for untargeted analysis and MS/MS analysis to evaluate the analytical system's performance.

4.3.3 LC-MS analysis

The Q-Exactive Plus mass spectrometer equipped with a Dionex U3000 UHPLC system was utilised for the LC-MS study. Using an HPLC flow rate of 300 L/min and a temperature of 45°C, metabolomics samples (10 µL, 4°C) were separated and eluted over a ZIC-pHILIC column (4.6×150 mm, 5m particle size, Merck SeQuant, Darmstadt, Germany). The gradients began with 20% A (20 mM ammonium carbonate in water) and 80% B (acetonitrile) and climbed to 95% A over 15 minutes, after which the composition was restored to its initial state in 2 minutes and the column was re-equilibrated for 7 minutes. The MS equipment was configured with ESI+ and ESI- switching acquisition modes for sample profiling and data-dependent MS/MS for QC sample identification. Detailed MS parameters are displayed as follows: Capillary voltage at 20 V (ESI+) and 15 V (ESI). Spray voltage at 4.5 kV (ESI+) and 3.5 (ESI). In both modes, the sheath, auxiliary, and sweep gas flow rates were 40, 5, and 1 (arbitrary unit) per minute respectively. The temperatures of the capillary and the heater were kept at 275°C and 150°C respectively. Data for LC-MS profiling were collected with a resolution of 70,000 from 70–1050 m/z . On the QC sample (n = 3), Top 5 ddMS/MS was done at a resolution of 17,500 and normalised collision energies (NEC) of 20, 30,

and 40.

Randomly selected cellular samples from the control group and ApoE4 KI group were evaluated using mixes of authentic standards and reagent blanks in a single LC-MS analytical run. Pooled QC (n = 4) was injected at the beginning of the analysis to condition the column, and also after every 3–5 samples (n = 6) to evaluate the analytical system's stability, robustness, repeatability, and performance.

4.3.4 Cell sample preparation for OrbiSIMS

The 5 groups of cells (Blank; 5 μM L-DOPA; 5 μM L-DOPA and 16 μM of 11c; 5 μM L-DOPA and 11m; 5 μM L-DOPA and Alpha-Arbutin) were seeded on glass slides merged in a complete culture medium for 48 hours. Cells were rinsed three times with a 150mM ammonium formate solution after adhering to glass slides. The slides were frozen in liquid nitrogen and dried for 48 hours in a freezer drier. Prior to OrbiSIMS analysis, the cell slides were kept at -80°C.

4.3.5 OrbiSIMS experimental methods

The 20 keV Ar_{3000}^{+} argon gas cluster ion beam (GCIB) of 20m diameter of SIMS was employed for sputtering ions of the cell samples, and Q Exactive HF mass spectrometry was utilised for the full-MS scan in the range of 75.0 to 1120.0 m/z for negative polarity. The Q Exactive depth profile was acquired on a 300 × 300 μm^2 region in random raster mode with crater size 384.6 × 384.6 μm and mass resolution 240,000 at 200 m/z. The cycle time was established at 200μs. The time for injection was set at 500 ms. Each sample was evaluated in three distinct regions, and each measurement lasted 300 scans.

4.3.6 Identification and annotation of metabolites

Compound Discoverer 3.3 was used to pre-process LC-MS data for untargeted metabolomics, univariate analysis, and metabolite identification. In addition, SIMCA P was used to conduct principal component analysis (PCA) and partial least squares-discriminant analysis (PLS-DA). Using the Compound Discoverer 3.3 software, metabolite identification was achieved by matching the retention time of identified peaks with legitimate standards, MS/MS fragmentation with the mzCloud database, and correct masses with human metabolites in the BioCyc database. A retention period of 0.5 min to 15 min (with an RT tolerance of 0.5 min), a mass range of 70-1050 m/z, and a mass tolerance of 5 ppm was utilised for peak selection and identification. According to the categorization guidelines of the standard metabolomics project, discovered metabolites can be categorised into four degrees of confidence. Level 2 confidence in metabolite identification is based on correct mass, retention duration, or MS/MS value. Level 3 confidence of metabolite identification is based on exact mass, while unknown is classed as level 4 after confidence selection.

Using GraphPad Prism, the data was analysed and reported as the mean standard deviation (SD). The significance of metabolite differences between the control and ApoE4 KI groups was determined using the Student's t-test, ANOVA test, and PLS-DA analysis. The combination of an FDR-adjusted p-value 0.05 and a VIP>1 was judged as statistically significant in LC-MS data analysis. For the OrbiSIMS Data analysis, the combination of a RAW-adjusted P value<0.05 and VIP>1 adjusted was

judged to be statistically significant.

3D OrbiSIMS is controlled by software supplied by SurfaceLab Version 9.0 (IONTOF, Germany), which uses the application programming interface (API) supplied by Thermo Fisher for both control of the Orbitrap MS section of the instrument and online data retrieval. Ions collected from the spectrum were searched and assigned by comparing the m/z value to the LIPID MAPS and HMDB databases with a mass deviation of less than 2 p.p.m.

4.3.7 Pathway and enrichment analysis

The web-based programme Metaboanalyst (https://www.metaboanalyst.ca/) was utilised for pathway and enrichment analysis.

4.4 Results and Discussion

4.4.1 Compounds 11c and 11m have negligible cytotoxicity in cell A375

The cytotoxicity of compounds 11c and 11m to cells A375 was determined by MTT, using Alpha-Arbutin as a positive control. The cytotoxicity was measured using a gradient of concentrations (1, 2, 4, 8, 16, 32, 64, 100 μM). The results displayed in **Figure 4-1**A and **Table 4-1** show that only at ultra-high concentrations greater than 64 μM did the cellular activity change significantly. At low concentrations, the cytotoxicity of compounds 11c and 11m was negligible. Thus, this fully demonstrates that compounds 11c and 11m are safe tyrosinase inhibitors.

4.4.2 Compounds 11c and 11m inhibit tyrosinase activity and reduce melanin content in cell A375.

L-DOPA was used as a stimulating agent to test the new compounds' inhibitory effect on tyrosinase activity. Cells were then treated with different concentrations (1, 2, 4, 8, 16, 32, 64, 100 μM) of 11c and 11m or the positive control Alpha-Arbutin. After 48 hours of incubation, the absorbance was measured at 490 nm using a microplate reader to assess intracellular tyrosinase activity.

Intracellular tyrosinase activity decreased significantly with increasing drug concentrations, as shown in **Figure 4-1**B and **Table 4-2**. The IC50 for 11c, 11m, and the positive control Alpha-Arbutin were 3.849 μM, 14.63 μM, and 3.227 μM respectively. The above results indicate that compounds 11c and 11m were able to inhibit intracellular tyrosinase activity in the same dose-dependent manner as Alpha-Arbutin, and that the ability of 11c to inhibit tyrosinase activity was similar to that of Alpha-Arbutin.

In order to assess the compounds' abilities to inhibit melanin, cells were again treated with different concentrations (1, 2, 4, 8, 16, 32, 64, 100 μM) of 11c, 11m, or the positive control Alpha-Arbutin. After 48 hours of incubation, the intracellular melanin content was measured according to the absorbance at 405 nm in a microplate reader.

As shown in **Figure 4-1**(C) and **Table 4-2**, the inhibition of melanin increased significantly with increasing concentrations of 11c, 11m, and

Alpha-Arbutin. The IC50 for 11c and 11m was 2.481 μM and 7.026 μM respectively, compared to 6.179 μM for the positive control Alpha-Arbutin. This indicates that 11c had a significantly higher ability to reduce melanin content than the positive control, while the effect of 11m was similar to that of the positive control. However, it can also be seen that the inhibitory effect on melanin was not further enhanced with increasing concentrations of the drug above 16 μM.

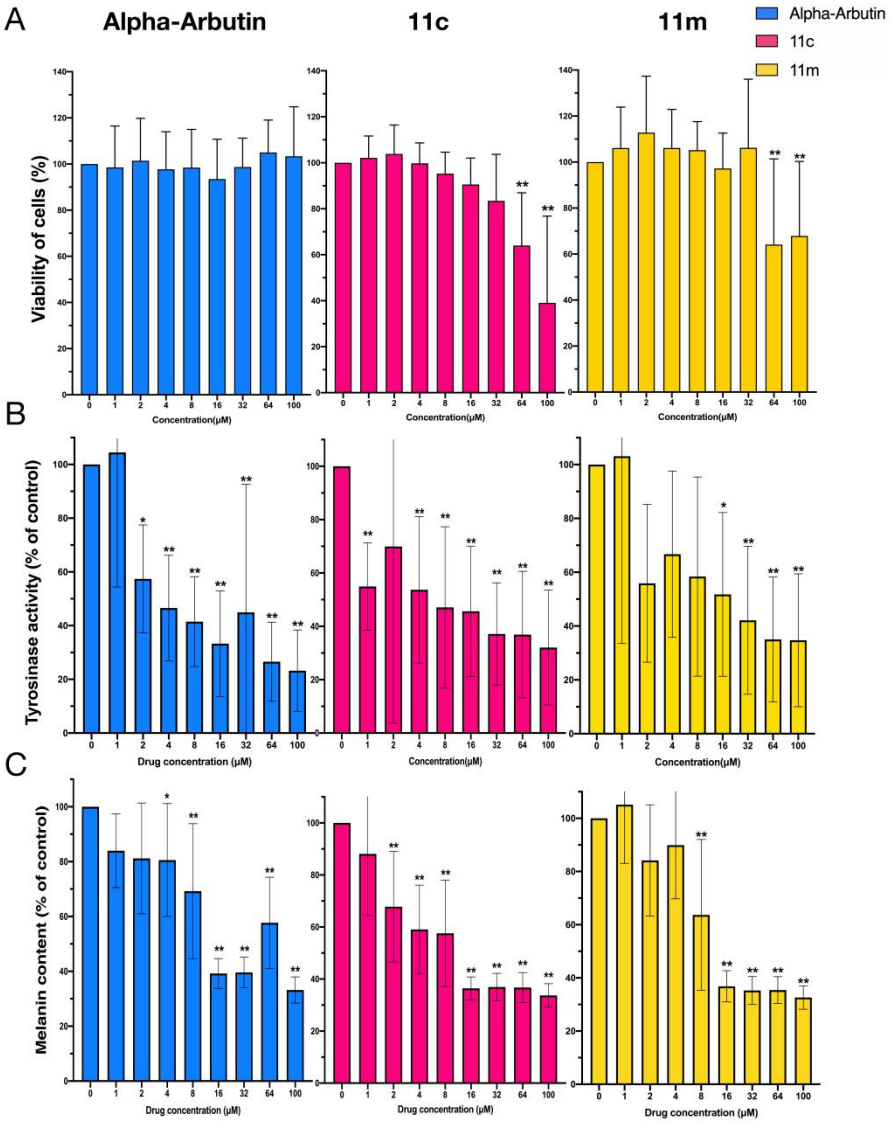


Figure 4-1 (A) Cytotoxicity of 11c, 11m and Alpha-Arbutin in cell A375; Total melanin content (B) and tyrosinase activity (C) in A375 melanoma cells after treatment with 11c, 11m and Alpha-Arbutin for 48h; A375 cells were exposed to 11c, 11m and Alpha-Arbutin at different concentrations for 48h, as shown in this figure. Data are expressed as absorbance levels. The statistical significance of differences was assessed using ANOVA one-way test. Values were significantly different from those of the control group. (A,n=4; B&C, n=9; values are means ± SE). *P < 0.05, **P < 0.01.

Table 4-1 Cytotoxicity of 11c, 11m, and Alpha-Arbutin in cell A375 in 48h

Cytotoxicity	Alpha-Arbutin	11c	11m
IC50 (μM)	4.904×10^{152}	82.3	128.1

Table 4-2 Inhibition of Tyrosinase and Melanin of by 11c, 11m, and Alpha-Arbutin in cell A375 in 48h

IC50 (μM)	Alpha-Arbutin	11c	11m
Melanin Inhibition	6.179	2.481	7.026
Tyrosinase Inhibition	3.227	3.849	14.63

4.4.3 LC-MS Metabolic profiles of melanoma cell A375 treated with L-DOPA only, or along with Alpha-Arbutin, 11c, and 11m.

The proliferation and apoptosis of melanoma cells are inextricably linked to the presence of a wide range of amino acids. In fact, relatively specific amino acid dependence has been found to be one of the metabolic abnormalities of melanoma cells[447,452,453]. It has been suggested in the literature that amino acids, particularly leucine and glutamine, are

essential for the growth, survival, and metabolism of tumour cells. Abnormal increases in some amino acids can even lead to the proliferation and metastasis of cancer cells[454]. Therefore, studying changes in metabolites such as amino acids is vital for understanding the effects of drugs on melanoma cells. To analyse the changes in polar metabolites such as amino acids in melanoma cells by L-DOPA and tyrosinase inhibitors, endogenous metabolites were chosen to be measured by hydrophilic interaction chromatography (HILIC) LC-MS in this study. A total of 1047 features were detected and then used for identification. Metabolite identification was performed by using the confidence levels recommended by the Metabolomics Standards Initiative (MSI). The databases used to assess metabolite confidence levels included the standards database for matching retention times of authentic standards, the mzCloud MS/MS database for matching MS/MS fragmentation databases, and the human database for matching accurate quality to metabolites. Following confidence selection, 108 metabolites were identified as high-confidence metabolites (Level 1 and 2) based on the MSI identification levels. These included Amino acids and pepides, Fatty Acids and Conjugates, TCA acids, Purines. Monosaccharides, Cholines, Pyrimkdines, Fatty esters, Pyridoxines, Nicatinamides, Sulfonic acids, Pyridinecarbaxylic acids and other organic acids (**Figure 4-2**B), and the score plot from the PLS-DA analysis showed a clear separation of metabolism between the five groups (**Figure 4-2**A). It is clear from the heat map analysis (**Figure 4-2**C) that most of the metabolites decreased significantly after the addition of L-DOPA e.g. Chenodeoxychol,

Hypoxanthine, Leucinic acid, and Acetoin. Only Hypoxanthine showed a significant increase after the addition of tyrosinase inhibitors.

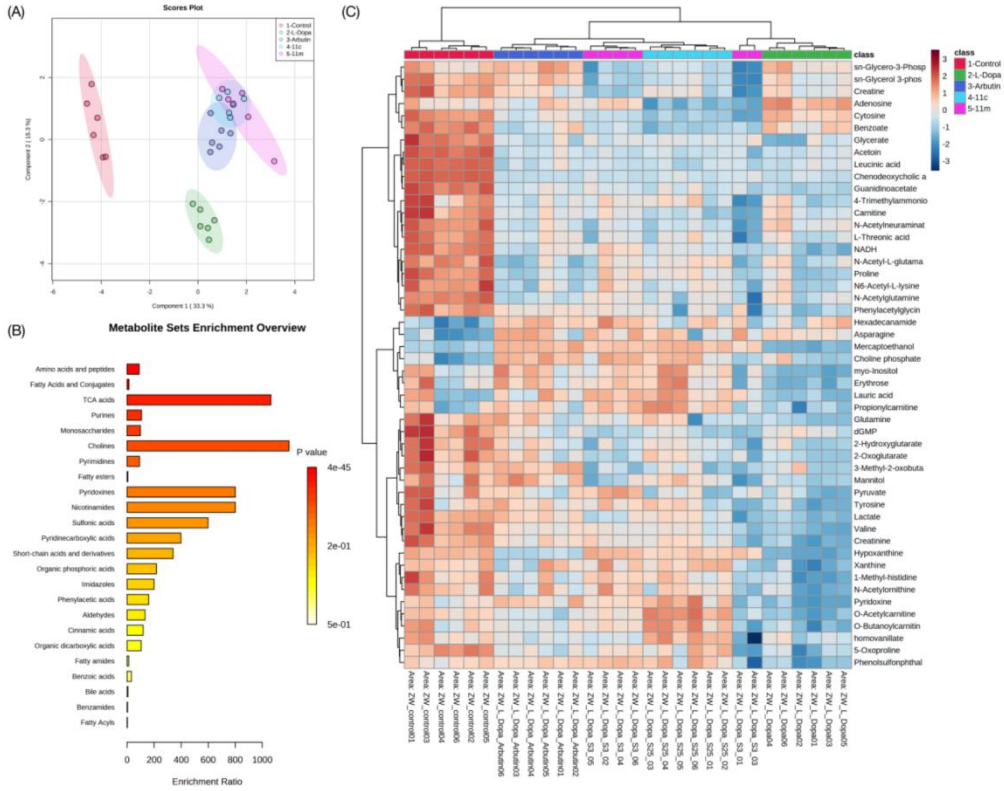


Figure 4-2 (A) The PLS-DA score plots for control, L-DOPA(5μM), Alpha-Arbutin(16μM), 11c(16μM), and 11m(16μM), in A375 cells. All groups except control contain L-DOPA (5 μM). R2=0.99 Q2=0.95. (B) The classification of annotated metabolites detected from A375 cells by LC-MS. (C) Heatmap of different metabolites for 5 groups. The top 50 identified differential metabolites were used to perform heatmap analyses. The color represents the metabolite concentration of each sample calculated by peak area normalization method.

In addition, in **Figure 4-3**, changes in metabolic profiles were compared between the control and L-DOPA groups and between the L-DOPA and 11c groups respectively. Between the control and L-DOPA grounds, 72 metabolites were considered to be statistically significant (FDR value < 0.05), while between the L-DOPA and 11c groups, 41 metabolites were considered statistically significant. The log normalised intensities of these features are shown in **Figure 4-4**.

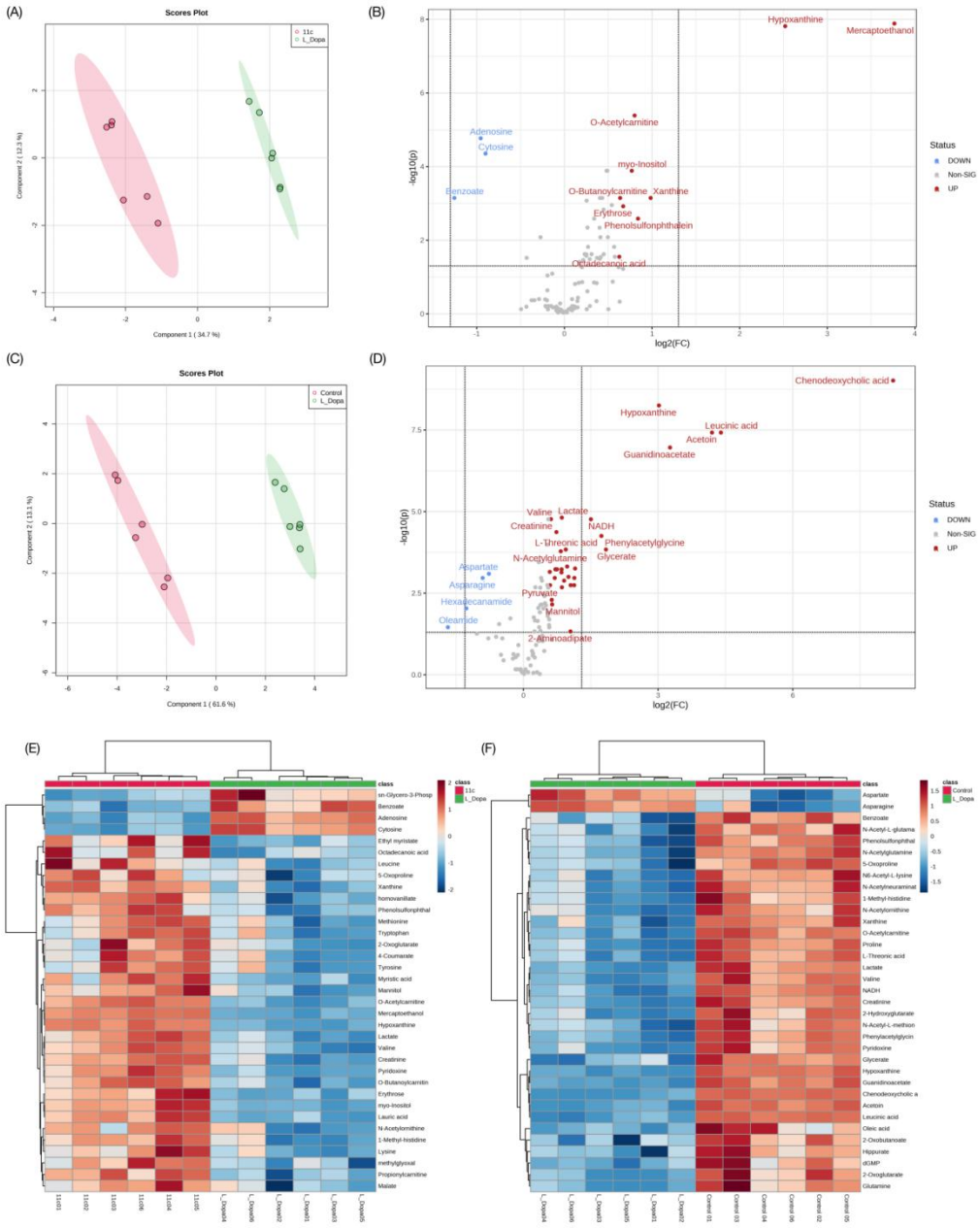


Figure 4-3 (A) The PLS-DA score plots, (B)volcano plot and (E) heatmap for control and 5μM L-DOPA group in A375 cells. R2=0.99 Q2=0.96 (C)The PLS-DA score plots, (D)volcano plot, and (F) heatmap for L-DOPA(5μM) and 11c group(16μM 11c & 5 μM L-DOPA) in A375 cells. R2=0.99 Q2=0.99. In the volcano plot, fold change threshold (x) 1.5 and p-value threshold (y) 0.05 were used. The red(up) and blue(down) dots

represent metabolites above the threshold. The top 35 identified differential metabolites were used to perform heatmap analyses. The colour represents the metabolite concentration of each sample calculated by peak area normalization method.

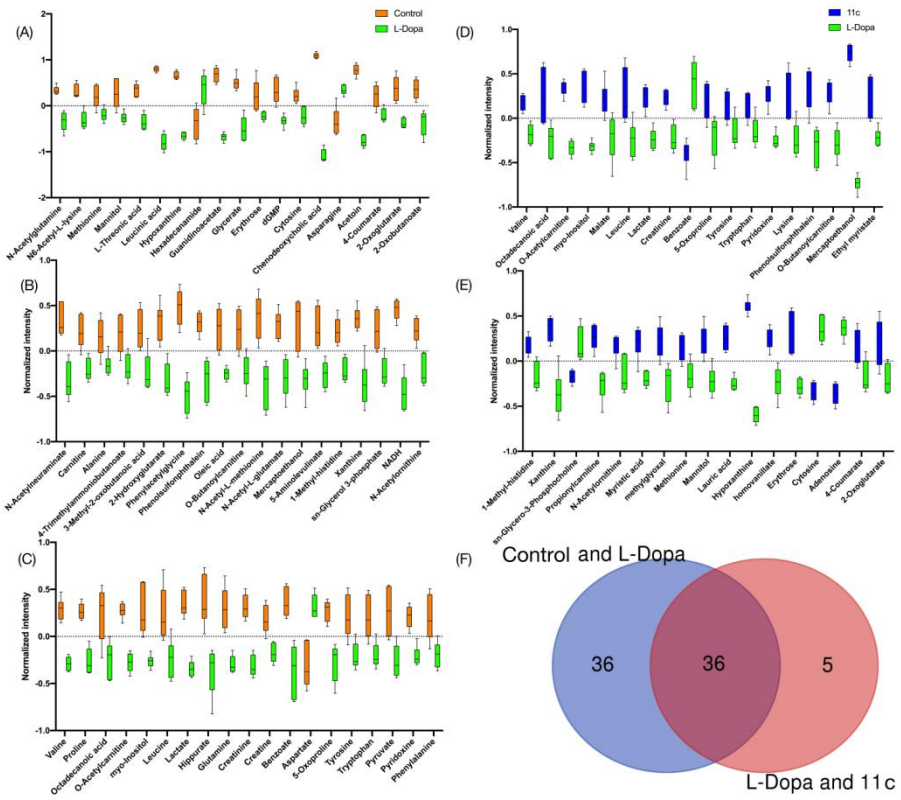


Figure 4-4 (A-E)The relative normalized intensity of significantly identified metabolites detected from LC-MS. (F)The Venn diagram of significantly different metabolites in the control and 5μM L-DOPA group compared with significantly different metabolites in the L-DOPA (5 μM) and 11c group (16μM 11c & 5 μM L-DOPA) group, in which 36 metabolites were found to be significantly different in both groups.

4.4.4 Tyrosinase modulators significantly perturb phenylalanine, tyrosine and tryptophan biosynthesis and Malate-Aspartate Shuttle

Pathway enrichment analysis using the characteristic metabolites from these two comparison groups (based on two different databases, KEGG and SMPDB) yielded that phenylalanine, tyrosine and tryptophan biosynthesis and Malate-Aspartate Shuttle were the two most important metabolic pathways (**Figure 4-5**). In the phenylalanine, tyrosine and tryptophan biosynthesis pathway, the expression of the metabolites phenylalanine and tyrosine was down-regulated in the L-DOPA group (**Figure 4-6**A). This was due to the addition of L-DOPA, which induced a rapid and dose-dependent increase in tyrosinase activity, thereby accelerating hydrolysis of the substrate (tyrosine) and phenylalanine. This coincided with the results of the changes in metabolites.

Moreover, phenylalanine and tyrosine showed a significant rebound after adding tyrosinase inhibitors. Of these, 11c was found to have a similar capacity to the positive control alpha-arbutin and was significantly better than 11m, which is consistent with our previous findings in Chapter 3. In addition, as an important intermediate in the tyrosine metabolic pathway, there was a change in the amount of L-DOPA obtained in the assay using OrbiSIMS. Unlike other tyrosinase inhibitors, the novel tyrosinase inhibitor 11c significantly inhibited the production of L-DOPA and thus effectively inhibited melanogenesis. L-DOPA is as an important intermediate in the tyrosine metabolic pathway and an oxidation product produced by the hydroxylation of tyrosine by the action of tyrosine hydroxylase[455].

Therefore, it can be assumed that 11c has an inhibitory effect on other enzymes, such as tyrosine hydroxylase.

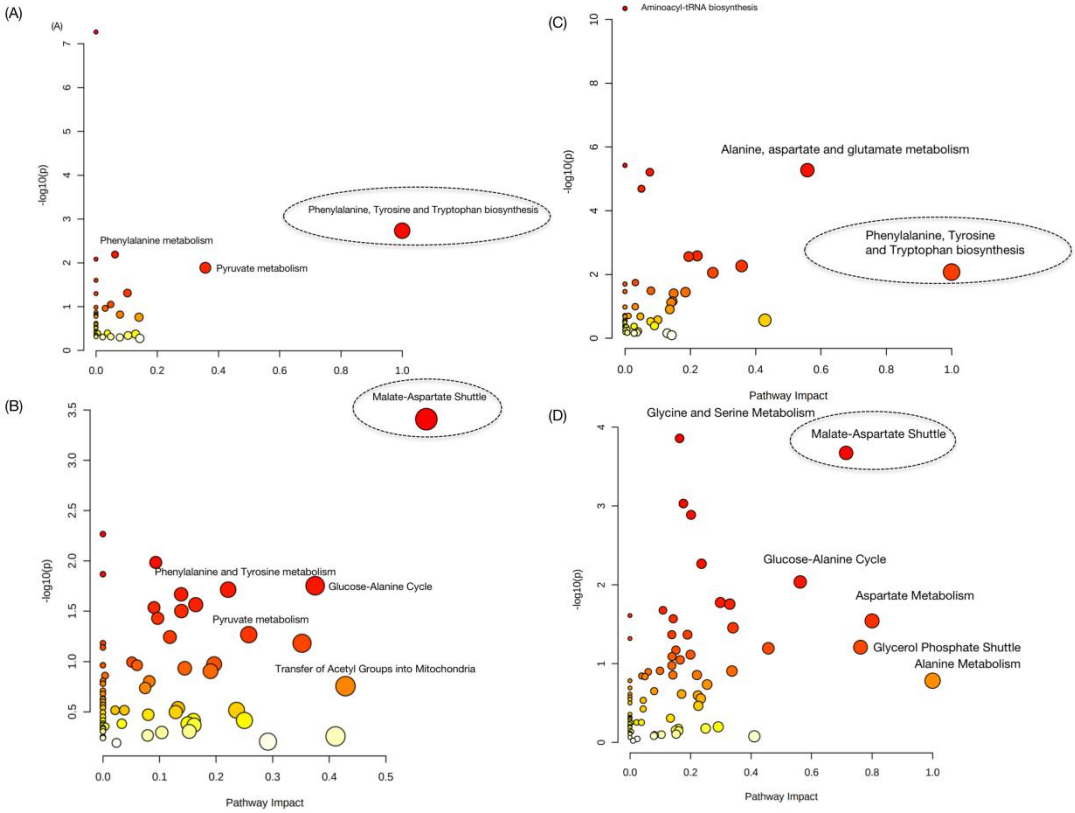


Figure 4-5 The pathway enrichment analysis of the control and 5 μM L-DOPA group in A375 cells with (A) KEGG and (B) SMPDB database. The pathway enrichment analysis of the L-DOPA group(5 μM) and 11c group(16μM 11c & 5 μM L-DOPA) in A375 cells with (C) KEGG and (D) SMPDB database.

In contrast, the apparent metabolic pathway obtained based on the SMPDB database (**Figure 4-5**B&D) was that of Malate-Aspartate Shuttle (**Figure 4-6**B), where Aspartate was found to be significantly up-regulated

and NADH and α-KG were significantly down-regulated in the L-DOPA group. Both Aspartate and NADH are closely associated with various types of cancer, especially melanoma. It has been shown that elevated levels of Aspartate promote cancer cell growth[456]. Most cancer cells rely on glycolysis to produce ATP, meaning Aspartate is essential for cell proliferation as it is a necessary metabolite in glycolysis. Moreover, asparate production results in cellular respiration, which leads to cell proliferation[457]. In our study, increased levels of Aspartate in the metabolites of the L-DOPA group were found to induce further proliferation of melanoma cells. However, this was not improved by the addition of tyrosinase inhibitors.

It has been suggested that NADH has an inhibitory effect on the growth of cancer cells and that there are different biochemical operating mechanisms and targets of NADH in the control of cancer cell growth[458]. Moreover, NADH has a preventive effect on cancer metastasis[459]. This is due to the fact that upon addition of NADH, the level of ATP in the cells can be increased, and when sufficient ATP is present in the cells, those regulatory factors that are necessary to stop cell division can be produced[460]. Therefore, the decrease in the level of NADH in the cells of the L-DOPA group indicates a decrease in the level of those regulatory factors necessary to stop cell division. As a result, the rate of cell proliferation increased. In contrast, after the addition of tyrosinase inhibitors, NADH levels were rebounded, with the most pronounced rebound found after the addition of 11m.

Alpha-ketoglutarate (α-KG, α-ketoglutarate) is an essential metabolite in the tricarboxylic acid (TCA) cycle and has an important regulatory role in physiological processes such as lipid synthesis, oxidative stress, protein modification, and cell death. Currently, several studies have been published suggesting that α-KG has potential antitumour effects[461].

The literature suggests that α-KG is an effector of p53-mediated tumour suppression and that accumulation of α-KG in p53-deficient tumours drives tumour cell differentiation and resists malignant tumour progression[462]. Moreover, α-KG also induces tumour cell scorching and inhibits breast cancer cell growth. Overall, α-KG levels have been found to be negatively correlated with cell proliferation capacity[463]. Therefore, in the L-DOPA group, the decreased level of α-KG indicates that cancer cells exhibited a significant proliferative and differentiation capacity. In contrast, the addition of the tyrosinase inhibitors alpha-arbutin and 11c resulted in a significant rebound in α-KG levels.

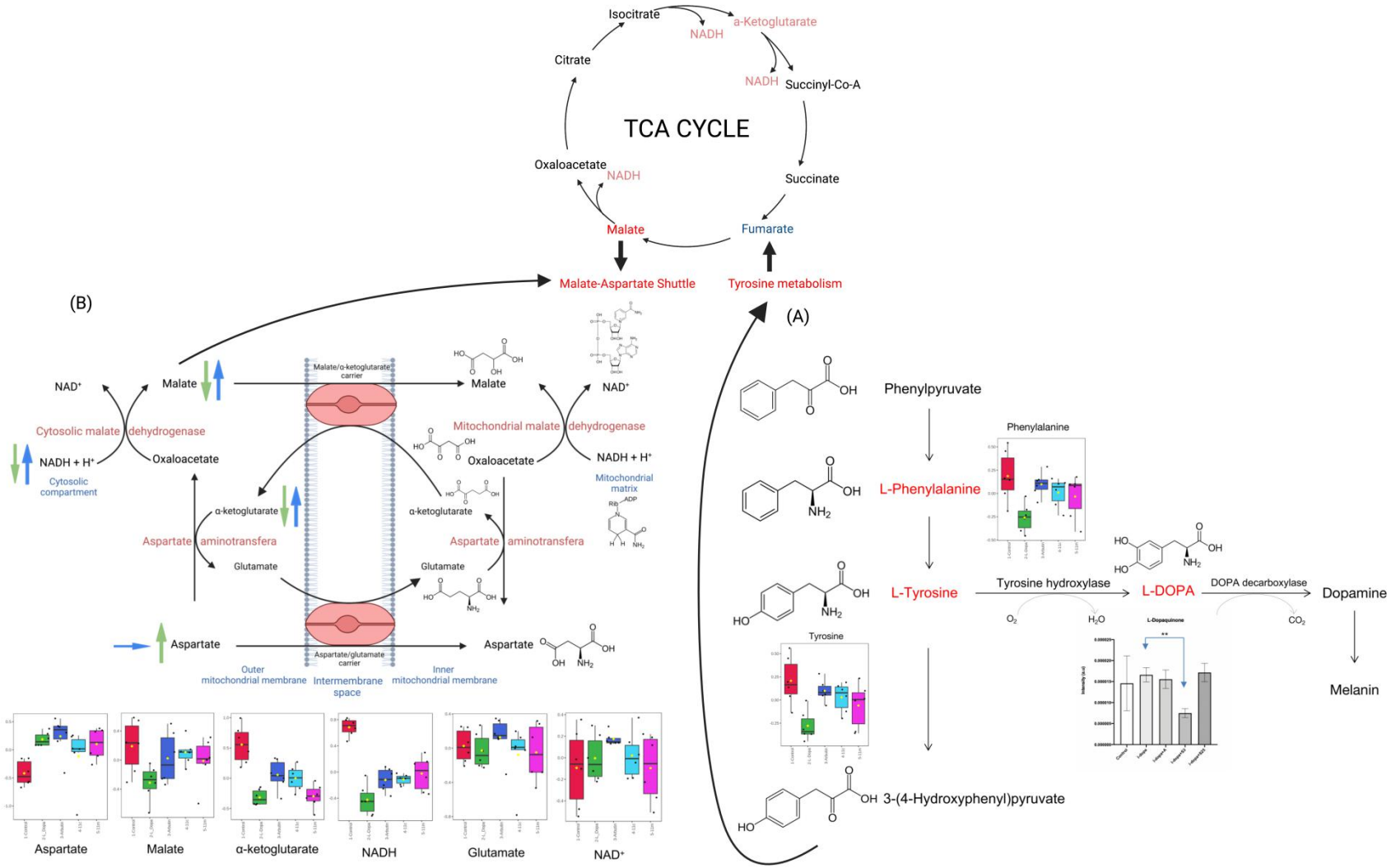

TCA CYCLE
Isocitrate
NADH
α-Ketoglutarate
NADH
Succinyl-Co-A
Succinate
Fumarate
Malate
NADH
Oxaloacetate
Citrate
Malate-Aspartate Shuttle
Tyrosine metabolism
(A)
Phenylpyruvate
L-Phenylalanine
L-Tyrosine
3-(4-Hydroxyphenyl)pyruvate
Phenylalanine
Tyrosine
Tyrosine hydroxylase
L-DOPA
DOPA decarboxylase
Dopamine
Melanin
(B)
NAD+
Malate
Cytosolic malate dehydrogenase
NADH + H+
Oxaloacetate
Cytosolic compartment
Malate/α-ketoglutarate carrier
Malate
NAD+
Mitochondrial malate dehydrogenase
Oxaloacetate
NADH + H+
Mitochondrial matrix
α-ketoglutarate
Aspartate aminotransfera
Glutamate
α-ketoglutarate
Aspartate aminotransfera
Glutamate
Aspartate
Aspartate/glutamate carrier
Aspartate
Outer mitochondrial membrane
Intermembrane space
Inner mitochondrial membrane
Aspartate
Malate
α-ketoglutarate
NADH
Glutamate
NAD+

Figure 4-6 The pathway network mapping. (A)Phenylalanine, tyrosine and tryptophan biosynthesis and tyrosine metabolism. Red font signals detected molecules and the bar chart shows the relative intensity of each species. (B)Malate-Aspartate Shuttle. The green arrow identifies the change of L-DOPA group to the control group. The blue arrow identifies the change of 11c group to the L-DOPA group. The bar chart shows the relative intensity of each detected species.

Overall, phenylalanine, tyrosine, and tryptophan biosynthesis and the Malate-Aspartate Shuttle are thought to be the two most affected pathways. These two metabolic pathways can be linked via the TCA cycle; fumaric acid is used as the posterior of tyrosine and participates in the TCA cycle to produce malate, thus affecting the Malate-Aspartate Shuttle pathway[464]. Of these two pathways, the effects of L-DOPA and tyrosine inhibitors on the phenylalanine, tyrosine, and tryptophan biosynthesis pathway are known. However, the effects on the Malate-Aspartate Shuttle (MAS) pathway have been a new discovery. Previous literature has shown that the MAS pathway is associated with lung cancer cells as well as melanoma[465]. Cancer cells use more oxygen than normal cells for oxidative phosphorylation and rely heavily on NADH in the cytoplasm for ATP production via the MAS pathway in the mitochondria. However, the effect of L-DOPA and tyrosinase inhibitors on the MAS pathway was previously unknown. Now, the results of metabolite analysis have demonstrated that L-DOPA and tyrosinase inhibitors significantly affect the

MAS pathway, thereby affecting ATP production and lipid metabolism. This is a significant new finding that will aid in future research.

The changes in individual metabolites shown above demonstrate the possible proliferative effect of L-DOPA on melanoma cells. The addition of tyrosinase inhibitors could improve this by increasing the expression of metabolites such as tyrosine, L-DOPA, α-KG, and NADH. It is suggested that these metabolites are new targets that should be considered for the treatment of melanoma, and that tyrosinase inhibitors could be used to some extent as an adjunct to promote the upregulation of cancer cell suppressors, thereby inhibiting the transitional differentiation of cancer cells.

4.4.5 OrbiSIMS lipid metabolic profiles of melanoma cell A375 in the presence of L-DOPA only, or with Alpha-Arbutin, 11c and 11m.

The changes in lipid metabolites in melanoma cells is another point of concern. Melanoma cells, being cancer cells, are able to provide the ATP and macromolecules needed for cell growth, division, and survival by reshaping their metabolism. Therefore, lipid synthesis and metabolism should be the focus of discussion in tumour cells. Moreover, based on the metabolic markers obtained using LC-MS analysis, it has been noted that phenylalanine, α-KG, and NADH all have important regulatory roles in lipid metabolism[466–468]. For example, phenylalanine is mostly oxidised to tyrosine in vivo through the catalytic action of phenylalanine hydroxylase, and together with tyrosine, it synthesises important neurotransmitters and

hormones and participates in glucose and lipid metabolism in the body. α-KG is not only an essential metabolite in the tricarboxylic acid (TCA) cycle, but also plays a vital role in lipid synthesis, oxidative stress, protein modification, and lipid metabolism. NADH can react with free radicals to inhibit lipid peroxidation and protect mitochondrial membranes and mitochondrial function. Therefore, changes in such lipid metabolites should also be an area of focus for research.

According to the current research literature, 3D OrbiSIMS has excellent potential for direct cellular analysis and in situ metabolite analysis as it has the advantage and sensitivity for the screening and detecting of lipid metabolites. Thus, the OrbiSIMS screening tool was selected to detect 115 putative annotated lipid metabolites against 5 different experimental groups. Score plots using PLS-DA analysis showed a clear separation of metabolic profiles between the 5 groups (**Figure 4-7**A). As shown in **Figure 4-7**B, 20 of the lipids had significant variation (p.value<0.01) according to ANOVA analysis, with 17 of these being fatty acids (FA). In addition, as shown in Figure 7 (D-I), changes in lipid metabolite profiles were compared between the control group and the L-DOPA group and between the L-DOPA group and the 11c group respectively. Both volcano and heatmap analyses clearly demonstrated that most lipid metabolites were significantly down-regulated by the addition of L-DOPA. However, upon addition of 11c, the intracellular lipid levels were significantly increased, returning to the same level as the control group. This indicates that both L-DOPA and 11c have significant, albeit different, effects on lipid

synthesis and metabolic pathways. In contrast, Alpha-Arbutin and 11m had no effect on lipid metabolites.

Figure 4-7 (E&F) shows 23 significantly altered metabolites (p.value<0.01) in the control and L-DOPA groups, while their log normalised intensities are shown in Figure 8A. Twenty of these were FA and all showed a decrease in the L-DOPA group. **Figure 4-7** (H&I) shows the 47 apparently altered metabolites in the L-DOPA and 11c groups, with their log normalised intensities shown in Figure 8B. All metabolites except for lipids PE(O-38:3) or PE(P-38:2) and SM(d16:1/17:0) showed a decrease in intracellular levels after the addition of 11c. All other apparent signatures showed an increasing trend, and 20 of them were Fatty Acids and Conjugates (**Table 4-3**).

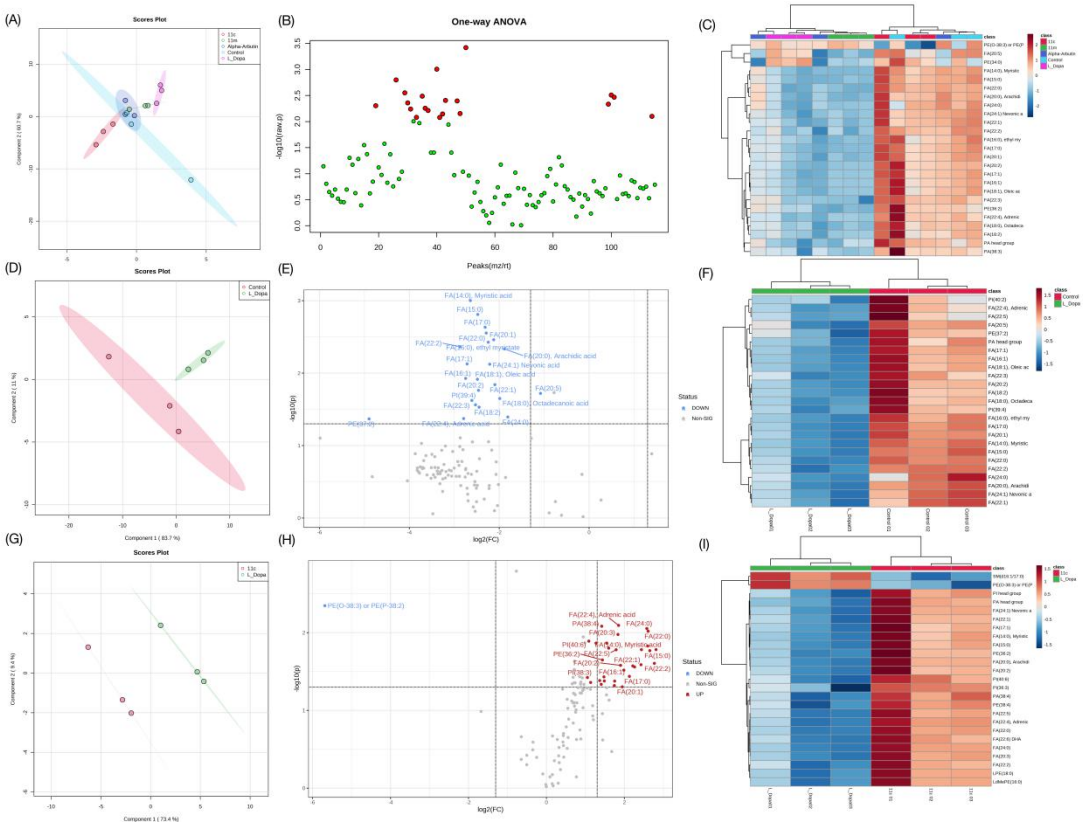


Figure 4-7 (A) The PLS-DA score plots, (B)ANOVA plot and (C)Heatmap of lipid metabolites for control, L-DOPA(5μM), Alpha-Arbutin(16μM), 11c(16μM), and 11m(16μM), in A375 cells. All groups except control contain L-DOPA (5 μM). The red dots represent the lipid metabolites with a significant difference. (D) The PLS-DA score plots (R2=0.99 Q2=0.59), (E) Volcano plot, and (F) Heatmap for control and 5 μM L-DOPA group in A375 cells. (G) The PLS-DA score plots (R2=0.99 Q2=0.76), (H) Volcano plot, and (I) Heatmap for L-DOPA (5 μM) and 11c group(16μM 11c & 5 μM L-DOPA) in A375 cells. The volcano plot has fold change threshold (x) 2 and p-value threshold (y) 0.1. The red (up) and blue (down) dots represent lipid metabolites above the threshold. The top 25 identified differential metabolites were used to perform heatmap analyses. The color represents the metabolite concentration of each sample calculated by peak area normalization method.

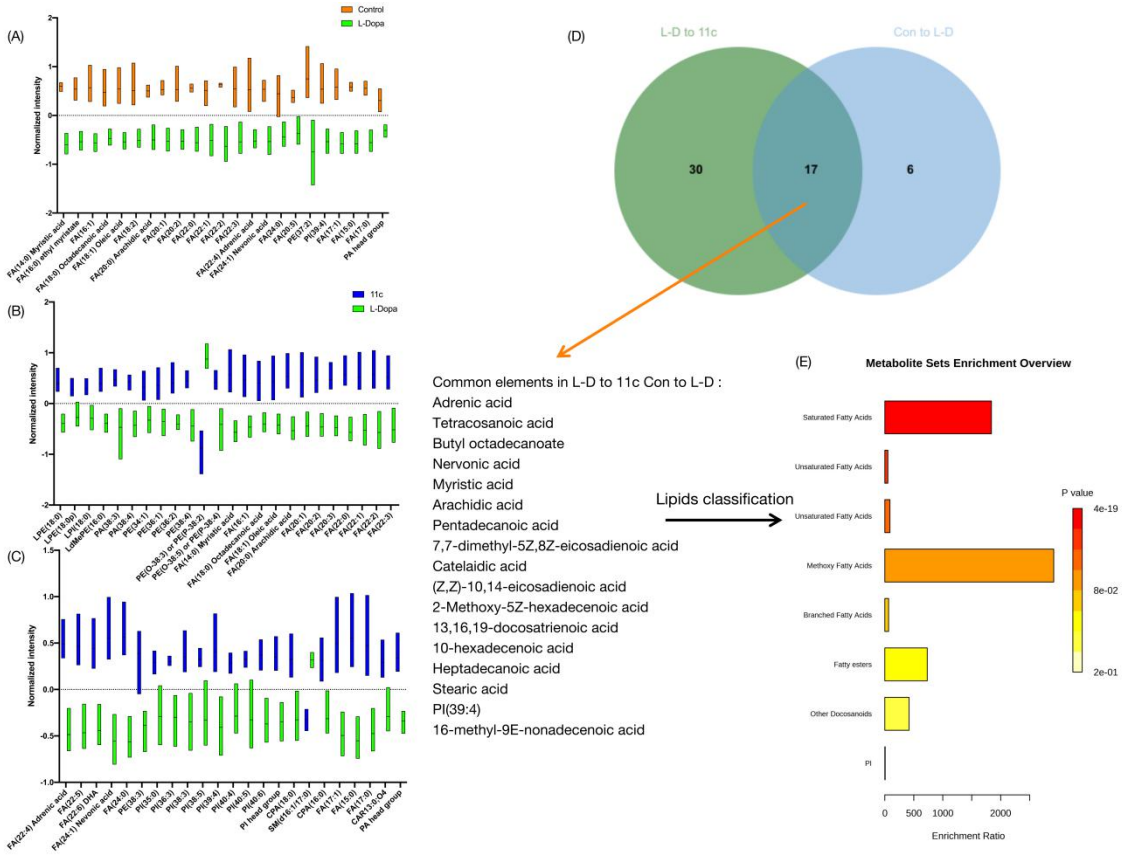


Figure 4-8 The relative normalized intensity of significantly identified lipid metabolites detected from OrbiSIMS, (A) Control, and 5 μM L-DOPA group in A375 cells; (B&C) L-DOPA (5 μM) and 11c group(16μM 11c & 5 μM L-DOPA) in A375 cells; (D) Venn diagram of significantly different lipid metabolites in the control and 5 μM L-DOPA group compared with the L-DOPA (5 μM) and 11c group(16μM 11c & 5 μM L-DOPA), in which 17 metabolites were significantly different across both groups. (E) The enrichment analysis of 17 lipid signatures in 1072 sub-chemical class metabolite sets.

Table 4-3 The classification of annotated lipid metabolites detected by OrbiSIMS.

Lipids metabolites classification	Control to L-DOPA (23)	L-DOPA to 11c (47)
Fatty Acids and Conjugates	20	18
Glycerophosphoethanolamines	1	11
Glycerophosphoinositols	1	9
Other Glycerophospholipids	0	1
Docosanoids	1	2
Steroids	0	1
Glycerophosphates	0	2
Sphingomyelins	0	1
Glycerophospholipids	0	2

4.4.6 Tyrosinase modulators significantly perturb the fatty acid metabolism

In addition, **Figure 4-8**D&E show that there were 17 significant change agents common to the two comparison groups, 15 of which were fatty acids. This demonstrates the importance of fatty acid metabolism in melanoma cells. It is well known that fatty acids, in addition to being structural components of the membrane matrix, are substrates for β-oxidation and can be used as a fuel source for energy production[469]. Fatty acids can be synthesised by fatty acid synthase (FASN), which is overexpressed in a variety of cancers, including melanoma. Its elevated expression is associated with tumour cell invasion and poor prognosis[470]. Uptake of fatty acids in the surrounding microenvironment and fatty acid β-oxidation and storage also play an important role in tumour cells. Recent studies have shown that FATP1/SLC27A1, a carrier of long-chain fatty

acids, is enriched in melanoma compared to other types of cancer, thus highlighting the importance of fatty acid uptake for melanoma progression[471].

Most studies nowadays focus only on either lipids or the expression of fatty acids in melanoma cells. However, the understanding of the relationship between tyrosinase regulators and fatty acids is still very limited, especially with regards to metabolic changes in melanoma cells. Intravenous injection of L-DOPA has been reported to increase plasma FFA and plasma glucose in dogs and humans[472]. In addition, L-DOPA has a specific structure similar to that of aromatic amino acids and is able to interact with the bilayer of different lipid components and reduce lipid peroxidation[473]. However, previous studies have only addressed the role of L-DOPA in neurodegenerative diseases such as PD, while studies in melanoma cells are still lacking.

Regarding the relationship between tyrosinase inhibitors and fatty acids, it has been documented that tyrosinase inhibitors usually have antioxidant effects and therefore reduce lipid peroxidation[166]. Much of the research has focused on the fact that fatty acids can act as tyrosinase inhibitors and reduce melanin production[474,475]. However, there has been no discussion on the role of tyrosinase inhibitors in melanoma cells for fatty acid metabolism. Therefore, this is the first discussion on the effect of tyrosinase modulators in melanoma cells on the metabolism of lipids such as fatty acids.

Overall, the results of the present study showed that the levels of fatty acids and other lipid metabolites in melanoma cells decreased significantly upon addition of L-DOPA and increased significantly upon addition of the novel tyrosinase inhibitor 11c. In contrast, the addition of Alpha-Arbutin and 11m had no significant effect on lipid metabolism. The evidence suggests that tyrosinase modulators are closely associated with fatty acid metabolic pathways. Furthermore, many studies have shown that fatty acid levels are usually higher in cancer cells than in normal tissue[476,477]. This suggests that at the fatty acid level, the activity of melanoma cells is inhibited after the addition of L-DOPA and activated after the addition of 11c. This is inconsistent with the conclusions obtained from the amino acid metabolism section, but this may also be the reason for the lack of significant cytotoxicity following the addition of tyrosinase inhibitors such as L-DOPA and 11c.

4.5 Conclusion

In conclusion, the novel tyrosinase inhibitor 11c had a similar tyrosinase inhibitory effect (IC50=3.849 μM) and an even better melanin inhibitory effect (IC50=2.481 μM) than Alpha-Arbutin. In addition, based on metabolomic and lipidomic analyses, we found that L-DOPA and 11c acted as stimulators of up- and down-regulation of tyrosinase activity respectively. We determined that tyrosinase modulators acting on melanoma cells A375 were significantly associated with the phenylalanine, tyrosine, and tryptophan biosynthesis pathway and for the first time, found a correlation with the Malate-Aspartate Shuttle metabolic pathway. In

addition, there was a significant correlation in the lipidome, especially for fatty acid metabolism. This provides a significant contribution to further studies on the role of tyrosinase modulators in melanoma. Helping researchers to understand the potential mechanisms by which tyrosinase modulators act on melanoma cells may lead to the identification of new targets, which could lead to the development of safer drugs. Furthermore, because of the complex interactions between oncogenic signalling, dysregulation of amino acid, and fatty acid metabolism in melanoma, it is important to further explore the effects of tyrosinase modulators such as L-DOPA and 11c on the metabolism of melanoma cells.

Chapter 5. General conclusions, future work and perspectives

5.1 General conclusion

Although hyperpigmentation as a skin disorder is not malignant, it can significantly impact a patient's daily life negatively. In addition, if left untreated, it can potentially worsen and lead to an increased risk of melanoma. It is therefore essential and urgent to find proper and effective treatment.

Existing hypomelanotic agents are mainly tyrosinase inhibitors. However, existing tyrosinase inhibitors have some drawbacks, so a targeted search to either improve existing tyrosinase inhibitors or explore new and superior tyrosinase inhibitors is a pressing need and a goal of this thesis. In addition, an extended exploration of the metabolomics and mechanisms of tyrosinase modulators in melanoma cell has been undertaken in this thesis. Overall, a range of approaches and results have been covered here and has furthered our understanding of tyrosinase inhibitors and potential treatment options.

It is well known that in the absence of microneedles, Alpha-Arbutin has a low permeation rate due to its high hydrophilicity. The first objective of my PhD project was to find a suitable microneedle delivery strategy that would enhance the intradermal delivery of Alpha-Arbutin. To achieve this goal, I chose to adapt two different microneedles, solid microneedle Dermapen®

and dissolving polymeric microneedle. The use of Dermapen® was also split into two different delivery sequences: pre-treatment application and post-treatment application. Afterwards, the permeation of Alpha-Arbutin in the skin was assessed by HPLC for three different commercial products, and the permeation of Alpha-Arbutin in the skin was visualised using OrbiSIMS to determine its spatial distribution.

One of the main findings of this thesis concerns the effect of mechanical insertion of solid microneedles and the sequence of drug delivery on the drug permeation capacity. HPLC analysis showed that the drug amount rate within the skin increased more significantly after solid microneedle post-treatment than pre-treatment. In addition, dissolving polymeric microneedles loaded with Alpha-Arbutin were also found to improve the intradermal permeation of Alpha-Arbutin significantly. However, there was no significant difference in the enhancement of the skin penetration capacity of solid microneedle post-treatment versus dissolved polymeric microneedle for Alpha-Arbutin when considering the proportion of intradermal content.

Subsequently, to further determine the difference in the drug permeation ability of the two different types of microneedles, the definitive location of arbutin retention within the skin was located. Therefore, in this experiment, for the first time, 3D OrbiSIMS and skin cross-section analysis were combined to assess the distribution of Alpha-Arbutin within the skin utilising 2D high-resolution imaging. It was found that dissolving polymer microneedles are more effective in increasing the amounts of Alpha-

Arbutin in the layer where melanocytes are located and in improving Alpha-Arbutin targeted delivery. This suggests that, overall, dissolving polymeric microneedles are better at reaching the target than solid microneedles. In addition, dissolving polymeric microneedles offer better prospects in terms of adherence and safety. This is because dissolvable microneedles are a straightforward way of administering drugs, which makes it simple and easy for patients to handle themselves. Moreover, there is no risk of the steel needle breaking off and remaining in the skin.

Thus, in an optimised protocol based on existing tyrosinase inhibitors, dissolving polymeric microneedles may be a promising delivery system that can be combined with Alpha-Arbutin to facilitate intradermal delivery for the treatment of pigmentation disorders.

However, due to the physical and chemical deficiencies of Alpha-Arbutin itself and the fact that a large number of existing melanin-reducing agents have several drawbacks, it is necessary to develop a new and effective melanin-reducing agent. As a key rate-limiting enzyme in melanogenesis, TYR has emerged as the most important target for melanogenesis inhibition. Thus, inhibition of TYR became a focus of this study.

A series of potential TYR inhibitors were synthesised with a dihydrochalcone backbone incorporating a resorcinol structure. They were then evaluated and screened on the basis of their biological activity. Compounds 11c and 11m showed the most potent inhibitory activity on mushroom tyrosinase. Furthermore, mechanistic validation experiments

showed that 11c might inhibit melanin production by inhibiting TYR function and reducing TYR content in a non-competitive manner. Moreover, there was satisfactory antioxidant activity. This makes it a very promising compound.

In Chapters 3 and 4, the low cytotoxicity of the novel tyrosinase inhibitors 11c and 11m in human-derived melanoma A375 cells, as well as their outstanding TYR inhibition and melanin inhibition, were successfully demonstrated. Compound 11c exhibited similar tyrosinase inhibition to Alpha-Arbutin (IC50=3.849 μM) and even better melanin inhibition than Alpha-Arbutin (IC50=2.481 μM). Furthermore, the HPLC results provide ample evidence of compound 11c with excellent performance in *in vitro* skin permeation tests, rapidly crossing the cutaneous stratum corneum and remaining within the skin. At the same time, OrbiSIMS spatial distribution analysis of the drug confirmed its ability of targeted drug delivery, staying in the basal layer and focusing only on melanocytes. More importantly, in an *in vivo* guinea pig model, 11c also exhibited a strong anti-melanogenic capacity. Overall, compound 11c can be considered as a low-toxic and potent TYR inhibitor for the further development of new therapies for the treatment of skin pigmentation disorders.

Having confirmed that compounds 11c and 11m have superior heterogeneous tyrosinase inhibitory abilities, the next step was to gain further insight into their mechanisms of action, particularly concerning metabolite changes in melanoma cells. A link between L-DOPA as a

tyrosinase stimulator and the appearance of melanoma was found. Therefore, to further understand this principle, metabolomics and lipidomics were chosen to analyse the metabolic pathways of the tyrosinase modulators L-DOPA and 11c in melanoma. Based on LC-MS analysis, it was shown that in melanoma cells A375, tyrosinase regulators are associated with the biosynthetic pathways of phenylalanine, tyrosine, and tryptophan. This is the first time that the relevance of tyrosinase modulators to the Malate-Aspartate Shuttle metabolic pathway has been specified and is one of the main findings of this thesis. In turn, Malate-Aspartate Shuttle influences the formation of ATP via the TCA cycle and affects cellular respiration. In addition, fatty acids showed significant changes in the lipidome. In accordance with previous literature, the importance of FA uptake on melanoma progression was highlighted and it was found that FA metabolism could regulate melanoma cell differentiation and progression.

These results demonstrate the significant regulatory role of L-DOPA and 11c on melanoma status and provide an important contribution to a deeper understanding of the mechanisms of tyrosinase regulators in melanoma. Overall, this demonstrates that Malate-Aspartate Shuttle and fatty acids are suitable new therapeutic targets, providing new directions for subsequent drug development against melanoma.

Overall, this thesis has explored three main topics that successfully address the main aims. Firstly, microneedles were used to optimise the intradermal permeation of the existing tyrosinase inhibitor Alpha-Arbutin.

Secondly, the novel tyrosinase inhibitor 11c was discovered to have higher bioactivity and permeation capacity. Lastly, the metabolomics of tyrosinase modulators in melanoma A375 was explored. It was found that Malate-Aspartate Shuttle and fatty acid metabolism had significant changes.

5.2 Future work and perspectives

A great deal of work has been done in this study to find suitable ways to increase the permeability of Alpha-Arbutin and evaluate the biological activity of novel tyrosinase inhibitors and metabolic pathways. As a result, this work offers many further possibilities that can be explored for the treatment of abnormal melanin deposition. However, a number of issues still need to be refined and further investigated.

The first concern is the choice of formulation for dissolving polymeric microneedles. In Chapter 2, only 2% Alpha-Arbutin was chosen to be loaded into the dissolving microneedles. Although this was a relatively small concentration, a relatively good enhancement effect was still achieved. Therefore, increasing the loading concentration of Alpha-Arbutin could be considered later to analyse the effect of dissolving microneedles containing higher concentrations of Alpha-Arbutin on the permeability of Alpha-Arbutin to find the most appropriate drug loading concentration.

In addition, more experimental time points should be added to the study on the effect of microneedle application time for drug permeability. At this stage of the experiment, the different time points were only tested up to 24 h, which is not sufficient. Because of the slow release of DMNs, which

require longer time to dissolve, the drug permeation should be tested after 36h, 48h and 72h. Therefore, this is a feasible experimental plan afterwards.

Moreover, the preliminary experiments were only done *in vitro*. Furthermore, frozen pig skin was used as the subject. A gap still exists between the characteristics of pig and human skin, which may impact the subsequent analysis of the permeation capacity of the drug. Therefore, this study proceeded to carry out studies in human skin. Young volunteers (20-35 years old) of different gender, skin colour, and ethnicity were used to avoid skin differences between different genders and ethnicities affecting the drug's penetration ability. Skin samples were collected using tape strips and the results were analysed using a combination of HLPC and OrbiSIMS, thus completing the aim of obtaining the distribution of Alpha-Arbutin in human skin.

The assessment of the cytotoxicity of the new compounds 11c and 11m needs to be refined by using a wider variety of cell lines for the assay. At this stage, only murine-derived melanoma cells B16F10 and human-derived melanoma cells A375 have been selected, leading to some limitations in the results. Other skin cell lines such as Human immortalised keratinocytes (HaCaT) and Human skin fibroblast (HSF) need to be selected to overcome this. Alternatively, 3D recombinant artificial skin models could be selected for *in vitro* alternative genotoxicity testing. EpiSkin™, EpiDerm™, and Skin Ethic™ are well-established commercial artificial skin models which are widely used. As for determining the

tyrosinase inhibitory activity of the new compounds 11c and 11m, besides the use of melanoma cells, the drug's ability to inhibit melanogenesis in normal human epidermal-derived melanocytes should also be considered. These are all directions that could be further delved into in the future.

At this stage, the permeability research for 11c is limited to the basic formulation, therefore, the next step could be to explore more suitable formulations to further enhance its permeability based on its drug ionic nature. In addition, an issue identified with 11c is that its drug stability is somewhat deficient and susceptible to oxidation. Therefore, exploring new and suitable formulations in combination with antioxidants will be the next research focus for the new compound 11c.

In terms of metabolomics, it is also necessary to consider the effect of different administration times on the changes of metabolites in the cells. Therefore, the next step is to investigate, at different time points, the changes of intracellular metabolites associated with L-DOPA and 11c as modulators of tyrosinase upregulation and downregulation respectively. This will lead to a deeper understanding of how tyrosinase modulators affect the metabolic pathways of melanoma cells and provide substantial support in exploring therapeutic modalities for melanoma.

Chapter 6. References

(1) Oh, M.-J.; Abdul Hamid, M.; Ngadiran, S.; Seo, Y.-K.; Sarmidi, M. R.; Park, C. S. Ficus Deltoidea (Mas Cotek) Extract Exerted Anti-Melanogenic Activity by Preventing Tyrosinase Activity in Vitro and by Suppressing Tyrosinase Gene Expression in B16F1 Melanoma Cells. *Archives of Dermatological Research* **2011**, *303* (3), 161–170.

(2) Ielo, L.; Deri, B.; Germano, M. P.; Vittorio, S.; Mirabile, S.; Gitto, R.; Rapisarda, A.; Ronsisvalle, S.; Floris, S.; Pazy, Y. Exploiting the 1-(4-Fluorobenzyl) Piperazine Fragment for the Development of Novel Tyrosinase Inhibitors as Anti-Melanogenic Agents: Design, Synthesis, Structural Insights and Biological Profile. *European journal of medicinal chemistry* **2019**, *178*, 380–389.

(3) Yamada, M.; Prow, T. W. Physical Drug Delivery Enhancement for Aged Skin, UV Damaged Skin and Skin Cancer: Translation and Commercialization. *Advanced Drug Delivery Reviews* **2020**, *153*, 2–17.

(4) Brenner, M.; Hearing, V. J. Modifying Skin Pigmentation–Approaches through Intrinsic Biochemistry and Exogenous Agents. *Drug Discovery Today: Disease Mechanisms* **2008**, *5* (2), e189–e199.

(5) Glenn, E. N. Yearning for Lightness: Transnational Circuits in the Marketing and Consumption of Skin Lighteners. *Gender & society* **2008**, *22* (3), 281–302.

(6) Armstrong, B. K.; Kricker, A. Skin Cancer. *Dermatologic Clinics* **1995**, *13* (3), 583–594.

(7) D'Orazio, J.; Jarrett, S.; Amaro-Ortiz, A.; Scott, T. UV Radiation and the Skin. *International journal of molecular sciences* **2013**, *14* (6), 12222–12248.

(8) Quevedo Jr, W. C.; Fitzpatrick, T. B.; Pathak, M. A.; Jimbow, K. Role of Light in Human Skin Color Variation. *American journal of physical anthropology* **1975**, *43* (3), 393–408.

(9) Pathak, M. A.; Jimbow, K.; Szabo, G.; Fitzpatrick, T. B. Sunlight and Melanin Pigmentation. In *Photochemical and photobiological reviews*; Springer, 1976; pp 211–239.

(10) Huang, W.; Wang, Y.; Hung, K.; Hsieh, P.; Fu, K.; Dai, L.; Liou, N.; Ma, K.; Liu, J.; Dai. High Correlation between Skin Color Based on CIELAB Color Space, Epidermal Melanocyte Ratio, and Melanocyte Melanin Content. *PeerJ* **2018**, *6*, 4815. https://doi.org/10.7717/peerj.4815.

(11) Yamaguchi, Y.; Hearing, V. J. Melanocytes and Their Diseases. *Cold Spring Harb Perspect Med* **2014**, *4* (5), a017046. https://doi.org/10.1101/cshperspect.a017046.

(12) HEARING, V. J. The Melanosome: The Perfect Model for Cellular Responses to the Environment. *Pigment Cell Research* **2000**, *13*, 23–34.

(13) Baxter, L. L.; Watkins-Chow, D. E.; Pavan, W. J.; Loftus, S. K. A Curated Gene List for Expanding the Horizons of Pigmentation Biology. *Pigment cell & melanoma research* **2019**, *32*, 348–358.

(14) Yamaguchi, Y.; Brenner, M.; Hearing, V. J. The Regulation of Skin Pigmentation. *Journal of biological chemistry* **2007**, *282* (38), 27557–27561.

(15) Benito-Martínez, S.; Salavessa, L.; Raposo, G.; Marks, M. S.; Delevoye, C. Melanin Transfer and Fate within Keratinocytes in Human Skin Pigmentation. *Integrative and Comparative Biology* **2021**, *61* (4), 1546–1555.

(16) Brenner, M.; Hearing, V. J. The Protective Role of Melanin Against UV Damage in Human Skin†. *Photochemistry and Photobiology* **2008**, *84* (3), 539–549. https://doi.org/10.1111/j.1751-1097.2007.00226.x.

(17) Agar, N.; Young, A. R. Melanogenesis: A Photoprotective Response to DNA Damage? *Mutation Research/Fundamental and Molecular Mechanisms of Mutagenesis* **2005**, *571* (1–2), 121–132.

(18) Tadokoro, T.; Kobayashi, N.; Zmudzka, B. Z.; Ito, S.; Wakamatsu, K.; Yamaguchi, Y.; Korossy, K. S.; Miller, S. A.; Beer, J. Z.; Hearing, V. J. UV-induced DNA Damage and Melanin Content in Human Skin Differing in Racial/Ethnic Origin. *The FASEB Journal* **2003**, *17* (9), 1177–1179.

(19) Plensdorf, S.; Martinez, J. Common Pigmentation Disorders. *American family physician* **2009**, *79* (2), 109–116.

(20) Baxter, L. L.; Pavan, W. J. The Etiology and Molecular Genetics of Human Pigmentation Disorders. *Wiley Interdisciplinary Reviews: Developmental Biology* **2013**, *2* (3), 379–392.

(21) Vashi, N.; Kundu, R. V. Acquired Hyperpigmentation Disorders.

(22) Cestari, T. F.; Dantas, L. P.; Boza, J. C. Acquired Hyperpigmentations. *An. Bras. Dermatol.* **2014**, *89*, 11–25. https://doi.org/10.1590/abd1806-4841.20142353.

(23) Vinay, K.; Bishnoi, A.; Kamat, D.; Chatterjee, D.; Kumaran, M. S.; Parsad, D. Acquired Dermal Macular Hyperpigmentation: An Update. *Indian Dermatol Online J* **2021**, *12* (5), 663–673. https://doi.org/10.4103/idoj.IDOJ_881_20.

(24) Rathee, P.; Kumar, S.; Kumar, D.; Kumari, B.; Yadav, S. S. Skin Hyperpigmentation and Its Treatment with Herbs: An Alternative Method. *Future Journal of Pharmaceutical Sciences* **2021**, *7* (1), 1–14.

(25) Nautiyal, A.; Wairkar, S. Management of Hyperpigmentation: Current Treatments and Emerging Therapies. *Pigment cell & melanoma research* **2021**, *34* (6), 1000–1014.

(26) Meys, R. Skin Pigmentation. *Medicine* **2017**, *45* (7), 438–443.

(27) Sato, N. Endocrine Environment in Adult Females with Chloasma. *Nihon Hifuka Gakkai zasshi. The Japanese journal of dermatology* **1987**, *97* (8), 937–943.

(28) Muller, I.; Rees, D. A. Melasma and Endocrine Disorders. *Pigmentary Disorders S* **2014**, *1*, 2376–0427.

(29) El-Sinbawy, Z. G.; Abdelnabi, N. M.; Sarhan, N. E.; Elgarhy, L. Clinical & Ultrastructural Evaluation of the Effect of Fractional CO2 Laser on Facial Melasma. *Ultrastructural Pathology* **2019**, *43* (4–5), 135–144.

(30) Findlay, G. H. Ochronosis Following Skin Bleaching with Hydroquinone. *Journal of the American Academy of Dermatology* **1982**, *6* (6), 1092–1093.

(31) Hoshaw, R. A.; Zimmerman, K. G.; Menter, A. Ochronosislike Pigmentation from Hydroquinone Bleaching Creams in American Blacks. *Archives of dermatology* **1985**, *121* (1), 105–108.

(32) Kang, H. Y.; Suzuki, I.; Lee, D. J.; Ha, J.; Reiniche, P.; Aubert, J.; Deret, S.; Zugaj, D.; Voegel, J. J.; Ortonne, J.-P. Transcriptional Profiling Shows Altered Expression of Wnt Pathway–and Lipid Metabolism–Related Genes as Well as Melanogenesis-Related Genes in Melasma. *Journal of investigative dermatology* **2011**, *131* (8), 1692–1700.

(33) Wang, Y.; Viennet, C.; Robin, S.; Berthon, J.-Y.; He, L.; Humbert, P. Precise Role of Dermal Fibroblasts on Melanocyte Pigmentation. *Journal of dermatological science* **2017**, *88* (2), 159–166.

(34) Passeron, T. Melasma Pathogenesis and Influencing Factors–an Overview of the Latest Research. *Journal of the European Academy of Dermatology and Venereology* **2013**, *27*, 5–6.

(35) Elpek, G. O. Molecular Pathways in Viral Hepatitis-Associated Liver Carcinogenesis: An Update. *World Journal of Clinical Cases* **2021**, *9* (19), 4890.

(36) Rigopoulos, D.; Gregoriou, S.; Katsambas, A. Hyperpigmentation and Melasma. *Journal of cosmetic dermatology* **2007**, *6* (3), 195–202.

(37) Lakhan, M. K.; Lynch, M. Skin Pigmentation. *Medicine* **2021**. https://doi.org/10.1016/j.mpmed.2021.04.010.

(38) Zaidi, K.; Ali, S.; Ali, A.; Thawani, V. Natural Melanogenesis Stimulator a Potential Tool for the Treatment of Hypopigmentation Disease. *Int. J. Mol. Biol. Open Access* **2017**, *2*, 00012.

(39) Delahanty, R. J.; Zhang, Y.; Bichell, T. J.; Shen, W.; Verdier, K.; Macdonald, R. L.; Xu, L.; Boyd, K.; Williams, J.; Kang, J.-Q. Beyond Epilepsy and Autism: Disruption of GABRB3 Causes Ocular Hypopigmentation. *Cell Reports* **2016**, *17* (12), 3115–3124. https://doi.org/10.1016/j.celrep.2016.11.067.

(40) Rodrigues, M.; Ezzedine, K.; Hamzavi, I.; Pandya, A. G.; Harris, J. E. New Discoveries in the Pathogenesis and Classification of Vitiligo. *Journal of the American Academy of Dermatology* **2017**, *77* (1), 1–13. https://doi.org/10.1016/j.jaad.2016.10.048.

(41) Sulaimon, S. S.; Kitchell, B. E. The Biology of Melanocytes. *Veterinary dermatology* **2003**, *14* (2), 57–65.

(42) Yamaguchi, Y.; Hearing, V. J. Physiological Factors That Regulate Skin Pigmentation. *Biofactors* **2009**, *35* (2), 193–199.

(43) Cao, W.; Zhou, X.; McCallum, N. C.; Hu, Z.; Ni, Q. Z.; Kapoor, U.; Heil, C. M.; Cay, K. S.; Zand, T.; Mantanona, A. J. Unraveling the Structure and Function of Melanin through Synthesis. *Journal of the American Chemical Society* **2021**, *143* (7), 2622–2637.

(44) Hirobe, T. Keratinocytes Regulate the Function of Melanocytes. *Dermatologica Sinica* **2014**, *32* (4), 200–204.

(45) Halder, R. M.; Roberts, C. I.; Nootheti, P. K. Cutaneous Diseases in the Black Races. *Dermatologic clinics* **2003**, *21* (4), 679–687.

(46) Plonka, P. M.; Passeron, T.; Brenner, M.; Tobin, D. J.; Shibahara, S.; Thomas, A.; Slominski, A.; Kadekaro, A. L.; Hershkovitz, D.; Peters, E.; Nordlund, J. J.; Abdel-Malek, Z.; Takeda, K.; Paus, R.; Ortonne, J. P.; Hearing, V. J.; Schallreuter, K. U. What are melanocytes really doing all day long...? *Experimental Dermatology* **2009**, *18*, 799–819.

(47) Agarwal, S.; Mendiratta, V.; Chander, R.; Jain, A.; Yadav, P. Study of Serum Levels of Vitamin B12, Folic Acid, and Homocysteine in Vitiligo. *Pigment Int* **2015**, *2*, 76–80.

(48) Xu, Y. G.; Aylward, J. L.; Swanson, A. M. Chapter 67: Nonmelanoma Skin Cancers. In *eds. Abeloff's Clinical Oncology*; Niederhuber, J. E., Armitage, J. O., Doroshow, J. H., Kastan, M. B., Tepper, J. E., Eds.; Elsevier: Philadelphia, Pa, 2020.

(49) Rok, J.; Rzepka, Z.; Respondek, M.; Beberok, A.; Wrześniok, D. Chlortetracycline and Melanin Biopolymer – The Risk of Accumulation and Implications for Phototoxicity: An in Vitro Study on Normal Human Melanocytes. *Chemico-Biological Interactions* **2019**, *303*, 27–34, 0009–2797.

(50) Slominski, R. M.; Sarna, T.; Płonka, P. M.; Raman, C.; Brożyna, A. A.; Slominski, A. T. Melanoma, Melanin, and Melanogenesis: The Yin and Yang Relationship. *Frontiers in Oncology* **2022**, *12*.

(51) Raposo, G.; Marks, M. S. Melanosomes—Dark Organelles Enlighten Endosomal Membrane Transport. *Nature reviews Molecular cell biology* **2007**, *8* (10), 786–797.

(52) Skoczyńska, A.; Budzisz, E.; Trznadel-Grodzka, E.; Rotsztejn, H. Melanin and Lipofuscin as Hallmarks of Skin Aging. *Advances in*

Dermatology and Allergology/Postępy Dermatologii i Alergologii **2017**, *34* (2), 97–103.

(53) Raposo, G.; Marks, M. S. The Dark Side of Lysosome-related Organelles: Specialization of the Endocytic Pathway for Melanosome Biogenesis. *Traffic* **2002**, *3* (4), 237–248.

(54) Hurbain, I.; Geerts, W. J.; Boudier, T.; Marco, S.; Verkleij, A. J.; Marks, M. S.; Raposo, G. Electron Tomography of Early Melanosomes: Implications for Melanogenesis and the Generation of Fibrillar Amyloid Sheets. *Proceedings of the National Academy of Sciences* **2008**, *105* (50), 19726–19731.

(55) Costin, G.-E.; Hearing, V. J. Human Skin Pigmentation: Melanocytes Modulate Skin Color in Response to Stress. *The FASEB journal* **2007**, *21* (4), 976–994.

(56) Slominski, A.; Tobin, D. J.; Shibahara, S.; Wortsman, J. Melanin Pigmentation in Mammalian Skin and Its Hormonal Regulation. *Physiological Reviews* **2004**, *84* (4), 1155–1228. https://doi.org/10.1152/physrev.00044.2003.

(57) Marles, L. K.; Peters, E. M.; Tobin, D. J.; Hibberts, N. A.; Schallreuter, K. U. Tyrosine Hydroxylase Isoenzyme I Is Present in Human Melanosomes: A Possible Novel Function in Pigmentation. *Experimental Dermatology* **2003**, *12* (1), 61–70. https://doi.org/10.1034/j.1600-0625.2003.120108.x.

(58) Devi, C. C.; Ramaiah, A.; Tripathi, R. K. PH-Dependent Interconvertible Allosteric Forms of Murine Melanoma Tyrosinase.

European Journal of Biochemistry **1987**, *166* (3), 705–711. https://doi.org/10.1111/j.1432-1033.1987.tb13569.x.

(59) Puri, N.; Gardner, J. M.; Brilliant, M. H. Aberrant PH of Melanosomes in Pink-Eyed Dilution (p) Mutant Melanocytes. *J Invest Dermatol* **2000**, *115* (4), 607–613. https://doi.org/10.1046/j.1523-1747.2000.00108.x.

(60) Moellmann, G.; Slominski, A.; Kuklinska, E.; Lerner, A. B. Regulation of Melanogenesis in Melanocytes. *Pigment Cell Research* **1988**, *1* (s1), 79–87. https://doi.org/10.1111/j.1600-0749.1988.tb00798.x.

(61) Fuller, B. B.; Spaulding, D. T.; Smith, D. R. Regulation of the Catalytic Activity of Preexisting Tyrosinase in Black and Caucasian Human Melanocyte Cell Cultures. *Experimental Cell Research* **2001**, *262* (2), 197–208. https://doi.org/10.1006/excr.2000.5092.

(62) Ancans, J.; Tobin, D. J.; Hoogduijn, M. J.; Smit, N. P.; Wakamatsu, K.; Thody, A. J. Melanosomal PH Controls Rate of Melanogenesis, Eumelanin/Phaeomelanin Ratio and Melanosome Maturation in Melanocytes and Melanoma Cells. *Exp Cell Res* **2001**, *268* (1), 26–35. https://doi.org/10.1006/excr.2001.5251.

(63) Abdel-Malek, Z.; Swope, V. B.; Suzuki, I.; Akcali, C.; Harriger, M. D.; Boyce, S. T.; Urabe, K.; Hearing, V. J. Mitogenic and Melanogenic Stimulation of Normal Human Melanocytes by Melanotropic Peptides. *Proceedings of the National Academy of Sciences* **1995**, *92* (5), 1789–1793. https://doi.org/10.1073/pnas.92.5.1789.

(64) Ashida, Y.; Denda, M.; Hirao, T. Histamine H1 and H2 Receptor Antagonists Accelerate Skin Barrier Repair and Prevent Epidermal

Hyperplasia Induced by Barrier Disruption in a Dry Environment. *J Invest Dermatol* **2001**, *116* (2), 261–265. https://doi.org/10.1046/j.1523-1747.2001.01238.x.

(65) Auböck, J.; Niederwieser, D.; Romani, N.; Fritsch, P.; Huber, C. Human Interferon-γ Induces Expression of HLA-DR on Keratinocytes and Melanocytes. *Arch Dermatol Res* **1985**, *277* (4), 270–275. https://doi.org/10.1007/BF00509079.

(66) ABDEL-MALEK, Z.; SCOTT, M. C.; SUZUKI, I.; TADA, A.; IM, S.; LAMOREUX, L.; ITO, S.; BARSH, G.; HEARING, V. J. The Melanocortin-1 Receptor Is a Key Regulator of Human Cutaneous Pigmentation. *Pigment Cell Research* **2000**, *13*, 156–162.

(67) Swope, V. B.; Abdel-Malek, Z. A. Significance of the Melanocortin 1 and Endothelin B Receptors in Melanocyte Homeostasis and Prevention of Sun-Induced Genotoxicity. *Frontiers in genetics* **2016**, *7*, 146.

(68) D'Mello, S. A.; Finlay, G. J.; Baguley, B. C.; Askarian-Amiri, M. E. Signaling Pathways in Melanogenesis. *International journal of molecular sciences* **2016**, *17* (7), 1144.

(69) Busca, R.; Ballotti, R. Cyclic AMP a Key Messenger in the Regulation of Skin Pigmentation. *Pigment Cell Research* **2000**, *13* (2), 60–69.

(70) PATERSON, E. K. *Modulate 0RW1S34RfeSDcfkexd09rT2MITF1RW1S34RfeSDcfkexd09rT2: A Novel Mechanism in the Regulation of Melanogenesis*; University of California: Irvine, 2015.

(71) Shakhova, O.; Cheng, P.; Mishra, P. J.; Zingg, D.; Schaefer, S. M.; Debbache, J.; Häusel, J.; Matter, C.; Guo, T.; Davis, S.; Meltzer, P.; Mihic-Probst, D.; Moch, H.; Wegner, M.; Merlino, G.; Levesque, M. P.; Dummer, R.; Santoro, R.; Cinelli, P.; Sommer, L. Antagonistic Cross-Regulation between Sox9 and Sox10 Controls an Anti-Tumorigenic Program in Melanoma. *PLOS Genetics* **2015**, *11* (1), e1004877. https://doi.org/10.1371/journal.pgen.1004877.

(72) Cronin, J. C.; Loftus, S. K.; Baxter, L. L.; Swatkoski, S.; Gucek, M.; Pavan, W. J. Identification and Functional Analysis of SOX10 Phosphorylation Sites in Melanoma. *PLOS ONE* **2018**, *13* (1), e0190834. https://doi.org/10.1371/journal.pone.0190834.

(73) Passeron, T.; Valencia, J. C.; Bertolotto, C.; Hoashi, T.; Le Pape, E.; Takahashi, K.; Ballotti, R.; Hearing, V. J. SOX9 Is a Key Player in Ultraviolet B-Induced Melanocyte Differentiation and Pigmentation. *Proceedings of the National Academy of Sciences* **2007**, *104* (35), 13984–13989.

(74) Steingrímsson, E.; Copeland, N.; Jenkins, N. Melanocytes and the Microphthalmia Transcription Factor Network. *Annual review of genetics* **2004**, *38*, 365–411. https://doi.org/10.1146/annurev.genet.38.072902.092717.

(75) Hossain, M. R.; Ansary, T. M.; Komine, M.; Ohtsuki, M. Diversified Stimuli-Induced Inflammatory Pathways Cause Skin Pigmentation. *International Journal of Molecular Sciences* **2021**, *22* (8), 3970.

(76) Arora, N.; Siddiqui, E. M.; Mehan, S. Involvement of Adenylate Cyclase/CAMP/CREB and SOX9/MITF in Melanogenesis to Prevent Vitiligo. *Molecular and Cellular Biochemistry* **2021**, 1–9.

(77) Lee, M.-H.; Lin, Y.-P.; Hsu, F.-L.; Zhan, G.-R.; Yen, K.-Y. Bioactive Constituents of Spatholobus Suberectus in Regulating Tyrosinase-Related Proteins and MRNA in HEMn Cells. *Phytochemistry* **2006**, *67* (12), 1262–1270.

(78) Simon, J. D.; Peles, D.; Wakamatsu, K.; Ito, S. Current Challenges in Understanding Melanogenesis: Bridging Chemistry, Biological Control, Morphology, and Function. *Pigment Cell & Melanoma Research* **2009**, *22*. https://doi.org/10.1111/j.1755-148X.2009.00610.x.

(79) Li, W.; Melton, D. W. Cisplatin Regulates the MAPK Kinase Pathway to Induce Increased Expression of DNA Repair Gene ERCC1 and Increase Melanoma Chemoresistance. *Oncogene* **2012**, *31* (19), 2412–2422.

(80) Pillaiyar, T.; Namasivayam, V.; Manickam, M.; Jung, S.-H. Inhibitors of Melanogenesis: An Updated Review. *J. Med. Chem.* **2018**, *61* (17), 7395–7418. https://doi.org/10.1021/acs.jmedchem.7b00967.

(81) Raper, H. S. The anaerobic oxidases. *Physiol. Rev* **1928**, *8*, 245–282.

(82) Mason, H. S. The Chemistry of Melanin. II. Mechanism of the Oxidation of Trihydroxyphenylalanine by Tyrosinase. *J. Biol. Chem.1948 172*, 83–99.

(83) Cooksey, C. J.; Garratt, P. J.; Land, E. J.; Pavel, S.; Ramsden, C. A.; Riley, P. A.; N.P.M, S. Evidence of the Indirect Formation of the Catecholic Intermediate Substrate Responsible for the Autoactivati on Kinetics of Tyrosinase. *J. Biol. Chem* **1997**, *272*, 26226–26235.

(84) Schallreuter, K. U.; Rubsam, K.; Gibbons, N. C.; Maitland, D. J.; Chavan, B. Methionine Sulfoxide Reductases A and B Are Deactivated by Hydrogen Peroxide (H2O2) in the Epidermis of Patients with Vitiligo. *J Invest Dermatol* **2008**, *128*, 808–815. https://doi.org/10.1038/sj.jid.5701100.

(85) Halaban, R.; Patton, R. S.; E., C.; Svedine, S.; Trombetta, E. S.; Wahl, M. L.; Ariyan, S.; Hebert, D. N. Abnormal Acidification of Melanoma Cells Induces Tyrosinase Retention in the Early Secretory Pathway. *J. Biol. Chem* **2002**, *277*, 14821–14828.

(86) Böhme, I.; Bosserhoff, A. K. Acidic tumor microenvironment in human melanoma. *Pigment Cell Melanoma Res* **2016**, *29*. https://doi.org/10.1111/pcmr.12495.

(87) E., B.; A, B. A re-examination of the Raper's scheme: cyclodopa as a biological precursor of eumelanin C. R. *Soc* **1895**, *Biol., 47*, 582–584.

(88) Zhu, T. H.; Cao, S. W.; Yu, Y. Y. Synthesis, Characterization and Biological Evaluation of Paeonol Thiosemicarbazone Analogues as Mushroom Tyrosinase Inhibitors. *International Journal of Biological Macromolecules* **2013**, *62*, 589–595.

(89) Bertrand, G. Sur Une Nouvelle Oxydase, Ou Ferment Soluble Oxidant, d'origine Végétale. *Comt. Rend. Acad. Sci. Paris* **1896**, No. 122, 1215–1217.

(90) Spritz, R. A.; Ho, L.; Furumura, M.; Hearing Jr, V. J. Mutational Analysis of Copper Binding by Human Tyrosinase. *Journal of investigative dermatology* **1997**, *109* (2), 207–212.

(91) Shi, S. Y. Online Extraction–HPLC–FRAP System for Direct Identification of Antioxidants from Solid Du-Zhong Brick Tea. *Food Chemistry, 288* **2019**, 215–220.

(92) Saeedi, M.; Eslamifar, M.; Khezri, K. Kojic Acid Applications in Cosmetic and Pharmaceutical Preparations. *Biomedicine & Pharmacotherapy* **2019**, *110*, 582–593. https://doi.org/10.1016/j.biopha.2018.12.006.

(93) Guo, N.; You, X.; Wu, Y.; Du, D.; Zhang, L.; Shang, Q.; Liu, W. Continuous Fluorometric Method for Determining the Monophenolase Activity of Tyrosinase on L-Tyrosine, through Quenching L-DOPA Fluorescence by Borate. *Analytical chemistry* **2020**, *92* (8), 5780–5786.

(94) Ismaya, W. T.; Rozeboom, H. J.; Weijn, A.; Mes, J. J.; Fusetti, F.; Wichers, H. J.; Dijkstra, B. W. Crystal Structure of Agaricus Bisporus Mushroom Tyrosinase: Identity of the Tetramer Subunits and Interaction with Tropolone. *Biochemistry* **2011**, *50* (24), 5477–5486.

(95) Fenoll, L. G.; Rodrí guez-López, J. N.; Garcí a-Molina, F.; Garcí a-Cánovas, F.; Tudela, J. Michaelis Constants of Mushroom Tyrosinase with Respect to Oxygen in the Presence of Monophenols and Diphenols. *The International Journal of Biochemistry & Cell Biology* **2002**, *34* (4), 332–336.

(96) Taofiq, O.; González-Paramás, A. M.; Martins, A.; Barreiro, M. F.; Ferreira, I. C. F. R. Mushrooms Extracts and Compounds in Cosmetics, Cosmeceuticals and Nutricosmetics—A Review. *Industrial Crops and Products* **2016**, *90*, 38–48.

(97) Ito, S.; Wakamatsu, K. Chemistry of Mixed Melanogenesis—Pivotal Roles of Dopaquinone. *Photochemistry and photobiology* **2008**, *84* (3), 582–592.

(98) Chen, Q.-X.; Song, K.-K.; Qiu, L.; Liu, X.-D.; Huang, H.; Guo, H.-Y. Inhibitory Effects on Mushroom Tyrosinase by P-Alkoxybenzoic Acids. *Food Chemistry* **2005**, *91* (2), 269–274.

(99) Xie, L.-P.; Chen, Q.-X.; Huang, H.; Wang, H.-Z.; Zhang, R.-Q. Inhibitory Effects of Some Flavonoids on the Activity of Mushroom Tyrosinase. *Biochemistry (Moscow)* **2003**, *68* (4), 487–491.

(100) Lerner, A. B. On the Metabolism of Phenylalanine and Tyrosine. *Journal of Biological Chemistry* **1949**, *181*, 281–294.

(101) Slominski, A.; Moellmann, G.; Kuklinska, E.; Bomirski, A.; Pawelek, J. Positive Regulation of Melanin Pigmentation by Two Key Substrates of the Melanogenic Pathway, L-Tyrosine and L-Dopa. *Journal of Cell Science* **1988**, *89* (3), 287–296. https://doi.org/10.1242/jcs.89.3.287.

(102) TOYOFUKU, K.; WADA, I.; SPRITZ, R. A.; HEARING, V. J. The Molecular Basis of Oculocutaneous Albinism Type 1 (OCA1): Sorting Failure and Degradation of Mutant Tyrosinases Results in a Lack of Pigmentation. *Biochemical Journal* **2001**, *355* (2), 259–269.

(103) Toyofuku, K.; Wada, I.; Hirosaki, K.; Park, J. S.; Hori, Y.; Jimbow, K. Promotion of Tyrosinase Folding in COS 7 Cells by Calnexin. *The Journal of Biochemistry* **1999**, *125* (1), 82–89.

(104) Slominski, A.; Zmijewski, M. A.; Pawelek, J. L-tyrosine and L-dihydroxyphenylalanine as Hormone-like Regulators of Melanocyte Functions. *Pigment cell & melanoma research* **2012**, *25* (1), 14–27.

(105) García-Borrón, J. C.; Solano, F. Molecular Anatomy of Tyrosinase and Its Related Proteins: Beyond the Histidine-bound Metal Catalytic Center. *Pigment Cell Research* **2002**, *15* (3), 162–173.

(106) Schallreuter, K. U.; Kothari, S.; Chavan, B.; Spencer, J. D. Regulation of Melanogenesis–Controversies and New Concepts. *Experimental dermatology* **2008**, *17* (5), 395–404.

(107) Saranya, G.; Sruthi, D.; Jayakumar, K. S.; Jiby, M. V.; Nair, R. A.; Pillai, P. P.; Jayabaskaran, C. Polyphenol Oxidase (PPO) Arm of Catecholamine Pathway Catalyzes the Conversion of L-Tyrosine to L-DOPA in Mucuna Pruriens (L.) DC Var. Pruriens: An Integrated Pathway Analysis Using Field Grown and in Vitro Callus Cultures. *Plant Physiology and Biochemistry* **2021**, *166*, 1032–1043.

(108) Olivares, C.; García-Borrón, J. C.; Solano, F. Identification of Active Site Residues Involved in Metal Cofactor Binding and Stereospecific Substrate Recognition in Mammalian Tyrosinase. Implications to the Catalytic Cycle. *Biochemistry* **2002**, *41* (2), 679–686. https://doi.org/10.1021/bi011535n.

(109) Whitten, M. M.; Coates, C. J. Re-evaluation of Insect Melanogenesis Research: Views from the Dark Side. *Pigment cell & melanoma research* **2017**, *30* (4), 386–401.

(110) Pomerantz, S. H.; Warner, M. C. 3, 4-Dihydroxy-l-Phenylalanine as the Tyrosinase Cofactor: Occurrence in Melanoma and Binding Constant. *Journal of biological Chemistry* **1967**, *242* (22), 5308–5314.

(111) Abu-Omar, M. M.; Loaiza, A.; Hontzeas, N. Reaction Mechanisms of Mononuclear Non-Heme Iron Oxygenases. *Chemical reviews* **2005**, *105* (6), 2227–2252.

(112) Ghanem, G.; Verstegen, J.; Libert, A.; Arnould, R.; Lejeune, F. Alpha-melanocyte-stimulating Hormone Immunoreactivity in Human Melanoma Metastases Extracts. *Pigment cell research* **1989**, *2* (6), 519–523.

(113) Herraiz, C.; Martínez-Vicente, I.; Maresca, V. The A-melanocyte-stimulating Hormone/Melanocortin-1 Receptor Interaction: A Driver of Pleiotropic Effects beyond Pigmentation. *Pigment cell & melanoma research* **2021**, *34* (4), 748–761.

(114) Bang, J.; Zippin, J. H. Cyclic Adenosine Monophosphate (CAMP) Signaling in Melanocyte Pigmentation and Melanomagenesis. *Pigment Cell & Melanoma Research* **2021**, *34* (1), 28–43.

(115) Rachmin, I.; Ostrowski, S. M.; Weng, Q. Y.; Fisher, D. E. Topical Treatment Strategies to Manipulate Human Skin Pigmentation. *Advanced drug delivery reviews* **2020**, *153*, 65–71.

(116) McLane, J.; Osber, M.; Pawelek, J. M. Phosphorylated Isomers of L-Dopa Stimulate MSH Binding Capacity and Responsiveness to MSH

in Cultured Melanoma Cells. *Biochemical and Biophysical Research Communications* **1987**, *145* (2), 719–725.

(117) Pawelek, J.; Bolognia, J.; McLane, J.; Murray, M.; Osber, M.; Słominski, A. A Possible Role for Melanin Precursors in Regulating Both Pigmentation and Proliferation of Melanocytes. *Progress in clinical and biological research* **1988**, *256*, 143–154.

(118) Kim, Y.-M.; Cho, S.-E.; Kim, S.-C.; Jang, H.-J.; Seo, Y.-K. Effects of Extremely Low Frequency Electromagnetic Fields on Melanogenesis through P-ERK and p-SAPK/JNK Pathways in Human Melanocytes. *International Journal of Molecular Sciences* **2017**, *18* (10), 2120.

(119) Perdomo, J.; Quintana, C.; González, I.; Hernández, I.; Rubio, S.; Loro, J. F.; Reiter, R. J.; Estévez, F.; Quintana, J. Melatonin Induces Melanogenesis in Human SK-MEL-1 Melanoma Cells Involving Glycogen Synthase Kinase-3 and Reactive Oxygen Species. *International journal of molecular sciences* **2020**, *21* (14), 4970.

(120) Collman, J. P.; Dey, A.; Barile, C. J.; Ghosh, S.; Decréau, R. A. Inhibition of Electrocatalytic O2 Reduction of Functional CCO Models by Competitive, Non-Competitive, and Mixed Inhibitors. *Inorganic chemistry* **2009**, *48* (22), 10528–10534.

(121) Shah, A. B.; Yoon, S.; Kim, J. H.; Zhumanova, K.; Ban, Y. J.; Lee, K. W.; Park, K. H. Effectiveness of Cyclohexyl Functionality in Ugonins from Helminthostachys Zeylanica to PTP1B and α-Glucosidase Inhibitions. *International Journal of Biological Macromolecules* **2020**, *165*, 1822–1831.

(122) Hanif, N.; Al-Shami, A. M. A.; Khalid, K. A.; Hadi, H. Plant-Based Skin Lightening Agents: A Review. *J. Phytopharm* **2020**, *9*, 54–60.

(123) Migas, P.; Krauze-Baranowska, M. The Significance of Arbutin and Its Derivatives in Therapy and Cosmetics. *Phytochemistry Letters* **2015**, *13*, 35–40. https://doi.org/10.1016/j.phytol.2015.05.015.

(124) Saeedi, M.; Khezri, K.; Seyed Zakaryaei, A.; Mohammadamini, H. A Comprehensive Review of the Therapeutic Potential of α-Arbutin. *Phytotherapy Research* **2021**, *35* (8), 4136–4154. https://doi.org/10.1002/ptr.7076.

(125) Ephrem, E.; Elaissari, H.; Greige-Gerges, H. Improvement of Skin Whitening Agents Efficiency through Encapsulation: Current State of Knowledge. *International Journal of Pharmaceutics* **2017**, *526* (1), 50–68. https://doi.org/10.1016/j.ijpharm.2017.04.020.

(126) Lin, Y.-S.; Chen, S.-H.; Huang, W.-J.; Chen, C.-H.; Chien, M.-Y.; Lin, S.-Y.; Hou, W.-C. Effects of Nicotinic Acid Derivatives on Tyrosinase Inhibitory and Antioxidant Activities. *Food Chemistry* **2012**, *132* (4), 2074–2080.

(127) Levitt, J. The Safety of Hydroquinone: A Dermatologist's Response to the 2006 Federal Register. *Journal of the American Academy of Dermatology* **2007**, *57* (5), 854–872.

(128) Ladizinski, B.; Mistry, N.; Kundu, R. V. Widespread Use of Toxic Skin Lightening Compounds: Medical and Psychosocial Aspects. *Ethnic Skin Diseases* **2011**, *29* (1), 111–123.

(129) Zhao, W.; Yang, A.; Wang, J.; Huang, D.; Deng, Y.; Zhang, X.; Qu, Q.; Ma, W.; Xiong, R.; Zhu, M. Potential Application of Natural

Bioactive Compounds as Skin-whitening Agents: A Review. *Journal of Cosmetic Dermatology* **2022**.

(130) Chai, W.-M.; Wei, M.-K.; Wang, R.; Deng, R.-G.; Zou, Z.-R.; Peng, Y.-Y. Avocado Proanthocyanidins as a Source of Tyrosinase Inhibitors: Structure Characterization, Inhibitory Activity, and Mechanism. *Journal of agricultural and food chemistry* **2015**, *63* (33), 7381–7387.

(131) Xiong, Z.; Liu, W.; Zhou, L. Mushroom (Agaricus Bisporus) Polyphenoloxidase Inhibited by Apigenin: Multi- Spectroscopic Analyses and Computational Docking Simulation [J. *Food Chemistry* **2016**, *203*, 430–439.

(132) Passi, S.; Nazzaro-Porro, M.; Picardo, M.; Mingrone, G.; Fasella, P. Metabolism of Straight Saturated Medium Chain Length (C9 to C12. *dicarboxylic acids. J Lipid Res* **1983**, *24* (9), 1140–1147.

(133) Momeni, J.; Kimbu, S. F.; Sondengam, B. L.; KHAN, M. T. H.; CHOUDHARY, M. I. Potent Inhibitors of Tyrosinase Activity from Citrullus Colocynthis Schrad.(Cucurbitaceae). *ACTA Pharmaceutica Sciencia* **2010**, *52* (3).

(134) Kaewduangdee, S.; Chaveerach, Prof. Dr. A.; Tanee, T.; Siripiyasing, P.; Runglawan, S. Effect of Dried Ethanol Extract of Arbutin-Containing Leaves from Artocarpus on Tyrosinase Inhibition and Postharvest Preservation. *ScienceAsia* **2020**, *46*, 420. https://doi.org/10.2306/scienceasia1513-1874.2020.053.

(135) Akiu, S.; Suzuki, Y.; Asahara, T.; Fujinuma, Y.; Fukuda, M. [Inhibitory effect of arbutin on melanogenesis--biochemical study

using cultured B16 melanoma cells]. *Nihon Hifuka Gakkai Zasshi* **1991**, *101* (6), 609–613.

(136) Dooley, T. Topical Skin Depigmentation Agents. *null* **1997**, *8* (4), 275–283. https://doi.org/10.3109/09546639709160535.

(137) Yoon, T.-J.; Hearing, V. J. Co-Culture of Mouse Epidermal Cells for Studies of Pigmentation. *Pigment Cell Research* **2003**, *16* (2), 159–163. https://doi.org/10.1034/j.1600-0749.2003.00028.x.

(138) Zhu, X.; Tian, Y.; Zhang, W.; Zhang, T.; Guang, C.; Mu, W. Recent Progress on Biological Production of α-Arbutin. *Applied Microbiology and Biotechnology* **2018**, *102* (19), 8145–8152. https://doi.org/10.1007/s00253-018-9241-9.

(139) Sugimoto, K.; Nishimura, T.; Nomura, K.; Sugimoto, K.; Kuriki, T. Inhibitory Effects of α-Arbutin on Melanin Synthesis in Cultured Human Melanoma Cells and a Three-Dimensional Human Skin Model. *Biological and Pharmaceutical Bulletin* **2004**, *27* (4), 510–514. https://doi.org/10.1248/bpb.27.510.

(140) Sugimoto, K.; Nishimura, T.; Nomura, K.; Sugimoto, K.; Kuriki, T. Syntheses of Arbutin-α-Glycosides and a Comparison of Their Inhibitory Effects with Those of α-Arbutin and Arbutin on Human Tyrosinase. *Chemical and Pharmaceutical Bulletin* **2003**, *51* (7), 798–801. https://doi.org/10.1248/cpb.51.798.

(141) Tang, H.-C.; Chen, Y.-C. Identification of Tyrosinase Inhibitors from Traditional Chinese Medicines for the Management of Hyperpigmentation. *SpringerPlus* **2015**, *4* (1), 184. https://doi.org/10.1186/s40064-015-0956-0.

(142) *PubChem Compound Summary for CID 440936, Arbutin*. National Center for Biotechnology Information. https://pubchem.ncbi.nlm.nih.gov/compound/Arbutin. (accessed 2023-01-09).

(143) Chandorkar, N.; Tambe, S.; Amin, P.; Madankar, C. Alpha Arbutin as a Skin Lightening Agent: A Review. **2021**, *13*, 3502–3510. https://doi.org/10.31838/ijpr/2021.13.02.446.

(144) Hu, Z.-M.; Zhou, Q.; Lei, T.-C.; Ding, S.-F.; Xu, S.-Z. Effects of Hydroquinone and Its Glucoside Derivatives on Melanogenesis and Antioxidation: Biosafety as Skin Whitening Agents. *Journal of Dermatological Science* **2009**, *55* (3), 179–184. https://doi.org/10.1016/j.jdermsci.2009.06.003.

(145) LIU, Y. T.; ZHANG, P. Effects of Base Materials of Cosmetics on Whitening Efficacy and Stability of α-Arbutin. China Surfactant Detergent & Cosmetics, 1, 2012.

(146) Xing, R.; Wang, F.; Dong, L. Inhibitory Effects of Na7PMo11CuO40 on Mushroom Tyrosinase and Melanin Formation and Its Antimicrobial Activities [J. *Food Chemistry* **2016**, *197*, 205–211.

(147) Yi, W.; Cao, R.; Wen, H. Synthesis and Biological Evaluation of Helicid Analogues as Mushroom Tyrosinase Inhibitors[J. *Bioorganic & medicinal chemistry letters* **2008**, *18*, 6490–6493.

(148) Cheng, A.-X.; Zhang, X.; Han, X.-J.; Zhang, Y.-Y.; Gao, S.; Liu, C.-J.; Lou, H.-X. Identification of Chalcone Isomerase in the Basal Land Plants Reveals an Ancient Evolution of Enzymatic Cyclization

Activity for Synthesis of Flavonoids. *New Phytologist* **2018**, *217* (2), 909–924.

(149) Iwashina, T. The Structure and Distribution of the Flavonoids in Plants. *Journal of Plant Research* **2000**, *113* (3), 287.

(150) Escobar-Cévoli, R.; Castro-Espín, C.; Béraud, V.; Buckland, G.; Zamora-Ros, R.; Béraud, G. B. V. An Overview of Global Flavonoid Intake and Its Food Sources. *Flavonoids-From Biosynthesis to Human Health* **2017**.

(151) Gan, F. F.; Zhang, R.; Ng, H. L.; Karuppasamy, M.; Seah, W.; Yeap, W. H. Novel Dual-Targeting Anti-Proliferative Dihydrotriazine-Chalcone Derivatives Display Suppression of Cancer Cell Invasion and Inflammation by Inhibiting the NF-KB Signaling Pathway. *Food and Chemical Toxicology* **2018**, *116*, 238–248.

(152) Abbas, I.; Noun, M.; Touboul, D.; Sahali, D.; Brunelle, A.; Ollero, M. Kidney Lipidomics by Mass Spectrometry Imaging: A Focus on the Glomerulus. *International Journal of Molecular Sciences* **2019**, *20* (7), 1623. https://doi.org/10.3390/ijms20071623.

(153) Vogel, S.; Barbic, M.; Jürgenliemk, G.; Heilmann, J. Synthesis, Cytotoxicity, Anti-Oxidative and Anti-Inflammatory Activity of Chalcones and Influence of A-Ring Modifications on the Pharmacological Effect. *European Journal of Medicinal Chemistry* **2010**, *45* (6), 2206–2213.

(154) Dan, W.; Dai, J. Recent Developments of Chalcones as Potential Antibacterial Agents in Medicinal Chemistry. *European Journal of Medicinal Chemistry* **2020**, *187*, 111980.

(155) Qin, H. L.; Zhang, Z. W.; Lekkala, R.; Alsulami, H.; Rakesh, K. P. Chalcone Hybrids as Privileged Scaffolds in Antimalarial Drug Discovery: A Key Review. *European Journal of Medicinal Chemistry* **2020**, *193*, 112215.

(156) Rashid, H.; Xu, Y.; Ahmad, N.; Muhammad, Y.; Wang, L. Promising Anti-Inflammatory Effects of Chalcones via Inhibition of Cyclooxygenase, Prostaglandin E2, Inducible NO Synthase and Nuclear Factor Kb Activities. *Bioorganic Chemistry* **2019**, *87*, 335–365.

(157) Ye, C.-L.; Liu, Y.; Wei, D.-Z. Antioxidant and Anticancer Activity of 3 '-Formyl-4', 6 '-Dihydroxy-2'-Methoxy-5 '-Methylchalcone and (2S)-8-Formyl-5-Hydroxy-7-Methoxy-6-Methylflavanone. *Journal of pharmacy and pharmacology* **2007**, *59* (4), 553–559.

(158) Nishida, J.; Gao, H.; Kawabata, J. Synthesis and Evaluation of 20, 40, 60-Trihydroxychalcones as a New Class of Tyrosinase Inhibitors[J. *Bioorg Med Chem* **2007**, *15*, 2396–2402.

(159) Nixha, A. R.; Arslan, M.; Atalay, Y. Synthesis and Theoretical Calculations of Carbazole Substituted Chalcone Urea Derivatives and Studies Their Polyphenol Oxidase Enzyme Activity. *Journal of Enzyme Inhibition and Medicinal Chemistry* **2013**, *Aug;28(4):808-815*.

(160) Sonmez, F.; Sevmezler, S.; Atahan, A. Evaluation of New Chalcone Derivatives as Polyphenol Oxidase Inhibitors[J. *Bioorganic & medicinal chemistry letters* **2011**, *21*, 7479–7482.

(161) Benavente-Garcia, O.; Castillo, J.; Del Baño, M. J.; Lorente, J. Improved Water Solubility of Neohesperidin Dihydrochalcone in

Sweetener Blends. *Journal of agricultural and food chemistry* **2001**, *49* (1), 189–191.

(162) Xiao, Z.; Wang, Y.; Wang, J.; Li, P.; Ma, F. Structure-Antioxidant Capacity Relationship of Dihydrochalcone Compounds in Malus. *Food chemistry* **2019**, *275*, 354–360.

(163) Kaouadji, M.; Champavier, Y.; Morand, J.-M. Platanus Acerifolia's Buds: Additional Non-Polar Metabolites and Structure Revision of Two Previous Dihydrochalcone-like Metabolites. *Tetrahedron Letters* **2013**, *54* (47), 6352–6357.

(164) Shang, A.; Liu, H.-Y.; Luo, M.; Xia, Y.; Yang, X.; Li, H.-Y.; Wu, D.-T.; Sun, Q.; Geng, F.; Gan, R.-Y. Sweet Tea (Lithocarpus Polystachyus Rehd.) as a New Natural Source of Bioactive Dihydrochalcones with Multiple Health Benefits. *Critical Reviews in Food Science and Nutrition* **2022**, *62* (4), 917–934.

(165) Zhang, Q.; Wang, L.; Zhao, Y. An Overview of Lithocarpus Polystachyus, with Dihydrochalcones as Natural-Derived Bioactive Compounds. *Food Reviews International* **2022**, 1–14.

(166) Solano, F.; Briganti, S.; Picardo, M.; Ghanem, G. Hypopigmenting Agents: An Updated Review on Biological, Chemical and Clinical Aspects. *Pigment Cell Research* **2006**, *19* (6), 550–571. https://doi.org/10.1111/j.1600-0749.2006.00334.x.

(167) Brunt, E. G.; Burgess, J. G. The Promise of Marine Molecules as Cosmetic Active Ingredients. *International journal of cosmetic science* **2018**, *40* (1), 1–15.

(168) Wang, J.; Xie, X.; Deng, Y.; Yang, H.; Du, X.; Liu, P.; Du, Y. SOX9 in Keratinocytes Regulates Claudin 2 Transcription during Skin Aging. *Contrast Media & Molecular Imaging* **2022**, *2022*.

(169) M Casanola-Martin, G.; Le-Thi-Thu, H.; Marrero-Ponce, Y.; A Castillo-Garit, J.; Torrens, F.; Rescigno, A.; Abad, C.; Tareq Hassan Khan, M. Tyrosinase Enzyme: 1. An Overview on a Pharmacological Target. *Current topics in medicinal chemistry* **2014**, *14* (12), 1494–1501.

(170) Ali, S.; Shabbir, M.; Shahid, N. The Structure of Skin and Transdermal Drug Delivery System-a Review. Res. *J. Pharm* **2015**, No. nol, 8, 103–109.

(171) Lee, S. H.; Jeong, S. K.; Ahn, S. K. An Update of the Defensive Barrier Function of Skin. *Yonsei medical journal* **2006**, *47* (3), 293–306.

(172) Boer, M.; Duchnik, E.; Maleszka, R.; Marchlewicz, M. Structural and Biophysical Characteristics of Human Skin in Maintaining Proper Epidermal Barrier Function. *Advances in Dermatology and Allergology/Postępy Dermatologii i Alergologii* **2016**, *33* (1), 1–5.

(173) Kolarsick, P. A.; Kolarsick, M. A.; Goodwin, C. Anatomy and Physiology of the Skin. *Journal of the Dermatology Nurses' Association* **2011**, *3* (4), 203–213.

(174) *What Is Skin Cancer? | CDC*. https://www.cdc.gov/cancer/skin/basic_info/what-is-skin-cancer.htm (accessed 2023-01-10).

(175) White, S. D.; Yager, J. A. Resident Dendritic Cells in the Epidermis: Langerhans Cells, Merkel Cells and Melanocytes. *Veterinary dermatology* **1995**, *6* (1), 1–8.

(176) Yousef, H.; Alhajj, M.; Sharma, S. Anatomy, Skin (Integument), Epidermis. **2017**.

(177) S.Z., A.; D.J., L.; R.Z, L. Normal Skin. *Atlas of Practical Mohs Histopathology* **2013**. https://doi.org/10.1007/978-1-4614-5161-7_2.

(178) *Structure and Function of Skin | Biology for Majors II*. https://courses.lumenlearning.com/suny-wmopen-biology2/chapter/structure-and-function-of-skin/ (accessed 2023-01-10).

(179) Honari, G.; Maibach, H. Chapter 1 - Skin Structure and Function. In *Applied Dermatotoxicology*; Maibach, H., Honari, G., Eds.; Academic Press: Boston, 2014; pp 1–10. https://doi.org/10.1016/B978-0-12-420130-9.00001-3.

(180) Akomeah, F. K.; Nazir, T. Basics of Topical Therapy. *Dermatological Treatments* **2012**, 3.

(181) van der Maaden, K.; Jiskoot, W.; Bouwstra, J. Microneedle Technologies for (Trans)Dermal Drug and Vaccine Delivery. *Journal of Controlled Release* **2012**, *161* (2), 645–655. https://doi.org/10.1016/j.jconrel.2012.01.042.

(182) Fresta, M.; Puglisi, G. Corticosteroid Dermal Delivery with Skin-Lipid Liposomes. *Journal of Controlled Release* **1997**, *44* (2), 141–151. https://doi.org/10.1016/S0168-3659(96)01519-2.

(183) Schubert, M. A.; Muller-Goymann, C. C. Novel Colloidal Delivery Systems for Dermal Application. *Journal of Drug Delivery Science and Technology* **2004**, *14* (6), 423–434. https://doi.org/10.1016/S1773-2247(04)50080-1.

(184) Harding, C. R. The Stratum Corneum: Structure and Function in Health and Disease. *Dermatologic Therapy* **2004**, *17* (s1), 6–15. https://doi.org/10.1111/j.1396-0296.2004.04S1001.x.

(185) McAfee, D. A.; Hadgraft, J.; Lane, M. E. Rotigotine: The First New Chemical Entity for Transdermal Drug Delivery. *European Journal of Pharmaceutics and Biopharmaceutics* **2014**, *88* (3), 586–593. https://doi.org/10.1016/j.ejpb.2014.08.007.

(186) Brankov, N.; Prodanovic, E. M.; Hurley, M. Y. Pigmented Basal Cell Carcinoma: Increased Melanin or Increased Melanocytes? *Journal of Cutaneous Pathology* **2016**, *43* (12), 1139–1142. https://doi.org/10.1111/cup.12819.

(187) Miettinen, M.; McCue, P. A.; Sarlomo-Rikala, M.; Biernat, W.; Czapiewski, P.; Kopczynski, J.; Thompson, L. D.; Lasota, J.; Wang, Z.; Fetsch, J. F. Sox10–a Marker for Not Only Schwannian and Melanocytic Neoplasms but Also Myoepithelial Cell Tumors of Soft Tissue: A Systematic Analysis of 5134 Tumors. The American Journal of Surgical Pathology, 39(6, 2015, 826–835. https://doi.org/10.1097/PAS.0000000000000398.

(188) Queiroz, M. L. B.; Shanmugam, S.; Santos, L. N. S.; Campos, C. de A.; Santos, A. M.; Batista, M. S.; Araujo, A. A. de S.; Serafini, M. R. Microneedles as an Alternative Technology for Transdermal Drug

Delivery Systems: A Patent Review. *Expert Opinion on Therapeutic Patents* **2020**, *30* (6), 433–452.

(189) Mezei, M.; Gulasekharam, V. Liposomes-a Selective Drug Delivery System for the Topical Route of Administration I. Lotion Dosage Form. *Life sciences* **1980**, *26* (18), 1473–1477.

(190) Sabri, A. H.; Ogilvie, J.; Abdulhamid, K.; Shpadaruk, V.; McKenna, J.; Segal, J.; Scurr, D. J.; Marlow, M. Expanding the Applications of Microneedles in Dermatology. *European Journal of Pharmaceutics and Biopharmaceutics* **2019**, *140*, 121–140.

(191) Larraneta, E.; Lutton, R. E.; Woolfson, A. D.; Donnelly, R. F. Microneedle Arrays as Transdermal and Intradermal Drug Delivery Systems: Materials Science, Manufacture and Commercial Development. *Materials Science and Engineering: R: Reports* **2016**, *104*, 1–32.

(192) Sabri, A. H.; Kim, Y.; Marlow, M.; Scurr, D. J.; Segal, J.; Banga, A. K. Intradermal and Transdermal Drug Delivery Using Microneedles – Fabrication, Performance Evaluation and Application to Lymphatic Delivery. *Advanced Drug Delivery Reviews* **2019**.

(193) Akhtar, N.; Singh, V.; Yusuf, M.; Khan, R. A. Non-Invasive Drug Delivery Technology: Development and Current Status of Transdermal Drug Delivery Devices, Techniques and Biomedical Applications. *Biomedical Engineering/Biomedizinische Technik* **2020**, *65* (3), 243–272.

(194) Ramteke, K. H.; Dhole, S. N.; Patil, S. V. Transdermal Drug Delivery System: A Review. *Journal of Advanced Scientific Research* **2012**, *3* (1), 22–35.

(195) Macedo, A. S.; Castro, P. M.; Roque, L.; Thomé, N. G.; Reis, C. P.; Pintado, M. E.; Fonte, P. Novel and Revisited Approaches in Nanoparticle Systems for Buccal Drug Delivery. *Journal of Controlled Release* **2020**, *320*, 125–141.

(196) Khan, S.; Hasan, A.; Attar, F.; Babadaei, M. M. N.; Zeinabad, H. A.; Salehi, M.; Alizadeh, M.; Hassan, M.; Derakhshankhah, H.; Hamblin, M. R. Diagnostic and Drug Release Systems Based on Microneedle Arrays in Breast Cancer Therapy. *Journal of Controlled Release* **2021**, *338*, 341–357.

(197) Sharma, M. Transdermal and Intravenous Nano Drug Delivery Systems: Present and Future. In *Applications of targeted nano drugs and delivery systems*; Elsevier, 2019; pp 499–550.

(198) Tuan-Mahmood, T.-M.; McCrudden, M. T. C.; Torrisi, B. M.; McAlister, E.; Garland, M. J.; Singh, T. R. R.; Donnelly, R. F. Microneedles for Intradermal and Transdermal Drug Delivery. *European Journal of Pharmaceutical Sciences* **2013**, *50* (5), 623–637. https://doi.org/10.1016/j.ejps.2013.05.005.

(199) Coulman, S.; Allender, C.; Birchall, J. Microneedles and Other Physical Methods for Overcoming the Stratum Corneum Barrier for Cutaneous Gene Therapy. *Critical Reviews™ in Therapeutic Drug Carrier Systems* **2006**, *23* (3).

(200) Williams, A. *Transdermal and Topical Drug Delivery from Theory to Clinical Practice*; Pharmaceutical press, 2003.

(201) Cole, G.; Dunne, N. J.; McCarthy, H. O. Microneedles for Gene Therapy: Overcoming Extracellular and Intracellular Barriers. In *Microneedles for Drug and Vaccine Delivery and Patient Monitoring*; Wiley-Blackwell, 2018; pp 129–175.

(202) Wiechers, J. W. The Barrier Function of the Skin in Relation to Percutaneous Absorption of Drugs. *Pharmaceutisch Weekblad* **1989**, *11* (6), 185–198.

(203) Paudel, K. S.; Milewski, M.; Swadley, C. L.; Brogden, N. K.; Ghosh, P.; Stinchcomb, A. L. Challenges and Opportunities in Dermal/Transdermal Delivery. *Therapeutic delivery* **2010**, *1* (1), 109–131.

(204) Jijie, R.; Barras, A.; Boukherroub, R.; Szunerits, S. Nanomaterials for Transdermal Drug Delivery: Beyond the State of the Art of Liposomal Structures. *Journal of Materials Chemistry B* **2017**, *5* (44), 8653–8675.

(205) Phatale, V.; Vaiphei, K. K.; Jha, S.; Patil, D.; Agrawal, M.; Alexander, A. Overcoming Skin Barriers through Advanced Transdermal Drug Delivery Approaches. *Journal of Controlled Release* **2022**, *351*, 361–380.

(206) Kapoor, M. S.; GuhaSarkar, S.; Banerjee, R. Stratum Corneum Modulation by Chemical Enhancers and Lipid Nanostructures: Implications for Transdermal Drug Delivery. *Therapeutic delivery* **2017**, *8* (8), 701–718.

(207) Higaki, K.; Amnuaikit, C.; Kimura, T. Strategies for Overcoming the Stratum Corneum. *American Journal of Drug Delivery* **2003**, *1* (3), 187–214.

(208) Rastogi, V.; Yadav, P. Transdermal Drug Delivery System: An Overview. *Asian Journal of Pharmaceutics (AJP)* **2012**, *6* (3).

(209) Ookubo, N.; Michiue, H.; Kitamatsu, M.; Kamamura, M.; Nishiki, T.; Ohmori, I.; Matsui, H. The Transdermal Inhibition of Melanogenesis by a Cell-Membrane-Permeable Peptide Delivery System Based on Poly-Arginine. *Biomaterials* **2014**, *35* (15), 4508–4516.

(210) Bouwstra, J. A.; Helder, R. W.; El Ghalbzouri, A. Human Skin Equivalents: Impaired Barrier Function in Relation to the Lipid and Protein Properties of the Stratum Corneum. *Advanced Drug Delivery Reviews* **2021**, *175*, 113802.

(211) Akinshina, A.; Jambon-Puillet, E.; Warren, P. B.; Noro, M. G. Self-Consistent Field Theory for the Interactions between Keratin Intermediate Filaments. *BMC biophysics* **2013**, *6* (1), 1–16.

(212) Benet, L. Z.; Kroetz, D.; Sheiner, L.; Hardman, J.; Limbird, L. Pharmacokinetics: The Dynamics of Drug Absorption, Distribution, Metabolism, and Elimination. *Goodman and Gilman's the pharmacological basis of therapeutics* **1996**, *3*, e27.

(213) C Silva, A.; Santos, D.; Ferreira, D.; M Lopes, C. Lipid-Based Nanocarriers as an Alternative for Oral Delivery of Poorly Water-Soluble Drugs: Peroral and Mucosal Routes. *Current medicinal chemistry* **2012**, *19* (26), 4495–4510.

(214) *Transcellular - an overview | ScienceDirect Topics*. https://www.sciencedirect.com/topics/agricultural-and-biological-sciences/transcellular (accessed 2023-01-10).

(215) Palmer, B. C.; DeLouise, L. A. Nanoparticle-Enabled Transdermal Drug Delivery Systems for Enhanced Dose Control and Tissue Targeting. *Molecules* **2016**, *21* (12), 1719. https://doi.org/10.3390/molecules21121719.

(216) Cichorek, M.; Wachulska, M.; Stasiewicz, A.; Tymińska, A. Skin Melanocytes: Biology and Development. *Advances in Dermatology and Allergology/Postępy Dermatologii i Alergologii* **2013**, *30* (1), 30–41.

(217) Duval, C.; Chagnoleau, C.; Pouradier, F.; Sextius, P.; Condom, E.; Bernerd, F. Human Skin Model Containing Melanocytes: Essential Role of Keratinocyte Growth Factor for Constitutive Pigmentation—Functional Response to α-Melanocyte Stimulating Hormone and Forskolin. *Tissue Engineering Part C: Methods* **2012**, *18* (12), 947–957.

(218) Brown, M.; Jones, S. Hyaluronic Acid: A Unique Topical Vehicle for the Localized Delivery of Drugs to the Skin. *Journal of the European Academy of Dermatology and Venereology* **2005**, *19* (3), 308–318. https://doi.org/10.1111/j.1468-3083.2004.01180.x.

(219) Tajima, R.; Oozeki, H.; Muraoka, S.; Tanaka, S.; Motegi, Y.; Nihei, H.; Yamada, Y.; Masuoka, N.; Nihei, K. Synthesis and Evaluation of Bibenzyl Glycosides as Potent Tyrosinase Inhibitors. *European journal of medicinal chemistry* **2011**, *46* (4), 1374–1381.

(220) Ullah, S.; Park, C.; Ikram, M.; Kang, D.; Lee, S.; Yang, J.; Park, Y.; Yoon, S.; Chun, P.; Moon, H. R. Tyrosinase Inhibition and Anti-Melanin Generation Effect of Cinnamamide Analogues. *Bioorganic chemistry* **2019**, *87*, 43–55.

(221) Anurova, M. N.; Demina, N. B.; Bakhrushina, E. O. Permeability Enhancers in Transdermal Delivery System Technology (Review). *Pharmaceutical Chemistry Journal* **2021**, *54* (11), 1162–1168. https://doi.org/10.1007/s11094-021-02336-w.

(222) Patel, H.; Trivedi, D.; Bhandari, A.; Shah, D. Penetration Enhancers for Transdermal Drug Delivery System: A Review. *International Journal of Pharmaceutical Innovations; Journal of Pharmaceutics and Cosmetology* **2011**, *1*, 67–80.

(223) Biniek, K. *Biomechanical Barrier Function of Human Stratum Corneum*; Stanford University, 2015.

(224) Thotakura, N.; Kaushik, L.; Kumar, V.; Preet, S.; Babu, P. V. Advanced Approaches of Bioactive Peptide Molecules and Protein Drug Delivery Systems. *Current pharmaceutical design* **2018**, *24* (43), 5147–5163.

(225) Zsikó, S.; Csányi, E.; Kovács, A.; Budai-Szűcs, M.; Gácsi, A.; Berkó, S. Methods to Evaluate Skin Penetration In Vitro. *Scientia Pharmaceutica* **2019**, *87* (3). https://doi.org/10.3390/scipharm87030019.

(226) Brown, M. B.; Martin, G. P.; Jones, S. A.; Akomeah, F. K. Dermal and Transdermal Drug Delivery Systems: Current and Future

Prospects. *null* **2006**, *13* (3), 175–187. https://doi.org/10.1080/10717540500455975.

(227) Sabri, A.; Ogilvie, J.; McKenna, J.; Segal, J.; Scurr, D.; Marlow, M. Intradermal Delivery of an Immunomodulator for Basal Cell Carcinoma; Expanding the Mechanistic Insight into Solid Microneedle-Enhanced Delivery of Hydrophobic Molecules. *Mol. Pharmaceutics* **2020**, *17* (8), 2925–2937. https://doi.org/10.1021/acs.molpharmaceut.0c00347.

(228) Morales, J. O.; Fathe, K. R.; Brunaugh, A.; Ferrati, S.; Li, S.; Montenegro-Nicolini, M.; Mousavikhamene, Z.; McConville, J. T.; Prausnitz, M. R.; Smyth, H. D. C. Challenges and Future Prospects for the Delivery of Biologics: Oral Mucosal, Pulmonary, and Transdermal Routes [J. *The AAPS Journal* **2017**, *19* (3), 652–668.

(229) Sabri, A. H.; Kim, Y.; Marlow, M.; Scurr, D. J.; Segal, J.; Banga, A. K.; Kagan, L.; Lee, J. B. Intradermal and Transdermal Drug Delivery Using Microneedles–Fabrication, Performance Evaluation and Application to Lymphatic Delivery. *Advanced drug delivery reviews* **2020**, *153*, 195–215.

(230) Dabholkar, N.; Gorantla, S.; Waghule, T.; Rapalli, V. K.; Kothuru, A.; Goel, S.; Singhvi, G. Biodegradable Microneedles Fabricated with Carbohydrates and Proteins: Revolutionary Approach for Transdermal Drug Delivery. *International Journal of Biological Macromolecules* **2021**, *170*, 602–621.

(231) Chen, X.; Wang, L.; Yu, H.; Li, C.; Feng, J.; Haq, F.; Khan, A.; Khan, R. U. Preparation, Properties and Challenges of the Microneedles-

Based Insulin Delivery System [J. *J. Controlled Release* **2018**, *288*, 173–188.

(232) Birchall, J. C.; Clemo, R.; Anstey, A.; John, D. N. Microneedles in Clinical Practice–an Exploratory Study into the Opinions of Healthcare Professionals and the Public [J. *Pharm Res* **2011**, *28* (1), 95–106.

(233) Escobar-Chavez, J. J.; Bonilla-Martinez, D.; Villegas-Gonzalez, M. A.; Molina-Trinidad, E.; Casas-Alancaster, N.; Revilla-Vazquez, A. L. Microneedles: A Valuable Physical Enhancer to Increase Transdermal Drug Delivery [J. *J Clin Pharmacol* **2011**, *51* (7), 964–977.

(234) Leone, M.; Mönkäre, J.; Bouwstra, J.; Kersten, G. Dissolving Microneedle Patches for Dermal Vaccination. *Pharmaceutical Research* **2017**, *34*. https://doi.org/10.1007/s11095-017-2223-2.

(235) E, R. S. The Use of Hydrofluoric Acid in Making Glass Microneedles. *Science* **1952**, *116* (3023).

(236) Garland, M. J.; Migalska, K.; Mahmood, T. M. T.; Singh, T. R. R.; Woolfson, A. D.; Donnelly, R. F. Microneedle Arrays as Medical Devices for Enhanced Transdermal Drug Delivery. *Expert review of medical devices* **2011**, *8* (4), 459–482.

(237) Hashmi, S.; Ling, P.; Hashmi, G.; Reed, M.; Gaugler, R.; Trimmer, W. Genetic Transformation of Nematodes Using Arrays of Micromechanical Piercing Structures. *BioTechniques* **1995**, *19* (5), 766–770.

(238) S., H.; V., M. D.; Gi, A. M. Microfabricated microneedles: a novel approach to transdermal drug delivery. *J. Pharm. Sci* **1998**, *87* (8), 922–925.

(239) Mittal, P.; Baddi, H. P. MICRONEEDLES BASED TRANSDERMAL DRUG DELIVERY. *consultant* **2013**, *3*, 0.

(240) Park, J.-H.; Allen, M. G.; Prausnitz, M. R. Biodegradable Polymer Microneedles: Fabrication, Mechanics and Transdermal Drug Delivery. *Journal of controlled release* **2005**, *104* (1), 51–66.

(241) Juster, H.; van der Aar, B.; de Brouwer, H. A Review on Microfabrication of Thermoplastic Polymer-based Microneedle Arrays. *Polymer Engineering & Science* **2019**, *59* (5), 877–890.

(242) Lee, J. W.; Han, M.-R.; Park, J.-H. Polymer Microneedles for Transdermal Drug Delivery. *Journal of drug targeting* **2013**, *21* (3), 211–223.

(243) Lee, J. W.; Prausnitz, M. R. Drug Delivery Using Microneedle Patches: Not Just for Skin. *Expert opinion on drug delivery* **2018**, *15* (6), 541–543.

(244) Sullivan, S. P.; Koutsonanos, D. G.; del Pilar Martin, M.; Lee, J. W.; Zarnitsyn, V.; Choi, S.-O.; Murthy, N.; Compans, R. W.; Skountzou, I.; Prausnitz, M. R. Dissolving Polymer Microneedle Patches for Influenza Vaccination. *Nature medicine* **2010**, *16* (8), 915–920.

(245) Shravanth, S. H.; Osmani, R. A. M.; Anupama, V. P.; Rahamathulla, M.; Gangadharappa, H. V. Microneedles-Based Drug Delivery for the Treatment of Psoriasis. *Journal of Drug Delivery Science and Technology* **2021**, *64*, 102668.

(246) Zhao, Z.; Chen, Y.; Shi, Y. Microneedles: A Potential Strategy in Transdermal Delivery and Application in the Management of Psoriasis. *Rsc Advances* **2020**, *10* (24), 14040–14049.

(247) Kim, Y.-C.; Park, J.-H.; Prausnitz, M. R. Microneedles for Drug and Vaccine Delivery. *Advanced Drug Delivery Reviews* **2012**, *64* (14), 1547–1568. https://doi.org/10.1016/j.addr.2012.04.005.

(248) Chen, S.; Wu, D.; Liu, Y.; Huang, Y.; Xu, H.; Gao, W.; Zhang, J.; Sun, J.; Zhuang, J. Optimal Scaling Analysis of Polymeric Microneedle Length and Its Effect on Transdermal Insulin Delivery. *Journal of Drug Delivery Science and Technology* **2020**, *56*, 101547.

(249) Ita, K. Transdermal Delivery of Drugs with Microneedles: Strategies and Outcomes. *Journal of Drug Delivery Science and Technology* **2015**, *29*, 16–23.

(250) Rejinold, N. S.; Shin, J.-H.; Seok, H. Y.; Kim, Y.-C. Biomedical Applications of Microneedles in Therapeutics: Recent Advancements and Implications in Drug Delivery. *Expert opinion on drug delivery* **2016**, *13* (1), 109–131.

(251) Roxhed, N.; Samel, B.; Nordquist, L.; Griss, P.; Stemme, G. Painless Drug Delivery through Microneedle-Based Transdermal Patches Featuring Active Infusion. *IEEE Transactions on Biomedical Engineering* **2008**, *55* (3), 1063–1071.

(252) J., V.; A, L. Microneedles for transdermal drug delivery: a minireview. *Front Biosci* **2008**, *13*, 1711–1715.

(253) Soltani-Arabshahi, R.; Wong, J. W.; Duffy, K. L.; Powell, D. L. Facial Allergic Granulomatous Reaction and Systemic Hypersensitivity

Associated with Microneedle Therapy for Skin Rejuvenation. *JAMA dermatology* **2014**, *150* (1), 68–72.

(254) Di Natale, C.; De Rosa, D.; Profeta, M.; Jamaledin, R.; Attanasio, A.; Lagreca, E.; Scognamiglio, P. L.; Netti, P. A.; Vecchione, R. Design of Biodegradable Bi-Compartmental Microneedles for the Stabilization and the Controlled Release of the Labile Molecule Collagenase for Skin Healthcare. *Journal of Materials Chemistry B* **2021**, *9* (2), 392–403.

(255) Yu, W.; Jiang, G.; Liu, D.; Li, L.; Chen, H.; Liu, Y.; Huang, Q.; Tong, Z.; Yao, J.; Kong, X. Fabrication of Biodegradable Composite Microneedles Based on Calcium Sulfate and Gelatin for Transdermal Delivery of Insulin. *Materials Science and Engineering: C* **2017**, *71*, 725–734.

(256) Yu, W.; Jiang, G.; Liu, D.; Li, L.; Tong, Z.; Yao, J.; Kong, X. Transdermal Delivery of Insulin with Bioceramic Composite Microneedles Fabricated by Gelatin and Hydroxyapatite. *Materials Science and Engineering: C* **2017**, *73*, 425–428.

(257) Battisti, M.; Vecchione, R.; Casale, C.; Pennacchio, F. A.; Lettera, V.; Jamaledin, R.; Profeta, M.; Di Natale, C.; Imparato, G.; Urciuolo, F. Non-Invasive Production of Multi-Compartmental Biodegradable Polymer Microneedles for Controlled Intradermal Drug Release of Labile Molecules. *Frontiers in bioengineering and biotechnology* **2019**, *7*, 296.

(258) Vecchione, R.; Coppola, S.; Esposito, E.; Casale, C.; Vespini, V.; Grilli, S.; Ferraro, P.; Netti, P. A. Electro-drawn Drug-loaded

Biodegradable Polymer Microneedles as a Viable Route to Hypodermic Injection. *Advanced Functional Materials* **2014**, *24* (23), 3515–3523.

(259) Waghule, T.; Singhvi, G.; Dubey, S. K.; Pandey, M. M.; Gupta, G.; Singh, M.; Dua, K. Microneedles: A Smart Approach and Increasing Potential for Transdermal Drug Delivery System. *Biomedicine & Pharmacotherapy* **2019**, *109*, 1249–1258. https://doi.org/10.1016/j.biopha.2018.10.078.

(260) Zahoor, I.; Singh, S.; Behl, T.; Sharma, N.; Naved, T.; Subramaniyan, V.; Fuloria, S.; Fuloria, N. K.; Bhatia, S.; Al-Harrasi, A. Emergence of Microneedles as a Potential Therapeutics in Diabetes Mellitus. *Environmental Science and Pollution Research* **2021**, 1–21.

(261) Aung, N. N.; Ngawhirunpat, T.; Rojanarata, T.; Patrojanasophon, P.; Opanasopit, P.; Pamornpathomkul, B. HPMC/PVP Dissolving Microneedles: A Promising Delivery Platform to Promote Trans-Epidermal Delivery of Alpha-Arbutin for Skin Lightening. *AAPS PharmSciTech* **2019**, *21* (1), 25. https://doi.org/10.1208/s12249-019-1599-1.

(262) Aung, N. N.; Ngawhirunpat, T.; Rojanarata, T.; Patrojanasophon, P.; Pamornpathomkul, B.; Opanasopit, P. Fabrication, Characterization and Comparison of α-Arbutin Loaded Dissolving and Hydrogel Forming Microneedles. *International Journal of Pharmaceutics* **2020**, *586*, 119508. https://doi.org/10.1016/j.ijpharm.2020.119508.

(263) Li, D.; Hu, D.; Xu, H.; Patra, H. K.; Liu, X.; Zhou, Z.; Tang, J.; Slater, N.; Shen, Y. Progress and Perspective of Microneedle System for Anti-Cancer Drug Delivery. *Biomaterials* **2021**, *264*, 120410.

(264) Amarnani, R.; Shende, P. Microneedles in Diagnostic, Treatment and Theranostics: An Advancement in Minimally-Invasive Delivery System. *Biomedical Microdevices* **2022**, *24* (1), 1–12.

(265) Kaufman, B.; Alexis, A. Skin Cancer Mortality in Patients with Skin of Color. *Cutis; cutaneous medicine for the practitioner* **2017**, *99*, 307–308.

(266) Oh, C.-M.; Cho, H.; Won, Y.-J.; Kong, H.-J.; Roh, Y. H.; Jeong, K.-H.; Jung, K.-W. Nationwide Trends in the Incidence of Melanoma and Non-Melanoma Skin Cancers from 1999 to 2014 in South Korea. *Cancer research and treatment: official journal of Korean Cancer Association* **2018**, *50* (3), 729–737.

(267) Ballerini, L.; Fisher, R. B.; Aldridge, B.; Rees, J. A Color and Texture Based Hierarchical K-NN Approach to the Classification of Non-Melanoma Skin Lesions. In *Color medical image analysis*; Springer, 2013; pp 63–86.

(268) Nihal, M.; Ahmad, N.; Mukhtar, H.; Wood, G. S. Anti-proliferative and Proapoptotic Effects of (−)-epigallocatechin-3-gallate on Human Melanoma: Possible Implications for the Chemoprevention of Melanoma. *International Journal of Cancer* **2005**, *114* (4), 513–521.

(269) Lorimer, P.; Milas, Z. Cutaneous Manifestations Associated with Malignancy of the Head and Neck. In *Seminars in Oncology*; Elsevier, 2016; Vol. 43, pp 353–358.

(270) Schmitt, J.; Haufe, E.; Trautmann, F.; Schulze, H.-J.; Elsner, P.; Drexler, H.; Bauer, A.; Letzel, S.; John, S. M.; Fartasch, M. Occupational UV-Exposure Is a Major Risk Factor for Basal Cell Carcinoma: Results of the Population-Based Case-Control Study FB-181. *Journal of occupational and environmental medicine* **2018**, *60* (1), 36–43.

(271) Andrews, G.; Anderson, B.; Neves, R. Appearance of Cutaneous Malignancies of the Head and Neck. *Operative Techniques in Otolaryngology-Head and Neck Surgery* **2013**, *24* (1), 2–8.

(272) Chien, A. J.; Conrad, W. H.; Moon, R. T. A Wnt Survival Guide: From Flies to Human Disease. *Journal of Investigative Dermatology* **2009**, *129* (7), 1614–1627.

(273) Gupta, A. K.; Bharadwaj, M.; Mehrotra, R. Skin Cancer Concerns in People of Color: Risk Factors and Prevention. *Asian Pacific journal of cancer prevention: APJCP* **2016**, *17* (12), 5257.

(274) C, G. F.; M, L.-T.; K, S. SS-Catenin Pathway Activation in Breast Cancer Is Associated with Triple-Negative Phenotype but Not with CTNNB1 Mutation[J. *Modern Pathology* **2011**, *24* (2), 209–231.

(275) Knackstedt, T.; Knackstedt, R. W.; Couto, R.; Gastman, B. Malignant Melanoma: Diagnostic and Management Update. Plast Reconstr Surg, 2018, *142*. https://doi.org/10.1097/PRS.0000000000004571.

(276) Albreski, D.; Sloan, S. B. Melanoma of the Feet: Misdiagnosed and Misunderstood. *Clinics in dermatology* **2009**, *27* (6), 556–563.

(277) Müller, C. S. Histology of Melanoma and Nonmelanoma Skin Cancer. *Sunlight, Vitamin D and Skin Cancer* **2014**, 141–159.

(278) di Ruffano, L. F.; Dinnes, J.; Deeks, J. J.; Chuchu, N.; Bayliss, S. E.; Davenport, C.; Takwoingi, Y.; Godfrey, K.; O'Sullivan, C.; Matin, R. N. Optical Coherence Tomography for Diagnosing Skin Cancer in Adults. *Cochrane Database of Systematic Reviews* **2018**, No. 12.

(279) Feller, L.; Khammissa, R. A. G.; Kramer, B.; Altini, M.; Lemmer, J. Basal Cell Carcinoma, Squamous Cell Carcinoma and Melanoma of the Head and Face. *Head & face medicine* **2016**, *12* (1), 1–7.

(280) Isola, A. L.; Eddy, K.; Chen, S. Biology, Therapy and Implications of Tumor Exosomes in the Progression of Melanoma. *Cancers* **2016**, *8* (12), 110.

(281) Karakaya, G.; Ercan, A.; Oncul, S.; Aytemir, M. D. Synthesis and Cytotoxic Evaluation of Kojic Acid Derivatives with Inhibitory Activity on Melanogenesis in Human Melanoma Cells. *Anti-Cancer Agents in Medicinal Chemistry- Anti-Cancer Agents)* **2018**, *18* (15), 2137–2148. https://doi.org/10.2174/1871520618666180402141714.

(282) Karakaya, G.; Ercan, A.; Oncul, S.; Aytemir, M. D. Kojic Acid Derivatives As Potential Anticancer Agents: Synthesis And Cytotoxic Evaluation On A375 Human Malignant Melanoma Cells. **2019**. https://doi.org/10.12991/jrp.2019.167.

(283) Wilhelm, S. M.; Adnane, L.; Newell, P.; Villanueva, A.; Llovet, J. M.; Lynch, M. Preclinical Overview of Sorafenib, a Multikinase Inhibitor That Targets Both Raf and VEGF and PDGF Receptor Tyrosine Kinase Signaling. *Molecular cancer therapeutics* **2008**, *7* (10), 3129–3140.

(284) Naidoo, C.; Kruger, C. A.; Abrahamse, H. Photodynamic Therapy for Metastatic Melanoma Treatment: A Review. *Technology in cancer research & treatment* **2018**, *17*, 1533033818791795.

(285) Xie, M.; Liu, D.; Yang, Y. Anti-Cancer Peptides: Classification, Mechanism of Action, Reconstruction and Modification. *Open Biology* **2020**, *10* (7), 200004.

(286) Nam, M. S.; Jung, D. B.; Seo, K. H.; Kim, B. I.; Kim, J. H.; Kim, B.; Baek, N. I.; Kim, S.H. Apoptotic Effect of Sanggenol L via Caspase Activation and Inhibition of NF-KB Signaling in Ovarian Cancer Cells. *Phytother Res., 30* **2016**, 90–96.

(287) Di Virgilio, F.; Sarti, A. C.; Falzoni, S.; De Marchi, E.; Adinolfi, E. Extracellular ATP and P2 Purinergic Signalling in the Tumour Microenvironment. *Nature Reviews Cancer* **2018**, *18* (10), 601–618.

(288) Mânica, A.; Bonadiman, B. da S. R.; Cardoso, A. M.; Paiz, A.; Siepko, C.; de Souza, J. V. G.; Moreno, M.; Moreno, A.; Schetinger, M. R. C.; Morsch, V. M. The Signaling Effects of ATP on Melanoma-like Skin Cancer. *Cellular Signalling* **2019**, *59*, 122–130.

(289) Conklin, K. A. Chemotherapy-Associated Oxidative Stress: Impact on Chemotherapeutic Effectiveness. *Integrative cancer therapies* **2004**, *3* (4), 294–300.

(290) Florea, A.-M.; Büsselberg, D. Cisplatin as an Anti-Tumor Drug: Cellular Mechanisms of Activity, Drug Resistance and Induced Side Effects. *Cancers* **2011**, *3* (1), 1351–1371.

(291) Corrie, P. G. Cytotoxic Chemotherapy: Clinical Aspects. *Medicine* **2008**, *36* (1), 24–28.

(292) Nurgali, K.; Jagoe, R. T.; Abalo, R. *Adverse Effects of Cancer Chemotherapy: Anything New to Improve Tolerance and Reduce Sequelae?*; Frontiers Media SA, 2018; Vol. 9, p 245.

(293) Chen, K. G.; Valencia, J. C.; Gillet, J.-P.; Hearing, V. J.; Gottesman, M. M. Involvement of ABC Transporters in Melanogenesis and the Development of Multidrug Resistance of Melanoma. *Pigment cell & melanoma research* **2009**, *22* (6), 740–749.

(294) Tacar, O.; Sriamornsak, P.; Dass, C. R. Doxorubicin: An Update on Anticancer Molecular Action, Toxicity and Novel Drug Delivery Systems. *Journal of pharmacy and pharmacology* **2013**, *65* (2), 157–170.

(295) Giard, D. J.; Aaronson, S. A.; Todaro, G. J.; Arnstein, P.; Kersey, J. H.; Dosik, H.; Parks, W. P. In Vitro Cultivation of Human Tumors: Establishment of Cell Lines Derived from a Series of Solid Tumors. *J Natl Cancer Inst* **1973**, *51* (5), 1417–1423. https://doi.org/10.1093/jnci/51.5.1417.

(296) Shahbazi, A.; Zargar, S. J.; Bajouri, A.; Mohammadi, P.; Aghdami, N. Evaluation of Cultured Melanocytes in Terms of Pigmentation, Genetic Stability and Tumorigenicity in Order to Vitiligo Patients Transplantation. **2022**.

(297) Romano, P.; Manniello, A.; Aresu, O.; Armento, M.; Cesaro, M.; Parodi, B. Cell Line Data Base: Structure and Recent Improvements towards Molecular Authentication of Human Cell Lines. *Nucleic Acids Research* **2009**, *37* (Database), D925–D932. https://doi.org/10.1093/nar/gkn730.

(298) Vert, M.; Doi, Y.; Hellwich, K.-H.; Hess, M.; Hodge, P.; Kubisa, P.; Rinaudo, M.; Schué, F. Terminology for Biorelated Polymers and Applications (IUPAC Recommendations 2012). *Pure and Applied Chemistry* **2012**, *84* (2), 377–410.

(299) Prinzinger, R. Programmed Ageing: The Theory of Maximal Metabolic Scope: How Does the Biological Clock Tick? *EMBO reports* **2005**, *6* (S1), S14–S19.

(300) Gerosa, L.; Sauer, U. Regulation and Control of Metabolic Fluxes in Microbes. *Current opinion in biotechnology* **2011**, *22* (4), 566–575.

(301) Obata, T.; Fernie, A. R. The Use of Metabolomics to Dissect Plant Responses to Abiotic Stresses. *Cellular and Molecular Life Sciences* **2012**, *69* (19), 3225–3243.

(302) Steuer, A. E.; Brockbals, L.; Kraemer, T. Metabolomic Strategies in Biomarker Research–New Approach for Indirect Identification of Drug Consumption and Sample Manipulation in Clinical and Forensic Toxicology? *Frontiers in Chemistry* **2019**, *7*, 319.

(303) Moco, S.; Vervoort, J.; Bino, R. J.; De Vos, R. C.; Bino, R. Metabolomics Technologies and Metabolite Identification. *TrAC Trends in Analytical Chemistry* **2007**, *26* (9), 855–866.

(304) Gaudillière, J.-P.; Rheinberger, H.-J. From Molecular Genetics to Genomics. *New York: Roudedge* **2004**.

(305) Mochida, K.; Shinozaki, K. Advances in Omics and Bioinformatics Tools for Systems Analyses of Plant Functions. *Plant and Cell Physiology* **2011**, *52* (12), 2017–2038.

(306) Gehlenborg, N.; O'donoghue, S. I.; Baliga, N. S.; Goesmann, A.; Hibbs, M. A.; Kitano, H.; Kohlbacher, O.; Neuweger, H.; Schneider, R.; Tenenbaum, D. Visualization of Omics Data for Systems Biology. *Nature methods* **2010**, *7* (3), S56–S68.

(307) Dettmer, K.; Hammock, B. D. Metabolomics--a New Exciting Field within the" Omics" Sciences. *Environmental health perspectives* **2004**, *112* (7), A396–A397.

(308) Johnson, C. H.; Ivanisevic, J.; Siuzdak, G. Metabolomics: Beyond Biomarkers and towards Mechanisms. *Nature reviews Molecular cell biology* **2016**, *17* (7), 451–459.

(309) Wishart, D. S. Metabolomics for Investigating Physiological and Pathophysiological Processes. *Physiological reviews* **2019**, *99* (4), 1819–1875.

(310) Forcisi, S.; Moritz, F.; Kanawati, B.; Tziotis, D.; Lehmann, R.; Schmitt-Kopplin, P. Liquid Chromatography–Mass Spectrometry in Metabolomics Research: Mass Analyzers in Ultra High Pressure Liquid Chromatography Coupling. *Journal of Chromatography A* **2013**, *1292*, 51–65.

(311) Weckwerth, W. Integration of Metabolomics and Proteomics in Molecular Plant Physiology–Coping with the Complexity by Data-dimensionality Reduction. *Physiologia Plantarum* **2008**, *132* (2), 176–189.

(312) Kim, Y. S.; Maruvada, P.; Milner, J. A. Metabolomics in Biomarker Discovery: Future Uses for Cancer Prevention. **2008**.

(313) Holmes, E.; Wilson, I. D.; Nicholson, J. K. Metabolic Phenotyping in Health and Disease. *Cell* **2008**, *134* (5), 714–717.

(314) Yang, Q.; Zhang, A.; Miao, J.; Sun, H.; Han, Y.; Yan, G.; Wu, F.; Wang, X. Metabolomics Biotechnology, Applications, and Future Trends: A Systematic Review. *RSC advances* **2019**, *9* (64), 37245–37257.

(315) Oliver, S. G.; Winson, M. K.; Kell, D. B.; Baganz, F. Systematic Functional Analysis of the Yeast Genome. *Trends in Biotechnology* **1998**, *16* (9), 373–378. https://doi.org/10.1016/S0167-7799(98)01214-1.

(316) Nicholson, J. K.; Lindon, J. C.; Holmes, E. “Metabonomics”: Understanding the Metabolic Responses of Living Systems to Pathophysiological Stimuli via Multivariate Statistical Analysis of Biological NMR Spectroscopic Data. *Xenobiotica* **1999**, *29* (11), 1181–1189.

(317) Fiehn, O. Metabolomics — the Link between Genotypes and Phenotypes. In *Functional Genomics*; Town, C., Ed.; Springer Netherlands: Dordrecht, 2002; pp 155–171. https://doi.org/10.1007/978-94-010-0448-0_11.

(318) Sun, H.; Zhang, A.; Liu, S.; Qiu, S.; Li, X.; Zhang, T.; Liu, L.; Wang, X. Cell Metabolomics Identify Regulatory Pathways and Targets of Magnoline against Prostate Cancer. *Journal of Chromatography B* **2018**, *1102*, 143–151.

(319) Dunn, W. B.; Broadhurst, D. I.; Atherton, H. J.; Goodacre, R.; Griffin, J. L. Systems Level Studies of Mammalian Metabolomes: The Roles

of Mass Spectrometry and Nuclear Magnetic Resonance Spectroscopy. *Chemical society reviews* **2011**, *40* (1), 387–426.

(320) Fritz, V.; Fajas, L. Metabolism and Proliferation Share Common Regulatory Pathways in Cancer Cells. *Oncogene* **2010**, *29* (31), 4369–4377.

(321) Vander Heiden, M. G. Targeting Cancer Metabolism: A Therapeutic Window Opens. *Nature reviews Drug discovery* **2011**, *10* (9), 671–684.

(322) Wheatley, D. N. Arginine Deprivation and Metabolomics: Important Aspects of Intermediary Metabolism in Relation to the Differential Sensitivity of Normal and Tumour Cells. In *Seminars in cancer biology*; Elsevier, 2005; Vol. 15, pp 247–253.

(323) Denkert, C.; Bucher, E.; Hilvo, M.; Salek, R.; Orešič, M.; Griffin, J.; Brockmöller, S.; Klauschen, F.; Loibl, S.; Barupal, D. K. Metabolomics of Human Breast Cancer: New Approaches for Tumor Typing and Biomarker Discovery. *Genome medicine* **2012**, *4* (4), 1–9.

(324) Hirayama, A.; Kami, K.; Sugimoto, M.; Sugawara, M.; Toki, N.; Onozuka, H.; Kinoshita, T.; Saito, N.; Ochiai, A.; Tomita, M. Quantitative Metabolome Profiling of Colon and Stomach Cancer Microenvironment by Capillary Electrophoresis Time-of-Flight Mass Spectrometry. *Cancer research* **2009**, *69* (11), 4918–4925.

(325) Catchpole, G. S.; Beckmann, M.; Enot, D. P.; Mondhe, M.; Zywicki, B.; Taylor, J.; Hardy, N.; Smith, A.; King, R. D.; Kell, D. B. Hierarchical Metabolomics Demonstrates Substantial Compositional Similarity between Genetically Modified and Conventional Potato

Crops. *Proceedings of the National Academy of Sciences* **2005**, *102* (40), 14458–14462.

(326) Cairns, R. A.; Harris, I. S.; Mak, T. W. Regulation of Cancer Cell Metabolism. *Nature Reviews Cancer* **2011**, *11* (2), 85–95.

(327) Fadaka, A.; Ajiboye, B.; Ojo, O.; Adewale, O.; Olayide, I.; Emuowhochere, R. Biology of Glucose Metabolization in Cancer Cells. *Journal of Oncological Sciences* **2017**, *3* (2), 45–51.

(328) Spratlin, J. L.; Serkova, N. J.; Eckhardt, S. G. Clinical Applications of Metabolomics in Oncology: A Review. *Clinical cancer research* **2009**, *15* (2), 431–440.

(329) Boroughs, L. K.; DeBerardinis, R. J. Metabolic Pathways Promoting Cancer Cell Survival and Growth. *Nature cell biology* **2015**, *17* (4), 351–359.

(330) DiNatale, R. G.; Sanchez, A.; Hakimi, A. A.; Reznik, E. Metabolomics Informs Common Patterns of Molecular Dysfunction across Histologies of Renal Cell Carcinoma. In *Urologic Oncology: Seminars and Original Investigations*; Elsevier, 2020; Vol. 38, pp 755–762.

(331) Junot, C.; Fenaille, F.; Colsch, B.; Bécher, F. High Resolution Mass Spectrometry Based Techniques at the Crossroads of Metabolic Pathways. *Mass spectrometry reviews* **2014**, *33* (6), 471–500.

(332) Li, M.; Yang, L.; Bai, Y.; Liu, H. Analytical Methods in Lipidomics and Their Applications. *Analytical chemistry* **2014**, *86* (1), 161–175.

(333) Navas-Iglesias, N.; Carrasco-Pancorbo, A.; Cuadros-Rodríguez, L. From Lipids Analysis towards Lipidomics, a New Challenge for the

Analytical Chemistry of the 21st Century. Part II: Analytical Lipidomics. *TrAC Trends in Analytical Chemistry* **2009**, *28* (4), 393–403.

(334) Han, X.; Gross, R. W. Global Analyses of Cellular Lipidomes Directly from Crude Extracts of Biological Samples by ESI Mass Spectrometry: A Bridge to Lipidomics. *Journal of lipid research* **2003**, *44* (6), 1071–1079.

(335) Wenk, M. R. The Emerging Field of Lipidomics. *Nature reviews Drug discovery* **2005**, *4* (7), 594–610.

(336) Smilowitz, J. T.; Zivkovic, A. M.; Wan, Y.-J. Y.; Watkins, S. M.; Nording, M. L.; Hammock, B. D.; German, J. B. Nutritional Lipidomics: Molecular Metabolism, Analytics, and Diagnostics. *Molecular nutrition & food research* **2013**, *57* (8), 1319–1335.

(337) Miao, Q.-Y.; Gao, W.; Li, J.; Chen, J. Progress on Lipidomics Analytical Methods and Their Applications in Studies of Traditional Chinese Medicines. *Zhongguo Zhong yao za zhi= Zhongguo Zhongyao Zazhi= China Journal of Chinese Materia Medica* **2019**, *44* (9), 1760–1766.

(338) Fahy, E.; Subramaniam, S.; Brown, H. A.; Glass, C. K.; Merrill, A. H.; Murphy, R. C.; Raetz, C. R.; Russell, D. W.; Seyama, Y.; Shaw, W. A Comprehensive Classification System for Lipids1. *Journal of lipid research* **2005**, *46* (5), 839–861.

(339) Fahy, E.; Cotter, D.; Sud, M.; Subramaniam, S. Lipid Classification, Structures and Tools. *Biochimica et Biophysica Acta (BBA)* -

Molecular and Cell Biology of Lipids **2011**, *1811* (11), 637–647. https://doi.org/10.1016/j.bbalip.2011.06.009.

(340) Li, H.; Feng, Z.; He, M.-L. Lipid Metabolism Alteration Contributes to and Maintains the Properties of Cancer Stem Cells. *Theranostics* **2020**, *10* (16), 7053.

(341) Huang, C.; Freter, C. Lipid Metabolism, Apoptosis and Cancer Therapy. *International journal of molecular sciences* **2015**, *16* (1), 924–949.

(342) Van Meer, G.; Voelker, D. R.; Feigenson, G. W. Membrane Lipids: Where They Are and How They Behave. *Nature reviews Molecular cell biology* **2008**, *9* (2), 112–124.

(343) Lee, C.-H.; Olson, P.; Evans, R. M. Minireview: Lipid Metabolism, Metabolic Diseases, and Peroxisome Proliferator-Activated Receptors. *Endocrinology* **2003**, *144* (6), 2201–2207.

(344) Deprince, A.; Haas, J. T.; Staels, B. Dysregulated Lipid Metabolism Links NAFLD to Cardiovascular Disease. *Molecular metabolism* **2020**, *42*, 101092.

(345) Santos, C. R.; Schulze, A. Lipid Metabolism in Cancer. *The FEBS journal* **2012**, *279* (15), 2610–2623.

(346) Deng, H.; Li, W. Monoacylglycerol Lipase Inhibitors: Modulators for Lipid Metabolism in Cancer Malignancy, Neurological and Metabolic Disorders. *Acta Pharmaceutica Sinica B* **2020**, *10* (4), 582–602.

(347) Dowhan, W. Molecular Basis for Membrane Phospholipid Diversity: Why Are There so Many Lipids? *Annual review of biochemistry* **1997**, *66* (1), 199–232.

(348) Gurr, M. I.; Harwood, J. L.; Frayn, K. N. *Lipid Biochemistry*; Springer, 2002; Vol. 409.

(349) Pellerin, L.; Carrié, L.; Dufau, C.; Nieto, L.; Ségui, B.; Levade, T.; Riond, J.; Andrieu-Abadie, N. Lipid Metabolic Reprogramming: Role in Melanoma Progression and Therapeutic Perspectives. *Cancers* **2020**, *12* (11), 3147. https://doi.org/10.3390/cancers12113147.

(350) Marzagalli, M.; Raimondi, M.; Fontana, F.; Marelli, M. M.; Moretti, R. M.; Limonta, P. Cellular and Molecular Biology of Cancer Stem Cells in Melanoma: Possible Therapeutic Implications. In *Seminars in Cancer Biology*; Elsevier, 2019; Vol. 59, pp 221–235.

(351) Lehuédé, C.; Dupuy, F.; Rabinovitch, R.; Jones, R. G.; Siegel, P. M. Metabolic Plasticity as a Determinant of Tumor Growth and MetastasisMetabolism and Cancer Metastasis. *Cancer research* **2016**, *76* (18), 5201–5208.

(352) Smith, L. K.; Arabi, S.; Lelliott, E. J.; McArthur, G. A.; Sheppard, K. E. Obesity and the Impact on Cutaneous Melanoma: Friend or Foe? *Cancers* **2020**, *12* (6), 1583.

(353) Lazar, I.; Clement, E.; Dauvillier, S.; Milhas, D.; Ducoux-Petit, M.; LeGonidec, S.; Moro, C.; Soldan, V.; Dalle, S.; Balor, S. Adipocyte Exosomes Promote Melanoma Aggressiveness through Fatty Acid Oxidation: A Novel Mechanism Linking Obesity and CancerAdipocyte Exosomes: A New Link between Obesity and Cancer. *Cancer research* **2016**, *76* (14), 4051–4057.

(354) Corn, K. C.; Windham, M. A.; Rafat, M. Lipids in the Tumor Microenvironment: From Cancer Progression to Treatment. *Progress in lipid research* **2020**, *80*, 101055.

(355) Bensaad, K.; Favaro, E.; Lewis, C. A.; Peck, B.; Lord, S.; Collins, J. M.; Pinnick, K. E.; Wigfield, S.; Buffa, F. M.; Li, J.-L. Fatty Acid Uptake and Lipid Storage Induced by HIF-1α Contribute to Cell Growth and Survival after Hypoxia-Reoxygenation. *Cell reports* **2014**, *9* (1), 349–365.

(356) Hoy, A. J.; Nagarajan, S. R.; Butler, L. M. Tumour Fatty Acid Metabolism in the Context of Therapy Resistance and Obesity. *Nature Reviews Cancer* **2021**, *21* (12), 753–766.

(357) Zhang, M.; Di Martino, J. S.; Bowman, R. L.; Campbell, N. R.; Baksh, S. C.; Simon-Vermot, T.; Kim, I. S.; Haldeman, P.; Mondal, C.; Yong-Gonzales, V. Adipocyte-Derived Lipids Mediate Melanoma Progression via FATP ProteinsAdipocyte-Derived Lipids Drive Melanoma Progression via FATP. *Cancer discovery* **2018**, *8* (8), 1006–1025.

(358) Mazurkiewicz, J.; Simiczyjew, A.; Dratkiewicz, E.; Ziętek, M.; Matkowski, R.; Nowak, D. Stromal Cells Present in the Melanoma Niche Affect Tumor Invasiveness and Its Resistance to Therapy. *International Journal of Molecular Sciences* **2021**, *22* (2), 529.

(359) Nguyen, P.; Leray, V.; Diez, M.; Serisier, S.; Bloc'h, J. L.; Siliart, B.; Dumon, H. Liver Lipid Metabolism. *Journal of animal physiology and animal nutrition* **2008**, *92* (3), 272–283.

(360) Edmunds, L. R.; Sharma, L.; Kang, A.; Lu, J.; Vockley, J.; Basu, S.; Uppala, R.; Goetzman, E. S.; Beck, M. E.; Scott, D. C-Myc Programs Fatty Acid Metabolism and Dictates Acetyl-CoA Abundance and Fate. *Journal of Biological Chemistry* **2014**, *289* (36), 25382–25392.

(361) Flavin, R.; Zadra, G.; Loda, M. Metabolic Alterations and Targeted Therapies in Prostate Cancer. *The Journal of pathology* **2011**, *223* (2), 284–295.

(362) Bastos, D. C.; Paupert, J.; Maillard, C.; Seguin, F.; Carvalho, M. A.; Agostini, M.; Coletta, R. D.; Noël, A.; Graner, E. Effects of Fatty Acid Synthase Inhibitors on Lymphatic Vessels: An in Vitro and in Vivo Study in a Melanoma Model. *Laboratory Investigation* **2017**, *97* (2), 194–206.

(363) Ubellacker, J. M.; Tasdogan, A.; Ramesh, V.; Shen, B.; Mitchell, E. C.; Martin-Sandoval, M. S.; Gu, Z.; McCormick, M. L.; Durham, A. B.; Spitz, D. R. Lymph Protects Metastasizing Melanoma Cells from Ferroptosis. *Nature* **2020**, *585* (7823), 113–118.

(364) Chen, S.; Zhu, B.; Yin, C.; Liu, W.; Han, C.; Chen, B.; Liu, T.; Li, X.; Chen, X.; Li, C. Palmitoylation-Dependent Activation of MC1R Prevents Melanomagenesis. *Nature* **2017**, *549* (7672), 399–403.

(365) Wei, H.; Movahedi, A.; Zhang, Y.; Aghaei-Dargiri, S.; Liu, G.; Zhu, S.; Yu, C.; Chen, Y.; Zhong, F.; Zhang, J. Long-Chain Acyl-CoA Synthetases Promote Poplar Resistance to Abiotic Stress by Regulating Long-Chain Fatty Acid Biosynthesis. *International Journal of Molecular Sciences* **2022**, *23* (15), 8401.

(366) Carracedo, A.; Cantley, L. C.; Pandolfi, P. P. Cancer Metabolism: Fatty Acid Oxidation in the Limelight. *Nat Rev Cancer* **2013**, *13* (4), 227–232. https://doi.org/10.1038/nrc3483.

(367) Liu, Q.; Luo, Q.; Halim, A.; Song, G. Targeting Lipid Metabolism of Cancer Cells: A Promising Therapeutic Strategy for Cancer. *Cancer letters* **2017**, *401*, 39–45.

(368) Cheli, Y.; Giuliano, S.; Fenouille, N.; Allegra, M.; Hofman, V.; Hofman, P.; Bahadoran, P.; Lacour, J. P.; Tartare-Deckert, S.; Bertolotto, C. Hypoxia and MITF Control Metastatic Behaviour in Mouse and Human Melanoma Cells. *Oncogene* **2012**, *31* (19), 2461–2470.

(369) Müller, J.; Krijgsman, O.; Tsoi, J.; Robert, L.; Hugo, W.; Song, C.; Kong, X.; Possik, P. A.; Cornelissen-Steijger, P. D.; Foppen, M. H. G. Low MITF/AXL Ratio Predicts Early Resistance to Multiple Targeted Drugs in Melanoma. *Nature communications* **2014**, *5* (1), 1–15.

(370) Magistrelli, A.; Salmona, M.; Tacconi, M. T. Phospholipid Composition, Phosphoinositide Metabolism and Metastatic Capacity in Murine Melanoma B16 Variants at Different Stages of Growth. *Melanoma Research* **1992**, *2* (4), 235–240.

(371) Kim, H.-Y.; Lee, H.; Kim, S.-H.; Jin, H.; Bae, J.; Choi, H.-K. Discovery of Potential Biomarkers in Human Melanoma Cells with Different Metastatic Potential by Metabolic and Lipidomic Profiling. *Scientific reports* **2017**, *7* (1), 1–14.

(372) Schroeder, F.; Gardiner, J. M. Membrane Lipids and Enzymes of Cultured High-and Low-Metastatic B16 Melanoma Variants. *Cancer research* **1984**, *44* (8), 3262–3269.

(373) Alicea, G. M.; Rebecca, V. W.; Goldman, A. R.; Fane, M. E.; Douglass, S. M.; Behera, R.; Webster, M. R.; Kugel, C. H.; Ecker, B. L.; Caino, M. C. Changes in Aged Fibroblast Lipid Metabolism Induce Age-Dependent Melanoma Cell Resistance to Targeted Therapy via the Fatty Acid Transporter FATP2FATP2 Enhances Therapy Resistance in Melanoma during Aging. *Cancer discovery* **2020**, *10* (9), 1282–1295.

(374) Falcon, A.; Doege, H.; Fluitt, A.; Tsang, B.; Watson, N.; Kay, M. A.; Stahl, A. FATP2 Is a Hepatic Fatty Acid Transporter and Peroxisomal Very Long-Chain Acyl-CoA Synthetase. *American Journal of Physiology-Endocrinology and Metabolism* **2010**, *299* (3), E384–E393.

(375) Qiu, P.; Wang, H.; Zhang, M.; Zhang, M.; Peng, R.; Zhao, Q.; Liu, J. FATP2-Targeted Therapies—A Role beyond Fatty Liver Disease. *Pharmacological Research* **2020**, *161*, 105228.

(376) Alicea, G. M. Metabolic Consequences of an Aging Microenvironment in Melanoma, University of the Sciences in Philadelphia, 2020.

(377) Crudele, L.; Piccinin, E.; Moschetta, A. Visceral Adiposity and Cancer: Role in Pathogenesis and Prognosis. *Nutrients* **2021**, *13* (6), 2101.

(378) Wang, Y.; Zeng, Z.; Lu, J.; Wang, Y.; Liu, Z.; He, M.; Zhao, Q.; Wang, Z.; Li, T.; Lu, Y. CPT1A-Mediated Fatty Acid Oxidation Promotes Colorectal Cancer Cell Metastasis by Inhibiting Anoikis. *Oncogene* **2018**, *37* (46), 6025–6040.

(379) Ma, Y.; Temkin, S. M.; Hawkridge, A. M.; Guo, C.; Wang, W.; Wang, X.-Y.; Fang, X. Fatty Acid Oxidation: An Emerging Facet of Metabolic Transformation in Cancer. *Cancer letters* **2018**, *435*, 92–100.

(380) Fares, J.; Fares, M. Y.; Khachfe, H. H.; Salhab, H. A.; Fares, Y. Molecular Principles of Metastasis: A Hallmark of Cancer Revisited. *Signal transduction and targeted therapy* **2020**, *5* (1), 1–17.

(381) Ng, S.-F.; Rouse, J. J.; Sanderson, F. D.; Meidan, V.; Eccleston, G. M. Validation of a Static Franz Diffusion Cell System for In Vitro Permeation Studies. *AAPS PharmSciTech* **2010**, *11* (3), 1432–1441. https://doi.org/10.1208/s12249-010-9522-9.

(382) Bartosova, L.; Bajgar, J. Transdermal Drug Delivery in Vitro Using Diffusion Cells. *Current medicinal chemistry* **2012**, *19* (27), 4671–4677.

(383) Venter, J. P.; Müller, D. G.; du Plessis, J.; Goosen, C. A Comparative Study of an in Situ Adapted Diffusion Cell and an in Vitro Franz Diffusion Cell Method for Transdermal Absorption of Doxylamine. *European journal of pharmaceutical sciences* **2001**, *13* (2), 169–177.

(384) Baert, B.; Boonen, J.; Burvenich, C.; Roche, N.; Stillaert, F.; Blondeel, P.; Bocxlaer, J.; Spiegeleer., B.; D. A New Discriminative

Criterion for the Development of Franz Diffusion Tests for Transdermal Pharmaceuticals. JOURNAL. *OF PHARMACY AND PHARMACEUTICAL* **2010**, *13* (2), 218–230.

(385) Boudry, I.; Blanck, O.; Cruz, C.; Blanck, M.; Vallet, V.; Bazire, A.; Capt, A.; Josse, D.; Lallement, G. Percutaneous Penetration and Absorption of Parathion Using Human and Pig Skin Models in Vitro and Human Skin Grafted onto Nude Mouse Skin Model in Vivo. *Journal of Applied Toxicology* **2008**, *28* (5), 645–657. https://doi.org/10.1002/jat.1317.

(386) Finnin, B.; Walters, K. A.; Franz, T. J. Vitro Skin Permeation Methodology. In *HAE Benson & AC Watkinson (eds), Transdermal and Topical Drug Delivery*; Principles and Practice. John Wiley & Sons, Hoboken NJ USA, 2012; pp 85-108 10 1002 9781118140505 5.

(387) Barbero, A. M.; Frasch, H. F. Pig and Guinea Pig Skin as Surrogates for Human in Vitro Penetration Studies: A Quantitative Review. *Toxicology in Vitro* **2009**, *23* (1), 1–13. https://doi.org/10.1016/j.tiv.2008.10.008.

(388) Wei, J. C. J.; Edwards, G. A.; Martin, D. J.; Huang, H.; Crichton, M. L.; Kendall, M. A. F. Allometric Scaling of Skin Thickness, Elasticity, Viscoelasticity to Mass for Micro-Medical Device Translation: From Mice, Rats, Rabbits, Pigs to Humans. *Scientific Reports* **2017**, *7* (1), 15885. https://doi.org/10.1038/s41598-017-15830-7.

(389) DICK, I. P.; SCOTT, R. C. Pig Ear Skin as an In-Vitro Model for Human Skin Permeability. *Journal of Pharmacy and Pharmacology*

1992, *44* (8), 640–645. https://doi.org/10.1111/j.2042-7158.1992.tb05485.x.

(390) Pizzo, S. V.; Lundblad, R. L.; Willis, M. S. *2016. Proteolysis in the Interstitial Space*; CRC Press.

(391) Paula, D. D.; Martins, C. A.; Bentley, M. V. L. B. Development and Validation of HPLC Method for Imiquimod Determination in Skin Penetration Studies. *Biomedical Chromatography* **2008**, *22* (12), 1416–1423. https://doi.org/10.1002/bmc.1075.

(392) Locatelli, M.; Melucci, D.; Carlucci, G.; Locatelli, C. RECENT HPLC STRATEGIES TO IMPROVE SENSITIVITY AND SELECTIVITY FOR THE ANALYSIS OF COMPLEX MATRICES. *null* **2012**, *40* (2–3), 112–137. https://doi.org/10.1080/10739149.2011.651668.

(393) Bonnin, E. A.; Rizzoli, S. O. Novel Secondary Ion Mass Spectrometry Methods for the Examination of Metabolic Effects at the Cellular and Subcellular Levels. Frontiers in Behavioral Neuroscience, 14, 2020.

(394) Agüi-Gonzalez, P.; Jähne, S.; N. Phan, N. T. SIMS Imaging in Neurobiology and Cell Biology. *Journal of Analytical Atomic Spectrometry* **2019**, *34* (7), 1355–1368. https://doi.org/10.1039/C9JA00118B.

(395) Passarelli, M. K.; Pirkl, A.; Moellers, R.; Grinfeld, D.; Kollmer, F.; Havelund, R.; Newman, C. F.; Marshall, P. S.; Arlinghaus, H.; Alexander, M. R.; West, A.; Horning, S.; Niehuis, E.; Makarov, A.; Dollery, C. T.; Gilmore, I. S. The 3D OrbiSIMS—Label-Free Metabolic Imaging with Subcellular Lateral Resolution and High

Mass-Resolving Power. *Nature Methods* **2017**, *14* (12), 1175–1183. https://doi.org/10.1038/nmeth.4504.

(396) Diehnelt, C. W. *Application of Polyatomic Primary Ions for Organic Secondary Ion Mass Spectrometry*; Texas A&M University, 2001.

(397) Patel, R. MALDI-TOF MS for the Diagnosis of Infectious Diseases. *Clinical Chemistry* **2015**, *61* (1), 100–111. https://doi.org/10.1373/clinchem.2014.221770.

(398) Israr, M. Z.; Bernieh, D.; Salzano, A.; Cassambai, S.; Yazaki, Y.; Suzuki, T. Matrix-Assisted Laser Desorption Ionisation (MALDI) Mass Spectrometry (MS): Basics and Clinical Applications. *Clinical Chemistry and Laboratory Medicine (CCLM)* **2020**, *58* (6), 883–896.

(399) Suvannapruk, W.; Edney, M. K.; Kim, D.-H.; Scurr, D. J.; Ghaemmaghami, A. M.; Alexander, M. R. Single-Cell Metabolic Profiling of Macrophages Using 3D OrbiSIMS: Correlations with Phenotype. *Analytical Chemistry* **2022**, *94* (26), 9389–9398.

(400) Hodgkinson, T.; Tsimbouri, P. M.; Llopis-Hernandez, V.; Campsie, P.; Scurr, D.; Childs, P. G.; Phillips, D.; Donnelly, S.; Wells, J. A.; O'Brien, F. J. The Use of Nanovibration to Discover Specific and Potent Bioactive Metabolites That Stimulate Osteogenic Differentiation in Mesenchymal Stem Cells. *Science Advances* **2021**, *7* (9), eabb7921.

(401) Meurs, J.; Scurr, D. J.; Lourdusamy, A.; Storer, L. C.; Grundy, R. G.; Alexander, M. R.; Rahman, R.; Kim, D.-H. Sequential Orbitrap Secondary Ion Mass Spectrometry and Liquid Extraction Surface Analysis-Tandem Mass Spectrometry-Based Metabolomics for

Prediction of Brain Tumor Relapse from Sample-Limited Primary Tissue Archives. *Analytical Chemistry* **2021**, *93* (18), 6947–6954.

(402) Theodoridis, G. A.; Gika, H. G.; Want, E. J.; Wilson, I. D. Liquid Chromatography–Mass Spectrometry Based Global Metabolite Profiling: A Review. *Analytica chimica acta* **2012**, *711*, 7–16.

(403) Nassar, A. F.; Wu, T.; Nassar, S. F.; Wisnewski, A. V. UPLC–MS for Metabolomics: A Giant Step Forward in Support of Pharmaceutical Research. *Drug discovery today* **2017**, *22* (2), 463–470.

(404) Xiao, J. F.; Zhou, B.; Ressom, H. W. Metabolite Identification and Quantitation in LC-MS/MS-Based Metabolomics. *TrAC Trends in Analytical Chemistry* **2012**, *32*, 1–14.

(405) Jian, W.; Edom, R. W.; Xu, Y.; Weng, N. Recent Advances in Application of Hydrophilic Interaction Chromatography for Quantitative Bioanalysis. *Journal of separation science* **2010**, *33* (6-7), 681–697.

(406) Villas-Bôas, S. G.; Mas, S.; Åkesson, M.; Smedsgaard, J.; Nielsen, J. Mass Spectrometry in Metabolome Analysis. *Mass spectrometry reviews* **2005**, *24* (5), 613–646.

(407) Unlu, A.; Onmaz, D. E.; Abusoglu, S.; Abusoglu, G. HPLC and LC-MS/MS Measurement Methods for the Quantification of Asymmetric Dimethylarginine (ADMA) and Related Metabolites. *Turkish Journal of Biochemistry* **2021**, *46* (4), 327–347.

(408) Erkmen, C.; Gebrehiwot, W. H.; Uslu, B. Hydrophilic Interaction Liquid Chromatography (HILIC): Latest Applications in the

Pharmaceutical Researches. *Current Pharmaceutical Analysis* **2021**, *17* (3), 316–345.

(409) t'Kindt, R.; Storme, M.; Deforce, D.; Van Bocxlaer, J. Evaluation of Hydrophilic Interaction Chromatography versus Reversed-Phase Chromatography in a Plant Metabolomics Perspective. *Journal of Separation Science* **2008**, *31* (9), 1609–1614. https://doi.org/10.1002/jssc.200700539.

(410) Zeki, Ö. C.; Eylem, C. C.; Reçber, T.; Kır, S.; Nemutlu, E. Integration of GC–MS and LC–MS for Untargeted Metabolomics Profiling. *Journal of Pharmaceutical and Biomedical Analysis* **2020**, *190*, 113509.

(411) Liu, X.; Zhou, L.; Shi, X.; Xu, G. New Advances in Analytical Methods for Mass Spectrometry-Based Large-Scale Metabolomics Study. *TrAC Trends in Analytical Chemistry* **2019**, *121*, 115665.

(412) Yang, L.; George, J.; Wang, J. Deep Profiling of Cellular Heterogeneity by Emerging Single-cell Proteomic Technologies. *Proteomics* **2020**, *20* (13), 1900226.

(413) Ruiz-Rodado, V.; Lita, A.; Larion, M. Advances in Measuring Cancer Cell Metabolism with Subcellular Resolution. *Nature Methods* **2022**, *19* (9), 1048–1063.

(414) Wouters, B.; Currivan, S. A.; Abdulhussain, N.; Hankemeier, T.; Schoenmakers, P. J. Immobilized-Enzyme Reactors Integrated into Analytical Platforms: Recent Advances and Challenges. *TrAC Trends in Analytical Chemistry* **2021**, *144*, 116419.

(415) Won, J.; Park, J. W. Improvement of Arbutin Trans-Epidermal Delivery Using Radiofrequency Microporation. *Tropical Journal of Pharmaceutical Research* **2014**, *13* (11), 1775–1781. https://doi.org/10.4314/tjpr.v13i11.1.

(416) Guillot, A. J.; Cordeiro, A. S.; Donnelly, R. F.; Montesinos, M. C.; Garrigues, T. M.; Melero, A. Microneedle-Based Delivery: An Overview of Current Applications and Trends. *Pharmaceutics* **2020**, *12* (6), 569. https://doi.org/10.3390/pharmaceutics12060569.

(417) Yang, J.; Liu, X.; Fu, Y.; Song, Y. Recent Advances of Microneedles for Biomedical Applications: Drug Delivery and Beyond. *Acta Pharmaceutica Sinica B* **2019**, *9* (3), 469–483. https://doi.org/10.1016/j.apsb.2019.03.007.

(418) Barde, M. P.; Barde, P. J. What to Use to Express the Variability of Data: Standard Deviation or Standard Error of Mean? *Perspect Clin Res* **2012**, *3* (3), 113–116. https://doi.org/10.4103/2229-3485.100662.

(419) Gupta, J.; Gill, H. S.; Andrews, S. N.; Prausnitz, M. R. Kinetics of Skin Resealing after Insertion of Microneedles in Human Subjects. *Journal of Controlled Release* **2011**, *154* (2), 148–155. https://doi.org/10.1016/j.jconrel.2011.05.021.

(420) Mann, T.; Gerwat, W.; Batzer, J.; Eggers, K.; Scherner, C.; Wenck, H.; Stäb, F.; Hearing, V. J.; Röhm, K.-H.; Kolbe, L. Inhibition of Human Tyrosinase Requires Molecular Motifs Distinctively Different from Mushroom Tyrosinase. *Journal of Investigative Dermatology* **2018**, *138* (7), 1601–1608. https://doi.org/10.1016/j.jid.2018.01.019.

(421) Lambert, M. W.; Maddukuri, S.; Karanfilian, K. M.; Elias, M. L.; Lambert, W. C. The Physiology of Melanin Deposition in Health and Disease. *Clinics in Dermatology* **2019**, *37* (5), 402–417. https://doi.org/10.1016/j.clindermatol.2019.07.013.

(422) Stulberg, D. L.; Clark, N.; Tovey, D. Common Hyperpigmentation Disorders in Adults: Part II. Melanoma, Seborrheic Keratoses, Acanthosis Nigricans, Melasma, Diabetic Dermopathy, Tinea Versicolor, and Postinflammatory Hyperpigmentation. *afp* **2003**, *68* (10), 1963–1969.

(423) Speeckaert, R.; Van Gele, M.; Speeckaert, M. M.; Lambert, J.; van Geel, N. The Biology of Hyperpigmentation Syndromes. *Pigment Cell & Melanoma Research* **2014**, *27* (4), 512–524. https://doi.org/10.1111/pcmr.12235.

(424) Davis, L. E.; Shalin, S. C.; Tackett, A. J. Current State of Melanoma Diagnosis and Treatment. *Cancer Biology & Therapy* **2019**, *20* (11), 1366–1379. https://doi.org/10.1080/15384047.2019.1640032.

(425) Saginala, K.; Barsouk, A.; Aluru, J. S.; Rawla, P.; Barsouk, A. Epidemiology of Melanoma. *Medical Sciences* **2021**, *9* (4), 63. https://doi.org/10.3390/medsci9040063.

(426) Yu, X.; Zheng, H.; Tse, G.; Chan, M. T.; Wu, W. K. Long Non-Coding RNAs in Melanoma. *Cell Proliferation* **2018**, *51* (4), e12457. https://doi.org/10.1111/cpr.12457.

(427) Rueth, N. M.; Cromwell, K. D.; Cormier, J. N. Long-Term Follow-up for Melanoma Patients: Is There Any Evidence of a Benefit? *Surg*

Oncol Clin N Am **2015**, *24* (2), 359–377. https://doi.org/10.1016/j.soc.2014.12.012.

(428) Pan, T.; Li, X.; Jankovic, J. The Association between Parkinson's Disease and Melanoma. *International Journal of Cancer* **2011**, *128* (10), 2251–2260. https://doi.org/10.1002/ijc.25912.

(429) Dalvin, L. A.; Damento, G. M.; Yawn, B. P.; Abbott, B. A.; Hodge, D. O.; Pulido, J. S. Parkinson Disease and Melanoma: Confirming and Reexamining an Association. *Mayo Clinic Proceedings* **2017**, *92* (7), 1070–1079. https://doi.org/10.1016/j.mayocp.2017.03.014.

(430) Bougea, A.; Spantideas, N.; Katoulis, A.; Stefanis, L. Levodopa-Induced Skin Disorders in Patients with Parkinson Disease: A Systematic Literature Review Approach. *Acta Neurol Belg* **2019**, *119* (3), 325–336. https://doi.org/10.1007/s13760-019-01195-3.

(431) Porcar Saura, S.; Guillén Climent, S.; Pinazo Canales, M. I.; Monteagudo, C. Melanocytic Hyperactivation Simulating an Acral Lentiginous Melanoma in a Patient With Parkinson Disease Treated by Levodopa. *The American Journal of Dermatopathology* **2021**, *43* (3), 238. https://doi.org/10.1097/DAD.0000000000001807.

(432) Inzelberg, R.; Rabey, J. M.; Melamed, E.; Djaldetti, R.; Reches, A.; Badarny, S.; Hassin-Baer, S.; Cohen, O.; Trau, H.; Aharon-Peretz, J.; Milo, R.; Schwartz, M.; Huberman, M.; Gilead, L.; Barchana, M.; Liphshiz, I.; Fitzer-Attas, C.; Giladi, N. High Prevalence of Malignant Melanoma in Israeli Patients with Parkinson's Disease. *J Neural Transm* **2011**, *118* (8), 1199–1207. https://doi.org/10.1007/s00702-011-0580-2.

(433) Disse, M.; Reich, H.; Lee, P. K.; Schram, S. S. A Review of the Association Between Parkinson Disease and Malignant Melanoma. *Dermatologic Surgery* **2016**, *42* (2), 141. https://doi.org/10.1097/DSS.0000000000000591.

(434) Min, K.; Park, K.; Park, D.-H.; Yoo, Y. J. Overview on the Biotechnological Production of L-DOPA. *Appl Microbiol Biotechnol* **2015**, *99* (2), 575–584. https://doi.org/10.1007/s00253-014-6215-4.

(435) Slominski, A.; Costantino, R. Molecular Mechanism of Tyrosinase Regulation by L-DOPA in Hamster Melanoma Cells. *Life Sciences* **1991**, *48* (21), 2075–2079. https://doi.org/10.1016/0024-3205(91)90164-7.

(436) Liu, R.; Gao, X.; Lu, Y.; Chen, H. Meta-Analysis of the Relationship between Parkinson Disease and Melanoma. *Neurology* **2011**, *76* (23), 2002–2009. https://doi.org/10.1212/WNL.0b013e31821e554e.

(437) Vermeij, J.-D.; Winogrodzka, A.; Trip, J.; Weber, W. E. J. Parkinson's Disease, Levodopa-Use and the Risk of Melanoma. *Parkinsonism Relat Disord* **2009**, *15* (8), 551–553. https://doi.org/10.1016/j.parkreldis.2009.05.002.

(438) Slominski, A.; Zbytek, B.; Slominski, R. Inhibitors of Melanogenesis Increase Toxicity of Cyclophosphamide and Lymphocytes against Melanoma Cells. *International Journal of Cancer* **2009**, *124* (6), 1470–1477. https://doi.org/10.1002/ijc.24005.

(439) Bakr, M. N.; Takahashi, H.; Kikuchi, Y. Analysis of Melanoma Gene Expression Signatures at the Single-Cell Level Uncovers 45-Gene

Signature Related to Prognosis. *Biomedicines* **2022**, *10* (7), 1478. https://doi.org/10.3390/biomedicines10071478.

(440) Meira, W. V.; Heinrich, T. A.; Cadena, S. M. S. C.; Martinez, G. R. Melanogenesis Inhibits Respiration in B16-F10 Melanoma Cells Whereas Enhances Mitochondrial Cell Content. *Experimental Cell Research* **2017**, *350* (1), 62–72. https://doi.org/10.1016/j.yexcr.2016.11.006.

(441) Li, C.; Kuai, L.; Cui, R.; Miao, X. Melanogenesis and the Targeted Therapy of Melanoma. *Biomolecules* **2022**, *12* (12), 1874. https://doi.org/10.3390/biom12121874.

(442) Bilska, B.; Schedel, F.; Piotrowska, A.; Stefan, J.; Zmijewski, M.; Pyza, E.; Reiter, R. J.; Steinbrink, K.; Slominski, A. T.; Tulic, M. K.; Kleszczyński, K. Mitochondrial Function Is Controlled by Melatonin and Its Metabolites in Vitro in Human Melanoma Cells. *Journal of Pineal Research* **2021**, *70* (3), e12728. https://doi.org/10.1111/jpi.12728.

(443) Miao, Y.; Sheng, J.; Wang, X.; Shi, C.; Sun, Q.; Liu, T.; Diwu, J. Melanin Nanoparticles as an Actinide in Vivo Sequestration Agent with Radiation Protection Effect. *New Journal of Chemistry* **2021**, *45* (21), 9518–9525. https://doi.org/10.1039/D1NJ00999K.

(444) Maher, S.; Mahmoud, M.; Rizk, M.; Kalil, H. Synthetic Melanin Nanoparticles as Peroxynitrite Scavengers, Photothermal Anticancer and Heavy Metals Removal Platforms. *Environ Sci Pollut Res* **2020**, *27* (16), 19115–19126. https://doi.org/10.1007/s11356-019-05111-3.

(445) Roulier, B.; Pérès, B.; Haudecoeur, R. Advances in the Design of Genuine Human Tyrosinase Inhibitors for Targeting Melanogenesis and Related Pigmentations. *J. Med. Chem.* **2020**, *63* (22), 13428–13443. https://doi.org/10.1021/acs.jmedchem.0c00994.

(446) Liu, L.; Yue, Q.; Ma, J.; Liu, Y.; Zhao, T.; Guo, W.; Zhu, G.; Guo, S.; Wang, S.; Gao, T.; Li, C.; Shi, Q. POU4F1 Promotes the Resistance of Melanoma to BRAF Inhibitors through MEK/ERK Pathway Activation and MITF up-Regulation. *Cell Death Dis* **2020**, *11* (6), 1–11. https://doi.org/10.1038/s41419-020-2662-2.

(447) Djehal, A.; Krayem, M.; Najem, A.; Hammoud, H.; Cresteil, T.; Nebigil, C. G.; Wang, D.; Yu, P.; Bentouhami, E.; Ghanem, G. E.; Désaubry, L. Targeting Prohibitin with Small Molecules to Promote Melanogenesis and Apoptosis in Melanoma Cells. *European Journal of Medicinal Chemistry* **2018**, *155*, 880–888. https://doi.org/10.1016/j.ejmech.2018.06.052.

(448) Kamo, H.; Kawahara, R.; Simizu, S. Tyrosinase Suppresses Vasculogenic Mimicry in Human Melanoma Cells. *Oncology Letters* **2022**, *23* (5), 1–9. https://doi.org/10.3892/ol.2022.13289.

(449) Slominski, A.; Tobin, D. J.; Shibahara, S.; Wortsman, J. Melanin Pigmentation in Mammalian Skin and Its Hormonal Regulation. *Physiological Reviews* **2004**, *84* (4), 1155–1228. https://doi.org/10.1152/physrev.00044.2003.

(450) Chen, C.; Gonzalez, F. J.; Idle, J. R. LC-MS-Based Metabolomics in Drug Metabolism. *Drug Metabolism Reviews* **2007**, *39* (2–3), 581–597. https://doi.org/10.1080/03602530701497804.

(451) Vergani, E.; Beretta, G. L.; Aloisi, M.; Costantino, M.; Corno, C.; Frigerio, S.; Tinelli, S.; Dugo, M.; Accattatis, F. M.; Granata, A.; Arnaboldi, L.; Rodolfo, M.; Perego, P.; Gatti, L. Targeting of the Lipid Metabolism Impairs Resistance to BRAF Kinase Inhibitor in Melanoma. *Front Cell Dev Biol* **2022**, *10*, 927118. https://doi.org/10.3389/fcell.2022.927118.

(452) Wang, Q.; Beaumont, K. A.; Otte, N. J.; Font, J.; Bailey, C. G.; van Geldermalsen, M.; Sharp, D. M.; Tiffen, J. C.; Ryan, R. M.; Jormakka, M.; Haass, N. K.; Rasko, J. E. J.; Holst, J. Targeting Glutamine Transport to Suppress Melanoma Cell Growth. *International Journal of Cancer* **2014**, *135* (5), 1060–1071. https://doi.org/10.1002/ijc.28749.

(453) Sheen, J.-H.; Zoncu, R.; Kim, D.; Sabatini, D. M. Defective Regulation of Autophagy upon Leucine Deprivation Reveals a Targetable Liability of Human Melanoma Cells In Vitro and In Vivo. *Cancer Cell* **2011**, *19* (5), 613–628. https://doi.org/10.1016/j.ccr.2011.03.012.

(454) Lieu, E. L.; Nguyen, T.; Rhyne, S.; Kim, J. Amino Acids in Cancer. *Exp Mol Med* **2020**, *52* (1), 15–30. https://doi.org/10.1038/s12276-020-0375-3.

(455) Haavik, J. L-DOPA Is a Substrate for Tyrosine Hydroxylase. *Journal of Neurochemistry* **1997**, *69* (4), 1720–1728. https://doi.org/10.1046/j.1471-4159.1997.69041720.x.

(456) Sullivan, L. B.; Luengo, A.; Danai, L. V.; Bush, L. N.; Diehl, F. F.; Hosios, A. M.; Lau, A. N.; Elmiligy, S.; Malstrom, S.; Lewis, C. A.;

Vander Heiden, M. G. Aspartate Is an Endogenous Metabolic Limitation for Tumour Growth. *Nat Cell Biol* **2018**, *20* (7), 782–788. https://doi.org/10.1038/s41556-018-0125-0.

(457) Wang, T.; Yao, W.; Li, J.; He, Q.; Shao, Y.; Huang, F. Acetyl-CoA from Inflammation-Induced Fatty Acids Oxidation Promotes Hepatic Malate-Aspartate Shuttle Activity and Glycolysis. *American Journal of Physiology-Endocrinology and Metabolism* **2018**, *315* (4), E496–E510. https://doi.org/10.1152/ajpendo.00061.2018.

(458) Kim, S.-Y. Cancer Energy Metabolism: Shutting Power off Cancer Factory. *Biomol Ther (Seoul)* **2018**, *26* (1), 39–44. https://doi.org/10.4062/biomolther.2017.184.

(459) Chikara, S.; Nagaprashantha, L. D.; Singhal, J.; Horne, D.; Awasthi, S.; Singhal, S. S. Oxidative Stress and Dietary Phytochemicals: Role in Cancer Chemoprevention and Treatment. *Cancer Letters* **2018**, *413*, 122–134. https://doi.org/10.1016/j.canlet.2017.11.002.

(460) Lee, J.-S.; Choi, J.; Lee, S.-H.; Kang, J. H.; Ha, J. S.; Kim, H. Y.; Jang, H.; Yook, J. I.; Kim, S.-Y. Oxoglutarate Carrier Inhibition Reduced Melanoma Growth and Invasion by Reducing ATP Production. *Pharmaceutics* **2020**, *12* (11), 1128. https://doi.org/10.3390/pharmaceutics12111128.

(461) Zdzisińska, B.; Żurek, A.; Kandefer-Szerszeń, M. Alpha-Ketoglutarate as a Molecule with Pleiotropic Activity: Well-Known and Novel Possibilities of Therapeutic Use. *Arch. Immunol. Ther. Exp.* **2017**, *65* (1), 21–36. https://doi.org/10.1007/s00005-016-0406-x.

(462) Morris, J. P.; Yashinskie, J. J.; Koche, R.; Chandwani, R.; Tian, S.; Chen, C.-C.; Baslan, T.; Marinkovic, Z. S.; Sánchez-Rivera, F. J.; Leach, S. D.; Carmona-Fontaine, C.; Thompson, C. B.; Finley, L. W. S.; Lowe, S. W. α-Ketoglutarate Links P53 to Cell Fate during Tumour Suppression. *Nature* **2019**, *573* (7775), 595–599. https://doi.org/10.1038/s41586-019-1577-5.

(463) Wen, Y.-A.; Xiong, X.; Scott, T.; Li, A. T.; Wang, C.; Weiss, H. L.; Tan, L.; Bradford, E.; Fan, T. W. M.; Chandel, N. S.; Barrett, T. A.; Gao, T. The Mitochondrial Retrograde Signaling Regulates Wnt Signaling to Promote Tumorigenesis in Colon Cancer. *Cell Death Differ* **2019**, *26* (10), 1955–1969. https://doi.org/10.1038/s41418-018-0265-6.

(464) Eroglu, E. C.; Tunug, S.; Geckil, O. F.; Gulec, U. K.; Vardar, M. A.; Paydas, S. Discovery of Metabolomic Biomarkers for Discriminating Platinum-Sensitive and Platinum-Resistant Ovarian Cancer by Using GC-MS. *Eur J Mass Spectrom (Chichester)* **2021**, *27* (6), 235–248. https://doi.org/10.1177/14690667211057996.

(465) Alkan, H. F.; Vesely, P. W.; Hackl, H.; Foßelteder, J.; Schmidt, D. R.; Vander Heiden, M. G.; Pichler, M.; Hoefler, G.; Bogner-Strauss, J. G. Deficiency of Malate-Aspartate Shuttle Component SLC25A12 Induces Pulmonary Metastasis. *Cancer & Metabolism* **2020**, *8* (1), 26. https://doi.org/10.1186/s40170-020-00232-7.

(466) Ueda, K.; Sanbongi, C.; Yamaguchi, M.; Ikegami, S.; Hamaoka, T.; Fujita, S. The Effects of Phenylalanine on Exercise-Induced Fat Oxidation: A Preliminary, Double-Blind, Placebo-Controlled,

Crossover Trial. *Journal of the International Society of Sports Nutrition* **2017**, *14*. https://doi.org/10.1186/s12970-017-0191-x.

(467) Nagaoka, K.; Mulla, J.; Cao, K.; Cheng, Z.; Liu, D.; William Mueller; Bay, A.; Hildebrand, G.; Lu, S.; Huang, C.-K. The Metabolite, Alpha-Ketoglutarate Inhibits Non-Alcoholic Fatty Liver Disease Progression by Targeting Lipid Metabolism. *Liver Research* **2020**, *4* (2), 94–100. https://doi.org/10.1016/j.livres.2020.04.001.

(468) Chen, G.-C.; Su, H.-M.; Lin, Y.-S.; Tsou, P.-Y.; Chyuan, J.-H.; Chao, P.-M. A Conjugated Fatty Acid Present at High Levels in Bitter Melon Seed Favorably Affects Lipid Metabolism in Hepatocytes by Increasing NAD+/NADH Ratio and Activating PPARα, AMPK and SIRT1 Signaling Pathway. *The Journal of Nutritional Biochemistry* **2016**, *33*, 28–35. https://doi.org/10.1016/j.jnutbio.2016.03.009.

(469) Koundouros, N.; Poulogiannis, G. Reprogramming of Fatty Acid Metabolism in Cancer. *Br J Cancer* **2020**, *122* (1), 4–22. https://doi.org/10.1038/s41416-019-0650-z.

(470) Long, X. H.; Mao, J. H.; Peng, A. F.; Zhou, Y.; Huang, S. H.; Liu, Z. L. Tumor Suppressive MicroRNA-424 Inhibits Osteosarcoma Cell Migration and Invasion via Targeting Fatty Acid Synthase. *Experimental and Therapeutic Medicine* **2013**, *5* (4), 1048–1052. https://doi.org/10.3892/etm.2013.959.

(471) Zhang, M.; Di Martino, J. S.; Bowman, R. L.; Campbell, N. R.; Baksh, S. C.; Simon-Vermot, T.; Kim, I. S.; Haldeman, P.; Mondal, C.; Yong-Gonzales, V.; Abu-Akeel, M.; Merghoub, T.; Jones, D. R.; Zhu, X. G.; Arora, A.; Ariyan, C. E.; Birsoy, K.; Wolchok, J. D.; Panageas, K. S.;

Hollmann, T.; Bravo-Cordero, J. J.; White, R. M. Adipocyte-Derived Lipids Mediate Melanoma Progression via FATP Proteins. *Cancer Discov* **2018**, *8* (8), 1006–1025. https://doi.org/10.1158/2159-8290.CD-17-1371.

(472) Rivera-Calimlim, L.; Bianchine, J. R. Effect of L-Dopa on Plasma Free Fatty Acids and Plasma Glucose. *Metabolism* **1972**, *21* (7), 611–617. https://doi.org/10.1016/0026-0495(72)90085-6.

(473) Soares, A. R.; Marchiosi, R.; Siqueira-Soares, R. de C.; Barbosa de Lima, R.; Dantas dos Santos, W.; Ferrarese-Filho, O. The Role of L-DOPA in Plants. *Plant Signaling & Behavior* **2014**, *9* (4), e28275. https://doi.org/10.4161/psb.28275.

(474) T.H. Khan, M. Novel Tyrosinase Inhibitors From Natural Resources – Their Computational Studies. *Current Medicinal Chemistry* **2012**, *19* (14), 2262–2272. https://doi.org/10.2174/092986712800229041.

(475) Vaezi, M. Structure and Inhibition Mechanism of Some Synthetic Compounds and Phenolic Derivatives as Tyrosinase Inhibitors: Review and New Insight. *Journal of Biomolecular Structure and Dynamics* **2022**, *0* (0), 1–13. https://doi.org/10.1080/07391102.2022.2069157.

(476) Currie, E.; Schulze, A.; Zechner, R.; Walther, T. C.; Farese, R. V. Cellular Fatty Acid Metabolism and Cancer. *Cell Metabolism* **2013**, *18* (2), 153–161. https://doi.org/10.1016/j.cmet.2013.05.017.

(477) Kuhajda, F. P. Fatty-Acid Synthase and Human Cancer: New Perspectives on Its Role in Tumor Biology. *Nutrition* **2000**, *16* (3), 202–208. https://doi.org/10.1016/S0899-9007(99)00266-X.

Chapter 7. Appendices

Appendix A



Figure A-1. Photograph of drug residue in the needle.

Table A-1. HPLC analysis of mean percentage of permeation of commercial Alpha-Arbutin products with Dermapen® post-treatment in different Franz cell components (donor wash, skin wash, tape strips, remaining skin and receptor fluid) following 24-hour permeation test.

Amount (μg)	Remain in needle	RF	DW	SW	TS	RS	Total amount	Recovery rate
HA	1348.23±324.2	4.98±11.02	543.09±241.8	550.2±340.44	270.03±243	50.95±33.75	2767.47	69.19%
AA	2362.96±501.73	5.34±13.64	1177.94±1352.61	279.94±256.06	27.23±19.05	13.13±11.54	3866.55	96.66%
INK	2842.43±200.79	16.31±32.72	328.55±282.93	585.09±475.42	75.68±39.13	49.02±24.55	3897.08	97.43%

Table A-2. HPLC analysis of mean Alpha-Arbutin permeation rates from remaining in skin of 24h penetration test of different formulations with and without microneedle pre-treatment. The data are expressed as means ± SD (Without MNs and CMNs pre-treatment, n=3; CMNs post-treatment, n=6; DMNs, n=4).

Percentage (%)	HA	AA	INK
Without MNs	1.1217±0.8646	0.4327±0.2239	0.8611±0.2148
CMNs pre-treatment	1.6901±1.5707	0.9393±1.8988	1.2156±0.3296
CMNs post-treatment	3.7536±1.7674	2.2446±3.217	6.5857±7.3408
	Pure Alpha-Arbutin		
DMNs	4.5772±1.2808		

Table A-3. HPLC analysis of mean Alpha-Arbutin from different Franz cell components, receptor fluid (RF), donor wash (DW), skin wash (SW), tape strips (TS) and remaining in skin (RS) following 24 hours permeation test by WMNs, CMNs and DMNs. The data are expressed as means ± SD (n=3 WMNs; n=6 for CMNs; n=4 for DMNs).

Franz Cell Components	Percentage of alpha-arbutin in total administration/ %									
	Commercial Alpha-Arbutin Products			Commercial Alpha-Arbutin Products with Dermapen® Pre-treatment			Commercial Alpha-Arbutin Products with Dermapen® Post-treatment			Alpha-Arbutin-Loaded PVPVA Microneedle
	HA	AA	INK	HA	AA	INK	HA	AA	INK	2% w/w Alpha-Arbutin
Donor Wash	57.53±15.12	87.43±5.19	57.84±21.14	66.78±19.79	92.12±8.92	70.11±18.83	41.46±16.04	56.13±39.23	24.31±11.37	4.34±4.55
Skin Wash	39.12±12.90	11.68±5.06	39.29±19.40	27.36±17.82	6.1±5.42	27.16±17.92	35.03±15.07	32.35±37.46	44.19±8.04	80.04±15.22
Tape Strips	2.20±1.53	0.42±0.10	1.96±1.92	3.59±4.41	0.67±1.26	1.47±1.01	19.44±20.80	4.09±4.03	11.71±5.16	9.79±8.88
Remaining within Skin	1.12±0.86	0.43±0.22	0.86±0.21	1.69±1.57	0.94±1.9	1.22±0.33	3.75±1.76	5.91±3.21	14.56±7.34	4.57±1.28
Receptor Fluid	0.01±0.02	0.02±0.04	0.02±0.02	0.59±0.62	0.16±0.37	0.05±0.08	0.30±0.59	1.48±4.72	5.21±3.60	1.23±2.46

Appendix B

1. Methods

1.1 Chemistry synthesis

*2,4-Bis(benzyloxy)benzaldehyde (**15**).* Compound **14** (1g, 7.24 mmol), K_2CO_3 (3 g, 21.72 mmol) and benzyl bromide (3.44 mL, 28.96 mmol) were added to methanol. The mixture was heated to reflux for 2 h. Then, methanol was removed in vacuo. Diluted with EtOAc and water, the biphasic solution was extracted three times with EtOAc. The combined organics were washed with brine, dried over anhydrous Na_2SO_4, and concentrated in vacuo. Purification of the residue by column chromatography with PE/EA (10:1) to give 2,4-bis(benzyloxy)benzaldehyde (**15**, 2 g, 6.3 mmol, 86.77%) as a white solid.

19a–n. Compound **15** (300 mg, 0.94 mmol), various acetophenone (1.05 eq.) and NaOH (188.44 mg, 4.71 mmol) were added to ethanol. The mixture was heated to reflux for 2–4 h. Then, ethanol was removed in vacuo. Diluted with EtOAc and water, the biphasic solution was extracted three times with EtOAc. The combined organics were washed with brine, dried over anhydrous Na_2SO_4, and concentrated in vacuo. Purification of the residue by column chromatography with PE/EA to give the target compounds **16a–n** as a yellow solid or oil with good yields.

17a–n. A pressure vial equipped with a magnetic stirring bar was charged with compounds **16a–n**, bis(pinacolato)diboron (3 eq.), Cs_2CO_3 (0.2 eq.) and ethanol. The vessel was flushed with argon, sealed with a crimp cap, and heated to 120–150 ℃ for 12–24 h. The reaction vessel was

removed from the oil bath when the reaction was finished, and cooled to room temperature. The precipitate, if appeared, was collected by filtration onto a sintered-glass funnel, washed with cold ethanol (3 × 50 mL), and dried in vacuo to give the target compounds. Otherwise, ethanol was removed in vacuo. Diluted with EtOAc and water, the biphasic solution was extracted three times with EtOAc. The combined organics were washed with brine, dried over anhydrous Na_2SO_4, and concentrated in vacuo. Purification of the residue by column chromatography with PE/EA to give the target compounds **17a–n** as a white solid with moderate yield.

11a–n. A two-neck flask was charged with compounds **17a–n**, pentamethylbenzene (1.5 eq. per benzyl to be removed) and dry DCM. Under the protection of Ar at 0 ℃ (the intermediate without methoxyl) or -78 ℃ (the intermediate with methoxyl), inject 1 M BCl_3 (1.5 eq. per benzyl to be removed) into the flask, the solution turned orange and reacted for 20 min. After the reaction was completed, water was added to quench the reaction. Diluted with EtOAc and water, the biphasic solution was extracted three times with EtOAc. The combined organics were washed with brine, dried over anhydrous Na_2SO_4, and concentrated in vacuo. Purification of the residue by column chromatography with DCM/MeOH to give the target compounds **11a–n** with moderate yields.

3-(2,4-Dihydroxyphenyl)-1-(4-methoxyphenyl)propan-1-one ***(11a).*** Yield 72.8%, yellow solid; ^{1}H NMR (300 MHz, $CDCl_3$) δ 8.55 (s, 1H), 7.96 (d, J = 8.5 Hz, 2H), 6.96 (s, 1H), 6.92 (d, J = 9.0 Hz, 2H), 6.54–6.45 (m, 1H), 6.39 (d, J = 8.2 Hz, 1H), 5.81 (s, 1H), 3.87 (s, 3H), 3.35 (t, J = 5.9 Hz,

2H), 3.09–2.85 (m, 2H); ^{13}C NMR (75 MHz, DMSO-d_6) δ 198.8, 163.5, 157.0, 156.3, 130.7, 130.6, 130.1, 118.1, 114.3, 106.4, 102.9, 56.0, 40.0, 25.0; HR-MS (ESI) *m/z*: calcd for $C_{16}H_{16}O_4$ $[M-H]^-$ 271.0975, found 271.0976; Purity: 99.358% (by HPLC).

*3-(2,4-Dihydroxyphenyl)-1-(m-tolyl)propan-1-one (**11b**).* Yield 80.2%, yellow oil. ^{1}H NMR (300 MHz, $CDCl_3$) δ 8.26 (s, 1H), 7.78 (d, J = 9.3 Hz, 2H), 7.43–7.29 (m, 2H), 6.95 (d, J = 8.1 Hz, 1H), 6.46 (d, J = 2.6 Hz, 1H), 6.39 (dd, J = 8.2, 2.5 Hz, 1H), 6.00 (s, 1H), 3.39 (t, J = 6.0 Hz, 2H), 2.95 (t, J = 6.0 Hz, 2H), 2.40 (s, 3H); ^{13}C NMR (75 MHz, $CDCl_3$) δ 202.9, 155.6, 155.2, 138.5, 136.1, 134.6, 131.3, 128.9, 128.5, 125.6, 119.9, 108.0, 104.4, 40.6, 23.0, 21.3; HR-MS (ESI) *m/z*: calcd for $C_{16}H_{16}O_3$ $[M-H]^-$ 255.1026, found 255.1028; Purity: 96.665% (by HPLC).

*1,3-Bis(2,4-dihydroxyphenyl)propan-1-one (**11c**).* Yield 64.2%, yellow oil. ^{1}H NMR (300 MHz, DMSO-d_6) δ 12.71 (s, 1H), 9.25 (s, 1H), 9.02 (s, 1H), 7.78 (d, J = 8.7 Hz, 1H), 7.17 (d, J = 25.3 Hz, 2H), 6.85 (s, 1H), 6.28 (m, 2H), 6.12 (s, 1H), 3.10 (s, 2H), 2.73 (d, J = 8.1 Hz, 2H); ^{13}C NMR (75 MHz, DMSO-d_6) δ 205.0, 165.2, 164.8, 157.1, 156.3, 133.4, 130.6, 117.8, 112.9, 108.6, 106.4, 102.9, 92.5, 29.5, 25.4; HR-MS (ESI) *m/z*: calcd for $C_{15}H_{14}O_5$ $[M-H]^-$ 273.0768, found 273.0767; Purity: 99.671% (by HPLC).

*3-(2,4-Dihydroxyphenyl)-1-(2-hydroxyphenyl)propan-1-one (**11d**).* Yield 82.7%, light yellow solid. ^{1}H NMR (300 MHz, DMSO-d_6) δ 11.99 (s, 1H), 9.23 (s, 1H), 8.99 (s, 1H), 7.92 (dd, J = 7.7, 1.7 Hz, 1H), 7.57–7.47 (m, 1H), 6.96 (d, J = 9.1 Hz, 2H), 6.85 (d, J = 8.1 Hz, 1H), 6.28 (d, J = 2.1 Hz, 1H), 6.18–6.08 (m, 1H), 3.24 (t, J = 7.6 Hz, 2H), 2.76 (t, J = 7.6 Hz, 2H); ^{13}C NMR (75 MHz, DMSO-d_6) δ 206.8, 161.2, 157.1, 156.3, 136.5, 131.2,

130.6, 120.6, 119.7, 118.1, 117.7, 106.4, 102.8, 25.0, 22.3; HR-MS (ESI) *m/z*: calcd for $C_{15}H_{14}O_4$ $[M-H]^-$ 257.0819, found 257.0818; Purity: 98.151% (by HPLC).

*1-(4-Bromophenyl)-3-(2,4-dihydroxyphenyl)propan-1-one (**11e**).* Yield 85.9%, pink oil. ^{1}H NMR (300 MHz, $CDCl_3$) δ 7.93 (s, 1H), 7.90–7.71 (m, 2H), 7.59 (d, J = 8.1 Hz, 2H), 6.95 (d, J = 8.2 Hz, 1H), 6.44–6.37 (m, 1H), 6.34 (d, J = 2.5 Hz, 1H), 4.86 (s, 1H), 3.36 (t, J = 5.9 Hz, 2H), 2.95 (t, J = 6.0 Hz, 2H); ^{13}C NMR (75 MHz, DMSO-d_6) δ 199.5, 157.0, 156.3, 136.1, 132.2, 130.5, 130.4, 127.6, 117.8, 106.4, 102.9, 24.7, 20.7; HR-MS (ESI) *m/z*: calcd for $C_{15}H_{13}BrO_3$ $[M-H]^-$ 318.9975, found 318.9976; Purity: 99.254% (by HPLC).

*3-(2,4-Dihydroxyphenyl)-1-(o-tolyl)propan-1-one (**11f**).* Yield 89.7%, yellow oil. ^{1}H NMR (300 MHz, $CDCl_3$) δ 8.09 (d, J = 3.8 Hz, 1H), 7.61 (dd, J = 7.6, 3.6 Hz, 1H), 7.31 (dd, J = 7.8, 4.1 Hz, 1H), 7.22–7.14 (m, 2H), 6.87 (dd, J = 8.2, 3.9 Hz, 1H), 6.38 (dd, J = 4.1, 2.5 Hz, 1H), 6.35–6.24 (m, 1H), 5.35 (s, 1H), 3.34–3.15 (m, 2H), 2.98–2.76 (m, 2H), 2.41 (d, J = 4.1 Hz, 3H); ^{13}C NMR (75 MHz, DMSO-d_6) δ 204.7, 157.0, 156.3, 138.6, 137.2, 132.0, 131.5, 130.5, 128.9, 126.3, 117.9, 106.3, 102.9, 41.9, 25.0, 21.0; HR-MS (ESI) *m/z*: calcd for $C_{16}H_{16}O_3$ $[M-H]^-$ 255.1026, found 255.1025; Purity: 98.650% (by HPLC).

*3-(2,4-Dihydroxyphenyl)-1-(4-hydroxyphenyl)propan-1-one (**11g**).* Yield 66.9%, colorless oil. ^{1}H NMR (300 MHz, $CDCl_3$) δ 8.49 (s, 1H), 7.89 (d, J = 9.0 Hz, 2H), 7.20 (s, 1H), 6.96–6.76 (m, 3H), 6.36 (d, J = 2.6 Hz, 1H), 6.29 (dd, J = 8.2, 2.6 Hz, 1H), 5.11 (s, 1H), 3.37–3.19 (m, 2H), 2.92–2.77 (m, 2H); ^{13}C NMR (101 MHz, $CDCl_3$) δ 201.1, 164.1, 155.6, 131.3,

130.8, 129.1, 120.3, 113.8, 107.9, 104.6, 40.3, 22.9; HR-MS (ESI) *m/z*: calcd for $C_{15}H_{14}O_4$ $[M-H]^-$ 257.0819, found 257.0815; Purity: 98.107% (by HPLC).

1-(2,4-Dichlorophenyl)-3-(2,4-dihydroxyphenyl)propan-1-one ***(11h).*** Yield 48.2%, pink oil. ^{1}H NMR (300 MHz, $CDCl_3$) δ 7.54–7.42 (m, 2H), 7.35–7.30 (m, 1H), 6.96 (d, J = 8.1 Hz, 1H), 6.46–6.34 (m, 2H), 5.08 (s, 2H), 3.36 (t, J = 6.2 Hz, 2H), 2.95 (t, J = 6.3 Hz, 2H); ^{13}C NMR (75 MHz, $CDCl_3$) δ 203.7, 155. 5, 155.1, 138.1, 136.3, 132.6, 131.3, 130.7, 130.6, 127.4, 119.4, 108.0, 104.1, 44.5, 23.3; HR-MS (ESI) *m/z*: calcd for $C_{15}H_{12}Cl_2O_3$ $[M-H]^-$ 309.0090, found 309.0094; Purity: 97.929% (by HPLC).

3-(2,4-Dihydroxyphenyl)-1-(2-hydroxy-4-methoxyphenyl)propan-1-one ***(11i).*** Yield 34.7%, pink solid. ^{1}H NMR (300 MHz, DMSO-d_6) δ 12.72 (s, 1H), 9.24 (s, 1H), 8.99 (s, 1H), 7.88 (d, J = 8.8 Hz, 1H), 6.85 (d, J = 8.2 Hz, 1H), 6.55–6.49 (m, 1H), 6.47 (d, J = 2.4 Hz, 1H), 6.28 (d, J = 2.4 Hz, 1H), 6.12 (dd, J = 8.1, 2.4 Hz, 1H), 3.82 (s, 3H), 3.22–3.13 (m, 2H), 2.74 (t, J = 7.7 Hz, 2H); ^{13}C NMR (101 MHz, DMSO-d_6) δ 205.4, 166.0, 164.7, 157.1, 156.3, 133.0, 130.6, 117.7, 113.8, 107.7, 106.4, 102.9, 101.3, 56.2, 40.0, 25.3; HR-MS (ESI) *m/z*: calcd for $C_{16}H_{16}O_5$ $[M-H]^-$ 287.0925, found 287.0924; Purity: 99.140% (by HPLC).

3-(2,4-Dihydroxyphenyl)-1-(4-isopropylphenyl)propan-1-one ***(11j).*** Yield 81.8%, yellow oil. ^{1}H NMR (300 MHz, $CDCl_3$) δ 8.43 (s, 1H), 7.95 (d, J = 7.8 Hz, 2H), 7.35 (s, 2H), 7.32 (d, J = 5.6 Hz, 1H), 6.99 (d, J = 8.1 Hz, 1H), 6.48 (d, J = 2.4 Hz, 1H), 6.41 (d, J = 8.3 Hz, 1H), 5.37 (d, J = 13.3 Hz, 1H), 3.43 (t, J = 5.9 Hz, 2H), 3.01–2.97 (m, 2H), 1.30 (d, J = 7.0 Hz, 6H); ^{13}C NMR (75 MHz, $CDCl_3$) δ 202.3, 155.6, 155.4, 154.5, 133.9, 131.3,

128.7, 126.8, 120.2, 107.9, 104.6, 40.6, 34.3, 23.6, 22.8; HR-MS (ESI) *m/z*: calcd for $C_{18}H_{20}O_3$ $[M-H]^-$ 283.1339, found 283.1334; Purity: 98.016% (by HPLC).

*3-(2,4-Dihydroxyphenyl)-1-(3-hydroxy-4-methoxyphenyl)propan-1-one (**11k**).* Yield 51.6%, white solid. ^1H NMR (300 MHz, $CDCl_3$) δ 9.37 (s, 1H), 9.20 (s, 1H), 8.98 (s, 1H), 7.48 (dd, J = 8.4, 2.1 Hz, 1H), 7.35 (d, J = 2.2 Hz, 1H), 6.99 (d, J = 8.5 Hz, 1H), 6.83 (d, J = 8.2 Hz, 1H), 6.27 (d, J = 2.3 Hz, 1H), 6.11 (dd, J = 8.1, 2.4 Hz, 1H), 3.83 (s, 3H), 3.06 (t, J = 7.6 Hz, 2H), 2.69 (t, J = 7.7 Hz, 2H); ^{13}C NMR (101 MHz, MeOD) δ 200.8, 156.4, 155.8, 152.2, 146.2, 130.1, 121.5, 118.6, 114.2, 113.5, 110.3, 106.0, 102.2, 55.0, 38.6, 25.2; HR-MS (ESI) *m/z*: calcd for $C_{16}H_{16}O_5$ $[M-H]^-$ 287.0925, found 287.0926; Purity: 98.408% (by HPLC).

*3-(2,4-Dihydroxyphenyl)-1-phenylpropan-1-one (**11l**).* Yield 52.9%, pink solid. ^1H NMR (300 MHz, $CDCl_3$) δ 8.25 (s, 1H), 8.03–7.98 (m, 2H), 7.61 (t, J = 7.4 Hz, 1H), 7.49 (d, J = 7.6 Hz, 2H), 7.46 (s, 1H), 6.99 (d, J = 8.2 Hz, 1H), 6.49 (d, J = 2.5 Hz, 1H), 6.42 (dd, J = 8.2, 2.6 Hz, 1H), 3.43 (t, J = 5.9 Hz, 2H), 2.99 (t, J = 6.0 Hz, 2H); ^{13}C NMR (75 MHz, $CDCl_3$) δ 202.6, 155.7, 155.3, 136.1, 133.8, 131.3, 128.7, 128.4, 119.9, 108.0, 104.5, 40.6, 23,0; HR-MS (ESI) *m/z*: calcd for $C_{15}H_{14}O_3$ $[M-H]^-$ 241.0870, found 241.0866; Purity: 98.017% (by HPLC).

*3-(2,4-Dihydroxyphenyl)-1-(4-hydroxy-3-methoxyphenyl)propan-1-one (**11m**).* Yield 63.2%, pink solid. ^1H NMR (300 MHz, MeOD) δ 7.57 (d, J = 7.7 Hz, 2H), 6.84 (dd, J = 11.8, 8.1 Hz, 2H), 6.29 (d, J = 2.4 Hz, 1H), 6.20 (dd, J = 8.2, 2.4 Hz, 1H), 3.89 (s, 3H), 3.15 (t, J = 7.7 Hz, 2H), 2.85 (t, J = 7.7 Hz, 2H); ^{13}C NMR (75 MHz, MeOD) δ 200.7, 156.4, 155.8, 152.3,

147.65, 130.2, 128.6, 123.3, 118.6, 114.5, 110.8, 106.0, 102.1, 54.9, 38.7, 19.5; HR-MS (ESI) *m/z*: calcd for $C_{16}H_{16}O_5$ $[M-H]^-$ 287.0925, found 287.0922; Purity: 95.521% (by HPLC).

1-([1,1'-Biphenyl]-4-yl)-3-(2,4-dihydroxyphenyl)propan-1-one ***(11n)***. Yield 49.8%, yellow oil. ^{1}H NMR (300 MHz, DMSO-d_6) δ 8.15 (s, 1H), 7.92 (s, 1H), 6.98 (d, J = 8.4 Hz, 2H), 6.74 (d, J = 8.3 Hz, 2H), 6.69–6.64 (m, 2H), 6.42 (d, J = 7.6 Hz, 2H), 6.15 (d, J = 7.4 Hz, 1H), 5.90 (d, J = 7.4 Hz, 1H), 5.80 (d, J = 8.2 Hz, 1H), 5.22 (d, J = 2.4 Hz, 1H), 2.15 (t, J = 7.6 Hz, 2H), 1.70 (t, J = 7.6 Hz, 2H); ^{13}C NMR (75 MHz, DMSO-d_6) δ 199.4, 156.5, 155.8, 144.4, 138.9, 135.5, 130.2, 129.1, 128.7, 128.4, 127.0, 126.9, 117.6, 106.0, 102.4, 38.7, 24.5; HR-MS (ESI) *m/z*: calcd for $C_{21}H_{18}O_3$ $[M-H]^-$ 317.1183, found 317.1182; Purity: 97.843% (by HPLC).

12a–n. Compounds **12a–n** were synthesized according to the synthetic routes of compounds **11a–n**.

1-(2,4-Dihydroxyphenyl)-3-(2,3-dimethoxyphenyl)propan-1-one ***(12a)***. Yield 54.1%, white solid. ^{1}H NMR (300 MHz, $CDCl_3$) δ 12.76 (s, 1H), 7.67 (d, J = 8.6 Hz, 1H), 6.99 (d, J = 7.5 Hz, 1H), 6.82 (d, J = 8.1 Hz, 2H), 6.35 (s, 2H), 5.83 (s, 1H), 3.86 (d, J = 3.8 Hz, 6H), 3.18 (d, J = 8.3 Hz, 2H), 3.09–2.95 (m, 2H); ^{13}C NMR (75 MHz, DMSO-d_6) δ 204.2, 165.2, 164.7, 152.8, 147.1, 134.7, 133.4, 124.3, 122.0, 112.9, 111.5, 108.7, 102.9, 60.5, 56.0, 25.0, 20.7; HR-MS (ESI) *m/z*: calcd for $C_{17}H_{18}O_5$ $[M-H]^-$ 301.1081, found 301.1082; Purity: 99.767% (by HPLC).

1-(2,4-Dihydroxyphenyl)-3-(4-hydroxyphenyl)propan-1-one ***(12b)***. Yield 74.7%, yellow solid. ^{1}H NMR (300 MHz, DMSO-d_6) δ 12.63 (s, 1H), 10.61 (s, 1H), 9.15 (s, 1H), 7.80 (d, J = 8.8 Hz, 1H), 7.05 (d, J = 8.3 Hz,

2H), 6.69–6.61 (m, 2H), 6.36 (dd, *J* = 8.8, 2.4 Hz, 1H), 6.24 (d, *J* = 2.2 Hz, 1H), 3.20 (t, *J* = 7.6 Hz, 2H), 2.81 (t, *J* = 7.6 Hz, 2H); ^{13}C NMR (75 MHz, DMSO-d_6) δ 204.3, 165.2, 164.7, 156.0, 133.5, 131.5, 129.7, 115.52, 113.0, 108.6, 102.9, 34.0, 29.5; HR-MS (ESI) *m/z*: calcd for $C_{15}H_{14}O_4$ [M-H]$^-$ 257.0819, found 257.0821; Purity: 96.941% (by HPLC).

1-(2,4-Dihydroxyphenyl)-3-(2,3,4-trimethoxyphenyl)propan-1-one ***(12c).*** Yield 48.2%, light yellow solid. ^{1}H NMR (300 MHz, DMSO-d_6) δ 12.60 (d, *J* = 1.4 Hz, 1H), 10.60 (s, 1H), 7.77 (d, *J* = 8.7 Hz, 1H), 6.89 (d, *J* = 8.5 Hz, 1H), 6.69 (d, *J* = 8.5 Hz, 1H), 6.37–6.31 (m, 1H), 6.26–6.20 (m, 1H), 3.77 (s, 3H), 3.73 (s, 3H), 3.71 (s, 3H), 3.14 (t, *J* = 7.6 Hz, 2H), 2.81 (t, *J* = 7.6 Hz, 2H); ^{13}C NMR (75 MHz, DMSO-d_6) δ 204.3, 165.3, 164.8, 152.5, 151.8, 142.2, 133.4, 126.7, 124.2, 112.9, 108.7, 108.2, 102.9, 61.1, 60.7, 56.2, 40.0, 25.0; HR-MS (ESI) *m/z*: calcd for $C_{18}H_{20}O_6$ [M-H]$^-$ 331.1187, found 331.1186; Purity: 96.389% (by HPLC).

1-(2,4-Dihydroxyphenyl)-3-(3-hydroxyphenyl)propan-1-one ***(12d).*** Yield 85.6%, light yellow solid. ^{1}H NMR (300 MHz, DMSO-d_6) δ 12.61 (s, 1H), 10.64 (s, 1H), 9.27 (s, 1H), 7.82 (d, *J* = 8.8 Hz, 1H), 7.07 (t, *J* = 7.7 Hz, 1H), 6.73–6.64 (m, 2H), 6.62–6.55 (m, 1H), 6.37 (dd, *J* = 8.9, 2.3 Hz, 1H), 6.26 (d, *J* = 2.4 Hz, 1H), 3.26 (t, *J* = 7.6 Hz, 2H), 2.85 (t, *J* = 7.5 Hz, 2H); ^{13}C NMR (75 MHz, DMSO-d_6) δ 204.0, 165.2, 164.7, 157.8, 142.9, 133.4, 129.7, 119.4, 115.8, 113.4, 113.0, 108.6, 102.9, 39.9, 30.2; HR-MS (ESI) *m/z*: calcd for $C_{15}H_{14}O_4$ [M-H]$^-$ 257.0819, found 257.0821; Purity: 99.268% (by HPLC).

1-(2,4-Dihydroxyphenyl)-3-(2-hydroxy-4-methoxyphenyl)propan-1-one ***(12e).*** Yield 61.5%, yellow solid. ^{1}H NMR (300 MHz, DMSO-d_6) δ 13.25–

13.05 (m, 1H), 11.07 (d, *J* = 15.1 Hz, 1H), 9.90 (d, *J* = 15.4 Hz, 1H), 8.33–8.18 (m, 1H), 7.44 (d, *J* = 9.7 Hz, 1H), 6.89 (d, *J* = 3.7 Hz, 1H), 6.85–6.80 (m, 1H), 6.80–6.74 (m, 1H), 6.71 (t, *J* = 5.6 Hz, 1H), 3.78 (s, 3H), 3.60 (d, *J* = 10.0 Hz, 2H), 3.10–2.90 (m, 2H); ^{13}C NMR (75 MHz, DMSO-d_6) δ 204.8, 165.2, 164.8, 159.1, 156.4, 133.4, 130.7, 119.7, 112.9, 108.6, 104.5, 102.9, 101.7, 55.3, 40.0, 25.2; HR-MS (ESI) *m/z*: calcd for $C_{16}H_{16}O_5$ $[M-H]^-$ 287.0925, found 287.0924; Purity: 97.871% (by HPLC).

1-(2,4-Dihydroxyphenyl)-3-(3-hydroxy-4-methoxyphenyl)propan-1-one ***(12f)****.* Yield 74.2%, white solid. ^{1}H NMR (300 MHz, DMSO-d_6) δ 12.61 (s, 1H), 8.78 (s, 1H), 7.81 (s, 1H), 6.80 (d, *J* = 8.2 Hz, 1H), 6.71–6.57 (m, 2H), 6.35 (d, *J* = 8.9 Hz, 1H), 6.24 (s, 1H), 3.72 (s, 3H), 3.19 (d, *J* = 7.2 Hz, 2H), 2.79 (t, *J* = 7.6 Hz, 2H); ^{13}C NMR (75 MHz, DMSO-d_6) δ 204.2, 165.2, 164.7, 146.78, 146.4, 134.1, 133.4, 119.2, 116.3, 113.0, 112.7, 108.6, 102.9, 56.1, 39.9, 29.6; HR-MS (ESI) *m/z*: calcd for $C_{16}H_{16}O_5$ $[M-H]^-$ 287.0925, found 287.0939; Purity: 98.746% (by HPLC).

1-(2,4-Dihydroxyphenyl)-3-(3,4,5-trimethoxyphenyl)propan-1-one ***(12g)****.* Yield 66.9%, white solid. ^{1}H NMR (300 MHz, DMSO-d_6) δ 12.61 (s, 1H), 7.83 (d, *J* = 8.9 Hz, 1H), 6.58 (s, 2H), 6.36 (d, *J* = 8.8 Hz, 1H), 6.25 (s, 1H), 3.74 (s, 6H), 3.61 (s, 3H), 3.27 (s, 2H), 2.86 (t, *J* = 7.9 Hz, 2H); ^{13}C NMR (75 MHz, DMSO-d_6) δ 204.2, 165.2, 164.7, 153.2, 137.2, 136.1, 133.6, 113.0, 108.6, 106.1, 102.8, 60.4, 56.2, 39.9, 30.7; HR-MS (ESI) *m/z*: calcd for $C_{18}H_{20}O_6$ $[M-H]^-$ 331.1187, found 331.1188; Purity: 96.984% (by HPLC).

1-(2,4-Dihydroxyphenyl)-3-(3,4-dimethoxyphenyl)propan-1-one ***(12h)****.* Yield 67.3%, light yellow solid. ^{1}H NMR (300 MHz, DMSO-d_6) δ 12.63 (s,

1H), 10.65 (s, 1H), 7.82 (d, *J* = 8.9 Hz, 1H), 6.87 (d, *J* = 10.1 Hz, 1H), 6.82 (s, 1H), 6.76 (d, *J* = 8.2 Hz, 1H), 6.36 (d, *J* = 8.8 Hz, 1H), 6.30–6.16 (m, 1H), 3.73 (s, 3H), 3.70 (s, 3H), 3.29–3.22 (m, 2H), 2.86 (t, *J* = 7.6 Hz, 2H); ^{13}C NMR (75 MHz, DMSO-d_6) δ 204.3, 165.2, 164.7, 149.1, 147.6, 133.9, 133.5, 120.6, 113.0, 112.8, 112.3, 108.6, 102.9, 56.0, 55.8, 39.95, 30.0; HR-MS (ESI) *m/z*: calcd for $C_{17}H_{18}O_5$ $[M-H]^-$ 301.1081, found 301.1085; Purity: 98.183% (by HPLC).

*1-(2,4-Dihydroxyphenyl)-3-(3-nitrophenyl)propan-1-one (**12i**).* Yield 60.2%, light yellow solid. ^{1}H NMR (300 MHz, DMSO-d_6) δ 12.49 (s, 1H), 10.66 (s, 1H), 8.19 (s, 1H), 8.14–8.03 (m, 1H), 7.84 (d, *J* = 8.9 Hz, 1H), 7.78 (d, *J* = 7.7 Hz, 1H), 7.59 (t, *J* = 7.9 Hz, 1H), 6.36 (dd, *J* = 9.0, 2.3 Hz, 1H), 6.25 (d, *J* = 2.3 Hz, 1H), 3.42–3.34 (m, 2H), 3.07 (t, *J* = 7.4 Hz, 2H); ^{13}C NMR (75 MHz, DMSO-d_6) δ 203.4, 165.2, 164.5, 148.2, 144.0, 136.0, 133.5, 130.1, 123.6, 121.5, 113.0, 108.6, 102.8, 39.9, 29.5; HR-MS (ESI) *m/z*: calcd for $C_{15}H_{13}NO_5$ $[M-H]^-$ 286.0721, found 286.0720; Purity: 98.228% (by HPLC).

*1-(2,4-Dihydroxyphenyl)-3-(2-hydroxyphenyl)propan-1-one (**12j**).* Yield 55.6%, yellow solid. ^{1}H NMR (300 MHz, DMSO-d_6) δ 12.66 (d, *J* = 2.3 Hz, 1H), 10.63 (d, *J* = 2.4 Hz, 1H), 9.42 (d, *J* = 2.5 Hz, 1H), 7.88–7.76 (m, 1H), 7.10 (d, *J* = 7.5 Hz, 1H), 6.99 (d, *J* = 8.0 Hz, 1H), 6.78 (d, *J* = 7.7 Hz, 1H), 6.71 (d, *J* = 7.8 Hz, 1H), 6.35 (d, *J* = 8.8 Hz, 1H), 6.29–6.18 (m, 1H), 3.17 (d, *J* = 7.8 Hz, 2H), 2.85 (d, *J* = 9.2 Hz, 2H); ^{13}C NMR (101 MHz, DMSO-d_6) δ 204.7, 165.2, 164.8, 155.6, 133.4, 130.3, 127.6, 127.4, 119.4, 115.3, 112.9, 108.6, 102.9, 38.1, 25.7; HR-MS (ESI) *m/z*: calcd for $C_{15}H_{14}O_4$ $[M-H]^-$ 257.0819, found 257.0819; Purity: 95.704% (by HPLC).

*1-(2,4-Dihydroxyphenyl)-3-(o-tolyl)propan-1-one (**12k**).* Yield 88.1%, light yellow solid. ^{1}H NMR (300 MHz, DMSO-d_6) δ 12.66–12.55 (m, 1H), 10.62 (s, 1H), 7.82 (d, J = 8.8 Hz, 1H), 7.19 (d, J = 6.2 Hz, 2H), 7.14–7.08 (m, 2H), 6.39–6.32 (m, 1H), 6.28–6.22 (m, 1H), 3.23 (t, J = 7.8 Hz, 2H), 2.90 (t, J = 7.7 Hz, 2H), 2.29 (s, 3H); ^{13}C NMR (101 MHz, DMSO-d_6) δ 204.1, 165.3, 164.7, 139.6, 136.2, 133.5, 133.5, 130.4, 129.0, 126.4, 113.0, 108.6, 102.9, 38.2, 27.6, 19.4; HR-MS (ESI) *m/z*: calcd for $C_{16}H_{16}O_3$ $[M-H]^-$ 255.1026, found 255.1029; Purity: 96.578% (by HPLC).

*1-(2,4-Dihydroxyphenyl)-3-(3-methoxyphenyl)propan-1-one (**12l**).* Yield 82.3%, light yellow solid. ^{1}H NMR (300 MHz, DMSO-d_6) δ 12.59 (d, J = 9.8 Hz, 1H), 10.64 (d, J = 10.0 Hz, 1H), 7.82 (t, J = 9.7 Hz, 1H), 7.18 (d, J = 9.9 Hz, 1H), 6.84 (d, J = 10.0 Hz, 2H), 6.75 (d, J = 11.3 Hz, 1H), 6.33 (d, J = 9.7 Hz, 1H), 6.27–6.18 (m, 1H), 3.73 (s, 3H), 3.30–3.19 (m, 2H), 2.88 (d, J = 9.3 Hz, 2H); ^{13}C NMR (75 MHz, $CDCl_3$) δ 203.8, 165.1, 163.1, 159.6, 142.5, 132.3, 129.7, 120.9, 114.3, 113.6, 111.6, 108.1, 103.6, 55.3, 39.6, 30.4; HR-MS (ESI) *m/z*: calcd for $C_{16}H_{16}O_4$ $[M-H]^-$ 271.0976, found 271.0978; Purity: 98.791% (by HPLC).

*1-(2,4-Dihydroxyphenyl)-3-(3,4-dihydroxyphenyl)propan-1-one (**12m**).* Yield 62.8%, yellow solid. ^{1}H NMR (300 MHz, DMSO-d_6) δ 12.68 (s, 1H), 10.67 (s, 0H), 8.75 (s, 1H), 7.82 (d, J = 8.8 Hz, 1H), 7.31–7.09 (m, 1H), 6.68–6.62 (m, 2H), 6.55–6.48 (m, 1H), 6.39 (dd, J = 8.9, 2.4 Hz, 1H), 6.28 (d, J = 2.4 Hz, 1H), 3.21 (t, J = 7.6 Hz, 2H), 2.78 (t, J = 7.6 Hz, 2H); ^{13}C NMR (75 MHz, DMSO) δ 204.0, 165.1, 164.5, 145.2, 143.5, 133.1, 132.0, 119.1, 116.0, 115.6, 112.6, 108.4, 102.6, 39.4, 29.4; HR-MS (ESI) *m/z*: calcd for $C_{15}H_{14}O_5$ $[M-H]^-$ 273.0768, found 273.0776; Purity: 99.871% (by

HPLC).

*1-(2,4-Dihydroxyphenyl)-3-(2,4-dimethoxyphenyl)propan-1-one (**12n**).* Yield 76.5%, yellow oil. ^{1}H NMR (300 MHz, $CDCl_3$) δ 7.80 (d, J = 8.4 Hz, 1H), 7.38 (d, J = 3.7 Hz, 1H), 7.35 (s, 1H), 6.89 (d, J = 8.2 Hz, 1H), 6.54 (d, J = 2.2 Hz, 1H), 6.51 (dd, J = 8.4, 2.2 Hz, 1H), 6.44 (d, J = 2.4 Hz, 1H), 6.37 (dd, J = 8.2, 2.5 Hz, 1H), 3.83 (s, 3H), 3.72 (s, 3H), 3.33–3.26 (m, 2H), 2.97–2.90 (m, 2H); ^{13}C NMR (75 MHz, DMSO-d_6) δ 204.2, 164.8, 164.4, 159.2, 158.0, 132.9, 130.0, 120.8, 112.5, 108.2, 104.4, 102.5, 98.3, 55.3, 55.1, 37.9, 24.7; HR-MS (ESI) *m/z*: calcd for $C_{17}H_{18}O_5$ $[M-H]^-$ 301.1081, found 301.1104; Purity: 98.515% (by HPLC).

13a–e. Compounds **13a–e** were synthesized according to the synthetic routes of compounds **11a–n**.

*3-(2,4-Dimethoxyphenyl)-1-(4-methoxyphenyl)propan-1-one (**13a**).* Yield 72.3%, pink oil. ^{1}H NMR (300 MHz, $CDCl_3$) δ 7.98 (d, J = 8.9 Hz, 2H), 7.12 (d, J = 8.1 Hz, 1H), 6.94 (d, J = 8.9 Hz, 2H), 6.48 (d, J = 2.4 Hz, 1H), 6.44 (dd, J = 8.1, 2.4 Hz, 1H), 3.88 (s, 3H), 3.83 (s, 3H), 3.81 (s, 3H), 3.23–3.15 (m, 2H), 3.02–2.94 (m, 2H); ^{13}C NMR (75 MHz, DMSO) δ 197.9, 163.0, 159.1, 158.0, 130.2, 129.9, 129.6, 121.1, 113.9, 104.3, 98.3, 55.5, 55.3, 55.1, 38.1, 24.4; HR-MS (ESI) *m/z*: calcd for $C_{18}H_{20}O_4$ $[M+H]^+$ 301.1435, found 301.1439; Purity: 99.215% (by HPLC).

*1-(2-Hydroxy-4-methoxyphenyl)-3-(2-hydroxyphenyl)propan-1-one (**13b**).* Yield 69.3%, white solid. ^{1}H NMR (300 MHz, $CDCl_3$) δ 7.66 (dd, J = 8.4, 0.9 Hz, 1H), 7.14–7.10 (m, 2H), 6.89 (s, 1H), 6.86 (d, J = 1.0 Hz, 1H), 6.40 (s, 2H), 3.82 (s, 3H), 3.39–3.34 (m, 2H), 3.02 (t, J = 6.3 Hz, 2H); ^{13}C NMR (75 MHz, $CDCl_3$) δ 204.8, 166.5, 165.4, 154.3, 131.8, 130.6, 128.0,

127.5, 120.8, 116.9, 113.2, 108.2, 100.9, 55.6, 39.3, 25.0; HR-MS (ESI) *m/z*: calcd for $C_{16}H_{16}O_4$ $[M-H]^-$ 271.0976, found 271.0968; Purity: 96.474% (by HPLC).

*3-(2-Hydroxyphenyl)-1-(4-methoxyphenyl)propan-1-one (**13c**).* Yield 75.7%, colorless oil. ^1H NMR (300 MHz, $CDCl_3$) δ 8.44 (s, 1H), 8.01 (d, J = 8.9 Hz, 2H), 7.18–7.12 (m, 2H), 6.99–6.93 (m, 3H), 6.91 (dd, J = 7.3, 1.3 Hz, 1H), 3.91 (s, 3H), 3.49–3.42 (m, 2H), 3.10–3.04 (m, 2H); ^{13}C NMR (75 MHz, $CDCl_3$) δ 200.6, 164.1, 154.7, 130.7, 130.6, 129.1, 128.0, 128.0, 120.6, 117.5, 113.8, 55.5, 40.1, 25.0; HR-MS (ESI) *m/z*: calcd for $C_{16}H_{16}O_3$ $[M-H]^-$ 255.1026, found 255.1023; Purity: 99.693% (by HPLC).

*1-(2-Hydroxy-4-methoxyphenyl)-3-(4-hydroxyphenyl)propan-1-one (**13d**).* Yield 56.8%, yellow solid. ^1H NMR (300 MHz, $CDCl_3$) δ 12.85 (s, 1H), 7.63 (d, J = 9.6 Hz, 1H), 7.10 (d, J = 8.4 Hz, 2H), 6.77 (d, J = 8.4 Hz, 2H), 6.45–6.33 (m, 2H), 3.83 (s, 3H), 3.24–3.14 (m, 2H), 3.02–2.91 (m, 2H); ^{13}C NMR (101 MHz, $CDCl_3$) δ 204.0, 166.1, 165.3, 154.2, 132.8, 131.6, 129.5, 115.5, 113.4, 107.8, 101.0, 55.6, 40.0, 29.6; HR-MS (ESI) *m/z*: calcd for $C_{16}H_{16}O_4$ $[M-H]^-$ 271.0976, found 271.0977; Purity: 99.733% (by HPLC).

*3-(4-Hydroxyphenyl)-1-(4-methoxyphenyl)propan-1-one (**13e**).* Yield 79.2%, yellow solid. ^1H NMR (300 MHz, $CDCl_3$) δ 8.03–7.93 (m, 2H), 7.16–7.09 (m, 2H), 7.01–6.93 (m, 2H), 6.86–6.78 (m, 2H), 3.90 (s, 3H), 3.26 (t, J = 7.7 Hz, 2H), 3.02 (t, J = 7.6 Hz, 2H); ^{13}C NMR (101 MHz, $CDCl_3$) δ 199.5, 163.7, 154.5, 132.8, 130.6, 129.8, 129.5, 115.6, 113.9, 55.5, 40.5, 29.7; HR-MS (ESI) *m/z*: calcd for $C_{16}H_{16}O_3$ $[M-H]^-$ 255.1026, found 255.1022; Purity: 98.584% (by HPLC).

1.2 Molecular docking. The X-ray crystal structure (PDB ID: 2Y9X) of TYR from *Agaricus bisporus* was downloaded from the protein database. The protein was then prepared through the Protein Preparation Wizard module in Schrödinger, and compounds **11c** and **11m** were prepared by the Ligprep module, and their force fields were minimized by OPLS-2005. Finally, Glide Extra Precision (Glide-XP) in Ligand Docking module was used for extra precision docking of compounds with proteins, and PyMOL Molecular Graphics System version 2.7 was used to process docking images.

1.3 TYR inhibitory mechanism study of 11c and 11m. Under different concentrations of L-Tyrosine (0.4 mM, 0.35 mM, 0.3 mM, 0.25 mM, 0.2 mM, 0.15 mM, 0.1 mM, 0.05 mM) and **11c** or **11m** (0 mM, 0.025 mM, 0.05 mM, 0.1 mM), the enzyme inhibition types of the compounds were analyzed and measured four times in parallel. The method was the same as that of IC_{50}. The inhibition type of the compounds on the enzyme was determined by using the Lineweaver-Burk double reciprocal diagram ($1/V = K_m/V_{max}\ 1/([S]) + 1/V_{max}$) with different concentrations of L-Tyrosine.

1.4 Antioxidant activity of representative compounds 11a–n. Representative compounds were tested for their DPPH free radical scavenging activity using methods reported in the literature[59,60] with some modifications. In a 96-well plate, 180 μL of DPPH in methanol (0.2 mM) were mixed with 20 μL of a representative compound in DMSO (0.5 mM).

L-ascorbic acid was used as standard reference material, and 20 μL of DMSO was added to the blank group. The 96-well plate was then incubated in the dark for 1 h. Absorbance was measured at 517 nm using a microplate reader and all experiments were repeated three times in parallel. The DPPH radical scavenging activity of representative compounds was calculated using the following formula: % radical scavenging rate = [(Ac-As)/Ac] × 100. Ac refers to the absorbance of the blank group, and As refers to the absorbance of the test group.

1.5 In vivo treatment of 11c on UV-induced skin pigmentation

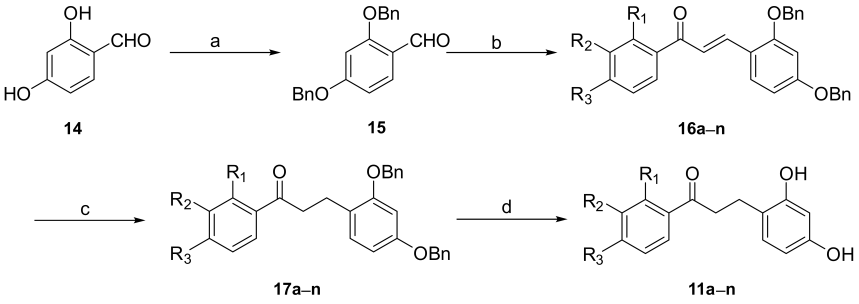
The animal experiments were performed using the previously reported method[44] with minor modifications. All the experiments were conducted on the basis of the approval and guidelines of the Ethics Review Committee of China Pharmaceutical University (animal experiment ethical review acceptance No. 2022-06-012), as well as the Animal Welfare Act and principles stated in the Guide for the Care and Use of Laboratory Animals of the National Research Council. Female guinea pigs (Dunkin−Hartley strain, 10 weeks old, 350−500 g, Nanjing, China) were used as experimental subjects. On the backs of the guinea pigs, four separate areas (2 × 2 cm^2) were shaved and received ultraviolet exposure from a UV lamp (SH1-B, Sigma, Shanghai, China), with a total UV dose of 30 mJ/cm^2/day. Each separate area was treated with different formulations with or without different doses of the compound. The effect of the compound was examined on the basis of a pigmentation model with two different methods of administration: topical administration of the compound 1) 6 h before UV radiation every day for 2 weeks, or 2) after exposure to

UV lamp for 5 days/week for two consecutive weeks. Three days after the final operation, the animals in both groups were sacrificed and skin samples were removed surgically. The skin samples were sent to KeyGEN Biotechnology Company (Nanjing, China) for tissue sectioning, staining, and photographing. Melanin content was assessed using a Fontana−Masson Stain Kit (Solarbio, Beijing, China) following the manufacturer's instruction. The proportion of the positive cells was the ratio of the number of positive cells to the number of epidermal cells in the same visual field with 10 different images for each skin sample

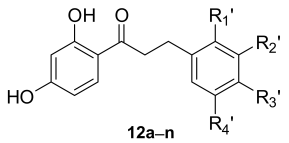
2. Results

2.1 Scheme B-1.

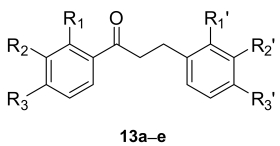
Synthesis of compounds **11a–n**, **12a–n** and **13a–e**[a]



11a $R_1 = R_2 = H$; $R_3 = OCH_3$
11b $R_1 = R_3 = H$; $R_2 = CH_3$
11c $R_1 = R_3 = OH$; $R_2 = H$
11d $R_1 = OH$; $R_2 = R_3 = H$
11e $R_1 = R_2 = H$; $R_3 = Br$
11f $R_1 = CH_3$; $R_2 = R_3 = H$
11g $R_1 = R_2 = H$; $R_3 = OH$
11h $R_1 = R_3 = Cl$; $R_2 = H$
11i $R_1 = OH$; $R_2 = H$; $R_3 = OCH_3$
11j $R_1 = R_2 = H$; $R_3 = CH(CH_3)_2$
11k $R_1 = H$; $R_2 = OH$; $R_3 = OCH_3$
11l $R_1 = R_2 = R_3 = H$
11m $R_1 = H$; $R_2 = OCH_3$; $R_3 = OH$
11n $R_1 = R_2 = H$; $R_3 = phenyl$



12a–n



13a–e

12a $R_1' = R_2' = OCH_3$; $R_3' = R_4' = H$
12b $R_1' = R_2' = R_4' = H$; $R_3' = OH$
12c $R_1' = R_2' = R_3' = OCH_3$; $R_4' = H$
12d $R_1' = R_3' = R_4' = H$; $R_2' = OH$
12e $R_1' = OH$; $R_2' = R_4' = H$; $R_3' = OCH_3$
12f $R_1' = R_4' = H$; $R_2' = OH$; $R_3' = OCH_3$
12g $R_1' = H$; $R_2' = R_3' = R_4' = OCH_3$
12h $R_1' = R_4' = H$; $R_2' = R_3' = OCH_3$
12i $R_1' = R_3' = R_4' = H$; $R_2' = NO_2$
12j $R_1' = OH$; $R_2' = R_3' = R_4' = H$
12k $R_1' = CH_3$; $R_2' = R_3' = R_4' = H$
12l $R_1' = R_3' = R_4' = H$; $R_2' = OCH_3$
12m $R_1' = R_4' = H$; $R_2' = R_3' = OH$
12n $R_1' = R_3' = OCH_3$; $R_2' = R_4' = H$
13a $R_1 = R_2 = R_2' = H$; $R_3 = R_1' = R_3' = OCH_3$
13b $R_1 = R_1' = OH$; $R_2 = R_2' = R_3' = H$; $R_3 = OCH_3$
13c $R_1 = R_2 = R_2' = R_3' = H$; $R_3 = OCH_3$; $R_1' = OH$
13d $R_1 = R_3' = OH$; $R_2 = R_1' = R_2' = H$; $R_3 = OCH_3$
13e $R_1 = R_2 = R_1' = R_2' = H$; $R_3 = OCH_3$; $R_3' = OH$

[a]Reagents and conditions: (a) Benzyl bromide, K_2CO_3, MeOH, reflux, 2 h; (b) Various acetophenone, NaOH, EtOH, reflux, 2–4 h; (c) Bis(pinacolato)diboron, Cs_2CO_3, EtOH, sealed tube, 130–150 ℃; (d) 1 M BCl_3, dry DCM, - 78 ℃ or 0 ℃, Ar, 20 min.

2.2 Molecular docking.

We used molecular docking to further explore the interaction mode of compounds **11c** and **11m** with TYR. The 3D structure of TYR used for docking was obtained from *Agaricus bisporus* (PDB ID: 2Y9X). The best docking mode is shown in Figure B-1. As shown in Figure B-2, the B-rings of **11c** and **11m** could occupy the spacious cavity around the active position formed by His61, His85, His259, Asn260, His263, Met280, Gly281, Ser282, Val283, Arg286, Phe292 and two copper ions, whereas the A rings were located at the inlet of the active pocket. The 2'-OH group of **11c** formed a significant hydrogen bond interaction with Met280, and the B ring formed a *π-π* stacking interaction with His85, His259 and His263, which further explained the reason why the activity of compounds was greatly reduced with B-ring without 2',4'-dihydroxy. The binding mode of the pharmacophore of **11m** and **11c** was similar. Moreover, neither **11c** nor **11m** interacted with copper ions. The docking results ulteriorly showed that compounds **11c** and **11m** mainly interacted with amino acid residues other than TYR active sites and were non-competitive inhibitors.

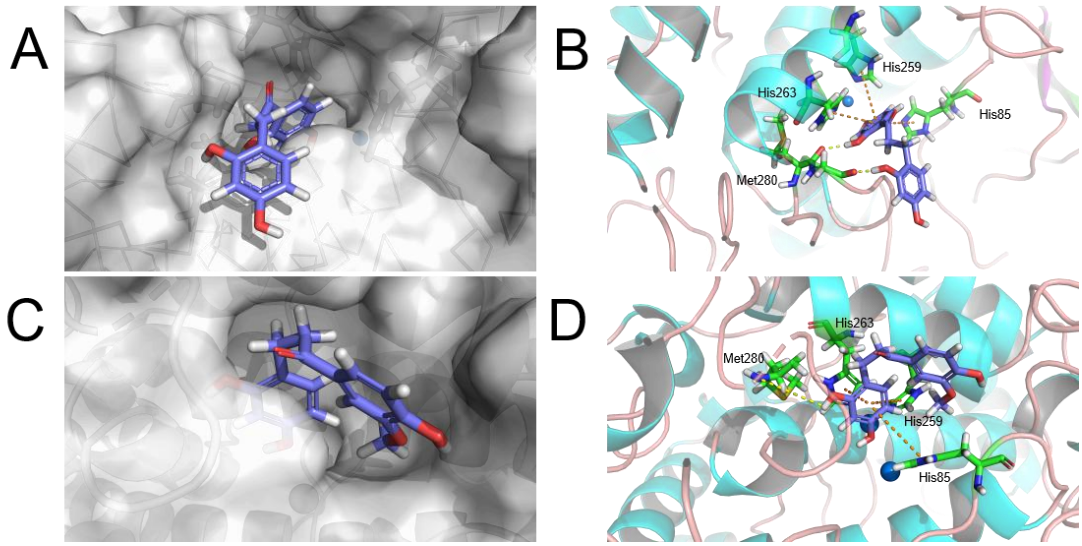


Figure B-1 Binding mode of **11c** (A and B) and **11m** (C and D); yellow dashed lines indicated hydrogen bonds; orange dashed lines indicated π–π stacking; the blue balls indicated copper ions.

2.3 Antioxidant activity of representative compounds 11a–n.

Since TYR can catalyze oxidation reactions, antioxidant compounds are capable of inhibiting TYR activity without direct contact with TYR.[53,54] Assessment of antioxidant activity helps to understand the mechanism of compounds inhibiting TYR further. Thus, 1,1-Diphenyl-2-picrylhydrazyl (DPPH) radical scavenging method was used to evaluate the antioxidant activity of representative compounds **11a–n** at 50 μM, L-ascorbic acid and kojic acid were used as the positive control, and the absorbance at 517 nm was measured by microplate reader. The results in Table B-1 showed that compounds **11a–n** had gratifying DPPH radical scavenging abilities, which were superior than that of positive control kojic acid. We speculated that the DPPH radical scavenging effect of compounds **11a–n** was part of its inhibition of melanin production.

Table B-1. Antioxidant activity of representative compounds **11a–n** at 50 μM.

Compd.	Scavenging activity (%)[a]	Compd.	Scavenging activity (%)[a]
11a	76.56 ± 1.31	**11i**	72.44 ± 0.98
11b	70.50 ± 0.97	**11j**	69.14 ± 1.09
11c	85.47 ± 1.21	**11k**	67.03 ± 0.62
11d	70.98 ± 1.57	**11l**	55.67 ± 0.99
11e	63.36 ± 2.21	**11m**	78.16 ± 1.27
11f	75.85 ± 0.97	**11n**	41.50 ± 0.21
11g	78.72 ± 1.87	kojic acid	28.20 ± 0.58
11h	71.30 ± 0.78	L-ascorbic acid	82.02 ± 2.48

[a]Scavenging activity values are expressed as means ± SD (n = 3).

2.4 Kinetic studies of TYR inhibition.

Due to the fact that, compounds **11c** and **11m** showed the strongest TYR inhibition, with IC_{50} values of 50 nM and 54 nM, respectively. Using Lineweaver Burk double-reciprocal plot, they were selected as representative compounds to analyze TYR inhibition. In the presence of **11c** and **11m**, the kinetic results of TYR were shown in Figure B-3, which showed four straight lines with 1/V varying with 1/[S], different slopes and intersecting on the horizontal axis. When the concentration of compounds increased, the V_{max} value decreased, while the K_m value remained

unchanged, indicating that compounds **11c** and **11m** were non-competitive inhibitors of mushroom TYR, which might exert the inhibitory effect of TYR by interacting with amino acid residues outside the active center.

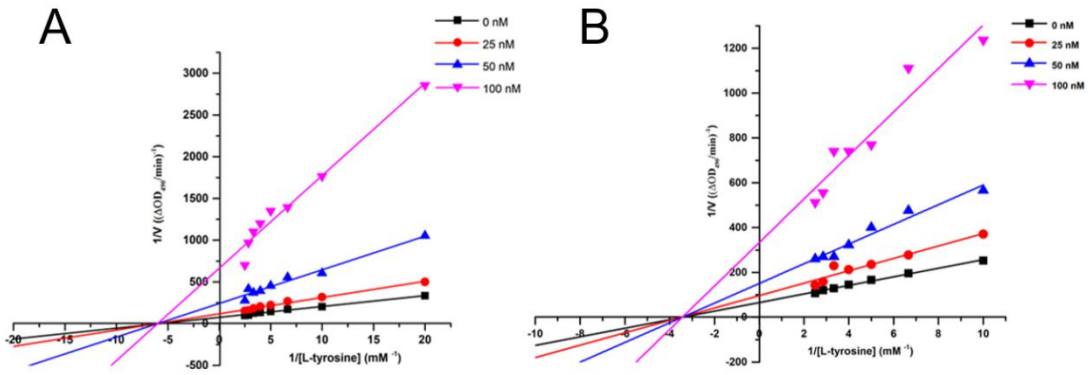


Figure B-2. TYR kinetic characteristic curves of **11c** (A) and **11m** (B).

2.5 In vivo treatment of 11c on UV-induced skin pigmentation in a guinea pig model

Two different methods were applied to evaluate the *in vivo* anti-melanin effect of **11c** in UV-induced skin pigmentation in a guinea pig model: as a prophylactic (**Figure B-3**A) and as a treatment for repair (**Figure B-4**A), that is, topical administration of the compound **11c** 6 h before UV radiation every day for 2 weeks, or after exposure to UV lamp for 5 days/week for two consecutive weeks.

From the result of preventing pigment formation, daily topical administration of **11c** inhibited the production of melanin in a dose-dependent manner (**Figure B-3**B). As shown in Figure B-4C and B-4D, the proportion of cells positive to the Fontana-Masson stain of the skin treated with 0.5 mM **11c** in PG was higher than that of 1 mM **11c** in PG.

Meanwhile, different solvents of **11c** had no significant effect on the inhibition of melanin, and duplicate concentration of **11c** in PG and carbomer (CP) hydrogel both reduced melanin level.

In the batch of repair experiments, compound **11c** in different formulations were applied after receiving UV radiation for 2 weeks. Similar conclusions could be drawn that **11c** was able to heal the scorching skin in a dose-dependent manner, and various solvents had limited influence on the experimental results (**Figure B-4**B-D).

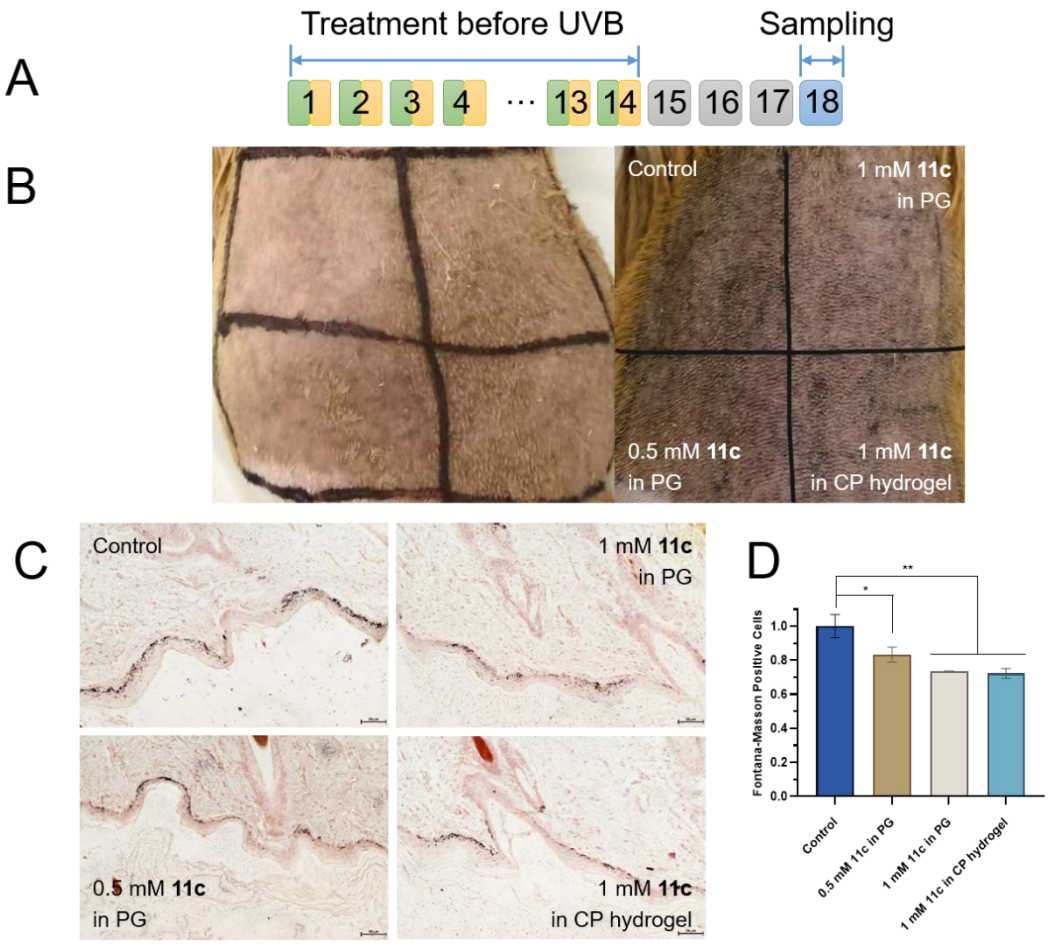


Figure B-3. Prophylactic effect of **11c** on UV-induced pigmentation in guinea pig skin. (A) Time schedule of UV irradiation and application of **11c**. (B) Images of the back of guinea pigs before (left) and after (right) UV

irradiation. (C) Biopsy specimens were taken from each of the four-square areas of the right guinea pig and silver-stained with a Fontana-Masson staining kit. Bars = 50 μM. (D) Statistics of cells positive for Fontana-Masson stain. The proportion of the positive cells was the ratio of positive cells to the number of epidermal cells in the same visual field with 10 different images for each skin sample. Statistical significance of differences was assessed using multiple t-test. *, $p < 0.05$; **, $p < 0.01$ *vs* control group.

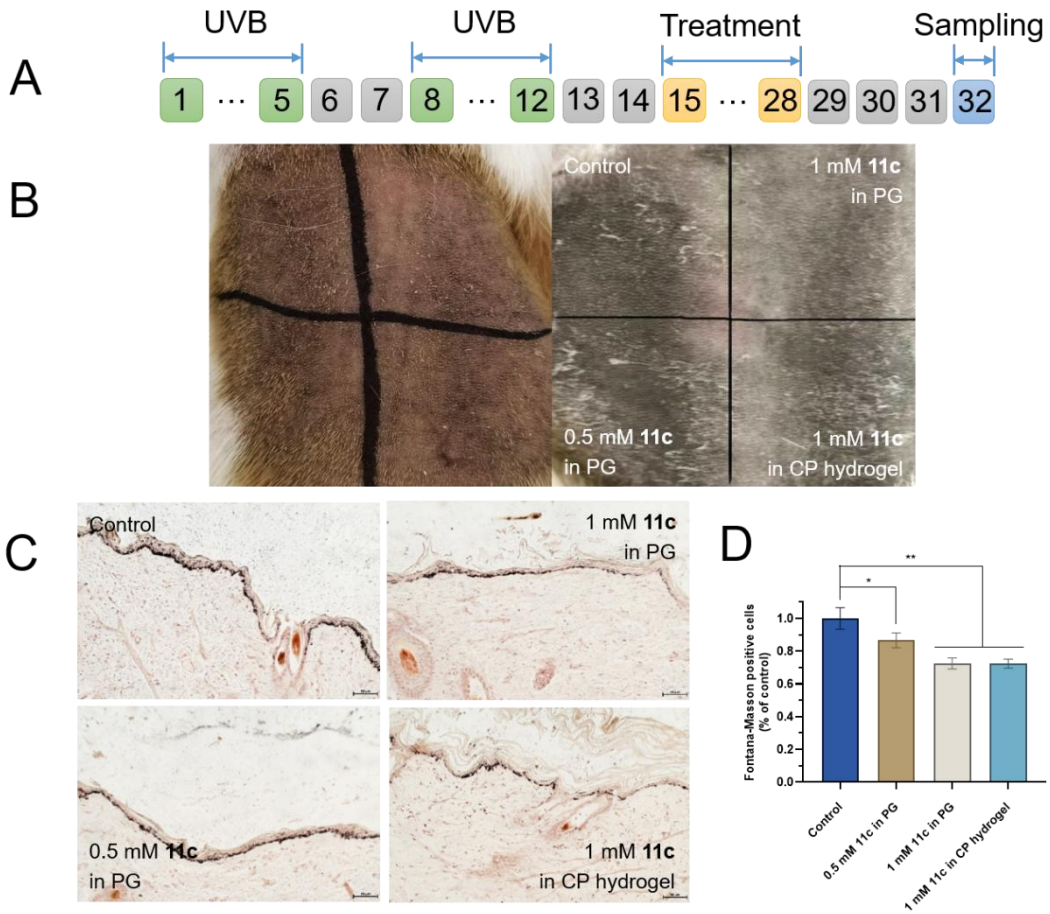


Figure B-4. Ability of **11c** to repair UV-induced pigmentation in guinea pig skin. (A) Time schedule of UV irradiation and application of **11c**. (B) Images of the back of guinea pigs after UV irradiation (left) and after UV

irradiation and treatment (right). (C) Biopsy specimens were taken from each of the four-square areas of the right guinea pig and silver-stained with a Fontana-Masson staining kit. Bars = 50 μM. (D) Statistics of cells positive for Fontana-Masson stain. The proportion of the positive cells was the ratio of positive cells to the number of epidermal cells in the same visual field with 10 different images for each skin samples. Statistical significance of differences was assessed using multiple t-test. *, $p < 0.05$; **, $p < 0.01$ *vs* control group.